

**OPTIMISING SLOPE STABILITY BY OPEN PIT SLOPE DESIGN AT
IKPOBIA MARBLE QUARRY, OKPELLA, SOUTHWESTERN NIGERIA**

BY

SENOUCI OUADADI

(Matriculation Number: 197335)

Bsc., Msc. (Department of Mining Engineering) University of Annaba, Algeria

A Thesis in the Department of Geology,

Submitted to the Faculty of Science,

In partial fulfilment of the requirements for the Degree of

DOCTOR OF PHILOSOPHY

of the

UNIVERSITY OF IBADAN

SEPTEMBER, 2021

ABSTRACT

The adoption of Open Pit Slope Design (OPSD) used in exploitation of minerals is known to impact mining outputs and safety if slope stability is properly determined. However, slope stability is dependent on the understanding of the rock mass properties and identification of critical features such as overburden materials, structural features, and groundwater system of the mines, all of which are usually not well defined. Therefore, this study was aimed at determining the rock mass properties and associated critical features of Ikpobia Marble Quarry, Okpella, Southwestern Nigeria towards optimising slope stability.

The quarry was divided into seven zones (1-7), each with approximately constant bench orientation. Geologic mapping of the quarry was conducted. Vertical Electrical Sounding (VES) using the Schlumberger array was done to determine the subsurface lithology. Quarry photographs were taken and used in photogrammetric analysis to create models of each of the seven zones. Rock mass classification (Geologic Strength Index, GSI) was carried out on the models. Core rock samples from the quarry were tested to determine Uniaxial Compressive Strength (UCS), indirect tensile strength, and density. Petrographic study and X-Ray Diffractometry (XRD) of the rocks were also undertaken. Joint sets orientations were determined from the photogrammetric models and used for kinematic analysis. Data from the analyses were used to determine rock mass properties and as input for analysis of slope stability.

The heights (m) and angles ($^{\circ}$) of slopes of the seven zones analysed were 25 and 85; 25 and 80; 20 and 80; 20 and 75; 30 and 80; 20 and 80; and 25 and 85, respectively. Rocks in the quarry were marble interbedded with calc-silicate gneiss, banded gneiss and quartz schist. The VES showed H-type curves to be dominant (62%) indicating three geoelectric layers made up of clayey sand topsoil, weathered bedrock, fractured and fresh bedrock. Joint sets observed in the zones ranged from 4 – 8 with the dominant orientation posing stability risk to the Northwest. The GSI ranged from 30 to 40. The UCS ranged from 45.7 to 52.3 MPa, tensile strength ranged from 1.5 to 4.6 MPa, and density ranged from 2710 to 2745 Kg/m³ which are in the low to medium range for intact rock. Minerals identified in the rocks were Calcite, Quartz, Alkali Feldspar, Chlorite, Apatite, Biotite, Muscovite, Epidote, Diopside, Phlogopite, Microcline and Albite. Kinematic analysis indicated low risk of slope failure across the zones but a toppling failure with 60% probability in zone 1. The current safety factors for each zone were 1.5, 1.43, 1.34, 1.69, 1.35, 1.34, and 1.5, respectively for zones 1 to 7. The optimum slope angles determined from finite element sensitivity analysis are 55°, 40°, 20°, 40°, 45°, 20° and 55° for zones 1 to 7, respectively.

The optimum slope angles for optimising slope stability were determined. The quarry rock mass properties, critical features assessment and measurements met the requisites standards for acceptable limits of safety.

Keywords: Slope stability, Slope failure, kinematic analysis, Rock mass strength.

Word Count: 478

ACKNOWLEDGEMENTS

To Almighty God: the creator, maker, giver, provider, protector, and doer of all good, be the glory and honour. You make it possible for me to born, grow, aspired and attained. May Allah name be praised.

To my supervisor, Prof. O. A. Okunlola, I appreciate your input into this work and into my life in particular. My learning under you has further shown to me that Ph.D is a process where everything about learner will be subjected to re-processing. Let me also acknowledge and appreciate my Co-Supervisor, Prof. Z. O. Opafunso of the Department of Mining Engineering, Federal University of Technology, Akure, for his inputs into this work.

I am eternally indebted to the Academic Staff Union of Universities in Nigeria (ASUU). The foundation, sub and super structures of this feat. Your commitment to ensuring equity, fairness, justice and truth has led to your extending opportunity to me to pursue my Ph.D in Nigeria. I salute your consistence and commitment to struggle of emancipation. Your act has taught me that the essence of a man is to live for others. The space here is far too small to write appreciation to the dependable body like ASUU, but I assure you I will live my life to extend your philosophy wherever I find myself in future.

My unflinching gratitude and appreciations go to ASUU members at the National level particularly the President, Prof. Emmanuel Osodeke, the Immediate Past President, Prof. Biodun Ogunyemi Dr. Dipo Fashina and Dr. Nasir Fagge, Prof. Sunny Ighalo and at the UI Branch level, the Immediate Past Chairman Prof. Ayodeji Omole who has been a father to me in Ibadan, Prof. Monica Odinko who has been a mother, sister and friend since my arrival to Nigeria, the Chairman, Prof. Ayo Akinwole, Dr. Dapo Adewole my brother and friend who contributed a lot in fulfilling this work, Prof. Demola Aremu, Prof. Segun Ajiboye, Prof. Tajudeen Akanji, Prof. Makinde Olapegba, Dr. Seun Garuba and the rest. Thank you all for accepting me as part of the wonderful ASUU family, giving me all the support and making sure that this work is completed.

I also appreciate the support and contribution of my highly respected lecturers including Professors G. O Adeyemi, O. A. Ehiniola, M. E. Nton, M. N. Tijani, Drs. A. I. Oyediran, A. T. Bolarinwa, A. S. Olatunji, M. A. Adeleye, O. A. Boboye, O. C.

Adeigbe, O. A. Omitogun, O. O. Osinowo and M. A. Oladunjoye. Thank you all for your guidance, constructive criticism and suggestions that made my work better. The support of all the non-teaching staff of the Department of Geology is also acknowledged.

Special thanks and appreciations go to my dear brother and friend who contributed immensely to this research work Dr. Mark Larson and all the great men and women that were contacted by him and made a significant participation to this work specially Dr. Bo Kim. I am equally grateful to the Department of Mining Engineering, University of Utah, USA for allowing the laboratory analyses to be carried out in their rock mechanics laboratory. I express my gratitude to Drs. Musa Idris and Gafar Oniyide of the Department of Mining Engineering, Federal University of Technology, Akure, for their input and contributions into this work. My thanks go to BUA Company management for giving me permission to use and to publish the data, my appreciation goes to the Quarry Engineers specially Mr. Emenike Kerrian, Mr. Tosin Olarinoye and Eng. Tafa Abubakar who helped me during the data collection at the site.

I also want to thank all my friends in Tafawa Balewa Hall of University of Ibadan for being a family to me and giving me all the support and encouragements. My sincere thanks go to my friends Mr. Imad Shaheen, Mr. Kamel Eddine Soltani, Mr. Khaireddin Samaali and from OFIL Company, Mr. Bassam Abdulsalam, Mr. Rassam Al-Wajeih, Mr. Hatim Abdelrahman, Mr. Ahmed Ginah and Mr. Wail Ashaibani for their help and support at all times. I want to thank my friend Labid Hamadha for the special friendship that he kept since secondary school. Many thanks to all my colleagues (research students) in Geology Department University of Ibadan for support in one way or the other.

Special and warm appreciation goes to the most wonderful parents in this world Mr. Mohamed-Salem Abd-Elwahab Senouci and Mrs. Embarka Lil Ramdan, the rare ones who have not failed in ensuring that I get to all my desired height using their time, care, efforts and prayers to support me. I appreciate your love, prayers, encouragement and words of wisdom always and pray that you shall live long in good health to witness and reap your seed. I sincerely appreciate my sisters Karama, Khadija, Najat and Leila and my brothers Mohamed-Lamin and Hamahou for their love, care, support

and being inspiration behind my struggle. I wish to thank my brothers-in-law Ahmed-Salem Senouci, Mohamed-Lamin Najem and special appreciation and thanks to the special one, Ahmed Sidi Ali, who supported me from the very beginning of this program till the end. I cannot forget my nephews and nieces that have always showed me that I am their favourite and most loved uncle, I love you all. My sincere appreciation goes to my uncle, Mr. Mohamed-Fadel Senouci and his lovely family, especially my Sister Sarah, for their participation in my education for a long period during my secondary school. Finally, my warm appreciations go to a very special and unique person in my life, my wife to be, Alia, you have been and will be always by my side. I love you to the moon and back “Forever”.

CERTIFICATION

I Certify that this work was carried out by Mr. Senouci Ouadadi in the Department of
Geology, University of Ibadan

.....

Supervisor

Olugbenga Akindeji Okunlola

B.Sc. (Ilorin), M.Sc. (Zaria), Ph.D. (Ibadan)

Professor, Department of Geology, University of Ibadan, Nigeria

.....

Co-Supervisor

Zacheus Olaniyan Opafunso

M.Sc. (Rapid City, USA), MBA (Vermillion, USA), Ph.D. (Akure, Nigeria), LL. B
(Abuja, Nigeria)

Professor, Department of Mining Engineering, University of Technology Akure

DEDICATION

I want to dedicate this research work and feat to the philosophy of truth, fairness, equity and lifting the trodden, epitomised by the Academic Staff Union of Universities of Nigeria (ASUU). May the strength of the union continue to wax stronger.

TABLE OF CONTENTS

	Page
Title page	i
Abstract	ii
Acknowledgements	iii
Certification	vi
Dedication	vii
Table of Contents	viii
List of Tables	xiv
List of Figure	xvi

CHAPTER ONE: INTRODUCTION

1.1 Study Background	1
1.2 Problem Statement	3
1.3 Aim and Objectives	4
1.4 Justification	4
1.5 Scope	5
1.6 Study Area	5
1.6.1 Location	5
1.6.2 Vegetation	6
1.6.3 Climate	6

CHAPTER TWO: LITERATURE REVIEW

2.1 Regional Geology of Nigeria	9
2.1.1 Precambrian Basement Complex	11
2.1.2 Geology of Northcentral Nigeria	11
2.1.3 Geology of Southwestern Nigeria	12
2.1.3.1 Migmatite–Gneiss–Quartzite Complex	12
2.1.3.2 Gneisses	13
i.) Early Gneiss	13
ii.) Mafic–Ultramafic Bands	13
iii.) Granitic or Felsic Component	13

2.1.3.3 Quartzites	14
2.1.3.4 Calc–Silicate Rocks and Marble	14
2.1.3.5 Slightly Migmatised to Unmigmatised	
Paraschists and Meta–igneous Rock (Schist Belts)	14
2.1.3.6 Ilesha Schist Belt	15
2.1.3.7 Igarra Schist Belt	15
2.1.3.8 Charnockitic Rocks	16
2.1.3.9 Older Granites	17
2.1.4 Geology of Southeastern Nigeria	18
2.1.4.1 The Ancient Migmatite – Gneiss Complex	19
2.1.4.2 Schist Belts	19
2.1.4.3 Older Granites	20
2.1.4.4 Younger Granites	20
2.1.5 Orogenic Episodes of The Nigerian Basement Complex	20
2.1.5.1 The Liberian Orogeny (Late Archean)	21
2.1.5.2 The Eburnean Orogeny (Early Proterozoic)	21
2.1.5.3 The Kibaran Orogeny (Mid Proterozoic – Late Proterozoic)	21
2.1.5.4 The Pan–African Orogeny (Late Proterozoic – Early Paleozoic)	22
2.1.6 Other Rock Types	24
2.1.6.1 Pegmatites	24
2.1.6.2 Quartz and Quartzo–Feldsparthic Veins	24
2.1.6.3 Dolerite Dykes	25
2.1.7 Structural Elements	25
2.1.7.1 Faults	25
2.1.7.2 Lineations	25
2.1.7.3 Major and Minor Folds	26
2.1.7.4 Foliations	26
2.1.8 Metamorphism	27
2.2 Carbonates in Nigeria	27
2.3 Mining Techniques	28
2.3.1 Surface mines	30
2.3.2 Underground Mines	31

2.4 Open Pit Slope Geometry	31
2.5 Open Pit Slope Design and Stability	32
2.6 Rock Slope Design Methods	39
2.6.1 Kinematic Analysis	39
2.6.2 Assessment of Rock Mass Properties	40
2.6.3 Numerical Modelling	44
2.6.3.1 Finite Element Method of Analysis	45
2.6.3.1.1 Basic Mechanics of Finite Element Analysis	46
2.6.3.1.2 Techniques of Determining Factor of Safety in Finite Element	47
2.7 Existing Open Pit Designs	47
2.7.1 The Aitik Copper mine in Sweden	47
2.7.2 The Escondida Mine in Chile	49
2.7.3 The Palabora Mine in South Africa	49
2.7.4 The Aznalcollar Mine in Spain	49
2.8 Recorded Accidents Caused by Slope Failure in Open Pit Mines	51
2.8.1 The Bingham Canyon Mine Slope Failure in 2013	51
2.8.2 Slope Failures at Pikeview Quarry in 2008 and 2009	53
2.8.3 Slope Failure at Dorli Opencast project I in 2014	54
2.8.4 Some Accidents Associated to Mine Failures in Jos, Nigeria	54
2.8.5 Landslides and Slope Failures in Nanka Area Southwestern Nigeria	54

CHAPTER THREE: METHODOLOGY

3.1 Field Investigation	57
3.1.1 Geological Investigation	57
3.1.1.1 Geological Mapping	57
3.1.1.2 Geological 3D Model of the Deposit	57
3.1.2 Geophysical and Groundwater Investigation	57
3.1.2.1 Data Processing and Interpretation of VES Results	59
3.1.3 Geomechanical Investigation	59
3.1.3.1 Joint Data Collection	61
i.) Building Photogrammetric Model	61

ii.) Determining Orientation of a Plane by Sampling on the Exposed Plane in the Model	62
iii.) Determination of Normal to Fitted Plane Via the Plane Equation	63
iv.) Determination of Normal to Fitted Plane Via Vectors Within the Plane	64
3.1.3.2 Rock Mass Classification	64
3.2 Laboratory Tests	68
3.2.1 Rock Samples Preparation	68
3.2.2 Determination of Uniaxial Compressive Strength	68
3.2.3 Triaxial Compression Strength Test	73
3.2.4 Brazil (Indirect Tensile) Test	73
3.2.5 Density Test	76
3.2.6 X-Ray Diffraction (XRD)	76
3.2.7 Petrographic Analysis	76
3.3 Pit Slope Stability Analysis	77
3.3.1 Kinematic Analysis	77
3.3.2 Estimation of Rock Mass Properties Using Hoek-Brown Failure Criterion	77
3.3.3 Numerical Analysis (Numerical Modelling)	78

CHAPTER FOUR: RESULTS AND DISCUSSION

4.1 Field Investigation	80
4.1.2 The Geology of the Study Area	80
4.1.3 X-Ray Diffractometry (XRD)	83
4.1.4 Petrographic Analyses	83
4.1.4.1 Marble Thin Section	83
4.1.4.2 Thins Section from Intrusion 1 (I1)	83
4.1.4.3 Thins Section from Intrusion 2 (I2)	89
4.1.4.4 Thins Section from Intrusion 3 (I3)	96
4.1.4.5 Summary of the Petrographic Analyses	102
4.1.5 Geological 3D Model of the Deposit	102

4.1.6 Geophysical, Hydrogeological and Groundwater Investigation	102
4.1.6.1 Data Processing and Interpretation of VES Results	106
4.1.6.2 Qualitative Interpretation	106
4.1.6.3 Relationship of the curve types with Geology	106
4.1.6.4 Geoelectric Sections	112
4.1.6.4.1 Geoelectric section along profile 1	112
4.1.6.4.2 Geoelectric section along profile 2	112
4.1.6.4.3 Geoelectric section along profile 3	112
4.1.6.4.4 Geoelectric section along profile 4	117
4.1.6.4.5 Geoelectric section along profile 5	117
4.1.6.5 Hydrogeology and Groundwater Flow	120
4.1.7 Geomechanical Investigation	124
4.1.7.1 Joint Data Collection (Photogrammetric Modelling)	124
4.1.7.1.1 Zone 1	124
4.1.7.1.2 Zone 2	124
4.1.7.1.3 Zone 3	124
4.1.7.1.4 Zone 4	130
4.1.7.1.5 Zone 5	130
4.1.7.1.6 Zone 6	130
4.1.7.1.7 Zone 7	130
4.1.7.2 Rock Mass Classification	140
4.2 Geomechanics Study	140
4.2.1 Uniaxial Compressive Strength	140
4.2.2 Triaxial Compression Test	144
4.2.3 Brazil (Indirect Tensile) Test	144
4.2.4 Density Test	153
4.3 Pit Slope Stability Analysis	157
4.3.1 Kinematic Analysis Stability	157
4.3.2 Estimation of Rock Mass Properties Using Hoek-Brown Failure Criterion	166

4.3.3 Numerical Analysis	166
4.3.3.1 Maximum Shear Strain Plots	171
4.3.3.2 Total Displacement Plots	171
4.3.3.3 Strength Reduction Factor	171
4.3.3.4 Sensitivity Analyses for the Deterministic Modelling	182
CHAPTER FIVE: CONCLUSIONS AND RECOMMENDATIONS	
5.1 Conclusions	198
5.2 Recommendations	200
5.3 Contribution to Knowledge	201

LIST OF TABLES

Table	Description	Page
Table 2.1	Generalized Geochronology for the Basement Rocks of Nigeria	23
Table 2.2	Aznalcollar Slope Design (Source: Sjöberg et al., 2001)	50
Table 2.3	Rescue Operations 1980-1993 (After: Mallo and Wazoh, 2014)	56
Table 3.1	Hoek-Brown Rock Mass Classification System	69
Table 4.1	XRD Analysis Results of a Marble Sample and 3 Intrusion Samples from the Ikpobia Quarry	84
Table 4.2	Thin Section Analyses Results for Intrusion 1	92
Table 4.3	Results of Thin Section Analyses for Intrusion 2	97
Table 4.4	Results of Thin Section Analyses for Intrusion 3	101
Table 4.5	Quantitative Interpretation of the VES Data from the Quarry	109
Table 4.6	Major Joint Sets of Zone 1	126
Table 4.7	Major Joint Sets of Zone 2	128
Table 4.8	Major Joint Sets of Zone 3	131
Table 4.9	Major Joint Sets of Zone 4	133
Table 4.10	Major Joint Sets of Zone 5	135
Table 4.11	Major Joint Sets of Zone 6	137
Table 4.12	Major Joint Sets of Zone 7	139
Table 4.13	Estimated GSI Values for Rock Masses in Ikpobia Quarry	141
Table 4.14	Dimensions and Some Properties of Specimens Prepared for UCS	143
Table 4.15	Uniaxial Compression Tests Results for the Ikpobia Quarry samples	147
Table 4.16	Dimensions of Samples Prepared for Triaxial Test	150
Table 4.17	Summary of the Triaxial Compression Test Results for the Ikpobia Quarry	152
Table 4.18	Dimensions of Disk Samples Prepared for Brazil Test	154
Table 4.19	Summary of the Brazil Test Results for the Ikpobia Quarry	156
Table 4.20	Summary of the Density Results for the Ikpobia Quarry	156
Table 4.21	Summary of Kinematic Analysis Results	165
Table 4.22	The Rock Mass Input Parameters of RocLab Software	167

Table 4.23 The Analytical Results of The Rock Mass Failure Criterion from RocLab	168
Table 4.24 Input Parameters for the Phase 2 Software for All the Zones	172
Table 4.25 Critical SRF of the Seven Zones of Ikpobia Quarry	181
Table 4.26 Summary of Sensitivity Analysis for Slope of the Zone 1 at Angle of 85°	191
Table 4.27 Summary of Sensitivity Analysis for Slope of the Zone 1 at 70 m Height	191
Table 4.28 Summary of Sensitivity Analysis for Slope of the Zone 2 at Angle of 80°	191
Table 4.29 Summary of Sensitivity Analysis for Slope of the Zone 2 at 70 m Height	192
Table 4.30 Summary of Sensitivity Analysis for Slope of the Zone 3 at Angle of 80°	192
Table 4.31 Summary of Sensitivity Analysis for Slope of the Zone 3 at 70 m Height	192
Table 4.32 Summary of Sensitivity Analysis for Slope of the Zone 4 at Angle of 75°	194
Table 4.33 Summary of Sensitivity Analysis for Slope of the Zone 4 at 70 m Height	194
Table 4.34 Summary of Sensitivity Analysis for Slope of the Zone 5 at Angle of 80°	194
Table 4.35 Summary of Sensitivity Analysis for Slope of the Zone 5 at 70 m Height	195
Table 4.36 Summary of Sensitivity Analysis for Slope of the Zone 6 at Angle of 80°	195
Table 4.37 Summary of Sensitivity Analysis for Slope of the Zone 6 at 70 m Height	195
Table 4.38 Summary of Sensitivity Analysis for Slope of the Zone 7 at Angle of 85°	196
Table 4.40 Summary of Sensitivity Analysis for Slope of the Zone 7 at 70 m Height	196

LIST OF FIGURES

Figure	Description	Page
Figure 1.1	Location Map of The Study Area	8
Figure 2.1	Geological Sketch Map of Nigeria Showing the Major Geological Components; Basement, Younger Granites, and Sedimentary Basins	10
Figure 2.2	Geological map of Nigeria Showing Limestone and Marble Occurrences (After Fatoye and Gideon, 2013)	29
Figure 2.3	Open Pit Wall Terminology (After Read and Stacey, 2009)	33
Figure 2.4	Joint Sets May be Stable or Present Various Types of Failure Modes at Different Locations in a Pit. After Wyllie and Mah (2004)	41
Figure 2.5	Kinematic Analysis of Blocks of Rock in Slope. (a) Discontinuity Sets in Slope; and (b) Daylight Envelopes on Equal Area Stereonet After Wyllie and Mah (2004)	42
Figure 2.6	Combined Kinematic and Simple Stability Analysis Using Friction Cone Concept. After Wyllie and Mah (2004)	43
Figure 2.7	6-Nodded and 3-Nodded Triangles Respectively (Rocscience, 2009)	47
Figure 2.8	Recommended Catch Bench (after Call <i>et al</i> , 1976; West <i>et al</i> , 1985) and Currently used Bench Geometry for the Northern Footwall of Aitik mine (After Sjöberg, 1999)	48
Figure 2.9	Photo of the 10 April 2013 Bingham Slope Failure (Copyright Kennecott Utah Copper, After Pankow <i>et al.</i> , 2014)	52
Figure 2.10	Photo of the 2008 and 2009 Slope Failures at Pikeview Quarry (After Varnier <i>et al.</i> , 2018)	53
Figure 2.11	Slope Failure at Dorli Opencast Project I (After Satyanarayana and Sinha, 2018)	55
Figure 3.1	Location of the Vertical Electrical Sounding Points and BH-Core-Holes at the Pit	58
Figure 3.2	Geopluse Campus Tiger Resistivity Meter used for VES	

Data Collection	60
Figure 3.3 Google Earth Image of the Pit Quarry Representing the Different Zones	65
Figure 3.4 Presentation of the Texture Photogrammetric Model Built by 3DF Zephyr Software for Zones 1 and 2	65
Figure 3.5 Presentation of the Texture Photogrammetric Model Built to Sample joint 2 in the Zone 1	66
Figure 3.6 Presentation of the Texture Photogrammetric Model Built to Sample Joints 3 and 4 in the Zone 1	66
Figure 3.7 Presentation of the Texture Photogrammetric Model Built to Sample Joints 1 in the Zone 3	67
Figure 3.8 Presentation of the texture photogrammetric model built to Sample Joints 6, 7 and 8 in the Zones 7 and 8	67
Figure 3.9 Sample Preparation at Geomechanics Laboratory, Mining Engineering Department of University of Utah, USA	70
Figure 3.10 Uniaxial Test Machine for Elastic and Compressive Strength Tests at Geomechanics Laboratory, Mining Engineering Department of University of Utah, USA 48	71
Figure 3.11 Samples During and After Strain Gauges Attachment at Geomechanics Laboratory, Mining Engineering Department of University of Utah, USA	72
Figure 3.12 Hoek Cell for Triaxial Tests at Geomechanics Laboratory, Mining Engineering Department of University of Utah, USA	74
Figure 3.13 Samples Ready for the Triaxial Test at Geomechanics Laboratory, Mining Engineering Department of University of Utah, USA	75
Figure 4.1 The Geological Map Okpella Region Indicating the Study Area (Modified after Jimoh <i>et al</i> , 2017)	81
Figure 4.2 The Geological Map of Ikpobia Quarry	82
Figure 4.3 Photomicrograph of Marble Area 1 In Transmitted Plane Polarized Light	85
Figure 4.4 Photomicrograph of Marble Area 3 in Transmitted Plane Polarized Light	85

Figure 4.5 Photomicrograph of Marble Area 3 in Transmitted Cross Polarized Light Indicating Cal (Calcite)	86
Figure 4.6 Photomicrograph of Marble Area 2 in Transmitted Cross Polarized Light Indicating Cal (Calcite)	86
Figure 4.7 Photomicrograph of Intrusion 1 Area 1 in Transmitted Plane Polarized Light Indicating Q (Quartz), Alf (Alkali Feldspar), B (Biotite), Ep (Epidote)	87
Figure 4.8 Photomicrograph of Intrusion 1 Area 2 in Transmitted Plane Polarized Light Indicating Q (Quartz), Alf (Alkali Feldspar), Bi (Biotite), Di (Diopside), Cl (Chlorite), Ap (Apatite), Opq (Opaque)	87
Figure 4.9 Photomicrograph of Intrusion 1 Area 3 in Transmitted Plane Polarized Light Indicating Q (Quartz), Alf/Plg (Alkali Feldspar)/ (Plagioclase), Bi (Biotite), Ep (Epidote), Ap (Apatite)	88
Figure 4.10 Photomicrograph of Intrusion 1 Area 1 in Transmitted Cross Polarized Light Indicating Q (Quartz), Alf (Alkali Feldspar), Bi (Biotite), Ep (Epidote)	90
Figure 4.11 Photomicrograph of Intrusion 1 Area 2 in Transmitted Cross Polarized Light Indicating Q (Quartz), Alf/Plg (Alkali Feldspar)/ (Plagioclase), Bi (Biotite), Ep (Epidote)	90
Figure 4.12 Photomicrograph of Intrusion 1 Area 3 in Transmitted Cross Polarized Light Indicating Q (Quartz), Alf/Plg (Alkali Feldspar)/ (Plagioclase), Bi (Biotite), Ep (Epidote), Sph (Sphene)	91
Figure 4.13 Photomicrograph of Intrusion 2 Area 1 in Transmitted Plane Polarized Light Indicating Q (Quartz), Alf (Alkali Feldspar), Cl (Chlorite), Ap (Apatite), Opq (Opaque)	93
Figure 4.14 Photomicrograph of Intrusion 2 Area 2 in Transmitted Plane Polarized Light Indicating Q (Quartz), Plg/Alf (Plagioclase/ Alkali Feldspar), Cl (Chlorite)	93
Figure 4.15 Photomicrograph of Intrusion 2 Area 3 in Transmitted Plane Polarized Light Indicating Q (Quartz), Alf (Alkali Feldspar), Bi (Biotite), Zr (Zircon), Ap (Apatite), Opq (Opaque)	94
Figure 4.16 Photomicrograph of Intrusion 2 Area 1 in Transmitted Cross	

Polarized Light Indicating Q (Quartz), Alf (Alkali Feldspar), Cl (Chlorite), Ap (Apatite), Opq (Opaque)	94
Figure 4.17 Photomicrograph of Intrusion 2 Area 2 in Transmitted Cross Polarized Light Indicating Q (Quartz), Plg/Alf (Plagioclase/ Alkali Feldspar), Cl (Chlorite)	95
Figure 4.18 Photomicrograph of Intrusion 2 Area 3 in Transmitted Cross Polarized Light Indicating Q (Quartz), Alf (Alkali Feldspar), Ap (Apatite)	95
Figure 4.19 Photomicrograph of Intrusion 3 Area 1 in Transmitted Plane Polarized Light Indicating Q (Quartz), Alf (Alkali Feldspar), Biotite (Bi) and Ap (Apatite)	98
Figure 4.20 Photomicrograph of Intrusion 3 Area 2 in Transmitted Plane Polarized Light Indicating Q (Quartz), Plg (Plagioclase), Biotite (Bi), Ap (Apatite) and Ep (Epidote)	98
Figure 4.21 Photomicrograph of Intrusion 3 Area 3 in Transmitted Plane Polarized Light Indicating Bi (Biotite), Ap (Apatite) and Opq (Opaque)	99
Figure 4.22 Photomicrograph of Intrusion 3 Area 1 in Transmitted Cross Polarized Light Indicating Q (Quartz), Alf (Alkali Feldspar) and Bi (Biotite)	99
Figure 4.23 Photomicrograph of Intrusion 3 Area 2 in Transmitted Cross Polarized Light Indicating Q (Quartz), Alf (Alkali Feldspar), Plagioclase (Plg), Bi (Biotite) and Trace Muscovite (Msc)	100
Figure 4.24 Photomicrograph of Intrusion 3 Area 3 In Transmitted Cross Polarized Light Indicating Q (Quartz), Alf (Alkali Feldspar), Plagioclase (Plg)	100
Figure 4.25 Concentration Map of the Deposit with Coreholes Superimposed	103
Figure 4.26 3-D Geological Model of the Deposit with Coreholes Superimposed	104
Figure 4.27 Fence Diagram of the Deposit	105
Figure 4.28 Representative VES Curves for Some Different Curve Types	107
Figure 4.29 The Distribution of the Curve Types	108
Figure 4.30 Geoelectric Profile Lines in the Ikpobia Quarry	113
Figure 4.31 Geoelectric Section Along Profile1 (VES1, VES20, VES19,	

VES18)	114
Figure 4.32 Geoelectric Section Along Profile 2 (VES8, VES7, VES5, VES4, VES3, VES2, VES1)	115
Figure 4.33 Geoelectric Section Along Profile 3 (VES4, VES23, VES21 & VES17)	116
Figure 4.34 Geoelectric Section Along Profile 4 (VES6, VES9, VES10, VES11, VES12, VES13 VES14)	118
Figure 4.35 Geoelectric Section Along Profile 5 (VES12, VES25, VES16, VES17, VES18)	119
Figure 4.36 Representative View of DEM of the Study Area	121
Figure 4.37 Pit Slope Picture Illustrating the Water Leakage Through Fractures	122
Figure 4.38 The Groundwater Flow Map Showing Recharged Area, Flow Direction and Hydraulic Gradient at the Quarry Site	123
Figure 4.39 Illustration of Joint Sets in Zone 1	125
Figure 4.40 Projection of Joint Sets of Zones 1 and 3 in Stereonet Software	127
Figure 4.41 Illustration of Joint Sets in Zone 3	129
Figure 4.42 Illustration of Joint Sets in Zone 4	132
Figure 4.43 Illustration of Joint Sets in Zone 5	134
Figure 4.44 Projection of Joint Sets of Zones 5 and 7 in Stereonet Software	136
Figure 4.45 Illustration of Joint Sets in Zone 7	138
Figure 4.46 Estimation of the Range of Geological Strength Index in Ikpobia Quarry	142
Figure 4.47 The sample C9A Before, During and After the Uniaxial Compression Test	145
Figure 4.48 Experimental Stress-Strain Diagram of Sample CA9	146
Figure 4.49 Experimental Stress-Strain Diagram of Sample C8A	146
Figure 4.50 Experimental Stress-Strain Diagram of Sample C7A	146
Figure 4.51 Plot of Peak Stresses Versus Confining Pressures	148
Figure 4.52 The Sample C1B Before, During and After the Triaxial Compression Test	149
Figure 4.53 The sample C4A Before, During and After the Triaxial Compression Test	149
Figure 4.54 Experimental Stress-Strain Diagram of Sample C7A	151

Figure 4.55 The sample D11B before, During and After the Brazil Test at Geomechanics Laboratory, Mining Engineering Department of University of Utah, USA	155
Figure 4.56 Kinematic Analysis for Zone 1	158
Figure 4.57 Kinematic Analysis for Zone 2	159
Figure 4.58 Kinematic Analysis for Zone 3	160
Figure 4.59 Kinematic Analysis for Zone 4	161
Figure 4.60 Kinematic Analysis for Zone 5	162
Figure 4.61 Kinematic Analysis for Zone 6	163
Figure 4.62 Kinematic Analysis for Zone 7	164
Figure 4.63 Hoek-Brown Failure Envelope for Zone 1	169
Figure 4.64 Mohr-Coulomb and Hoek Brown Failure Envelopes for Zone 1	170
Figure 4.65 Maximum shear strain for slope at Zone 1	173
Figure 4.66 Maximum shear strain for slope at Zone 2	174
Figure 4.67 Maximum shear strain for slope at Zone 3	174
Figure 4.68 Maximum shear strain for slope at Zone 4	175
Figure 4.69 Maximum shear strain for slope at Zone 5	175
Figure 4.70 Maximum shear strain for slope at Zone 6	176
Figure 4.71 Maximum shear strain for slope at Zone 7	176
Figure 4.72 Total Displacement for slope of Zone 1	177
Figure 4.73 Total Displacement for slope of Zone 2	177
Figure 4.74 Total Displacement for slope of Zone 3	178
Figure 4.75 Total Displacement for slope of Zone 4	178
Figure 4.76 Total Displacement for slope of Zone 5	179
Figure 4.77 Total Displacement for slope of Zone 6	179
Figure 4.78 Total Displacement for slope of Zone 7	180
Figure 4.79 Maximum Shear Strain plot for the Slope of Zone 1 at 70 m height and 85°	183
Figure 4.80 Total Displacement plot for Slope at 70 m height and angle of 85°	183
Figure 4.81 Deformation contour for the Slope of Zone 1 at 70 m height and 85°	184
Figure 4.82 Maximum Shear Strain plot for the Slope of Zone 1 at 70 m	

height and 75°	184
Figure 4.83 Total Displacement plot for Slope at 70 m height and angle of 75	185
Figure 4.84 Deformation contour for the Slope of Zone 1 at 70 m height and 75°	185
Figure 4.85 Maximum Shear Strain plot for the Slope of Zone 1 at 70 m height and 65°	186
Figure 4.86 Total Displacement plot for Slope at 70 m height and angle of 65	187
Figure 4.87 Deformation contour for the Slope of Zone 1 at 70 m height and 65°	187
Figure 4.88 Maximum Shear Strain plot for the Slope of Zone 1 at 70 m height and 60°	188
Figure 4.89 Total Displacement plot for Slope at 70 m height and angle of 60°	188
Figure 4.90 Deformation contour for the Slope of Zone 1 at 70 m height and 60°	189
Figure 4.91 Maximum Shear Strain plot for the Slope of Zone 1 at 70 m height and 55°	189
Figure 4.92 Total Displacement plot for Slope at 70 m height and angle of 55°	190
Figure 4.93 SRF Results of the Slope Angle Optimization Analyses for the Ikpobia Quarry	197

CHAPTER ONE

INTRODUCTION

1.1 Study Background

The economic depression is driving many counties in Africa to leverage on exploitation of their natural resources. This assertion may be buttressed by the reaction of mining companies that are attempting to restructure and reorganize their African interests, either by changing their investment objective or by separating African assets into distinct businesses. The purpose of this restructuring is to increase the value of their broader portfolio's assets (Woods and Lane, 2015). This development does not exclude the current situation in Nigeria where Nigeria's government is attempting to diversify its economy away from oil production by executing a significant mining sector reorganization program. Its goal is to attract private investors (Piper, 2012). One of the objectives of Nigeria's new national solid mineral strategy is to ensure the coordinated development of the country's mineral resources, though Nigeria is rich in a range of solid minerals, ranging from precious metals to various stones, as well as industrial minerals. The majority of these minerals have yet to be mined. Hence, international mining companies are interested in investing in mineral resources of Nigeria.

One other significant features of the mining reforms in Africa revolves around the liberalization of the investment climate as a key factor of attracting foreign direct investment. Many African governments were heavily indebted in the early 1980s, prompting the World Bank to become more involved in devising reforms for the continent's mining industry. The World Bank presented the first comprehensive presentation of reforms that it deemed required to address Africa's low mineral performance and development in its strategy for African mining (UNECA, 2011).

Apart from forest resources that are renewable, mineral resources are not renewable as may be corroborated by the observation of Ibrahim *et al.*, (2010) that in a broader sense, mining refers to the extraction of any non-renewable resource. In the scope of

this study, the non-renewable processes under review had been aptly captured by Warhurst (1999) to include parts of metal production, such as mine development, extraction, and smelting, re-mining and waste management. Hence its exploitation has to be guided by scientific principle to aid production yield to allow environmental sustainability. The three main pillars of the sustainable development are economic, environmental, and social development. Although mining has a many different socio-economic benefits, it also has significant environmental and social consequences in terms of land conversion and degradation, habitat alteration, and water and air pollution if not properly managed (Twerefou, 2009).

Safety is very important in mining but thousands of people are murdered or injured every year in the mining industry around the world (Dhillon, 2010). Therefore, a more proactive approach to all aspects of safety, such as design, engineering safeguards, and promoting safe choices, is necessary. Hence, there is need to build an operational approach around theoretically developed databases to aid production yield and to augment safety. Pit wall failures are a daily occurrence for many operational mines, and they pose a significant risk. At its most basic level, mining is about two things: safety and profitability. Opafunso (2002a), observed that greater concerns have been raised in the recent times about the relationship between slope stability and the economics of open pit mines. The true amount of risk, that is, the level that occurs in practice, is demonstrated by a number of recent safety events and, in economic terms, by the performance of many of the medium- to large-scale mines (Sullivan, 2006).

Mining is defined as the process of extracting mineral wealth from the earth by excavating from the surface to the mineral deposit (Hartman and Mutmansky, 2002). Mining is very important to any nation's economy because it is the way to make mineral resources available for human usage. It has been judged as one of the major sources of raw material supplies to the nation's industries for production of secondary materials and ready merchandise. It was reported that the mining industry is a major factor in the global economy, playing a key role in the resource supply chain. Despite this, its role fluctuates and differs widely from one economy to the next at the national level, and it is poorly documented and sometimes incomprehensible (Dorin *et al.*, 2014). Generally, mining is the extraction of minerals from the earth using two major methods, surface mining and underground mining methods. Surface mining method is the most common method used in

the world on account of security and other factors like ore recovery, operational flexibility, productivity, and cost effectiveness. It involves quarries and mines. Some can reach several hundred meters deep, which could be dangerous because of the risk of slope failure. The risk of slope failure increases as an operator tries to increase the economic benefit by lowering the stripping ratio. Therefore, the proper design of slopes is very important to optimize economics and keep the risk of slope failure at an acceptable level.

The overall goal of hard rock pit slope design is to find the steepest viable slope angles for an open pit mine so that the operator can extract as much ore as possible. On the other hand, steep slopes are more likely to cause slope stability concerns, which could have an impact on worker safety, productivity and, as a result, profitability (Opafunso, 2002b). The strategy is to base the pit design on obtaining an acceptable level of risk, which is then factored into the stability assessments as a component of safety and failure probability. If no instability arises during operations, the pit slopes are overly conservative. As a result, some little instability can be tolerated and monitored during pit construction.

Generally, all fields of earth sciences and mechanical sciences are used in the design of slope mines, including engineering geology, geotechnics, soil and rock mechanics, and hydrogeology. In order to better understand the nature of the rock and identify the most important deformation and failure causes, an overall factor of safety that represents conditions must be determined. In Nigeria there is a dearth or sometimes a total absence of information on the aspect of open pit slope design for many quarries. The reason for initiating this research work, entitled Open pit Slope Design for Production Optimization of BUA Ikpobia Quarry in Okpella, Southwestern Nigeria, is to gain additional information about the rock at this quarry and demonstrate an approach toward improved design.

1.2 Problem Statement

Geological, hydrogeological, and geomechanical investigations provide detailed information, including important properties which increase the confidence of an analysis and allow the geotechnical engineers to optimise slope designs and blast designs on a regular basis (Little, 2006). However, there is no evidence of the existence of these information and properties at most of the quarries in Nigeria including BUA Ikpobia quarry. Hence necessitating a need for the provision of such data as provided in this study.

Several studies have shown that the intact rock properties are not enough to assess the stability and to design the slope. These studies have insisted on the need to assess the rock mass properties to be able to study the slope stability and design it. Therefore, the need to have data on properties of the rock mass at the BUA Ikpobia quarry.

Modelling is important to break down the database into more understandable segments like showing the data in 3D isometric views, which will help geologists and miners to understand the deposit better.

The examination of probable failure modes that could damage the slope benches is crucial to the establishment of slope design criteria. The level of stability should be assessed and put in consideration for safety levels and economic risk.

At BUA Ikpobia quarry the slope consists of only one bench, and as mining progresses, the height of the bench increases. The increasing height augments the incidence of rock failure and poses a threat to both workers and equipment. This threat calls for serious attention to address the problem and, thus, requires a design for the slope.

1.3 Aim and Objectives

The aim of this research is to design pit slope for BUA Ikpobia quarry, Southwestern Nigeria with a view to increase production and enhance mining safety. The objectives are to:

- i.) conduct geological, hydrogeological and geomechanical investigations of the BUA Ikpobia marble deposit;
- ii.) assess the rock mass properties using the Hoek-Brown failure criterion;
- iii.) estimate possible slope mode of failures using kinematic analysis; and
- iv.) analyse the present slope stability and design the slope using inputs from above parameters

1.4 Justification

The design of the slope in BUA Ikpobia quarry is a must to optimize the production and enhance the safety at the quarry. Currently the slope consists only of a bench, which is hazard prone, especially with any increment of slope height that increases the risk of rock fall to unacceptable levels. The solution to this is to develop a proper design according to the slope stability analysis as this is vital for designing safe slopes in open-pit mines. A

good slope design not only improves slope stability and safety, but it also saves money, extends the mine's life, and lowers the stripping ratio. Nevertheless, preliminary information on geological, hydrogeological and geomechanical properties of the deposit must be available. But there is dearth of information on geological, hydrogeological and geomechanical information about the BUA Ikpobia quarry. This may have been the challenge that has limited the ability of the site's geotechnical engineers to determine an optimized design of the BUA Ikpobia quarry slope. If this study is able to generate such information, the BUA geotechnical engineers will be able to use or build upon such information and design work to improve current and future slope design to attain optimisation and safety.

The properties of jointed rock masses are difficult to assess because the laboratory tests on intact rock and the site investigations are not representative of the rock masses. The rock mass properties are important in any slope stability analysis or design. The use of Hoek-Brown failure criterion is common in the rock mechanics field as a widely accepted approach to assess the rock mass properties (Hoek and Brown, 2019). At BUA Ikpobia quarry, the Hoek-Brown failure criterion should be used to assess the rock mass properties.

This study uses the modelling of the deposit characteristics and shows its importance to break down the database into more understandable segments like showing the data in 3D isometric views. Thus, this study upon conclusion will help the geologists and miners to understand the deposit characteristic for proper optimization of the quarry exploitation.

1.5 Scope

This research covered the Ikpobia quarry of Okpella deposit that is under the operation of BUA Group Company. The study in this thesis focused on the design of the overall slope angles at the quarry and does not cover the design of benches and ramps and other elements of the pit.

1.6 Study Area

1.6.1 Location

Okpella is located in the northern region of Edo state in Nigeria. It lies between Latitude 7° and 7.25° North and Longitude 6.15° and 6.38° East, covering an area of about 231.2 sq.km, shown in Figure 1.1. To the North and North-East of Okpella is Okene local

government area in Kogi state, to the West are the Akoko-Edo local government area, villages of Ososo, Oja, Dangbala, Ojirami and Atte. To the south is the Uzairue clan and to the South-West are the north Ibie clans (Okpekpe and the tree Ibies) (Fadugba *et al*, 2015). The area lies within the Precambrian Basement complex of southwestern Nigeria.

1.6.2 Vegetation

The vegetation in the area is derived savannah ecosystem with a mix of few forests' flora, the area is a community of regenerating savannah plants which has been left to fallow. Generally, the area was tempered by human activities mainly for agricultural purposes. Imported cultivated plants in the area are casava (*Manihot esculenta*), maize (*Zea mays*), bean (*Vinga unguiculata*), yam (*Dioscorea esculenta*), pepper and fruits (Mango, Orange).

1.6.3 Climate

In 1956, the World Meteorological Organization proposed a minimum duration of thirty to thirty-five years for averaging climatic data before detecting variability (Trewin, 2007). That is why a set of data of 39 years (from 1973 – 2012) was obtained from the Nigeria Meteorological Agency (NIMET). Okpella is located within the humid tropical climate with a moisture index between -19.5 and + 18.5 based on Thornthwaite classification scheme. Rain falls for about 9 months of the year in Okpella and its environs the rainy season starts in March and lasts until November. The twin peak features common in the southern section of the country are plainly visible, and Okpella has a "little dry season" around August. Rain falls on more than (i.e. > 30%) of the days in every month from March to October, and on little less than 5 (i.e. > 16%) of the days between November and February. Overall, a total of approximately 2006.60mm of rain is recorded annually.

Due to the latitudinal location of the Ikpobia quarry in relation to the equator, the temperature is reasonably high and consistent throughout the year, while there is a significant variation between the rainy and dry seasons in temperature. The general annual average daily temperature is 27.9⁰C. The minimum average daily temperature is about 26.38⁰C and daily maximum is about 29.54⁰C. The region is characterized by a relatively high relative humidity (RH) as a result of the prevailing tropical maritime (TM) air mass blowing over the environment almost all year round. Overall, an average of 91.25% and 68.27% are recorded at 10.00 hours and 16.00 hours local time. The mean annual sunshine hour in the area is about 1,642 hours. The mean monthly values vary between 45 and 172

hours in the months of July and January respectively. The wind pattern in the area follows the Inter – Tropical Convergence Zone (ITCZ). Thus, it is mainly south westerly during the rainy season and north easterly during the dry season and north easterly during the dry season. The wind spread varies between 2 and 5knots for most of the year with an average speed of about 5 knots.

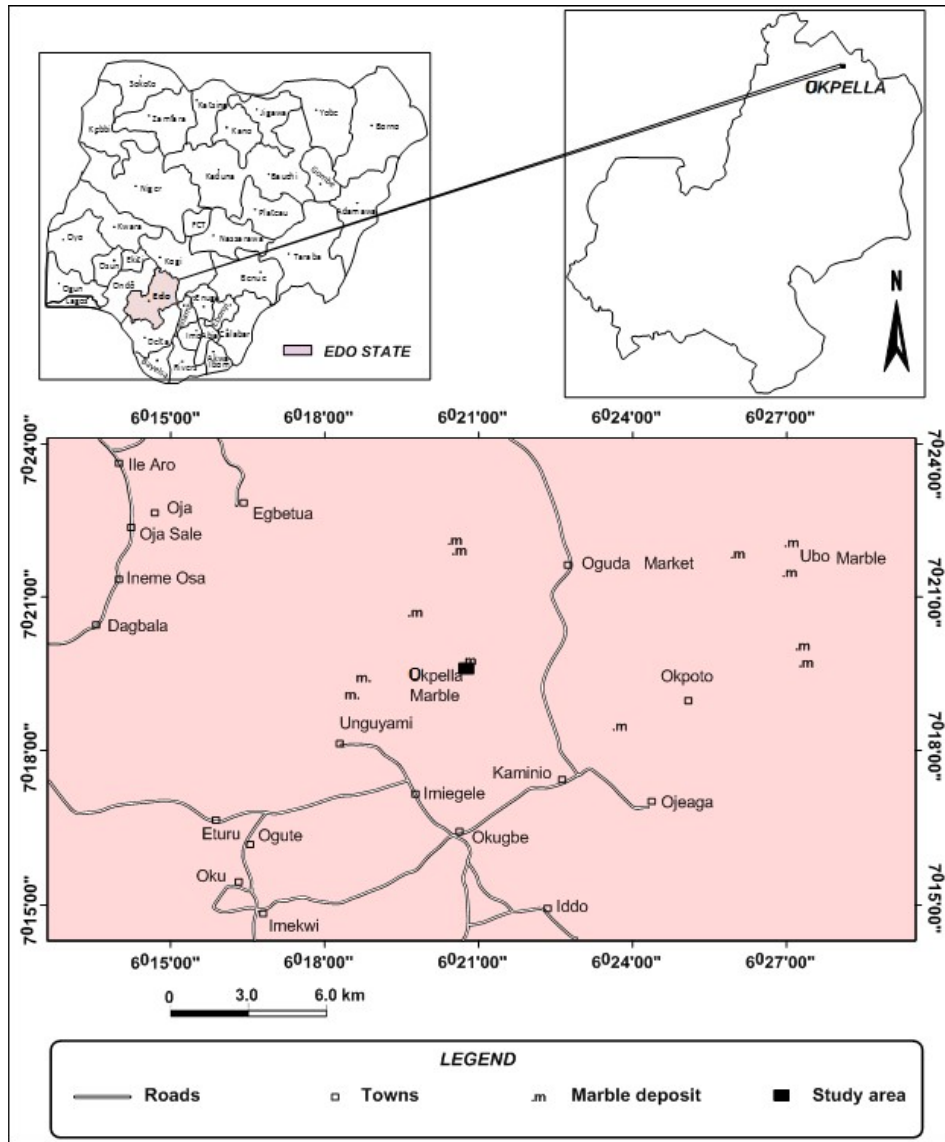


Figure 1.1: Location Map of the Study Area

CHAPTER TWO

LITERATURE REVIEW

2.1 Regional Geology of Nigeria

Nigeria lies between the longitudes of 3° E and 14° E, and the latitudes of 4° N and 14° N (Obaje, 2009). It falls within the Benin-Nigeria shield, which is part of the Pan-African mobile belt. Between the West African craton and the West African sub-region, a major geotectonic domain was structurally consolidated during the Eburnean tectono-thermal event (c2000ma), and it divided the two recognized regions of Pan African orogenic activity in West Africa (Odeyemi, 1979). This occurs to the east of this craton as the Dahomeyan through the Nigeria/ Haggar belt, and to the west as the southern end of the Mauritania belt, which stretches from Liberia in the south to Morocco in the east. It stretches northwards to the Taureg or Hoggar region, which is divided into three structural zones (Black, 1980). The Dahomeyan basement, which stretches all the way to Nigeria, is gneissic in nature and carries the signature of the pan-African orogeny. It also includes migmatites and supra crustal rocks that were folded together on a north-south axis (Odeyemi, 1988).

Nigeria's geology as described by Obaje (2009), is made up of three general litho-petrological components which are:

- Basement Complex
- Younger Granites
- Sedimentary Basins

Figure 2.1 illustrates the geological sketch map of Nigeria showing the major geological components (Obaje, 2009).

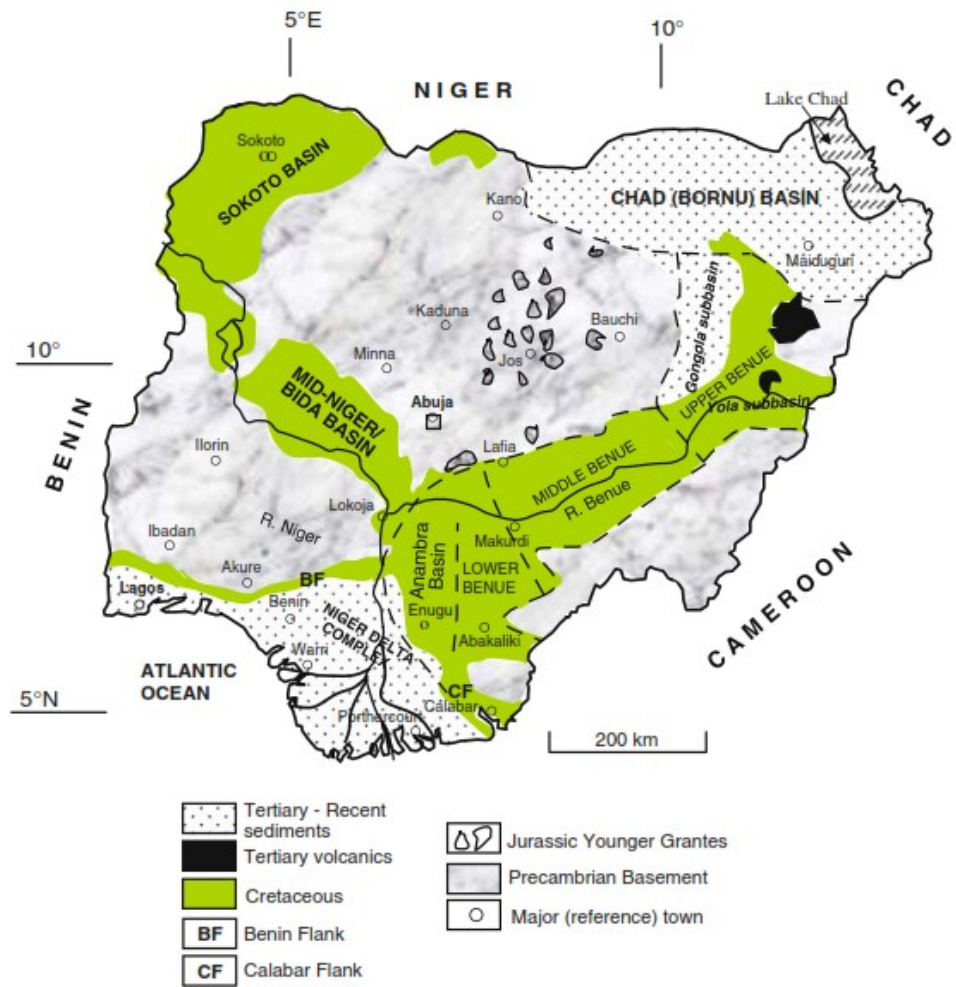


Figure 2.1: Geological Sketch Map of Nigeria Showing the Major Geological Components; Basement, Younger Granites, and Sedimentary Basins
Source : (Obaje, 2009)

2.1.1 Precambrian Basement Complex

The Nigerian basement complex is located between the West African and Congo Cratons, south of the Tuareg Shield, and is part of the Pan-African mobile belt (Black, 1980). The Mesozoic calc-alkaline ring complexes (Younger Granites) of the Jos Plateau intrude on it, while Cretaceous and younger sediments are unconformably overlain. The 600 Ma Pan-African orogeny impacted the Nigerian basement, and it now occupies the reactivated zone that resulted from plate collision between the passive continental margin of the West African craton and the active Pharusian continental margin (Burke and Dewey, 1972). There are four major petro-lithological units in Nigeria's Basement Complex.

The Basement Complex rocks of Nigeria are closely associated with the overall evolution of the African Continent. Hence to unravel the geology of the Southwestern Basement Complex, it is imperative to understand the basement complex's regional geology general. The Nigerian Basement Complex's Rocks are of Precambrian to Late Proterozoic age and occur east of the Craton of West Africa. These rocks have undergone at least more than two orogenic events (tectono-metamorphic cycle), otherwise known as polyphase metamorphism and deformation. They are mainly crystalline igneous and metamorphic rocks and are overlain by Mesozoic to Recent sediments. The Precambrian basement rocks cover around half of Nigeria's land area, and they outcrop in the West (Lokoja-Abeokuta-Babana), Southeast (Plateau bordering Cameroon) and North central (Bauchi-Kano-Anka-Kotangora) areas (FMMP, 1974). For descriptive purposes, the Nigerian basement can be divided into four (4) regions namely; Northwest, Southwest, Northcentral – Northeast, and Southeast. In the Nigerian Basement Complex's central areas there have been intrusions by high level granites and porphyries of Jurassic age known as the Younger Granite Ring Complexes.

Three parts of Nigeria are underlain by Precambrian Basement Complex rocks: southwest area, adjacent to Benin Republic; southeast area, adjacent to Cameroon; and northcentral area, including the Jos Plateau.

2.1.2 Geology of Northcentral Nigeria

Gneisses, migmatites, granites, schists, phyllites, and quartzites make up the rocks found in the North-central region. Igneous rocks, pelitic schists, phyllites, and banded ironstones are found in the narrow, severely folded north-south trending Schist Belts of

northern Nigeria (Obaje, 2009). Amphibolites, diorites, gabbros, marbles, and pegmatites constitute a transition zone between the schist belt of northern Nigeria and the granites of the Jos Plateau to the east in the migmatite–gneiss complex. Older Granites of the Precambrian epoch are abundant there. Younger granites from the Jurassic period have intruded them, forming ring complex formations. The Jos Plateau and adjacent plateau areas have olivine basalts, trachytes, rhyolites, and tuffs that are overlaying or interbedded with coarse grained alluvial sediments from the Mesozoic to Tertiary periods. Weathering has formed a sequence of laterites on the surfaces of these volcanic lava flows. Interbedded sandstones, clays, and limestones dip northwest in the Mesozoic and Tertiary layers of the Sokoto section of the Iullemeden Basin in northwestern Nigeria (Obaje, 2009). Laterite covers the tops of these formations. The late Jurassic to early Cretaceous Illo and Gundumi Formations, the Maastrichtian Rima Group, the late Paleocene Sokoto Group, and the Eocene–Miocene Gwandu Formation make up the sedimentary sequence. During a succession of overlapping maritime transgressions, they were deposited. The down-warped Sokoto Basin contains around 1250m of sediments that lie unconformably on top of Precambrian Basement rocks. Alluvial deposits from the Quaternary period can be found along the Sokoto River's course (Kogbe, 1989).

2.1.3 Geology of Southwestern Nigeria

The Precambrian Basement rocks of southwestern Nigeria, as found in the Dahomeyan (Benin) Basin, are composed of migmatites, banded gneisses, and granite gneisses, intruded by Pan–African age granites and charnockites, with low grade metasedimentary and metavolcanic schists (Oyawoye, 1972). Pegmatite veins and dykes frequently intrude on migmatites and gneissic metasediments (Oluyide *et al.*, 1998). The Precambrian basement of southwestern Nigeria also includes older granites, granodiorites, and syenites, as well as dolerite dykes.

2.1.3.1 Migmatite–Gneiss–Quartzite Complex

This group of rocks is the most pervasive in the Southwestern Basement Complex. It is typified by gneisses, quartzites (characterized by Ibadan and Iseyin–type quartzites), calc–silicate rocks, biotite–hornblende schists and amphibolites. They are the basement “*sensu stricto*”. Deformative, shearing and folding, granitization, and migmatization processes are hypothesized to have resulted in the migmatite–gneiss complex.

2.1.3.2 Gneisses:

They are generally medium to coarse grained with gneissose foliation that is characterized by the alternating layers or bands of light and dark-coloured minerals (Obiora and Umeji, 2004). The foliations may be weak or well pronounced. The migmatite–gneisses are composed of three main components which may be observed in a single outcrop. They include:

- i.) **Early Gneiss:** This is a granodioritic to quartz dioritic quartzo–feldspathic rock with foliated biotite and/or hornblende. The mineral components in the light layers include; orthoclase/microcline, plagioclase of andesine/oligoclase composition, and quartz while dark bands are composed of biotite and/or hornblende. Accessory minerals include; zircon, apatite, sphene and epidote. Alternating mafic and quartzo–feldspathic material sometimes define a fine banding. The contact between mafic and felsic material is gradational. The early gneiss is best seen in the migmatites around Ibadan, Iseyin and Ikare.
- ii.) **Mafic–Ultramafic Bands:** They are generally amphibolites, biotite and biotite hornblende schists or meta–gabbros. They are frequently strongly foliated with foliation parallel to that of enclosing rocks. These rock sub–group may be completely absent in some outcrops.
- iii.) **Granitic or Felsic Component:** This is mainly granitic in nature and can range from aplitic to granitic to pegmatitic in composition. Swarms of augen–shaped porphyroblasts of microcline aligned along the pre–existing foliation in the host rock; concordant to discordant veins and dykes of pegmatite.

Depending on the relationship between these three components various types of gneisses can be distinguished and they encompass the following:

- (a) *Banded Gneiss* which consists of alternating parallel bands of light and dark colored mineral and is the most abundant;
- (b) *Granite Gneiss* (a more uniform gneiss);
- (c) *Semi–banded Gneiss* forms the transition between the banded and granite gneiss. It has also been described as transition gneiss.
- (d) Agmatite
- (e) Augen Gneiss
- (f) Porphyroblastic and Cataclastic Gneiss

The migmatites are a composite group of rocks in which a discrete leucocratic granitic component alternates with more basic gneisses.

2.1.3.3 Quartzites:

Quartzites on the other hand, form good topographic features above the surrounding terrains (about 100m). They generally outcrop poorly but a few good outcrops occur around Ibadan, Okemesi and Iseyin. These quartzites usually consist of at most eight minerals, with only three or four occurring more frequently. Quartz in this rock is usually more than 90% with slight amounts of muscovite, sillimanite, staurolite, garnet, hematite, graphite, tourmaline and zircon, most quartz schist samples from the Nigerian metasedimentary belt yielded similar results (Elueze and Okunlola, 2003; Okunlola *et al.*, 2006). A quartzite from Iseyin described by Rahaman (1973) contained clinopyroxene, epidote, tremolite, actinolite, calcite and sphene.

2.1.3.4 Calc–Silicate Rocks and Marble:

Calc–silicate rocks outcrop as low–lying bodies in the migmatitic gneisses of the Basement Complex. They are continuous for only a few meters and occur differently from the calc–schist of the Younger meta–sediments.

2.1.3.5 Slightly Migmatised to Unmigmatised Paraschists and Meta–igneous Rock (Schist Belts)

These rocks are also referred to as “*Younger Meta–sediments*”. They overlie the migmatite gneiss complex and were previously thought to occur only in the western half of the country until they were found in the central and south eastern parts. They are mapped predominantly as meta–sediments with subordinate mafic–ultramafic units. These rocks occupy the N–S trending, with synformal troughs infolded into the Archean migmatite–gneiss complex. They are largely sediment dominated with the most important lithologies being pelites and semi–pelites. Metamorphic grade varies widely ranging from chlorite to sillimanite grade. The meta–sediments consist of low to medium grade mica–schists, quartz schists, quartzites, meta–conglomerates and concordant amphibolites (rock rich in hornblende). The amphibolites are often products of meta–igneous (basic) rocks but sometimes are often of meta–sedimentary (shale) origin. Rahaman (1973) described biotite; biotite–garnet and biotite garnet–staurolite schist, together with talc–tremolite chlorite rocks. These Younger Meta–sediments are

also associated with marbles, dolomites and calc–silicate rocks which are products of the metamorphism of limestones, marls and calcareous sediments. Some belts with chemical sediments are also present as Banded Iron Formations (BIF). The schist belts generally, which are conspicuous in the western part, show unique petrological, structural and metallogenic features. Schist belts in the southwest include the Igarra, Egbe-Isanlu, Iseyin, Ife-Ilesha, and Lokoja (Elueze and Okunlola, 2003). Two major schist belts exist in Southwestern Basement Complex and they are:

2.1.3.6 Ilesha Schist Belt:

This belt lies east of Ibadan and has a N–S orientation. Elueze (1982), based on the field occurrence, petrology and geochemistry, grouped the rocks of the Ilesha Schist Belt into three major units: (a) the Ilesha Amphibolite Complex; (b) the Ilesha meta–clastics and; (c) the Efon Quartzitic Sequence (Efon Psammite).

- a) The Ilesha Amphibolite Complex includes generally meta–basalts and meta–ultramafites exposed as lenticular and ovoid bodies within the meta–clastics. The meta–sedimentary complex (the meta–clastic and Efon Psammite) consists of sequences of supracrustals that have generally undergone low to medium grade metamorphism.
- b) The meta–clastics include a variety of micaceous schists that are essentially of pelitic to greywacke affinity.
- c) The Efon Psammite overlies the meta–clastics and are principally meta–sandstones consisting of quartzites, quartz schists and granulites which occur largely East of Ilesha and runs for nearly 180km in a general NNE–SSW direction (Dempster, 1967). Some undifferentiated schists (amphibolite schist and talcose rocks) are associated with the Efon Psammite east and west of the area.

The Ilesha Schist Belt has mineral occurrences which include sulphides and oxide minerals. It is also gold bearing.

2.1.3.7 Igarra Schist Belt:

This is the most–easterly belt in Southwestern Nigeria. It trends in the NNW–SSE direction with a distance of 60km. Characteristic rock types include biotite schist which is dominant, meta–conglomerates, marbles, calc–silicate rocks, and quartzites. The pelitic schists in places form impressive and continuous ridges with crests which are

made of narrow bands of quartzite. South of Igarra, the calc–silicate rocks form extensive outcrops which give the most continuous expression of folding in the area. Marble occurrences of economic value have been reported and are being exploited at Jakura, Igbetti and Ukpilla. The marble is composed predominantly of calcite with minor amounts of graphite and calc–silicates minerals and they have varying colors such as white, grey, cream and pale green. The schist belts are Nigeria's best-studied geological formation (Russ, 1957) but the age relationship and geodynamic setting of the schist belts is still unresolved.

2.1.3.8 Charnockitic Rocks

As an end–member of the charnockite series, charnockite is applied to any orthopyroxene–bearing granite made primarily of quartz, perthite or antiperthite, and orthopyroxene (typically hypersthene) (Le Maitre *et al.*, 2005). The charnockite series includes a variety of rocks, some acidic and rich in quartz and microcline, others basic and rich in pyroxene and olivine, and intermediate variations mineralogically corresponding to norites, quartz–norites, and diorites. The presence of extremely pleochroic, reddish or green hypersthene is a frequent trait in several members of the group. They can be named by adding orthopyroxene or especially hypersthene to the conventional igneous nomenclature (e.g. hypersthene–granite), but specialized names such as norite, mangerite, enderbite, jotunite, farsundite, opdalite, and charnockite are also in general usage (in the strict sense). Charnockites from the southwestern basement complex, in general, appear as smooth, spherical boulders that are widely scattered. Although they form solitary hills in areas like Oke–Patara and Osuntedo, it has been determined that their centers are frequently coarser grained than their edges. Charnockites can be found west of Ibadan as dyke–like bodies strewn across a large area. These rocks have been emplaced in migmatite–gneiss terrains to the east of Ibadan and have an oval to circular shape. The charnockites have three major modes of occurrences.

- i.) They commonly occur in the core of an aureole of granitic rocks and typical examples are seen at Wasimi and Oke–Patara. The most complete section is at Wasimi, where a central area of charnockite is followed outwards by granodiorite, porphyritic biotite and biotite hornblende granite and finally migmatites.

- ii.) Charnockites also occur along the margin of Older Granite bodies especially porphyritic biotite granite and an example of this occurs north of Akure and west of Egosi.
- iii.) They also occur as discrete individual bodies in the gneiss complex such as the occurrences at Lagun and Awo.

Charnockites are composed of quartz, alkali feldspars, plagioclase, pyroxenes, and hornblende, biotite and accessory amounts of opaque ore, apatite, zircon and allanite. The alkali feldspars are mesoperthitic and zoned. Plagioclase feldspars present are usually range from andesine to labradorite in composition (Cooray, 1972), but subordinate oligoclase may also be present in some charnockites. Randomly oriented inclusions of various rock types are not uncommon in charnockites. They vary from inclusions of finely foliated amphibolites and syenites to xenoliths of contorted schist granulites and calc-silicate rocks. These inclusions could indicate the nature of the country rocks in which they (charnockite) were emplaced.

The nature of the contact between charnockites and their host rocks is variable. For the Wasimi charnockite, its contact with the surrounding Older Granite is gradational (Hubbard, 1968) and at Iwo it is abrupt. On fresh surfaces though, the contact between the granite and charnockite is often indistinguishable since both feldspars in the granites and charnockite appear greenish.

2.1.3.9 Older Granites

These rocks were initially categorised from the “*younger*” alkaline granites by Falconer and Woods, (1911). In addition to that they are known as Pan-African Granites and vary in size from batholiths to plutons. The forms of bodies seem to be related to the environment in which they were emplaced. It has been observed that, while circular to elliptical bodies are associated with schists more elongate bodies are known amongst migmatite-gneiss terrain. The Older Granite suite is made up of a variety of rocks. Porphyritic/porphyroblastic muscovite granites, biotite granites, hornblende-biotite granites, non-porphyritic/porphyroblastic fine to medium grained granites, granodiorites, adamellites, quartz monzonites, syenites, aplites, diorites, quartz diorites, and pegmatites although granitic and granodioritic compositions are the most prevalent.

The most abundant and most typical member of the Older Granite suite is coarse porphyritic granite as named by Oyawoye (1972). It occurs as discrete bodies several

kilometers across and forms prominent topographic features. They are typified by large feldspars whose color maybe white, pink, purple, yellowish brown or dark grey in a groundmass rich in quartz, feldspar and biotite and/or hornblende. In some cases as was seen in biotite granite found at Iwerre-Ile, these large phenocrysts of feldspars were so abundant that the matrix is subordinate. In other instances, these feldspars show a kind of zoning and they vary in size from about 0.5cm in length at Igarra to about 10cm in the Abeokuta granite. They are usually euhedral to subhedral and have an average length of 3–5cm. Most Older Granites possess a foliation which is concordant with that in the surrounding rocks and is defined by the parallelism of the large feldspars and an alignment of the mafic minerals generally in a N–S direction (Rahaman, 1989). This foliation is variable and sometimes tends towards gneissosity. There are some bodies of Older Granites however, in which these feldspar megacrysts are haphazardly arranged and as such, the granite lacks foliation. Inclusions of surrounding country rocks have been observed in a few cases as in occurrences of garnet in mica schist in the large feldspar granite in Iseyin area. It has also been observed that the contact between the Older Granite rocks and their host rock is gradational in most cases, even though sometimes, it can abrupt. Under the microscope, the phenocrysts (customarily microcline) are twinned under the combined Carlsbad–Tartan twin law, with a strong to weak perthitic intergrowth and may occasionally be zoned. They are set in a granitic groundmass of quartz, microcline, plagioclase of albite to oligoclase composition, muscovite, biotite and/or hornblende. Moreso, petrologically and geochemically, they are known to be calc–alkaline in nature; As a result, they are products of subduction/collision or mountain-building processes, both of which are associated with convergent or compressional tectonics. Therefore, they are known as orogenic granites (Obiora and Umeji, 2004).

2.1.4 Geology of Southeastern Nigeria

Along the border with Cameroon, the Precambrian Basement rocks of southeastern Nigeria are found in three blocks. Biotite-hornblende gneiss, kyanite gneiss, migmatite gneiss, and granite are among the well-fractured crystalline rocks (Ekwueme, 1987).

Within the Nigerian Province, thrust and shear zones allow for the division of the region into numerous units. They are:

2.1.4.1 The Ancient Migmatite – Gneiss Complex

It is made up of Archean polycyclic grey gneisses of predominantly granodioritic to tonalitic nature, migmatites, quartzites, marble, mica schist and talc schist (Jones and Hockey, 1964), amphibolites which occur as relicts within the gneisses and migmatites or are interlayered with them. This reactivated basement occupies fifty percent of the Nigerian Precambrian. They are believed to be the basement “*sensu stricto*” and are considered to be of predominantly sedimentary origin and have undergone a long history of sedimentations, deformations, metamorphisms, and igneous intrusions before the deposition of the Younger meta-sediments and emplacement of the Older Granites (Russ, 1957). According to Rahaman and Ocan (1978), the gneisses are of two basic types; the biotite gneiss and the banded gneiss. Very little is known about the evolution of the migmatite–gneiss complex but age data indicates that they incorporate rocks of the Liberian, Eburnean, possibly Kibaran and Pan–African ages (Ajibade and Wright, 1988). Radiometric ages obtained from the ancient migmatite–gneisses are notably between 2.8Ga and 2.0Ga, these suites' rocks are mostly sedimentary with a few small igneous rocks that have been changed in various ways by metamorphic, migmatic, and granitic processes (Rahaman, 1988; Okunlola 2005). Older dates (>3.0Ga) have been derived (Dada, 1998).

2.1.4.2 Schist Belts

These are composed of low–grade meta–sedimentary (pelitic and semi–pelitic schists and phyllites) and meta–volcanic rocks that were thought to be limited to the western half of the country. These low–grade rocks have steeply dipping foliations and tight to isoclinal folding, as well as gradational, faulted, or sheared interfaces with the surrounding migmatite–gneiss complexes. These so–called Older Metasediments, which are characterized by schists and meta–quartzites inside banded gneisses, are best known in the Ibadan–Ife region. The Northwestern Nigerian schist belts are interpreted as typical volcano–sedimentary assemblages with tensional and compressional associated rocks, demonstrating the influence of paleo–rift systems. Other rocks that make up this unit include; meta–conglomerates, marbles, calc–silicate rocks and subordinate meta–igneous rocks. Isotopic field data reported by Ajibade *et al.*, (1979), have demonstrated that the schist belts are younger than the migmatite–gneiss complex. However, the age of the schist belts is still a matter of controversy.

2.1.4.3 Older Granites

The rocks belonging to this suite include plutonic rocks such as granites, coarse/porphyritic granites, adamellites, granodiorites, quartz diorites, tonalities, charnockites (common in Bauchi and south western Nigeria) and true granites. In several places of the Basement Complex, they appear as significant batholithic masses. The term "Older Granite" also distinguishes these rocks from the Jos Plateau's high-level intrusive Jurassic granites (the Younger Granites). They have consistently yielded broadly, Pan-African ages but the exact time and sequence of emplacement is still unclear. The rocks belonging to the Older Granite suite are believed to have intruded into both migmatite–gneiss complex and schist belts (basement *sensu stricto*).

2.1.4.4 Younger Granites

These accompanied minor intrusions of Jurassic age form a large part of the Jos Plateau of central Nigeria. Tin (cassiterite) mineralization is frequently linked with these. On the Jos Plateau and the eastern plateau sections, tertiary volcanic rocks (basalts and rhyolites) can be found occasionally above basement rocks.

The remaining areas of Nigeria are covered in Mesozoic and younger sediments, which are found in a number of sedimentary basins, including the Benue Basin (Central) Valley/Trough, Sokoto (Northwest border), Chad (Northeast), Bida (Central, along the Niger Valley), Benin–Dahomey (Southwest), Anambra (Southeast) and the Niger Delta (South) Basins.

2.1.5 Orogenic Episodes of The Nigerian Basement Complex

Four significant orogenies have been discovered disturbing the Precambrian history of Nigeria's Basement Complex based on structural, lithostratigraphic, and geochemical data, and their age pattern has been grouped as follows:

1. The Liberian Orogeny (2800 ± 150 m.y.)
2. The Eburnean Orogeny (2000 ± 200 m.y.)
3. The Kibaran Orogeny (1100 ± 100 m.y.)
4. The Pan African Orogeny (600 ± 150 m.y.)

2.1.5.1 The Liberian Orogeny (Late Archean)

Grant (1970) and Oversby (1975) argued that part of the migmatite–gneiss complex is Liberian based on geochronological evidence. The later author obtained a Pb–Pb age of 2750Ma for aplites that intruded on the Ibadan Banded Gneiss and its surrounding rocks. As a result, the Liberian age of these para–gneisses is confirmed. It has become difficult to distinguish the distinct lithostratigraphic units of the Liberian Orogeny in Nigeria due to the obliterating impacts of later deformational processes, migmatization, and erosion.

2.1.5.2 The Eburnean Orogeny (Early Proterozoic)

The consequence of the widespread granitic processes that accompanied the Eburnean Orogeny in West Africa can be seen in the basement rocks of Nigeria. Some basement gneisses in Nigeria have been dated to the Eburnean epoch, however these ages appear to indicate more deformation and basement reactivation than sedimentation. As a matter of fact, it's impossible to prove the existence of undisputable Eburnean meta-sediments, and there's no evidence of any sedimentation during this time. However, Grant (1971) determined a whole rock Rb–Sr age of 2190 ± 30 Ma for the Ibadan granite and a Rb–Sr age of 2220 ± 30 Ma for the Kaduna migmatite. Moreso, Ogezi (1977) obtained indications of Eburnean and older ages from gneisses and migmatites from various parts of northwestern Nigeria.

2.1.5.3 The Kibaran Orogeny (Mid Proterozoic – Late Proterozoic)

The Kibaran orogeny is the most hotly contested in the Nigerian Precambrian and this is because, rocks of the Kibaran are not very common in Nigeria and this has prompted some workers to believe that the Kibaran orogeny did not occur in Nigeria. The published whole rock isochron age of 1150 ± 140 ma for granite gneiss from Ile–Ife by Grant *et al.*, (1972) which according to them, reflects a major metamorphic event that reworked and isotopically homogenized pre-existing granitic rocks suggests a Kibaran age in the Nigerian Basement Complex but this was queried by Hubbard (1975) who re–interpreted the geology of the Ibadan–Ife–Iwo areas in the light of the Kibaran age quoted above.

Ogezi (1977) obtained a 10–point Rb/Sr whole rock isochron age of 1065–65m.y. on the Maru phyllites. This age was interpreted as dating the metamorphism of the phyllites

and aided him in the conclusion that the Kibaran was a major orogenic event in Northwestern Nigeria.

2.1.5.4 The Pan–African Orogeny (Late Proterozoic – Early Paleozoic)

The Pan-African Orogeny has been established in Nigeria like in other parts of West Africa. The Pan-African Orogeny is the most recent orogeny, and it is responsible for the majority of the rocks in Africa's mobile belts which includes the Nigerian Basement Complex. It refers to the Late Precambrian thermotectonic event which led to the “structural differentiation of an original shield into craton and circum–structural (orogenic) areas” (Ajibade and Fitches, 1988). Rahaman (1989), has showed the Effon Psammite Formation in Southwestern Nigeria was deposited throughout the late stages of this orogeny while Ogezi (1977) described the Anka Conglomerates in Northwestern Nigeria as a mollase facie of the Pan–African. Studies by authors such as Ogezi (1977), Ajibade (1980) and others have gone a long way to establish that the Older Granites belong to the Pan–African event *sensu stricto*.

The Pan–African orogeny is the most dated in Nigeria and this is so because; the porphyritic granites and related acidic plutons on which the age determinations are carried out are common and moreso, older rocks bear the imprint of the Pan-African Orogeny. Table 2.1 presents the generalized geochronology for the Basement rocks of Nigeria after McCurry (1989).

TABLE 2.1: Generalized Geochronology for the Basement Rocks of Nigeria

AGE (MA)	PERIOD (OR EPOCH)	ACTIVITY	REMARKS
540 + 40Ma	Late Pan-African	Uplift, cooling, faulting, high level magmatic activity	Gold Mineralization, Rare metals and Pegmatite
650 - 580Ma	Pan African	Granitic intrusion, pegmatite and aplite development	Older Granite Magmatism
650 - 850Ma	(Main Phase)	Orogenesis: deformation, metamorphism, migmatization and reactivation of pre-existing rocks	
800 - 1000Ma	Katangan	Geosynclinal deposition, intrusion of hypersthene-bearing rocks	Katangan metasediments
1900 ± 250Ma	Eburnean	Granite intrusion Orogenesis: folding, metamorphism and reactivation of pre-existing rocks	Eburnean Granites
2500Ma	Birimian	Geosynclinal deposition	Birimian metasediments
2800 ± 200Ma?	Liberian Cycle?	Possible formation of banded gneiss complex near Ibadan (Grant, 1970)	
>2800Ma	Dahomeydan	Crystalline basement	

Source: McCurry, 1989 (Modified)

2.1.6 Other Rock Types

2.1.6.1 Pegmatites

Pegmatites in Southwestern Nigeria are typically extremely coarse grained, show great variation in grain size and are composed of essentially microcline and quartz (Rahaman, 1989). Besides these, they may also contain small amounts of muscovite or biotite, tourmaline, occasional garnet and hornblende. Occasionally, these minerals are arranged zonally or there may be graphic intergrowth between quartz and K-feldspar in the coarse central zone of the pegmatite. They are frequently found associated with the Older Granites and gneisses. They range from veinlets a few millimeters wide to bodies a few kilometers thick. According to Rahaman (1989), they are obviously absent from the main areas of the slightly migmatized to unmigmatized parashists and meta-igneous rocks except at the margins of the belts containing these rocks with the gneissic basement. In the gneisses, these pegmatites may be conformable to foliation but are generally known to cross-cut, but in the Older Granites, they habitually cross-cut. The concordant pegmatites in the gneisses usually have very irregular form and have quartz at their centers bounded by feldspars at their peripheries. The largest pegmatite body is known to be 4km long and 2km wide.

2.1.6.2 Quartz and Quartzo-Feldspathic Veins

These are veins (1cm – 20cm across), composed essentially of quartz and/or feldspars (Obiora and Umeji, 2004). Quartz veins and lenses can be found in all of the Basement Complex's major rock types. They cross-cut (discordant) as well as follow (concordant) the trends of foliation in the rocks in which they are found. The concordant ones are usually thought to have been involved in the tectonism affecting their hosts while the discordant ones have been known to be structureless. In some cases, they vary in thickness from a few millimeters to about a meter and show great irregularities in their form (thin out at some point or begin to widen). Plates of muscovite and biotite may be found associated with large quartz veins. They are generally younger than the Basement Complex rocks within which they are emplaced along weak planes or fractures.

2.1.6.3 Dolerite Dykes

These are considered to be the youngest members of the Basement Complex (Rahaman, 1988). Grant (1970) obtained a whole rock K–Ar age which is $478 \pm 19\text{Ma}$ on an unmetamorphosed dolerite dyke from Ibadan. Dolerite dykes are widespread in the Southwestern Basement Complex and occur in association with the gneisses and Older Granites. They trend in an essentially NE–SW and ENE–WSW direction (Rahaman, 1973). They occur as tabular, unmetamorphosed bodies that crosscut the foliation of their host rocks and can be as little as a few millimeters to as large as a meter. They have chilled margins and sharp contacts at points of intrusion. It has been observed in some cases that closely spaced joints, parallel to the trend of the dyke are observed in the host rock, in the immediate vicinity of the dyke. Xenoliths of the country rock have also been found in these rocks.

Dolerites in this area are generally fine grained and black in colour but in some cases, pale green spots of olivine may be observed in hand specimen. They typically exhibit a diabasic texture (intermediate) and are composed largely of augite, andesine or labradorite as plagioclase.

2.1.7 Structural Elements

The structural elements of the Southwestern Basement Complex of Nigeria include:

- a. Faults
- b. Lineations
- c. Major and Minor folds
- d. Foliations

2.1.7.1 Faults

Major faulting is not evident. Fault trends on the western side trend west of north. Post Older Granite tectonic activity is said to be responsible for the well–developed ENE–NE trends of joints and subsidiary faults (Jones and Hockey, 1964).

2.1.7.2 Lineations

Mineral lineation marked by the preferred orientation of biotite, amphibole and quartz are the most common types (Rahaman, 1989). Other types include the corrugation of

the foliation by crests and troughs of minor folds giving rise to a crenulation foliation. These two types are usually parallel to one another.

2.1.7.3 Major and Minor Folds

The fundamental structure of the western part of southwestern Nigeria is an anticlinorium with a northward plunging migmatitic core (Jones and Hockey, 1964). The initial fold is said to have been along a NW trending axis while the second folding has an axis, west of north. The axial plane trace of the early antiform was recognized by Grant (1970) while Rahaman (1973) proved that a synform plunging northwards occurs northwest of the area described by Grant (1970) at Iseyin. This structure is outlined by the complex outcrop pattern of quartzites to the east of Iseyin town. At the Effon Psammite Formation, a complex pattern of tight to isoclinal refolded folds with the axial traces of the late folds trending in the NNE–SSW direction occur. Minor folds are very common features found in the gneisses and schists. They are of two main sets with differing styles in the Iseyin area.

The first sets are similar folds that are tight to isoclinal with small dihedral angles, limbs that dip in the same direction, a strike of the axial plane that is normal to the trend of the fold axes and a dip of axial plane always less than 20° (Fleuty, 1964). The second sets of folds contrast sharply to the first sets in the attitude of their axial planes. Folds of the second set vary from open to isoclinal and are usually more common than the first set of folds. Over most of the southwestern region, these folds plunge to the north and rarely exceed 25° although steeper plunges may be observed in some areas.

2.1.7.4 Foliations

Foliation in rocks of this complex, are frequently parallel to color banding and only one foliation is dominant. Most of the western region has a regional strike of foliation roughly constant in a N–S direction, with variation between the NW–SE and NE–SW directions. In the gneisses, the most conspicuous surface is marked by parallel layers consisting of alternating light and dark minerals. In the quartzites, quartzitic component bands can be peeled off along micaceous laminae parallel to lithologic banding. In amphibolites, a fine differentiation lamination defines the foliation and the amphiboles are aligned parallel. Foliations in these rocks are of tectonic origin and this is confirmed by the presence of small, tight to isoclinal folds on the straight limbs of the folds, crescent-shaped attenuated closures and rootless folds which represent relicts

of earlier folds whose limbs have been sheared, and the fact that large scale lithologic banding and foliation are almost but not simultaneous. Foliation generally in this part of the Basement Complex is parallel to the limbs of major folds.

2.1.8 Metamorphism

Mineral assemblages correspond to the amphibolite facies grade of metamorphism and this metamorphic activity can be compared to the Older Granite (Pan–African) activity (Jones and Hockey, 1964). Rahaman (1973) deduced that in this area, regional metamorphism reached green schist to amphibolite facies with the metamorphic grade decreasing rapidly from the amphibolite facies in the southeast to the green schist facies in the northwest. A zonation of metamorphic index minerals and Barrovian type of metamorphism was observed in places such as Aiyetoro. Quartzites are thought to be associated with a metasomatic phase of metamorphism involving water, fluorine and boron and not relict from an earlier high-grade metamorphism (Rahaman, 1973).

2.2 Carbonates in Nigeria

Carbonate sediments and rocks are rocks that contain over half carbonate minerals, these minerals are composed of CO_3^{2-} and one or more cations. The most widely recognized carbonate mineral is calcite (CaCO_3), which is the foremost part of limestones and marble. Carbonate sediments are discovered today in numerous marine and some earthbound settings however the site of their most noteworthy wealth is on the floor of shallow tropical oceans (Scoffin, 1986). The formation of Carbonates is usually by precipitation from carbonate-saturated water by biochemical or chemical processes and accumulate in a variety of ways. For instance, as pre-existing rocks or skeletal remains, inorganic growths that nucleate on fine mobile debris in shallow seas, as crusts within arid soils, and laminated precipitates on the walls of limestone caves or on the ground around hot springs (Scoffin, 1986). Sedimentary rocks while forming take a very long deposition period of time, as the sediment cement and compact into hard beds or strata.

Akinniyi and Ola (2016), stated that Nigeria is endowed with large deposits of limestone and marble situated in all parts of the nation. The Basement Complex, Younger Granites, and Sedimentary Basins are the three basic litho-petrological components of Nigerian geology. The Migmatite-Gneiss Complex, the Schist Belts, and the Older Granites are all part of the Precambrian Basement Complex. Several

Jurassic magmatic ring complexes make up the Younger Granites. They differ from the Older Granites in terms of structure and petrology. The Niger Delta, the Benue Trough, the Chad Basin, the Sokoto Basin, the Mid-Niger (Bida/Nupe) Basin, and the Dahomey Basin are the Sedimentary Basins, which include sediment fill from the Cretaceous to Tertiary ages (Fatoye and Gideon, 2013). Limestone and marble can be found in both Basement rocks and Sedimentary Basins throughout Nigeria (Figure 2.2). The country's cement plants are situated near suitable limestone or marble deposits quarries. On the basis of geological age, Nigerian limestone, marble, and dolomite can be divided into three categories: Precambrian marble, Cretaceous limestone, and Tertiary limestone (Fatoye and Gideon, 2013). The schist belts of the western part of Nigeria west of longitude 8°E contain Precambrian limestone that has been re-crystallized to create marble. When they are relatively pure, they are white and grayish. Mica, calcilicates, and small inclusions of gneiss, pegmatite, and quartz, as well as reaction products, are found in varying proportions. The wide range of applications of marble and associated lime-rich rocks, particularly in construction, as well as recent increases in urban development and new opportunities in solid minerals development, have prompted both local and foreign entrepreneurs to express an interest in exploitation of marble deposits in Nigeria which shows the importance of Nigeria's marble deposits because of their suitable physical and chemical characteristics (Okunlola *et al.*, 2015). The Okpella deposit in Edo State is currently used for the manufacture of cement and calcium carbonate by BUA group in the area of Okpella, Edo state, which is the study area in this project.

2.3 Mining Techniques

Mining is an engineering discipline that involves the practice, the theory, the science, the technology, and application of extracting and processing minerals from a naturally occurring environment (Mallo, 2012). Mining can be said the second of mankind's earliest activities after agriculture that was the first. The two activities rank together as the major or elementary industries of the early civilization. Little practices have changed in the significance and importance of these industries since the beginning of civilization. Considering fishing and lumbering as part of agriculture and oil and gas production as part of mining, will definitely continue making agriculture and mining to supply all of modern civilization's fundamental resources (Hartman and Mutmanky, 2002). Construction materials are part of the mining resources supplied to the use of

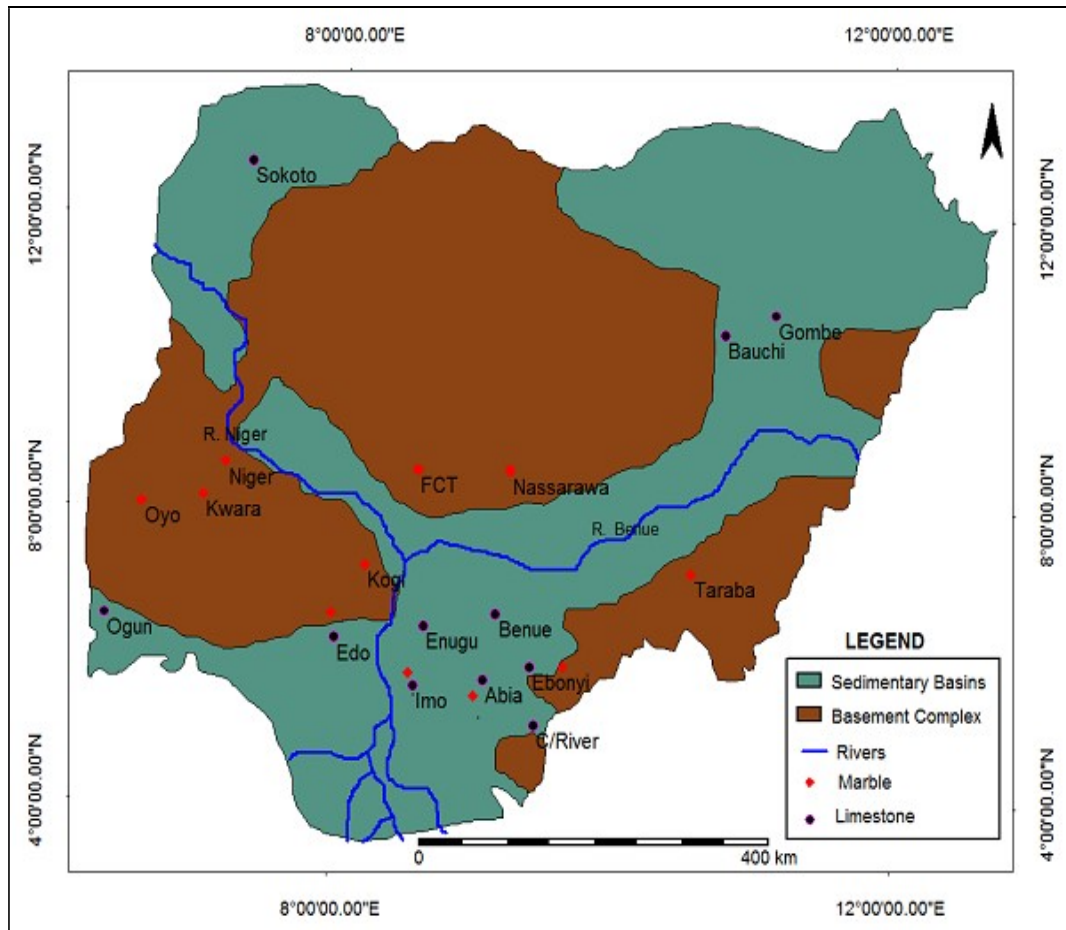


Figure 2.2: Geological Map of Nigeria Showing Limestone and Marble Occurrences (After Fatoye and Gideon, 2013)

modern civilization and because of the daily growth of the world and its expansion there is a need to optimize and enhance construction materials production. To accomplish this purpose, mining processes need to be developed that include the optimized design of slopes, which is the aim of this research. In mining, the extraction of minerals from the earth is to construct an excavation or an opening to gain access from the surface to the mineral deposit. The particular details of the technique, design, equipment, and method used to extract the minerals are usually determined by the geologic, physical, environmental, economic, and legal conditions that prevail (Hartman and Britton, 1992). The basic aim of selecting and implementing a specific mine plan should always be to mine a mineral deposit with a maximum profit depending on the uniqueness of the deposit in terms of its characteristics, location, current market prices for the mined mineral, safety implementation, and environment. Depending on these characteristics the mining method is chosen, such as surface mining, or underground mining methods.

2.3.1 Surface Mining

Surface mining is a word that refers to methods for extracting ore minerals from the surface, which typically entails removing the top soil and rock covering the deposit in order to gain access to the ore minerals (Opafunso, 2011). The practice of surface mining involves a number of complex operations including: site preparation (overburden drilling, blasting, loading and hauling), deposit exploitation (drilling, blasting, loading and hauling of the ore) and finally site reclamation. Surface mining methods are generally classified as open-pit mining, which includes quarrying, strip mining, contour mining, and dredging (National Research Council, 2002). Open-pit mining is the most commonly used method worldwide, where the waste is sent to a disposal site, while the ore is taken to a processing site. According to Ericsson (2012), open-pit mining contributes for roughly 83% of global metal ore production, while underground operations account for the remaining 17%. The choice of method is affected by the topography and physical characteristics of the deposit. Open-pit mining method uses a sequence of benches from the surface to the deposit, which is similar in quarrying with few differences in type of minerals in quarrying which is aggregates and dimension stone, and in the number of benches which is fewer in quarrying, and that most of the material extracted in quarrying is marketable unlike in open-pit mining (National Research Council, 2002). Surface mining necessitates a significant capital

investment, but it typically yields great production, cheap operating costs, and favourable safety conditions (Hartman and Mutmansky, 2002).

2.3.2 Underground Mining

Underground mining method is used when the deposit is too deep and the surface mining is not applicable (Hustrulid, 1982). Underground mining is complex because it requires shaft sinking for the transportation of people, equipment and material (Quadrat-Ullah and Panthallor 2020). The deposit is accessed from the surface through vertical shafts, horizontal adits, or inclines. In underground mines, deposits are designed and developed by cross-crossing openings called levels or cross-cuts, which are used to create blocks of ore to be extracted and to provide access for workers and equipment, the transportation of ore and waste, and adequate ventilation. The basic mining operations (drilling, blasting, loading, and transporting of ore) in active working zones (faces) are carried out according to a mining plan. In hard rock mines these activities are carried out carefully, drilling into the ore and blasting with dynamite or ammonium-nitrate explosives and transporting to the surface. In exceptional cases Opafunso and Ozigis (2008), opined that very efficient use of explosive energy is required to cut the rock according to design to prevent cracks or back break. However, if the deposit is soft, such as coal, potash, or salt, mechanical methods can be used to cut and load it, eliminating the need for drilling and blasting. There are various types of underground mining methods, including unsupported, supported, and caving methods. The most common unsupported methods are open stopes, room-and-pillar, and sublevel stopping; the most common supported underground mining method is cut-and-fill stopping, where the fill is often waste from the mine and mill tailings. Open stopping with caving techniques is employed wherever possible due to the significant expenses associated with supported and unsupported mining processes (National Research Council, 2002).

2.4 Open Pit Slope Geometry

Designing an open pit slope means determining the slope geometry which is mainly benches, inter-ramps and overall slope angles. The smallest unit of a slope are benches, which are separated by catch benches, these catch benches or widths are constructed to catch falling rocks from upper levels. Generally, is common to use double benching (the catch bench is left only every second bench), as it allows more catching capacity

(Hustrulid and Kuchta, 1995). The open pit slope design should determine the bench face angle. The second unit of an open pit mine is the inter-ramp slope, which can be defined as the slope between ramps, which is constituted of the benches between ramps. The inter-ramp angle is the line linking bench toe to bench toe (Sjöberg, 1999). The open pit design should determine the inter-ramp slope angle which depends upon the bench face angle and also its height and width. The last and the one contains all pit components, the overall pit slope, which considers all ramps and inter-ramps. Its design is to define the overall slope angle, which is measured from toe at the pit bottom to its crest (Figure 2.3).

The three slope units should be designed separately. And their design may vary in the same mine depending on different regions or sectors in the pit. Requiring different slope angles in different sectors. Common in the majority of existing design methods is the concept of design sector in open pit mines. A design sector is a region in the open pit mine that has similar geotechnical parameters that influence slope stability and are different from parameters in other regions in the same pit. These parameters comprise mainly lithology, discontinuities and rock mass properties.

2.5 Open Pit Slope Design and Stability

According to Hartman and Britton (1992), open pit mining is the excavation of near surface ore deposits, via horizontal benches to extract the ore. But the establishment of benches or slopes raises the issue of stability which is crucial in open pit mines because it can lead to safety problems. Opafunso (2002a), noted that much emphasis is placed on the subject of pit design due to the dire consequences of slope failure in surface mines. Hence, the need for design optimum overall slope angle that ensures minimizing the amount of stripped waste to lower production costs under safe conditions. Read and Ogden (2006), stated that slope design is a basic section of open pit planning and needs a suitable understanding of rock mass characteristics and the type of discontinuities that are dominant in the deposit. The slope design process in large open pit mines, has been limited in the past by critical gaps in our knowledge and understanding of rock masses particularly the relationships between the strength and deformability and the likely mechanism of failure. This gap can only be bridged through research on the rock masses and their mechanisms of failure. This will

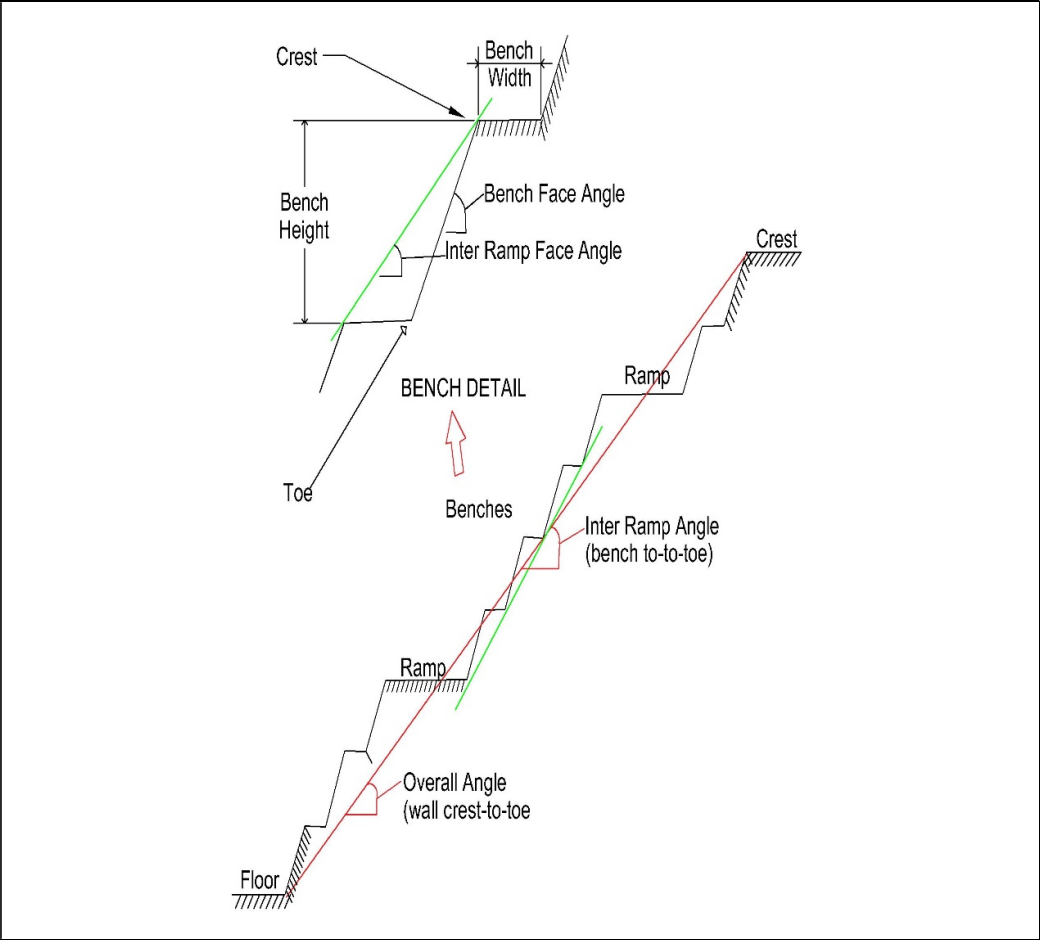


Figure 2.3: Open Pit Wall Terminology (Modified After Read and Stacey, 2009)

enhance the human performance on slope design in mining as envisaged by the focus of this study. Read and Stacey (2009) stated that the purpose of an open pit mine design is to achieve an optimum excavation in the frame of safety, ore recovery and economic profit. The walls established by the slope design are expected to be stable during the life of the open pit, and are likely to last longer than the closure. At the very least, any potential instability should be controllable. This is true at all scales of the walls, from individual benches to overall slopes. Safety and economic benefits are required in any study on open pit slope design, in order to meet the goal of maximum gain from mineral extraction, and this is the primary need for the Okpella slope design. The design of slope for Okpella quarry should ensure safety, which requires a flat slope. However, a flat slope generally means more waste excavation, which will increase the excavation cost. So, the achievement of an appropriate open pit slope design requires slope flat enough to ensure safety and at the same time, it must be steep enough to minimize the cost of excavation. For example, Adebimpe and Akande (2014), reported that safety and cost aspects to minimize waste excavation are substantial for an appropriate open pit slope design. Mine or civil engineering operations in mine and quarry slopes that can reach hundreds of meters deep must be classified as "geotechnical operations". Keeping in mind that their design and implementation must adhere to general practice guidelines, with the overall goal of ensuring the structure's safety while minimizing the volume of material to be excavated and, as a result, the project's final cost (Fleurisson, 2012). Mining and civil engineering designs are generally geotechnical works but when they reach a depth of a hundred meters, they become very critical and even dangerous. This level of danger is what we want to avoid at BUA Ikpobia quarry at the Okpella site. Currently the non-designed slope poses a significant risk, with less probability of economic benefit as it gets deeper if further excavation is accomplished without optimized design.

The general objective of hard-rock pit slope design is the determination of the steepest applicable slope angles for the open pit mine, therefore the extraction of the ore resource can be maximized by the operator. On the other hand, is the increment of possibility that slope stability problems will arise as a result of steep slopes, which may have an influence on worker safety, productivity, and, as a result, mine profitability. The strategy entails planning the pit design to attain an acceptable level of risk and combining it with stability analyses as a factor of safety (FOS) or probability

of failure (POF). If no instability arises during operations, the pit slopes are pretty conservative. During pit development, some small instability must now be monitored. (Taseko Mines Limited, 2012). That means the slope we are trying to achieve at BUA Ikpobia quarry should avoid any significant instability. Such instability is very possible if we don't study the rock mass well and define a very precise factor of safety from a very detailed stability study of the rock mass. The stability of the slope results from an appropriate slope design which must be steep and ensures safety. In addition, it was stated by Call (1972) that steepness of the pit walls is essential and sometimes a critical aspect of the design and operation of an open pit mine, in general, the steeper the pit wall the lower the stripping cost and, therefore, the greater the profitability of the mine. Consequently, slope design consists primarily of determining the maximum angle at which a pit wall stands without failure. The same idea was supported by Steffen *et al.*, (2008) where they asserted that the ideal slope design of a pit involves the determination of the most economic pit limit which normally comes in steep slope angle and as result the excavation of waste is minimized. Kennedy (1990) mentioned the importance of the stability to achieve a steep and safe slope when submitted that the wall's stability should be analysed very carefully because it needs to stay stable during the period that mining activities are in that area.

The criticality of the slope design in mines or quarries was stated by Read and Stacey (2009), when they stated that for an open pit mine, the most important challenge is the design of the slopes at every stage of planning and operation. Which shows the need to design a slope at BUA Ikpobia quarry, that requires a major knowledge of the geology, because of the usually complexity of orebodies, and of the material properties, which are often tremendously variable.

According to Read and Stacey (2009), over the past quarter of century the formulating of pit slope design has been established. Though some of the methodologies vary between practitioners, the process is still relatively standard. The process is standard to some extent—for example, for slopes, benches, and inter-ramps—but the difference in these examples is in the height and angles of the slope, bench and inter-ramp. The challenge is determining what are these parameters at the point- of stability limit. That is what the design of BUA Ikpobia quarry slope will ensure. This concept was emphasised by Mathis *et al.* (2009), when they stated that for effective excavation and economic optimization of a rock slope, it is necessary to design and evaluate catch

bench angle, inter-ramp slope angle, and overall slope angle separately and in combination.

Stacey (2006), stated that since the mid-1970's there have been important ameliorations in the tools from the technical perspective, especially analytical techniques that are available to slope designers. Also, there is an extended awareness and comprehension of a detailed geological model, with strong importance of structure and alteration for the platform for the slope designs to be formed. Nevertheless, the basic technology for the determination of the rock strength aspects has changed slightly, though an important growing experience has been used extensively and has a high level of comfort in its application for heights of up to 500 meters. Slope management is also an important aspect of the execution of slope designs, and it has been aided by ongoing advancements in slope monitoring systems. All of these efforts have resulted in the decrease of mining accidents in the last 50 years and emphasize the need to keep enhancing the understanding the technical, geological and geotechnical properties of the rock mass to achieve an appropriate slope design, to which goal this research will contribute (Breuer *et al.*, 2002). The same idea was submitted by Fleurisson (2012), when he stated that well-controlled methodology is required for the slope design in open pit mines because of the uniqueness of each rock mass characterized by its geological structures, therefore what will be achieved at BUA quarry will be truly valuable because the solution will be applicable to the site, and the method might be applicable elsewhere.

Hoek (2009), reported that good geological, geotechnical, and groundwater models, as well as an understanding of the hazards and economic consequences of slope instability, are required to assess slope stability. The design that incorporates all previous elements to produce a balanced compromise between safety in a side and operational and economic efficiency on the other side, is a good design. The formulation of a good design is not the end in itself because the stability should be maintained and controlled during the mine operation. This also was stated by Hoek (2009), that an ongoing evaluation of the stability of the slopes generated during the development of an open pit mine is required through the overall management of these slope.

Stacey (2004), submitted that design must be optimized during the development of the mine to minimize the risk which involves factors like safety, cost, productivity, water and labour, etc. and also to optimize the production and minimize the waste. There is value in designing the pit for the Ikpobia quarry so that the production can be improved and safety can be maintained and assured.

The rock-mass conditions control the slope angle, the determination of the slope angle is through a detailed rock mass investigation to design the slope. Dempers *et al.*, (2011), stated that variability in rock mass conditions can be caused by major geological structures, large fault zones, and areas of closely spaced jointing, geological structures carrying water, weak rock, intense alteration, and excessive rock bridges. Therefore, it is important to characterize all of these conditions at a site so that a good slope design can be accomplished.

Kennedy (1990), summarised the slope design when he stated that rock strength, joints, faults, presence of water, and other geologic information are important factors in the assessment of the suitable slope angle. The slope may be stated as a simple, overall average for the pit (e.g., 45°), but a more thorough investigation can indicate that the physical properties of the deposit lead the pit slope to vary depending on the rock type, sector location, elevation, or orientation within the pit. All of these items might show significant variability. A correct slope assessment will give the slopes that allow the pit walls to remain stable. To minimize the strip ratio pit walls should be set as steep as possible. The angle to be used between the roads in the pit is determined by the pit slope analysis. The overall pit slope utilised for design is required to be flatter to allow for the road system in the ultimate pit. It will be shown this project that the detailed study of the geological and geotechnical investigation lead to the slope design depending on the variability of rocks.

The importance of geological and geotechnical investigations was described in a paper that was published by Hoek (2009) except that he emphasized the importance of understanding the risks and economic consequences, and of ongoing overall management and valuation of the slopes created throughout the progress of an open pit mine. This evaluation is based on accurate geological, geotechnical, and groundwater models, as well as a comprehension of the hazards and costs associated with slope instability. The slope instability is very critical in open pit slope design and it can lead

to economic consequences, but the construction of good geological and geomechanical models can control the slope stability. Also, we can see the same concept was followed by Hustrulid *et al.*, (2001), where they concluded that the geological model is the forms of the fundamental basis for all designs and it should form the basis for all geotechnical and hydrogeological studies which are, rock mass properties, role of groundwater, impact of alteration, and in situ rock stress. The geological model in this study is the overall investigations done on the field which are referred to in this study as the geological, hydrogeological and geomechanical models.

Dunn (2014), described the geotechnical model as “the cornerstone of any underground or open pit mining geotechnical design”, and stated that it outfits the foundation for developing geotechnical domains and analysis inputs. The meaning of this is that the geotechnical model is directly associated with design assurance and reliability. The geotechnical model is also related to the project life cycle, from the study through the feasibility to implementation and operations stages. There is also a relation between the geotechnical model and the declaration of resources and reserves. All this information about the geotechnical investigation show the importance of the investigation to our research project.

In the same line with the above scholars Fillion and Hadjigeorgiou (2013), reported that geotechnical stability analysis and design need to reach to representative geological, structural and rock mass models. These models should be constantly updated during the life of the project from the visionary study through the feasibility, design and construction. It is well-known that there are issues related to data uncertainty that can have serious consequences. The consequences are the result of the instability of slopes and can be very critical if the investigation is not well done.

Dunn (2014), stated according to Read and Stacey (2009) that the geotechnical term is largely used and it can mean various things to various people, but in simple terms, the geotechnical model is a combination of the geological, structural, hydrogeological and rock mass models, and he added that typically the level of confidence of each component changes relying on the geotechnical environment and the relative importance of each component. It also must be suited for purpose in both complexity and for the project life cycle stage.

Hawley and Stewart (1987), described the geotechnical model as an engineering geology and stated that its understanding is the success of any coherent slope design program. Therefore, it is substantial to collect pertinent data and construct an engineering model of the rock-mass at an initial stage of mine development. The preliminary mining design and the rock-mass model are both based on the primary geological research, which includes geologic, topographic, and structural mapping. Also, in addition to field and laboratory investigations, detailed investigations such as geotechnical core, logging, and core orientation, detailed geologic structural mapping, hydrogeology studies, and rock mechanics are required to substantiate and refine the rock-mass model and establish the range of critical engineering geology parameters.

2.6 Rock Slope Design Methods

The main aim of design methods for rock slopes is the determination and prediction of the occurrence of failure, depending on the measure of loads acting on a slope and their comparison with the strength of the rock mass constituting the slope. Kinematic analysis, empirical design methods, limit equilibrium methods, and numerical modelling analysis are some of the methods that can be employed for slope design analyses (Sjöberg, 1999). In this research, two methods were chosen, kinematic analysis and numerical modelling, because of the limitations in empirical design method and the limit equilibrium method, they only satisfy equations of statics and they do not consider strain and displacement compatibility. This in addition to the assessment of the rock mass properties through the Hoek-Brown failure criterion which parameters are used in the numerical analysis.

2.6.1 Kinematic Analysis

Given the need to optimize resource and ensure safety, a reasonably simple approach is needed that can easily determine possible types of failures and determine whether a bench face is likely to be stable. In order to determine the possibility for planar, wedge, and toppling failures, a kinematic analysis considers the geometry of the discontinuities, the slope orientation, and the friction angle along the discontinuity surfaces. Stereographic techniques are used in these investigations. A kinematic analysis seems to meet that need for simplicity. Such an analysis does not guarantee total accuracy, but represents a significant step toward design and analysis of rock slopes. A kinematic analysis does not discount a possible need for more detailed

analyses, but it is a first step that can be followed by more analysis like numerical analysis (Senouci and Okunlola, 2019).

The need for analysis by zone is illustrated well by Figure 2.4 from Wyllie and Mah (2004). The fictitious pit has a reasonably constant joint set. Depending upon the bench orientation and the slope angle of the face, different failure modes may be likely, or the bench may be stable.

Using equal area stereographic projection of planes and their normal lines or poles, and projecting a cone representing a friction angle, one can easily assess possible failure modes or stability.

For example, in Figure 2.5, the orientation of a bench with discontinuities in (a) is projected onto the stereonet in (b) along with the daylight envelopes for planar failure and wedge failure. Planar envelope is restricted by about 20° from either side of the bench pole direction. Wedge failures are possible with the poles of two joints fall within the wedge daylight envelope. Similarly, toppling failure may occur when the pole of a joint lies within the toppling envelope. The friction cone is plotted over the top of these envelopes, further restricting the envelopes, as shown in Figure 2.6 (Senouci and Okunlola, 2019).

2.6.2 Assessment of Rock Mass Properties

The most significant input parameter to any analysis of slope stability and design is the rock mass strength. Valerio *et al.*, (2017) stated that the design of the pit slope is dependent on the proper selection of design strength parameters. The larger volume of rock mass makes its parameters difficult to be assessed. For a safe, realistic and sound analysis of an engineering project, geotechnical design necessitates numerical estimation of a series of geotechnical properties and parameters of the geomaterials (Marinos, 2019). Geological data acquisition or estimation of rock mass properties can be achieved by implementing one or more of the following methods: a) laboratory testing, b) in situ testing, c) use of rock mass classifications (GSI, RMR, Q), and d) back analysis (Marinos, 2019, Marinos and Carter, 2018). The laboratory tests on core samples cannot be representative of a rock mass which makes the problem of rock mass properties determination especially the rock mass strength one of the greater challenges in rock mechanics. Currently, the most accepted approach to this problem is

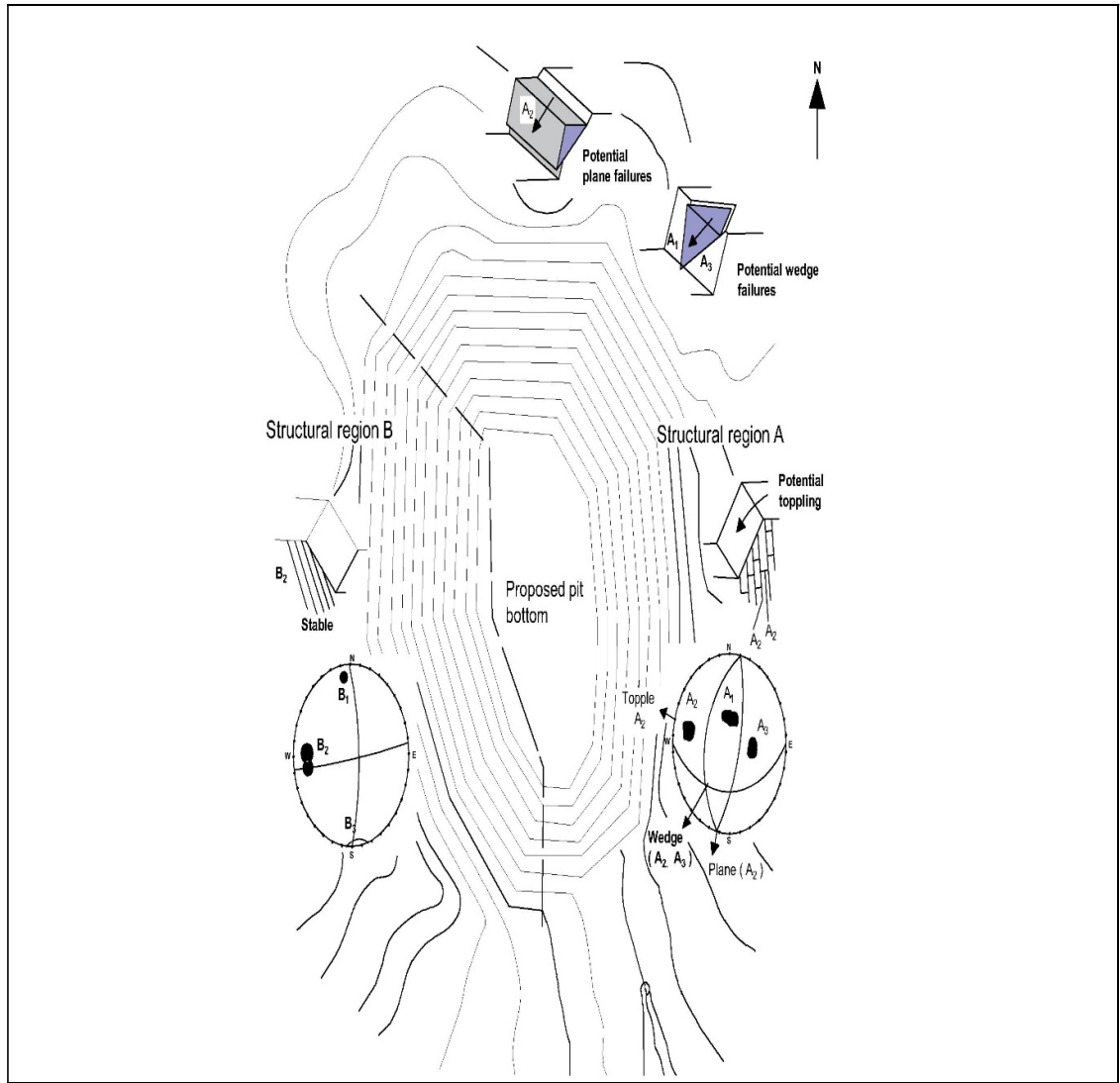


Figure 2.4: Joint Sets May Be Stable or Present Various Types of Failure Modes at Different Locations in a Pit. Modified After Wyllie and Mah (2004)

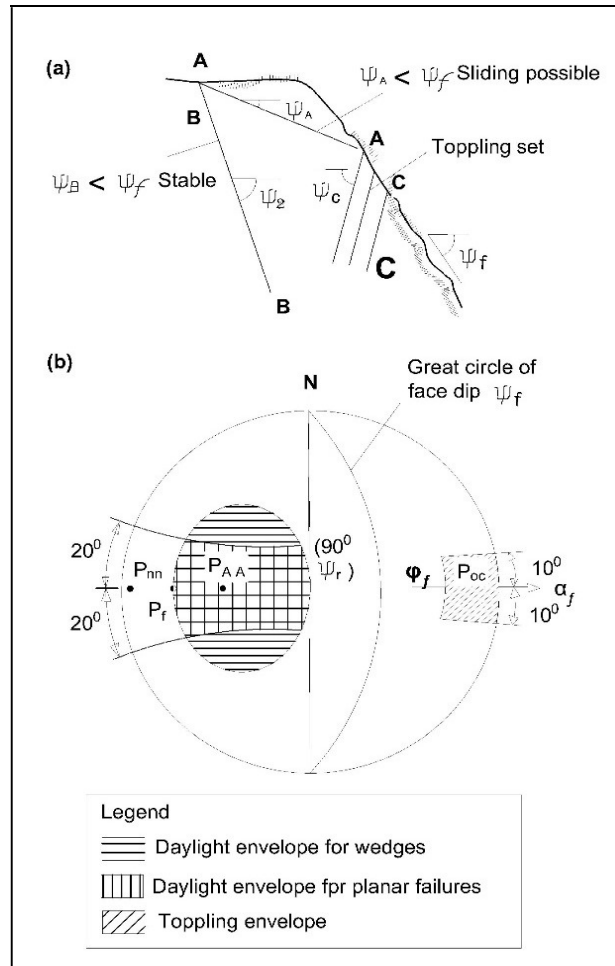


Figure 2.5: Kinematic Analysis of Blocks of Rock in Slope. (a) Discontinuity Sets in Slope; and (b) Daylight Envelopes on Equal Area Stereonet. Modified After Wyllie and Mah (2004)

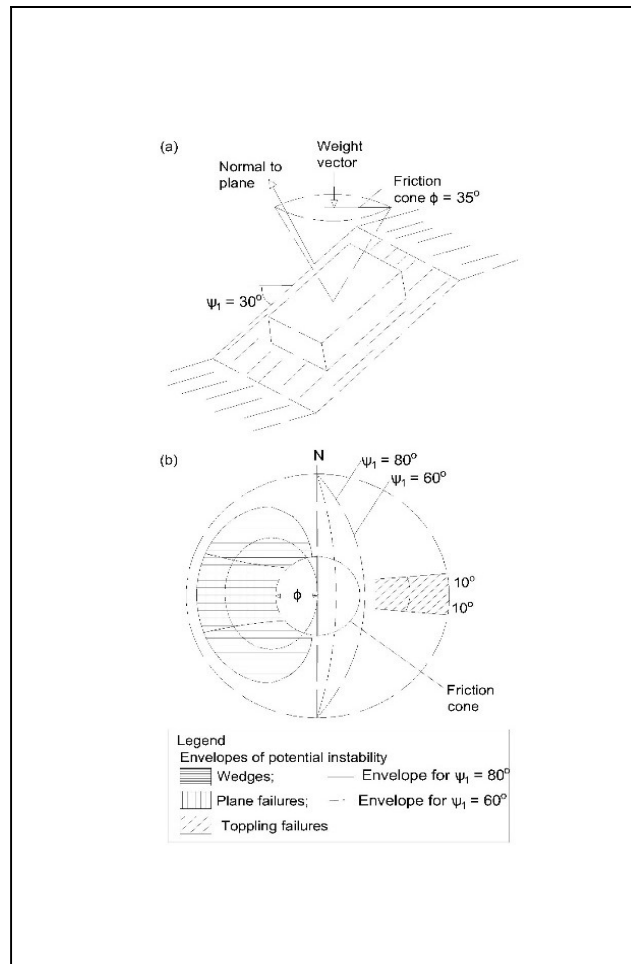


Figure 2.6: Combined Kinematic and Simple Stability Analysis Using Friction Cone Concept. Modified After Wyllie and Mah (2004)

the estimation of rock mass parameters using the Hoek-Brown failure criterion that uses the rock mass classification tool Geological Strength Index GSI (Sjöberg, 1997). Hoek and Brown (2019) stated that Griffith's (1924) brittle fracture theory, which was modified by McClintock and Walsh (1962) to account for friction on sliding surfaces, was the basis for Hoek and Brown's (1980) nonlinear failure criterion for intact rock, which was also derived from Hoek's (1965) brittle failure research and Brown's model studies of jointed rock mass behaviour (1970). The Hoek-Brown failure criterion determines the rock mass properties which represent the rock mass behaviour by means of both laboratory tests and geotechnical field survey.

The criterion has been updated many times since 1980 (Hoek *et al.* 1992, 2002) but the empirical parameters of the criterion were always linked to the Bieniawski's Rock Mass Rating (RMR) classification system (Bieniawski, 1976). In the 2002 version Hoek *et al.* (2002) introduced new classification system called Geological Strength Index (GSI) that was related to the empirical parameters of the Hoek-Brown criterion.

2.6.3 Numerical Modelling

Numerical modelling is capable to solve the equilibrium equations, strain compatibility equations and the constitutive equations for a material for described boundary conditions. Numerical modelling has main benefits that can be summarized as follow:

a) The stress and the displacements can be calculated b) Different constitutive relations can be employed (Sjöberg, 1999). Jing (2003) provided an inclusive review of the numerical techniques utilised in modelling in rock mechanics. This divides numerical methods to two classes as follow:

1. Boundary methods. Which entails dividing the excavation's boundaries into elements and representing the interior of the rock mass as an infinite mathematical continuum; and
2. Domain methods. Where the interior of the rock mass is divided into elements with specific material properties, and these elements are integrated to model the rock mass's overall behaviour. This method includes finite element, finite difference, and distinct element methods.

The conceptualization of the rock mass in a model is one of the most important tasks of numerical modelling, and there are two types of numerical models used: continuous and discontinuous.

The continuum methods (Boundary Element Methods, Finite Element Methods (FEM), Finite Difference Methods), and discontinuum method (Discrete Element Method). In boundary element methods, just the boundaries of a problem need to be discretized into elements. In the other hand, the finite element and finite difference methods, the whole problem domain must be discretized into elements. While in the discrete element method discontinuities that are existing in the rock mass are modelled explicitly (Sjöberg, 1999). The selection of either of the methods is done based on the scale of the problem. Nevertheless, it is known that the rock behaves both as a continuum and discontinuum and both methods can complement each other. The difference can be in the selection of material properties, where the discontinuum selects easily material properties from laboratory tests, and the continuum model requires representative properties of the rock mass as whole (Stewart, 2007). The Finite Element Method is a general drive that can be used to calculate different engineering interests which include, according to Liu and Quek (2014), the simulation and calculation of stresses, pore pressure, and displacement of rocks. And it can also assess the slope stability by driving factor of safety from the use of Strength Reduction Method (SRM) based on Finite Element Method (Lane and Griffiths, 2000). This research project focuses on the slope stability analysis to determine the failure within the rock mass of the Okpella quarry. This aim can be achieved by using FEM to investigate the slope stability based on the Hoek-Brown failure criterion to calculate the factor of safety and display the potential failure mechanisms. The commercial finite element computer program, Rocscience Phase 2, 7.0 program (Rocscience, 2009a) is used in this research study.

2.6.3.1 Finite Element Method of Analysis

Finite element technique is a numerical method belonging together with the finite difference technique to the domain discretization numerical methods (Hoek, 2010), also called stress deformation methods (Chowdhury *et al.*, 2009) or continuum methods (Eberhardt and Wallmersperger, 2015). Historical records credit the first implementation of this method for slope stability solutions to Zienkiewicz in 2000

(Zheng *et al.*, 2009, Griffith and Lane, 1999). Hoek and Brown (1997) mentioned that both are essentially the same technique that treats rock mass as a continuum and even go further to discuss them in the same light. It has been argued by Eberhardt (2003) that finite element method is more suitable for solving complex geometries because of its holistic approach unlike the finite difference method that solves stiffness equation of individual element, an approach he says may result in problematic approximation between grid points.

2.6.3.1.1 Basic Mechanics of Finite Element Analysis

Two-dimensional analysis generally uses the plain strain assumption in which stresses and their resultant strains and displacements act only in x and/or y directions. The plane strain assumption is particularly valid for slopes whose third dimension, i.e. z, is very long and an infinite extent assumption in that direction is valid. The first step in the analysis is the discretization and meshing of the rock mass and selection of element type. This usually follows after delineation and the slope boundary definition. It involves dividing the soil mass internally into finite smaller elements that are separated at the edges but connected at their nodes (Chowdury *et al.*, 2009). Triangular elements are preferred because they allow a perfect discretization of an irregularly shaped body and the ensuing global stiffness equations are relatively simple (Hoek and Bray 1981, Chowdury *et al.*, 2009). Linear Strain Triangles (LST) or six-noded triangles are generally more recommendable than Constant Strain Triangles (CST) or 3-noded triangles (Figure 2.7). The results obtained by Rocscience (2014) give credibility to this claim. In that study, the results for both CST and LST were compared with the results of bishop LE and Griffiths FE methods and it was found that LST gives closer result than CST. This is so because some rock masses are highly nonlinear in behavior and the corresponding LST displacement function is nonlinear (quadratic). Furthermore, Rocscience (2009), recommends the use of 1500 elements for simple geometries and up to 3500 elements for complex ones. Choosing a large number of elements to mesh the soil slope is known as finer-mesh generation.

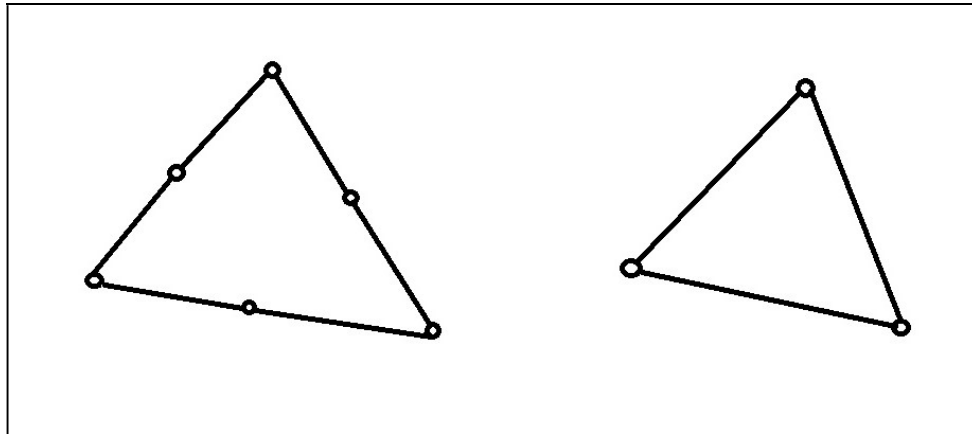


Figure 2.7: 6-nodded and 3-nodded Triangles Respectively (Rocscience, 2009b).

2.6.3.1.2 Techniques of Determining Factor of Safety in Finite Element

In determining the Factor of Safety (FOS) of finite element analysis, two methods are commonly used which are shear strength reduction (SRF) method that is the most widely applied FEM computational scheme in slope stability calculations, and the gravity increase (GI) method (Sternik, 2013). GI method fixes strength parameters but varies gravity while SRF method varies strength parameters but fixes gravity. The former method is limited in its application and therefore may not be applied unconditionally. Sternik (2013) computed FOS results with both methods and found that the GI method is less accurate. SRF is equivalent to limit equilibrium factor of safety FOS. Many researchers have proposed different critical factor of safety. However, the most recommended value of factor of safety is 1.3. Wesseloo *et al.*, (2009), suggested a critical factor of safety that ranges between 1.2 and 1.3.

2.7 Existing Open Pit Slope Designs

Every mine in the world should have a special design that fits the different properties of the rock mass and different conditions at the mine site. Some examples of present open pit designs are given bellow:

2.7.1 The Aitik Copper Mine in Sweden

The Aitik Mine is an open pit mine located about 60 km north Arctic Circle in northern Sweden, at $67^{\circ} 07' N$ and $21^{\circ} E$. The mine is under operation of the mining company Boliden Ltd. The current mine design (Figure 2.8) is focused on the probability of

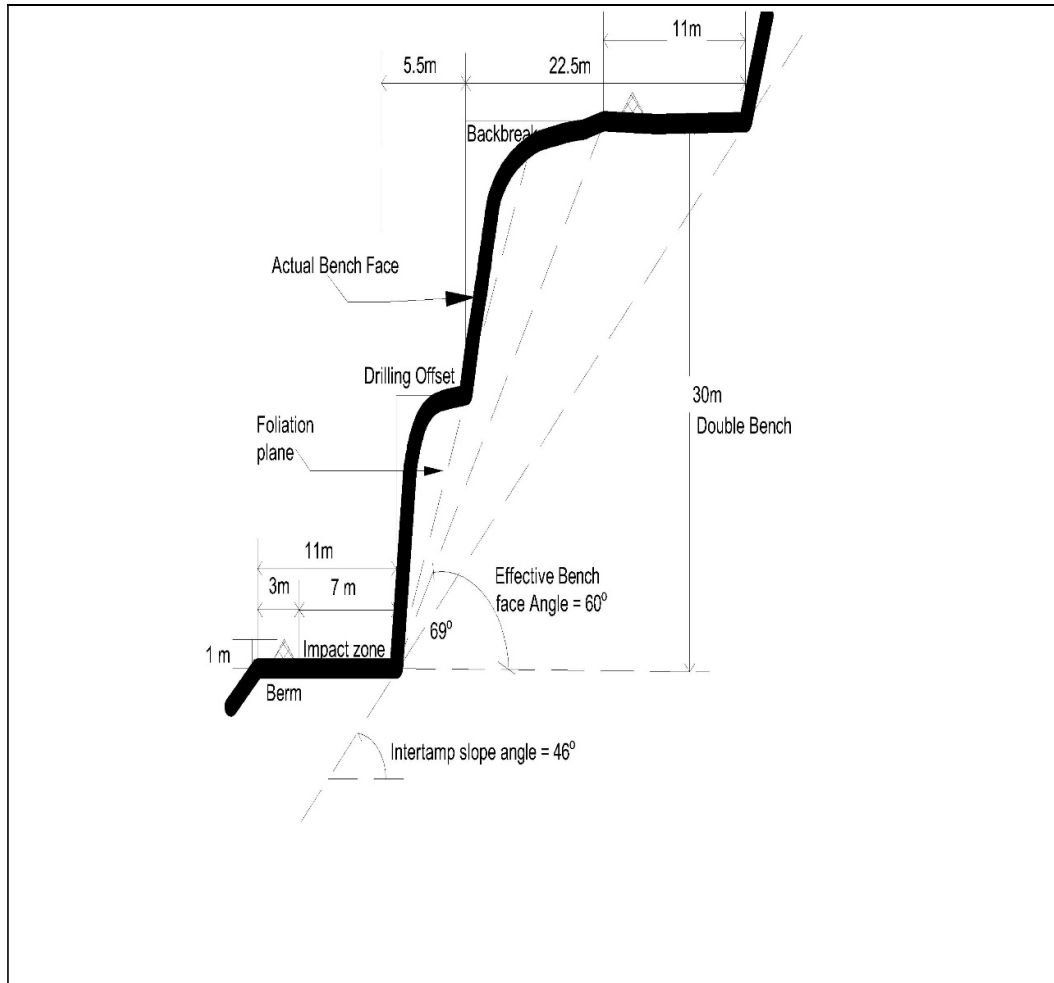


Figure 2.8: Recommended Catch Bench (after Call *et al*, 1976; West *et al*, 1985) and Currently Used Bench Geometry for the Northern Footwall of Aitik Mine (After Sjöberg, 1999)

small-scale failures. This design was proposed by Call *et al.* (1976, 1977) and West *et al.* (1985) in their studies. The studies recommended the use of double bench configuration for the inter-ramp angles. They recommended also 15-meter height for bench, with an offset drilling of 5.5 meters between each single bench. It was based on a foliation dip angle of 69° in the north and middle footwall. And a catchment area left for each double bench. With a bench face angle of at least 60° and an inter-ramp slope angle of 46° (Sjöberg, 1999).

2.7.2 The Escondida Mine in Chile

The Escondida Mine was discovered 1981, and it is the world largest copper mine. It is located in the second region of Chile, 160 km southeast of the Antofagasta city, at an elevation of 3100 m above sea level.

It was known that the rock masses at Escondida had a kind of medium-to-low competence, that the structural condition of the ore body was very complex, and that there was a natural water below the ground surface. The mine was designed with a single inter-ramp angle of 40° for the entire pit, with a mining plan based on 15 m height benches (Valdivia and Lorig, 2000).

2.7.3 The Palabora Mine in South Africa

The Palabora copper mine is located in northern South Africa near the town of Phalaborwa. Operational mining at Palabora began 1964, and production started 1966. The current design was implemented 1980, it recommended overall slope angle 45° to 50° , and 30.5 m height double benches in all areas, except in the weathered MPY and glimmerite unites where single (15.2 m or 12.2 m high) benches, and about 80° bench face angle, the slope interramp angles implemented were of 37° to 40° (Stewart *et al.*, 2000).

2.7.4 The Aznalcollar Mine in Spain

The Aznalcollar open pit mine is located in southern Spain, to the northwest of Seville city. The pit measured at the end of mining about 1300 by 700 meters with a depth of 270 meters. The overall slope angles range from 30° to 38° . Despite the slope height which is relatively moderate with flat angles, the mine had suffered numerous large-scale failures of the footwall slopes, which occurred in 1983, 1987, 1988, 1989, and 1992 (Sjöberg, 1997). Sjöberg *et al.* (2001) recommended the following slope design for the mine (Table 2.2).

Table 2.2: Aznalcollar Slope Design (Source: Sjöberg *et al.*, 2001)

Slope	Max. Slope Angles	Slope Height Range
South Lode, Rio Tinto	32°-34°	70-140 m
Aznalcollar, Central Zone	32°-34°	150-220 m
Aznalcollar, Eastern Zone	35°-36°	240- 270 m

they also submitted that predicting safe angles for the Aznalcollar slopes on the ongoing deformations is extremely difficult.

2.8 Recorded Accidents Caused by Slope Failure in Open Pit Mines

Mining industry produce billions of tons of products that worth trillions of dollars and employs millions of people all around the world every year but the same industry is the cause that thousands of people to loose their lives or get injured throughout the world (Dhillon, 2010). Mallo and Yarekes (2012), stated that when soil is loaded, it distorts just like any other engineered material and the structure falls as a result of this distortion and the structure's eventual collapse could result in massive losses in terms of both economic value and human lives, which is exactly the case in manes. Mining companies loose billions of dollars as economic impact of occupational injuries and much more than that as equipment and time west because of mining accidents generally.

Mining accidents have various causes including dust explosions, leaks poisonous or explosive natural gases, mechanical errors from malfunctioning mining equipment, flooding or collapsing (Terazawa *et al.*, 1985, Kucuker, 2006). One of the leading causes of fatalities at the United States surface mining operations is the slope stability accidents, between 1995 and 2000, 33 miners lost their lives as a result of surface ground control accidents (Girard and McHugh, 2000). Many accidents have occurred all around the world that were caused by slope failures, following are some examples:

2.8.1 The Bingham Canyon Mine Slope Failure in 2013

The Bingham Canyon Mine is the world largest man-made excavation at more than 970 m deep and 4 km wide (Pankow *et al.*, 2014). The mine is located 30 km south-west of Salt Lake City, Utah, USA. On April 10, 2013 pit wall slides occurred along a geotechnical fault on the north-east wall of the mine (Figure 2.9) (Llano-Serna *et al.*, 2016). Pankow *et al.* (2014) submitted that local news agencies reported that the initial cost estimates related to the Bingham slope failure approaches one billion dollars which makes it the most expensive landslide in U.S history.

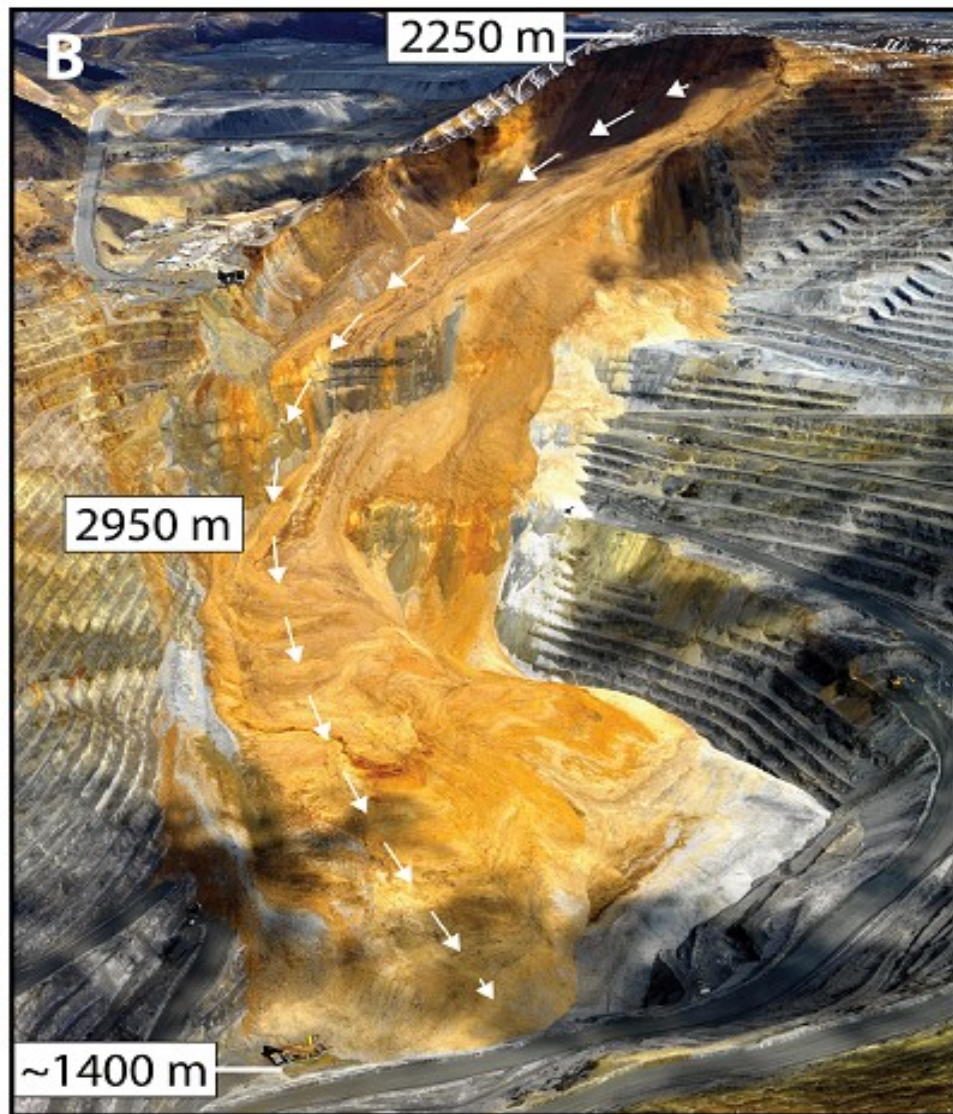


Figure 2.9: Photo of the 10 April 2013 Bingham Slope Failure (Copyright Kennecott Utah Copper, After Pankow *et al.*, 2014)

2.8.2 Slopes Failures at Pikeview Quarry in 2008 and 2009

The Pikeview Quarry is an aggregate quarry located northwest of Colorado Spring in El Paso County, CO, USA. A large slope failure occurred on December 2, 2008, which stopped the activities at the quarry. A second slope failure occurred on September 13, 2009 which was located immediately adjacent to the initial 2008 failure (Figure 2.10). The 2008 failure involved an area of 3.6 to 4 ha and 1.15 million to 1.22 million m³ of material which is big economic lost (Varnier *et al.*, 2018).



Figure 2.10: Photo of the 2008 and 2009 Slope Failures at Pikeview Quarry (After Varnier *et al.*, 2018)

2.8.3 Slope Failure at Dorli Opencast project I in 2014

The Dorli Opencast project-I is operated by M/s Singareni Collieries Company Limited and is located in North western extremity of Gadavari valley coalfield, India. A large slope failure occurred on October 13, 2014, and its result was the collapse of all the seven benches consisting of soil and clay from the surface to a depth of 50m (Figure 2.11). After the collapse, the monitoring station got disturbed. When investigation was conducted on slope profile and based on previous experiences of slope failures, it was found that the major influencing factors for the cause of the failure of this pit slope were: slope angle, groundwater, weak strata and rainfall (Satyanarayana and Sinha, 2018).

2.8.4 Some Accidents Associated to Mine Failures in Jos, Nigeria

Some accidents recorded in Jos, north Nigeria, were associated to abandoned mine ponds and spoils. Mallo and Wazoh (2014), defined mining ponds as large pits with varied depths that have been filled with water as a result of earth excavation during mining, and defined mine spoils as piles of "waste" rocks and soils that remain after mines have been excavated, and overlying vegetations, soils, and rocks are stripped away throughout the mining operation to allow for the recovery of the ore. Both mine ponds and spoils can cause a good number of accidents and threats to human and cattle lives. These ponds and spoils have become a major source of concern for both the government and the general population. Table 2.3 gives some data rescue operations in mine ponds from 1980 to 1993 (Mallo and Wazoh, 2014). The number of deaths caused by mine ponds (106) during 14 successive years is alarming and calls for special attention to mining sector in Nigeria.

2.8.5 Landslides and Slope Failures in Nanka Area South-eastern Nigeria

Slopes in Nanka frequently fail after short or lengthy periods of heavy rain, especially towards the start of the rainy season. High pore water pressures caused by rains during the wet season, as well as the swelling behaviour of active clay minerals in interbedded clay/shale units, have been documented as landslide mechanisms in Nanka (Igwe and Una, 2019). Landslides have had a negative impact on the Nanka settlement area. The 1988 landslide in this area, according to Okagbue (1992), destroyed many homes and forced over 50 families to evacuate.



Figure 2.11: Slope Failure at Dorli Opencast project I (After Satyanarayana and Sinha, 2018)

Table 2.3: Rescue Operations 1980-1993 (After: Mallo and Wazoh, 2014)

MINE PONDS		
YEARS	ALIVE	DEAD
1980	-	4
1981	-	20
1982	-	23
1983	-	20
1984	1	4
1985	-	2
1986	-	10
1987	-	3
1988	-	-
1989	4	5
1990	1	1
1991	-	-
1992	7	6
1993	-	8
TOTAL	13	106

SOURCE: Adiuku-Brown, 1999

CHAPTER THREE

METHODOLOGY

3.1 Field Investigation

Field investigation was conducted at Ikpobia quarry operated by BUA Group, Okpella, Edo State, Nigeria. It included geological, geophysical, groundwater, and geomechanical investigations.

3.1.1 Geological Investigation

This includes geological mapping, geological 3D solid modelling using borehole drilling results and geophysical and ground water investigation.

3.1.1.1 Geological Mapping

This was mainly based on field observation and involves recording the pit boundaries coordinates and recording the existing types of rocks within and surrounding the quarry and was carried out with compass clinometer, GPS for geographical locations and geological hammer.

3.1.1.2 Geological 3D Model of the Deposit

This was achieved using the results of borehole drilling that were provided by BUA Okpella geologists (Figure 3.1). And using Surfer 12 and ArcGIS software.

3.1.2 Geophysical and Groundwater Investigation

This was carried out using the Vertical Electrical Sounding (VES) conventional Schlumberger array method which is based on the gradual increasing of interelectrode spacing about fixed center of array. It employs a four-electrode system that is placed linearly with varying interelectrode spacing, with the potential electrode remaining somewhat fixed at the spread's center and the current electrode expanding progressively around the spread's center (Parasnis, 2012). Twenty-six (26) vertical electrical sounding (VES) points were carried out in this study, 20 surrounding the pit

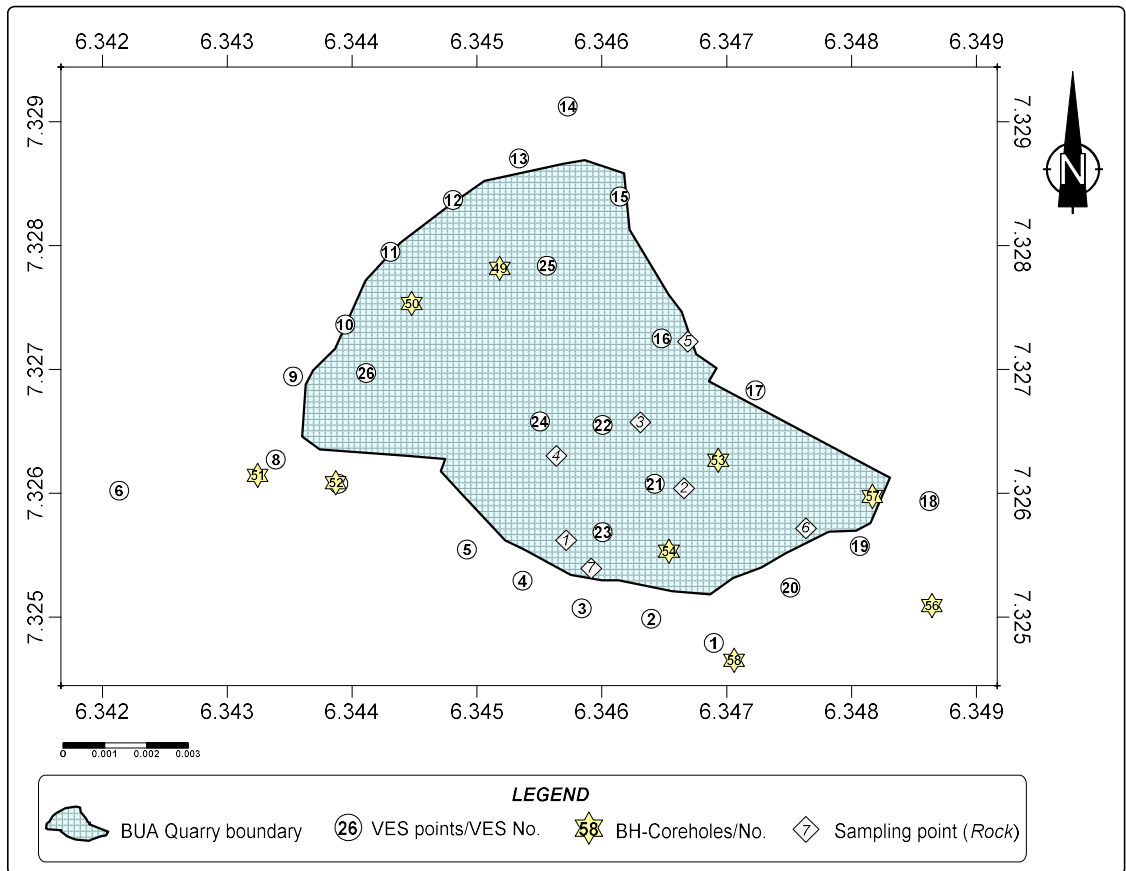


Figure 3.1: Location of the Vertical Electrical Sounding Points and BH-core-holes at the Pit

and six inside the pit. The Geopulse Campus Tigre resistivity meter was used for data collection (Figure 3.1) and Global Positioning System (GPS) was used to record the geographic coordinates of the VES stations (Figure 3.2).

3.1.2.1 Data Processing and Interpretation of VES Results

This comprises the calculation of apparent resistivity (ρ_a) through the multiplication of the resistance got from the field and the geometric factors i. e. $\rho_a = 2\pi(a^2/b - b/4)R$ for schlumberger array. These measurements of each VES station were plotted graphically on a transparent log-log graph sheet with an electrode spacing AB/2 on the X-axis and apparent resistivity (ρ_a) on the Y-axis to give VES curves. Curve matching technique is very accurate method of interpretation (Keller and Frischknect, 1966). This technic was carried out for the interpretation of the curves which involves the determination of the thickness and resistivity of different horizons and is a quantitative interpretation.

Using the WINRESIST computer software, the results of the curve matching were inserted into the computer as a starting model parameter in an iterative forward modelling process. The inversion method was then frequently employed in the interpretation of geophysical data. An iterative process guided by a mathematical equation known as inversion (Nicholas, 1986). From the field data, a model was proposed and supplied into a computer, where an inversion program was performed, yielding a new model with parameters that were compared to the field data. These parameters were changed and the computer was run again. This process was repeated until a model was established and best matches the field data in terms of calculated data. Layer parameter charts were created using the inversion results (layer resistivity and thickness). In order to estimate the relationship between the different arrays employed, statistical calculations (tests of significance) and the coefficient of correlation “R” of the statistical-plots of the layer parameters were performed (Oladunjoye and Jekayinfa, 2015).

3.1.3 Geomechanical investigation

This includes structural investigation (joint data collection) and rock mass classification and requires strong observation and attention to the field data gathering.



Figure 3.2: Geopulse Campus Tigre Resistivity Meter Used for VES Data Collectio

The Ikpobia marble quarry was divided to 7 zones depending on the structural characteristics of each zone.

3.1.3.1 Joint Data Collection

Gathering joint set orientations is one of the most important structural modelling activities. This data gathering can be achieved by different mapping techniques, including, line mapping, window mapping and digital mapping. In this study digital mapping was used in building the structural model and analyzing joint sets in the pit faces through digital photogrammetry. The decision of choosing the digital photogrammetry for the mapping was because it allows structural geologic mapping to be conducted on rock faces that are not accessible for conventional mapping. It also ensured safety and saved time. This was carried out using 3DF Zephyr Free Software following 4 steps:

i.) Building Photogrammetric Model

1. Photographs from various viewpoints were taken, such that the direction from the object to the camera has a wide overall range of angles covering three-dimensions.
2. The photogrammetry software analysed the photographs and built a cloud or surface grid model.
3. Multiple measurements between identifiable points were obtained so that it allows to compare measurements to measurements between the same points using the cloud developed by the photogrammetric model. The factor of the ratio between the two was indicative of the calibration that one must attempt. The factor should be reasonably constant. An average constant can be used to obtain real coordinates. This factor is a calibration factor to adjust camera coordinates to meaningful real coordinates. This adjustment is not needed to determine dip and dip direction.
4. The axes definition or horizontal plane normal vector utility in the photogrammetric software was used to orient the axes of the model. If that is not possible, then one must determine the orientation of the model coordinate system so that any orientations determined from the cloud can be rotated to the global coordinate system that a mine or researcher uses or that a researcher has established for a domain of constant bench orientation.
5. The orientation of an exposed joint was measured.

ii.) **Determining Orientation of a Plane by Sampling Points on the Exposed Plane in the Model**

One of the best ways to measure the average orientation of a plane is to sample points in that plane. A joint will not always be planar. An average orientation of that pseudo-plane is the objective to represent that surface orientation. To sample, a selection of about 10 points is desired over the area of the exposed surface. The coordinates of each point are recorded. A plane can be represented by the equation

$$ax + by + c = z, \quad (3.1)$$

where a , b , and c = constants of a fitted plane.

For each individual point represented by the index i , the error between the point and a fitted point—that is the error in the z-direction, can be represented by

$$e_i = z_i - ax_i - by_i - c, \quad (3.2)$$

where e_i = error between the i th point and the fitted plane.

The average plane can be fitted by a number of techniques. Here, we used the criterion of minimizing the sum of the square of the error. That is, minimizing that quantity with respect to each of the parameters to be fit (a , b , and c).

Therefore,

$$\sum e_i^2 = \sum z_i^2 + \sum a^2 x_i^2 + \sum b^2 y_i^2 + \sum c^2 - \sum 2ax_i z_i - \sum 2b y_i z_i - \sum 2c z_i + \sum 2abx_i y_i + \sum 2acx_i + \sum 2bcy_i \quad (3.3)$$

The next step is to take the derivative of $\sum e_i^2$ with respect to each parameter and set each to zero to minimize the sum of the square of the error.

A system of equations results, and the answer provides values for a , b , and c .

In matrix form, this same process can be simply represented. Set the system of equations of the form in equation 3.1 be represented by

$$Ap = b, \quad (3.4)$$

Where:

$$A = \begin{bmatrix} x_1 & y_1 & 1 \\ x_2 & y_2 & 1 \\ x_3 & y_3 & 1 \\ \dots & \dots & \dots \\ x_n & y_n & 1 \end{bmatrix} \quad (3.5)$$

$$p = \begin{bmatrix} a \\ b \\ c \end{bmatrix}, \text{ and} \quad (3.5)$$

$$b = \begin{bmatrix} z_1 \\ z_2 \\ z_3 \\ \dots \\ z_n \end{bmatrix} \quad (3.6)$$

The least squares fit is obtained by the following operations:

$$p = (A^T A)^{-1} A^T b, \quad (3.7)$$

The method of determining dip and dip direction involves determination of the upper normal to the fitted plane. There are two ways to do this, and both should be used as a check.

iii.) Determination of Normal to Fitted Plane Via the Plane Equation

The normal to the fitted plane is

$$n = \begin{bmatrix} a \\ b \\ -1 \end{bmatrix}, \quad (3.8)$$

The unit vector is determined by dividing each component by the length of n .

The unit vector components are represented as u , v , and w . If w is negative, then the sign of each component should change so that w is positive, meaning that the normal is in the upward direction. The u and v can be used to represent dip direction.

Dip may be found with the following equation:

$$Dip = \cos^{-1} w, \quad (3.9)$$

And the angle counter clockwise from the x-axis is

$$\alpha = \text{atan2}(u, v). \quad (3.10)$$

Here, `atan2` is a function that accounts for the quadrants of the coordinates so that the answers range from $-\pi$ to $+\pi$, or -180° to 180° with most computers and calculators. This angle can be converted easily to azimuth from north.

iv.) Determination of Normal to Fitted Plane Via Vectors Within the Plane

Once the plane equation is fitted to the points sampled, the fitted equation can be used to determine a series of points that are exactly on the plane. Typically, this might be done by determining the range of x and y in the sampled points. A regular grid of x and y points might be established, and a spreadsheet used to calculate the Z value for each point. One can then determine a vector along the x axis, and another along the y axis. If these vectors are, respectively V_1 and V_2 , then the vector in the normal direction is determined by the cross product of these two vectors, namely,

$$V_3 = V_1 \times V_2, \quad (3.11)$$

V_3 can then be normalized to a unit vector, and the same Dip and dip direction can be determined with equations 10 and 11.

The dip direction can be converted easily to azimuth from north. Different joint sets were observed in the 7 zones of the pit quarry of Ikpobia and were analysed to get their different properties. In Zone 1 five joints (5), Zone 2 five joints (5), in Zone 3 six joints (6), in Zone 4 six joints (6), in Zone 5 four joints (4), in Zone 6 five joints (5) and eight joints (8) in the Zone 7 that were analysed together. Google earth image representing the seven zones was used for the determination of the bench orientation of each zone (Figure 3.3). Figures 3.4 – 3.8 give examples of some joints that were sampled in the model that was built by the 3DF Zephyr Software.

3.1.3.2 Rock Mass Classification

Many rock mass classifications were used for the rock mass strength properties including Rock Mass Rating system (RMR), Laubscher's In-situ Rock Mass Rating system (IRMR) and Geological Strength Index (GSI) among others. In this study GSI was used as a tool of rock mass classification and its values were obtained for seven zones of the pit. GSI system was introduced by Hoek and his research partners (Hoek, 1994; Hoek *et al.*, 1995), and it is based heavily on the fundamental geological

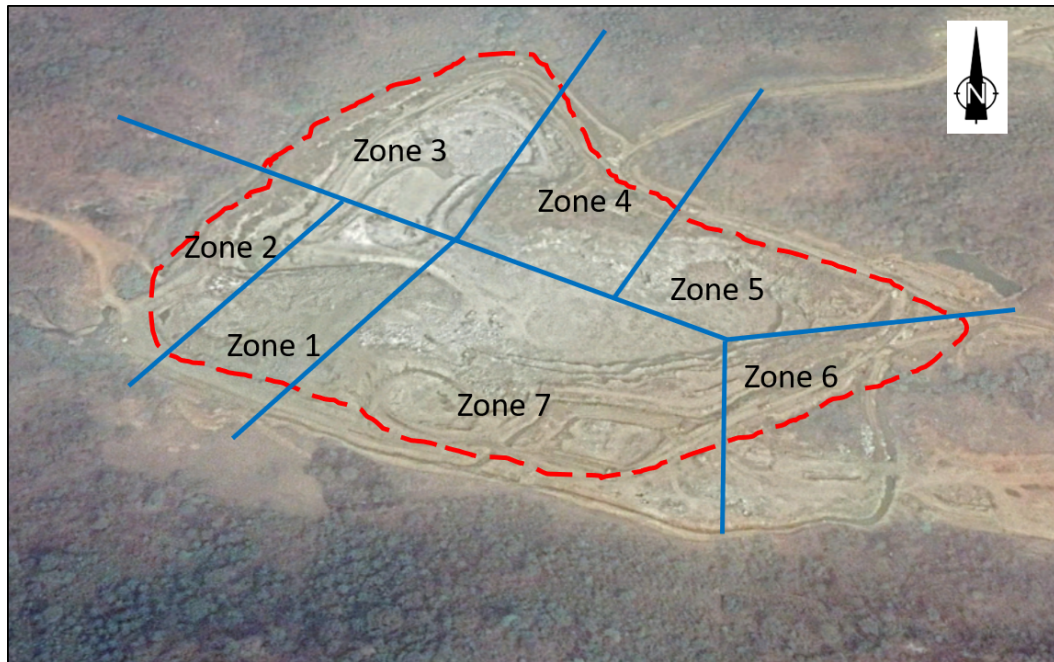


Figure 3.3: Google Earth Image of the Pit Quarry Representing the Different Zones

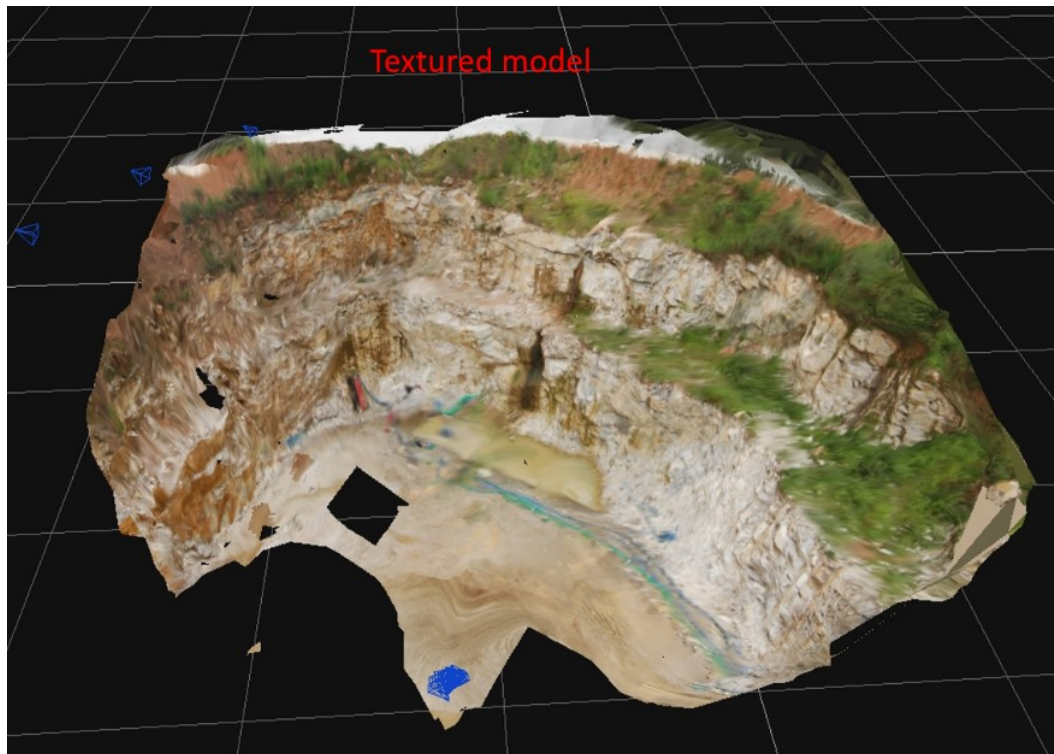


Figure 3.4: Presentation of the Texture Photogrammetric Model Built by 3DF Zephyr Software for Zones 1 and 2

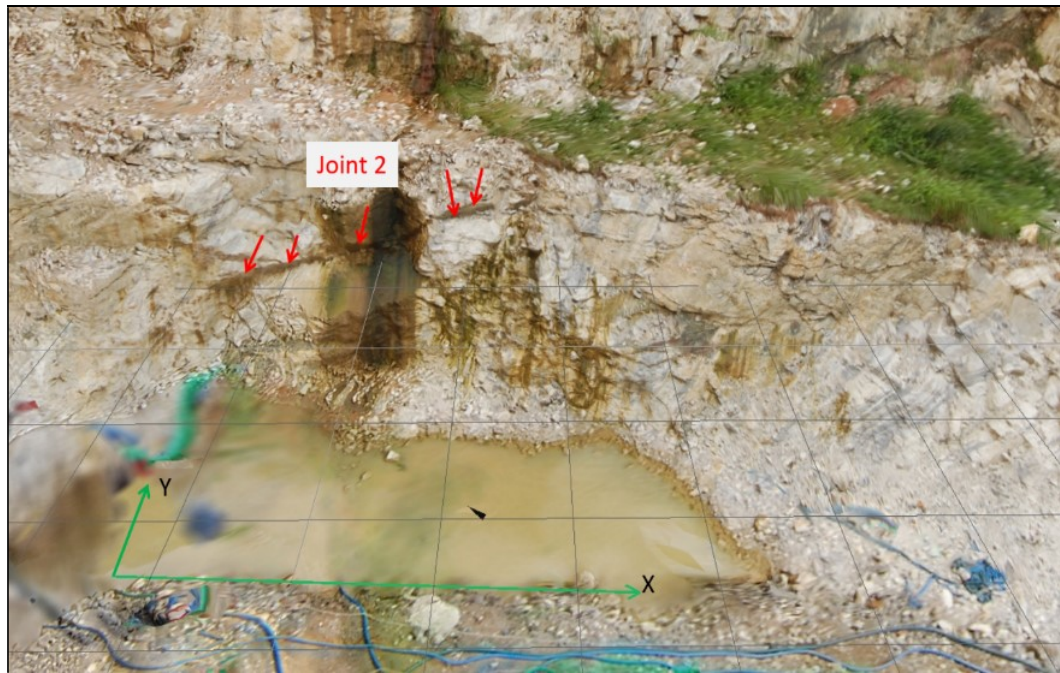


Figure 3.5: Presentation of the Texture Photogrammetric Model Built to Sample Joint 2 in the Zone 1

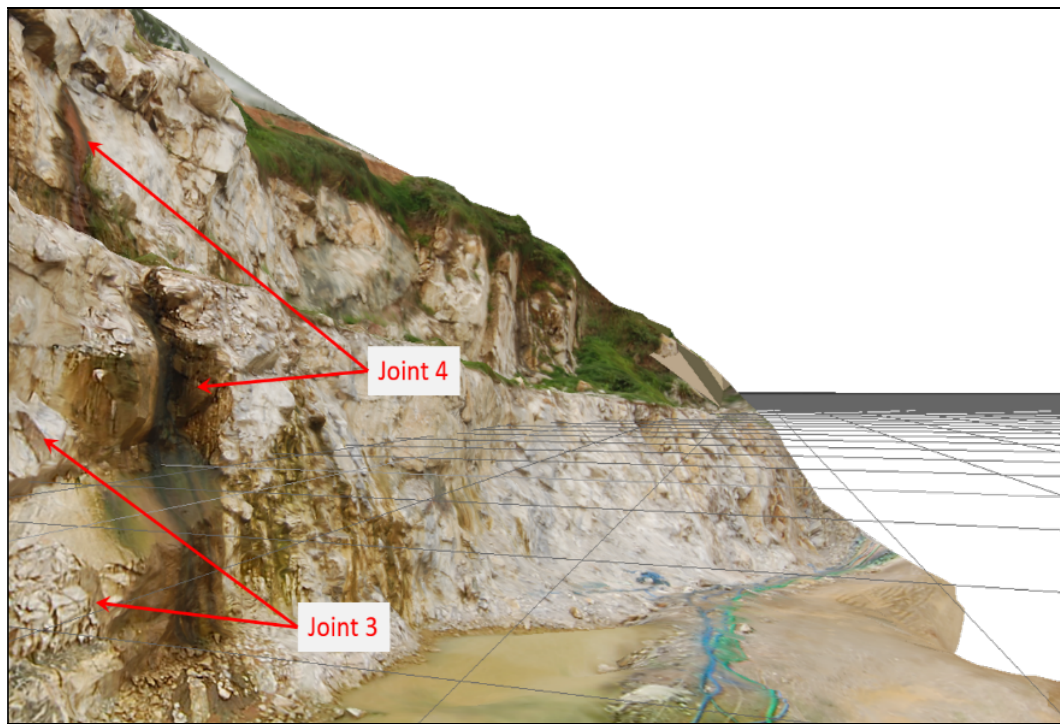


Figure 3.6: Presentation of the Texture Photogrammetric Model Built to Sample Joints 3 and 4 in the Zone 1

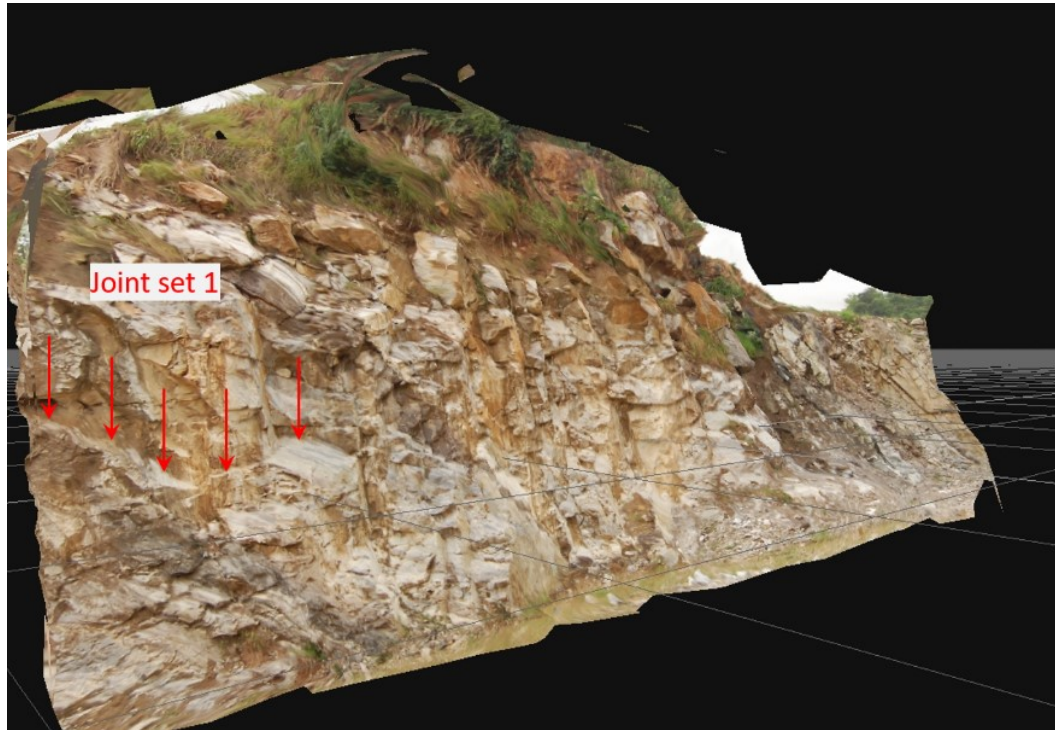


Figure 3.7: Presentation of the Texture Photogrammetric Model Built to Sample Joints 1 in the Zone 3

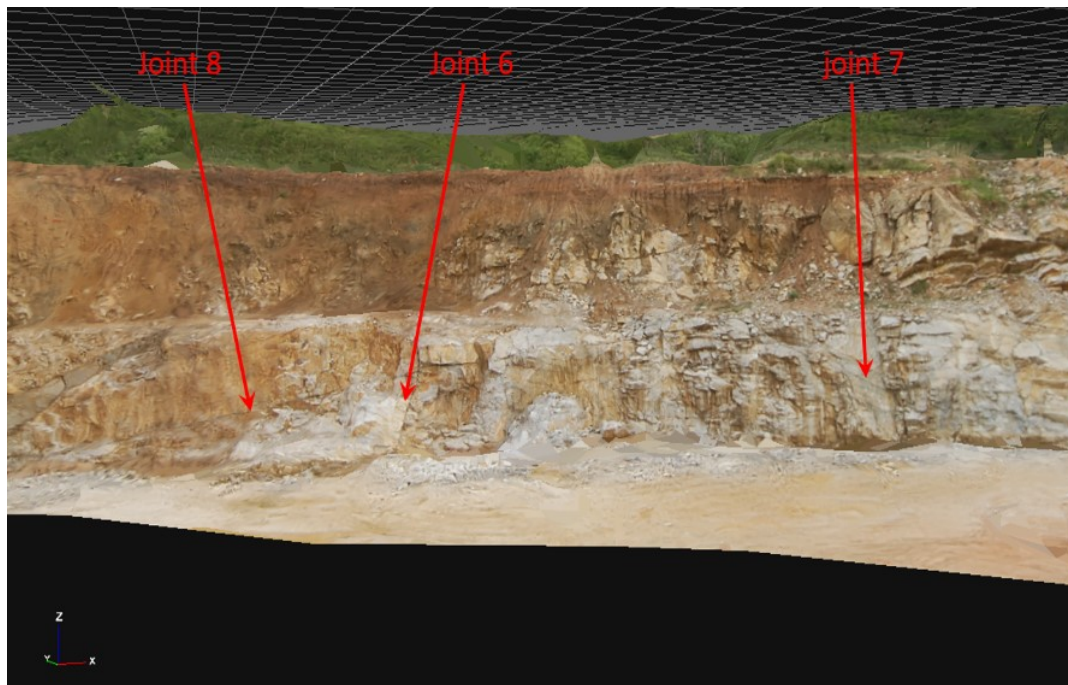


Figure 3.8: Presentation of the Texture Photogrammetric Model Built to Sample Joints 6, 7 and 8 in the Zone 7

observation of the blockiness and the rock mass structure of the rock mass and the condition of the joint surfaces using a range between 0 and 100 (Table 3.1).

3.2 Laboratory Tests

This section presents the methodology and equipment for all the laboratory tests conducted in the study. All the tests followed the suggested methods given by the International Society for Rock Mechanics (ISRM) and American Society for Testing and Measurements (ASTM). Tests were conducted in the Geomechanics Laboratory at the Mining Engineering Department of the University of Utah.







3.2.1 Rock Samples Preparation

The specimens were prepared according to the Standard ASTM D4543 (2008). Seven cylindrical specimens were prepared with approximately height-to-width ratio between 2.0 to 2.5, and seven disks, with diameter to depth ratio of approximately 2.0. The ends of the specimen were cut and ground parallel to each other, and at right angle to the longitudinal axis, the parallelism of the upper and lower surfaces should be less than 0.02 mm (Figure 3.9). The specimens were prepared using saw and grinder. Measurements were taken with digital calipers. Height and diameter were determined by averaging 3 measurements.

3.2.2 Determination of Uniaxial Compressive Strength

The UCS test is also known as the uniaxial compressive strength test. Uniaxial test machine for elastic and compressive strength tests was used for the determination of the UCS (Figure 3.10). Three UCS samples, C9A, C8A, and C7A were prepared for testing. In order to determine some elastic properties, Young's modulus (E) and Poisson's ratio (μ), four strain gauges were attached to each sample (Figure 3.11). Test procedure involves subjecting the cylindrical rock specimens to an axial load, without any lateral confinement. The axial load was increased gradually until the specimen fails. The vertical normal stress on the specimen, when failure occurs, is known as the unconfined compressive strength or uniaxial compressive strength, fondly known as UCS. By monitoring the vertical deformations, the vertical normal strains can be computed. By plotting the stress–strain curve, the Young's modulus (E) can be

Table 3.1: Hoek-Brown Rock Mass Classification System

<p>GEOLOGICAL STRENGTH INDEX JOINED ROCK MASSES (modified from Marinos & Hoek (2000))</p> <p>From the lithology, structure and surface condition of the structures, estimate the average value of <i>GSI</i>.</p> <p>DO NOT try to be too precise. Quoting a range $33 \leq GSI \leq 37$ is more realistic than stating that $GSI = 35$. <u>Note that this table does not apply to structurally controlled failures.</u> Where weak planar structural planes are present in an unfavourable orientation with respect to the excavation face, these will dominate the rock mass behavior.</p> <p>The shear strength of surfaces in rocks that are prone to deterioration, as a result of changes in moisture content, will be reduce if water is present. When working with rocks in the fair to very poor categories, a shift to the right may be made for wet conditions. Water pressure is dealt with by effective stress analysis.</p>		<p>JOINT SURFACE CONDITIONS</p> <p>VERY GOOD Very rough, fresh unweathered surfaces.</p> <p>GOOD Rough, slightly weathered, iron stained surfaces.</p> <p>FAIR Smooth, moderately weathered and altered surfaces.</p> <p>POOR Slacksided, highly weathered surfaces with compact coatings or fillings of angular fragments.</p> <p>VERY POOR Slacksided, highly weathered surfaces with soft clay coatings or fillings.</p>				
<p>ROCK MASS STRUCTURE</p>		<p>□ DECREASING SURFACE QUALITY →</p>				
 <p>INTACT or MASSIVE ‘Intact’ rock specimens. Massive in situ rock with few widely spaced structures.</p>	<p>90</p>			N/A	N/A	
 <p>BLOCKY Well interlocked undisturbed rock mass consisting of cubical blocks formed by three intersecting sets of structures.</p>	<p>80</p> <p>75</p>		55	50	40	
 <p>VERY BLOCKY Interlocked, partially disturbed rock mass with multi-faceted angular blocks, formed by four or more sets of structures.</p>	<p>70</p>				30	
 <p>BLOCKY/DISTURBED/SEAMY Folded rock mass with angular blocks formed by many intersecting structural sets. Persistence of bedding planes or schistosity.</p>	<p>60</p>				20	
 <p>DISINTEGRATED Poorly interlocked, heavily broken rock mass with mixture of angular and rounded rock pieces.</p>					10	
 <p>LAMINATED / SHEARED Lack of blockiness due to close spacing of weak schistosity or shear planes.</p>		N/A	N/A			

Source: Marinos and Hoek (2000)



Figure 3.9: Sample Preparation at Geomechanics Laboratory, Mining Engineering Department of University of Utah, USA

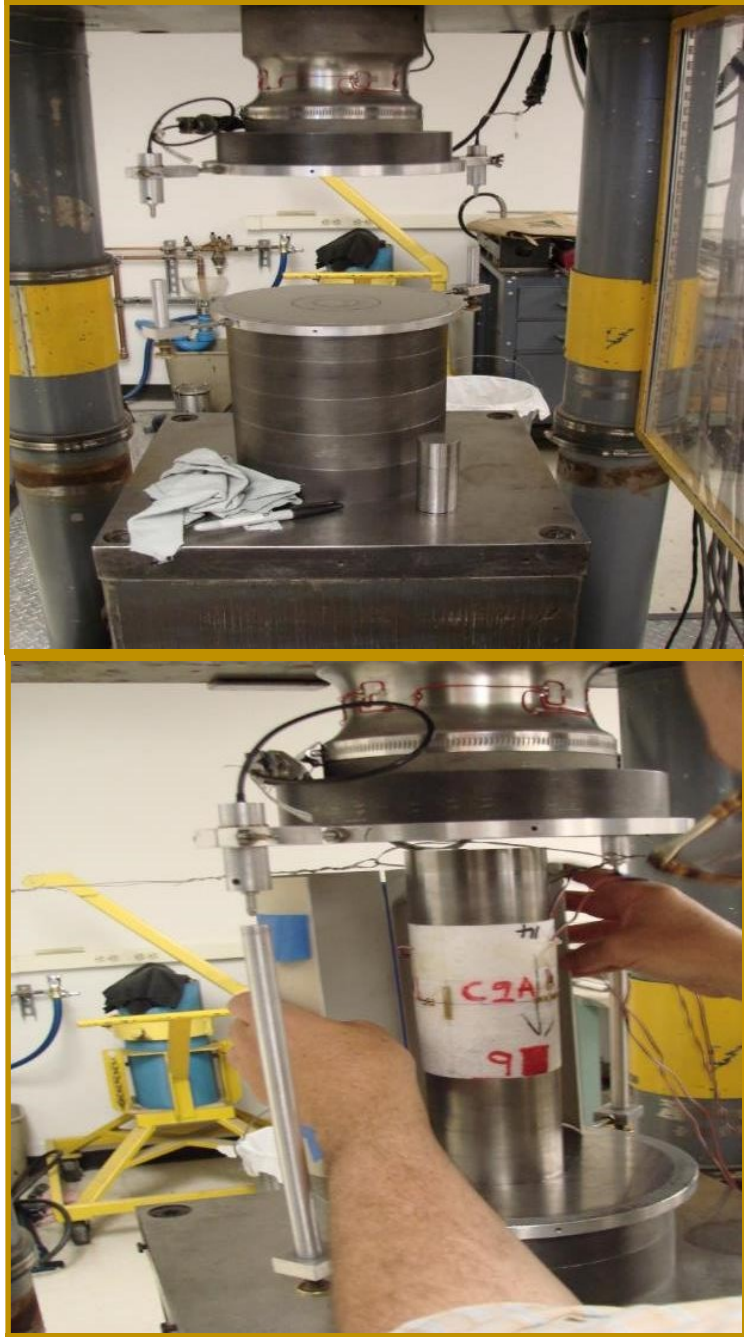


Figure 3.10: Uniaxial Test Machine for Elastic and Compressive Strength Tests at Geomechanics Laboratory, Mining Engineering Department of University of Utah, USA

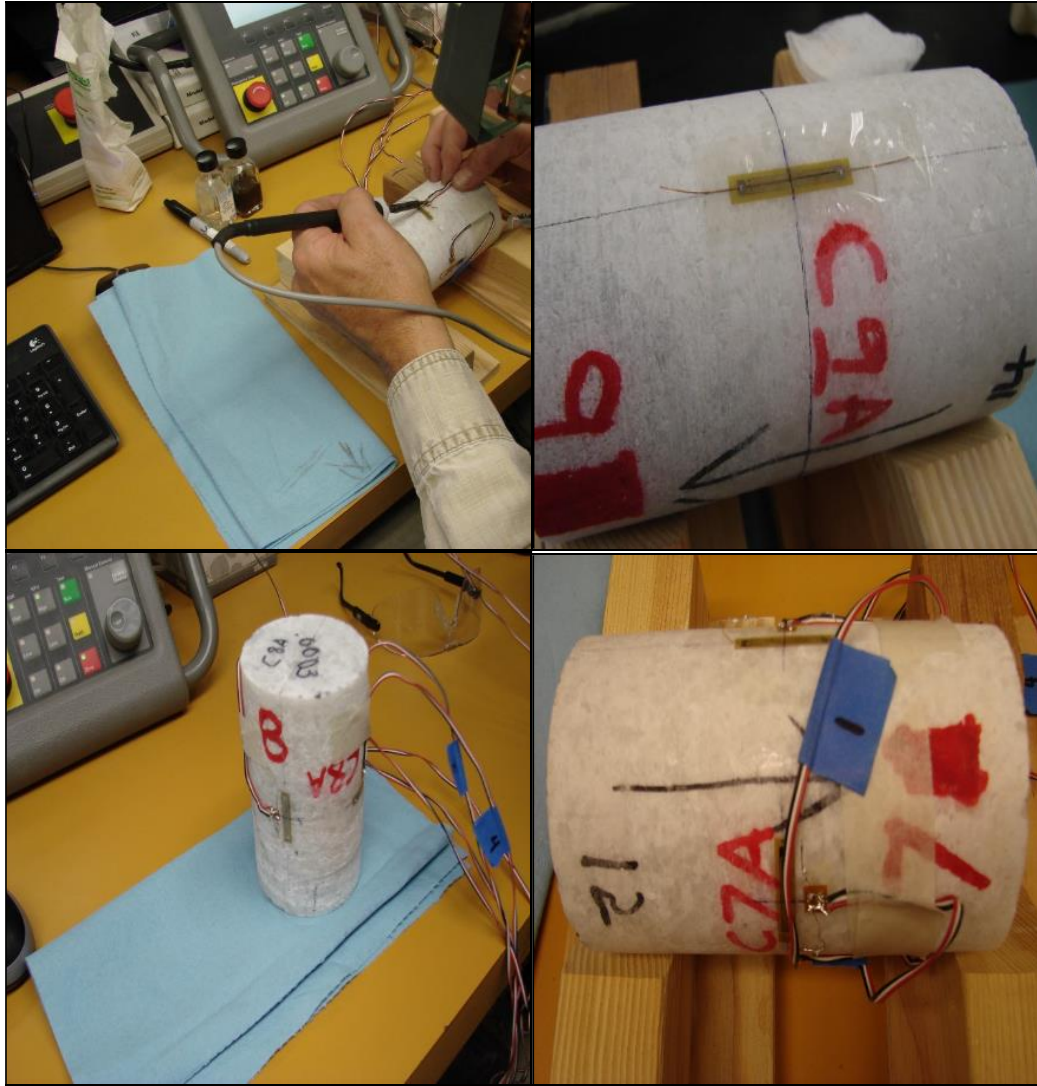


Figure 3.11: Samples During and After Strain Gauges Attachment at Geomechanics Laboratory, Mining Engineering Department of University of Utah, USA

determined. By monitoring the lateral or circumferential deformation, the Poisson's ratio can be computed too (Sivakugan *et al* 2013).

3.2.3 Triaxial Compression Strength Test

The Mohr-Coulomb failure envelope is defined by the triaxial compressive strength test, which may be used to determine the friction (ϕ) and cohesion (c) shear strength parameters for intact rock. Failure occurs only when the combination of normal stress and shear stress is such that the Mohr circle is tangential to the failure envelope in triaxial compression, when the rock sample is loaded not only axially but also radially by a confining pressure kept constant throughout the test (Read and Stacey, 2009). The triaxial test was performed on 6 samples, C1A, C1B, C2A, C3A, C4A and C5A to determine the strength envelope, within initial plan for confining stress at the following percentages of average unconfined compressive strength: 1.0%, 2.0%, 5.0%. Triaxial tests were performed according to ASTM Standard D7012 (2010), Using Hoek cell (Figure 3.12). The objective here is to capture as much of the post-peak strength specimen behaviour as possible. Figure 3.13 represents samples that were prepared for the Triaxial test.

3.2.4 Brazil (Indirect Tensile) Test

The Brazilian test was performed on seven disk samples D1A, D2A, D2B, D3A, D5A, D11A and D11B in order to obtain the tensile strength of rocks. Samples were compressed between conical steel platens of a portable light weight tester until failure occurs. The tester is quick and can be conducted on regular or irregular rock fragments. The apparatus of the tests consists of a rigid frame, two point load patterns and hydraulic activated ram with pressure gauge and a device for measuring the distance between the loading points. This work was carried out in accordance with ISRM standards for indirect testing of tensile strength. This involves loading the specimens continuously at a constant rate of 200 N/s until failure occurs. The Brazilian tensile strength is different from the tensile strength that is obtained from the direct tension test. The tensile strength, σ_t , is calculated from the Brazil test as follow:

$$\sigma_t = 0.636 P / Dt \text{ (MPa)} \quad (3.12)$$

where P is the load at failure (N),

D and t are the diameter and the thickness of the test specimen respectively (mm).



Figure 3.12: Hoek Cell for Triaxial Tests at Geomechanics Laboratory, Mining Engineering Department of University of Utah, USA



Figure 3.13: Samples Ready for the Triaxial Test at Geomechanics Laboratory, Mining Engineering Department of University of Utah, USA

3.2.5 Density Test

The dry density can be defined as per unit volume of completely dry sample. The sample of rock to be tested should be dry completely before the testing. The complete dry rock sample is now immersed in the water for 24 hours. The voids are available in the rock are also included in to the volume.

The dry of any materials or sample can be obtained by the followed formulae.

$$\gamma_d = W_d/V \quad (3.13)$$

Where γ_d = Dry density.

W_d = Weight of dry rock.

V = Total volume of rock sample.

3.2.6 X-Ray Diffractometry (XRD)

Four samples from the Ikpobia Quarry were evaluated with the use of X-ray Diffraction technique (XRD), one sample of marble and three samples from the three different intrusions in the quarry. These analyses were carried out using a Bruker D8 Advance X-ray powder diffractometer with filtered Cu-K α radiation ($\lambda = 1.542$) operating at a beam voltage and current of 40 kV and 40 mA, respectively. The XRD patterns were recorded in the range of $2\theta = 5^\circ - 90^\circ$ using a step size of 0.034° and scan step time of 71.6 s. The diffractometer was attached to a computer to analyse the results using X'pert HighScore Plus software.

3.2.7 Petrographic Study

One sample of marble and other three samples of intrusions from the Ikpobia Quarry were cut off along selected direction using diamond saw to get thin slides. The slides were polished to a perfectly smooth and flat surface and then were attached to a thin glass using a special cement. Then the slides thicknesses were reduced in special machine by rotary grinding with different grades of carborundum powder. After the machine grinding the slides were then removed and grinded by hand on a glass plate until the thickness of approximately 0.03 mm. After that the slides were washed and dried and covered with thin glass cover slip attached with the same above-mentioned cement. Then, the BX41 OLYMPUS petrographic microscope with a mounted DVC camera connected to a computer, was used to observe the thin sections.

Photomicrographs were taken with microscope NICON ECLIPSE 90i. The analysis was performed under both polarized and cross polarized light at 409 magnification.

3.3 Pit Slope Stability Analysis

There are several methods to investigate the slope stability analysis. In this study kinematic analysis was used to investigate the possible failure modes. The Hoek-Brown failure criterion was used to estimate the rock mass properties and numerical analysis to assess the stability through the calculation of the stress and the displacement of rock mass.

3.3.1 Kinematic Analysis

This is done based on the geological structures and the stress state of the rock mass. It can easily determine the stability state of a bench face through the geometry of the discontinuities, the slope orientation and the friction angle along the discontinuity surfaces in order to determine the potential for planar, wedge and toppling failures. For the rock slopes investigated at the site, the kinematic analysis was performed for bench faces of the seven zones to estimate the possibility of slope failure. Rocscience DIPS 7.0 program (Rocscience, 2019) was used to plot the data for the kinematic analysis in order to test the possibility of each of three basic slope failure modes: “planar failure, wedge failure and toppling failure.

3.3.2 Estimation of Rock Mass Properties Using Hoek-Brown Failure Criterion

Rock mass properties were determined based on the geological visual observation (GSI) and laboratory analysis results that were used as inputs for the generalized Hoek-Brown failure criterion. The criterion is expressed according to (Hoek et al, 2002) by the following equation:

$$\sigma_1 = \sigma_3 + \sigma_{ci} \left(m_b \frac{\sigma_2}{\sigma_{ci}} + s \right)^\alpha \quad (3.14)$$

Where σ_1 and σ_3 are the major and minor effective principal stresses at failure,

- σ_{ci} is the uniaxial compressive strength of the intact rock material
- m_i and s are material constants, where $s = 1$ for intact rock
- m_b is a reduced value of the material constant m_i and is given by

$$m_b = m_i \exp\left(\frac{GSI-100}{28-14D}\right) \quad (3.15)$$

- s and a are constants for the rock mass given by the following relationships:

$$s = \exp\left(\frac{GSI-100}{9-3D}\right) \quad (3.16)$$

$$a = \frac{1}{2} + \frac{1}{6}\left(e^{-GSI/15} - e^{-20/3}\right) \quad (3.17)$$

- D is a factor which depends upon the degree of disturbance to which the rock mass has been subjected by blast damage and stress relaxation. It varies from 0 for undisturbed in situ rock masses to 1 for very disturbed rock masses.
- GSI (Geological Strength Index) a rock mass classification system.

The deformation of rock mass E_m is calculated as follow using some of the above parameters,

$$E_m = \left(1 - \frac{D}{2}\right) \sqrt{\frac{\sigma_{ci}}{100}} \times 10 \left(\frac{GSI-10}{40}\right) \quad (3.18)$$

Because most geotechnical codes employ Mohr-Coulomb in the calculations, the equivalent Mohr-Coulomb parameters, cohesion (c), and friction angle (ϕ) must be determined from the Hoek Brawn failure envelope, which, according to Hoek and Brown, (1997) and Hoek *et al.*, (2002), is translated to Mohr-Coulomb failure criterion. In this study the free Software RocLab (Rocscience, 2007) was used in the estimation of the rock mass properties.

3.3.3 Numerical Analysis (Numerical Modelling)

In this project Finite Element Method (FEM) was chosen to model the material behaviour. The commercial finite element computer program, Phase 2, was used to conduct deterministic numerical modelling analysis. The FEM modelling program was used because it provides the factor of safety that leads to stability of the overall pit slope. Factor of safety was calculated using Phase 2 Software through the method known as the Shear Strength Reduction (SSR) method. The shear strength reduction method was used to calculate the critical shear reduction factor (SRF) by progressively

reducing or increasing the shear strength of the material to bring the slope to state of limiting equilibrium (Zienkiewicz *et al.*, 1975). The critical SRF is identical to the Factor of Safety adopted by conventional limiting equilibrium method for slope stability analyses. The software Phase 2 allows the utilisation of Hoek-Brown failure criterion parameters and Mohr-Coulomb criterion in the analyses. In this project the Mohr-Coulomb parameters were used for the analyses to model slope stability.

Elastic – perfectly plastic Mohr-Coulomb model was used to describe the behaviour of the slope materials hence the SRF was defined according to the following equations:

$$C_f = \frac{C}{SRF} \quad (3.19)$$

$$\varphi_f = \tan^{-1} \left(\frac{\tan \varphi}{SRF} \right) \quad (3.20)$$

where C_f and C are the cohesive strength on the sliding surface and cohesive strength of the slope material, respectively. Also, φ_f and φ are the friction angle on the sliding surface and friction angle of the slope material, respectively.

Series of simulation was made using different trial values of SRF, starting from initial estimate of 1, to reduce the strength parameters (i.e. cohesion and friction angle) of the slope materials, until the slope failure occurs. The critical SRF value at which the slope failure occurs was found by bracketing and bisection method (Dawson *et al.*, 1999). The lower limit of bracket represents the trial SRF when the simulation converges and the initial upper limit was any trial SRF when the simulation does not converge. The next value of SRF was selected by bisecting the interval between the lower and upper limit. If the simulation converges with this new SRF then it was chosen as the new lower limit. Otherwise, it replaces the upper limit. The process was repeated until the difference between two succeeding upper and lower values of trial SRF was lower than 0.01.

CHAPTER FOUR

RESULTS AND DISCUSSION

4.1 Field Investigation

The investigation at the quarry site was carried out at several phases and following are the results

4.1.2 The Geology of the Study Area

In Okpella, the study region, the Upper Proterozoic Igarra Schist belt is found in association with metacarbonates between longitudes $N7^{\circ}19'$ and $7^{\circ}21'$ and latitudes $E6^{\circ}20'$ and $6^{\circ}23'$ Figure 4.1. This is a Proterozoic portion of Nigeria's basement complex, which comprises of metavolcanic and metasedimentary rocks of high quality (Fitches *et al.*, 1985; Obaje, 2009). The Schist belt, trends NNW–SSE and covers about 60 km of the basement complex, and contains the metacarbonates deposit (Rahaman *et al.*, 1983). These Precambrian rocks are found in Dahomeyan tectono-metamorphic terrain, which carries Pan-African orogeny traces. The Precambrian basement complex in this area is made up of three primary types of rocks: migmatite–gneiss, meta-sediments (calc-silicate and marble), and intrusive older granite (Obaje, 2009). The rocks in this area have a north–south trends and a western direction dip Figure 4.1 (Jimoh *et al.*, 2017). The migmatite–gneiss complex, meta-sediments (calc-silicate and marble), and intrusive older granite are the three major groups of rocks that make up the Precambrian basement complex in the study area (Figure 4.1). Rocks in the Ikpobia Quarry deposit were marble interbedded with calc-silicate gneiss, banded gneiss and quartz schist and some biotite granite and laterites beside the pit (Figure 4.2).

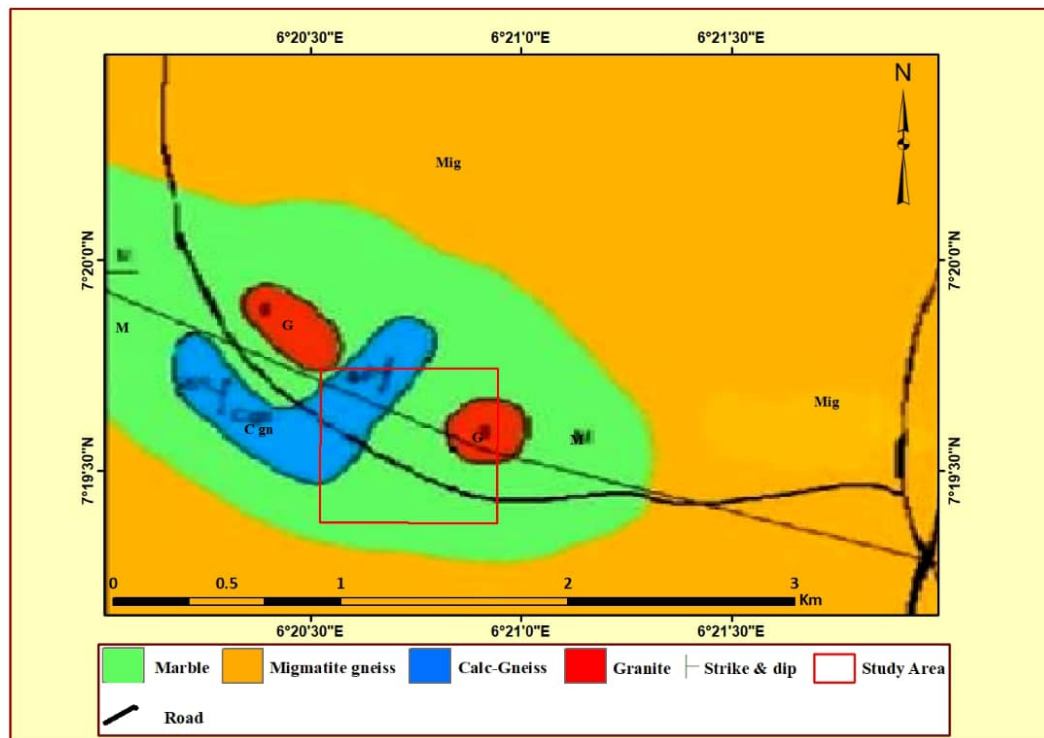


Figure 4.1: The Geological Map Okpella Region Indicating the Study Area
(Modified After Jimoh *et al*, 2017)

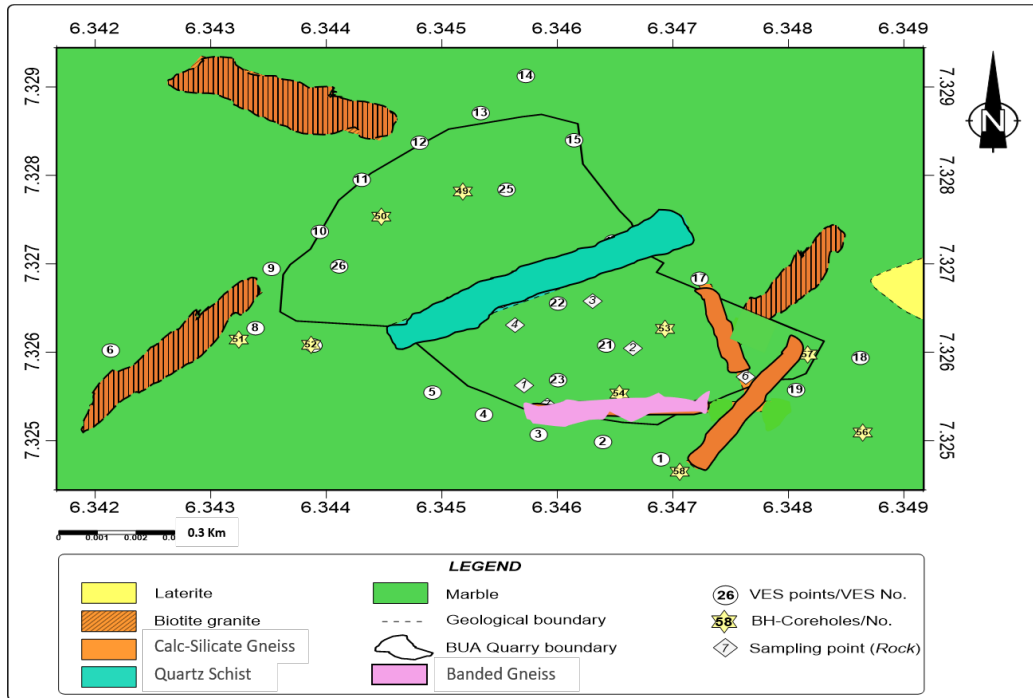


Figure 4.2: The Geological Map of Ikpobia Quarry

4.1.3 X-Ray Diffractometry (XRD)

X-Ray Diffractometry analysis revealed that the marble sample from the quarry site contains 100% of Calcite, while the samples from the three intrusions I1, I2 and I3 differ in their mineral content and the number of minerals. In sample I1 two minerals are dominant, Albite (33.2%) and Quartz (32.6%) and other minerals in different quantities, Actinolite (20.8%), Phlogopite (7.6%), Chlorite (5.1%) and Palygorskite (0.7%). The XRD analysis of the sample I2 shows a domination of Diopside (44.9%) and in less quantities Phlogopite, Microcline and Quartz estimated at 22.9%, 16.2% and 14.6% respectively and minor quantities of Bassanite and Vermiculite estimated at 0.5% and 0.95% respectively.

While the analysis of sample I3 shows a domination of Microcline (40%) and in less quantity Quartz (28.3) and Albite (25.1%). It is also observed from the analysis a small quantity of Muscovite-2M1 of 4% and minor quantities of Vermiculite and Bassanite estimated at 1.53% and 0.7%. Table 4.1 represents the XRD analysis results of a marble sample and three intrusion samples from the Ikpobia Quarry with an all error of +/- 3%.

4.1.4 Petrographic Analyses

Petrographic analyses were done on one sample of marble and other three samples from intrusions in Ikpobia Quarry and the results are as follow.

4.1.4.1 Marble Thin Section

The analysis of thin section of the marble sample was done in three areas of the section, area 1 and 3 in transmitted plane polarized light (Figures 4.3 and 4.4) and area 2 and 3 in transmitted cross polarized light (4.5 and 4.6). These analyses indicated 99% Calcite in coarse-grained marble. Grain boundaries are irregular. So, they are subhedral to anhedral grains. The sizes of these are 2 to 4 mm. The calcite shows distinct cleavage. There are trace amounts of quartz, feldspar, zircon, and apatite, all less than 1mm in size.

4.1.4.2 Thins Section from Intrusion 1 (I1)

Analyses of I1 thin section were done in six areas of the section, area 1, 2 and 3 in transmitted plane polarized light (Figures 4.7, 4.8 and 4.9) and area 1, 2, and 3 in

Table 4.1: XRD Analysis Results of a Marble Sample and 3 Intrusion Samples from the Ikpobia Quarry

Sample ID	Mineralogy	Percentage %
Marble	Calcite	100
I1	Quartz	32.6
	Albite	33.2
	Actinolite	20.8
	Phlogopite	7.6
	Chlorite	5.1
	Palygorskite	0.7
I2	Quartz	14.6
	Microcline	16.2
	Phlogopite	22.9
	Diopside	44.9
	Bassanite	0.5
	Vermiculite	0.95
I3	Quartz	28.3
	Microcline	40
	Albite	25.1
	Muscovite-2M1	4
	Bassanite	0.7
	Vermiculite	1.53

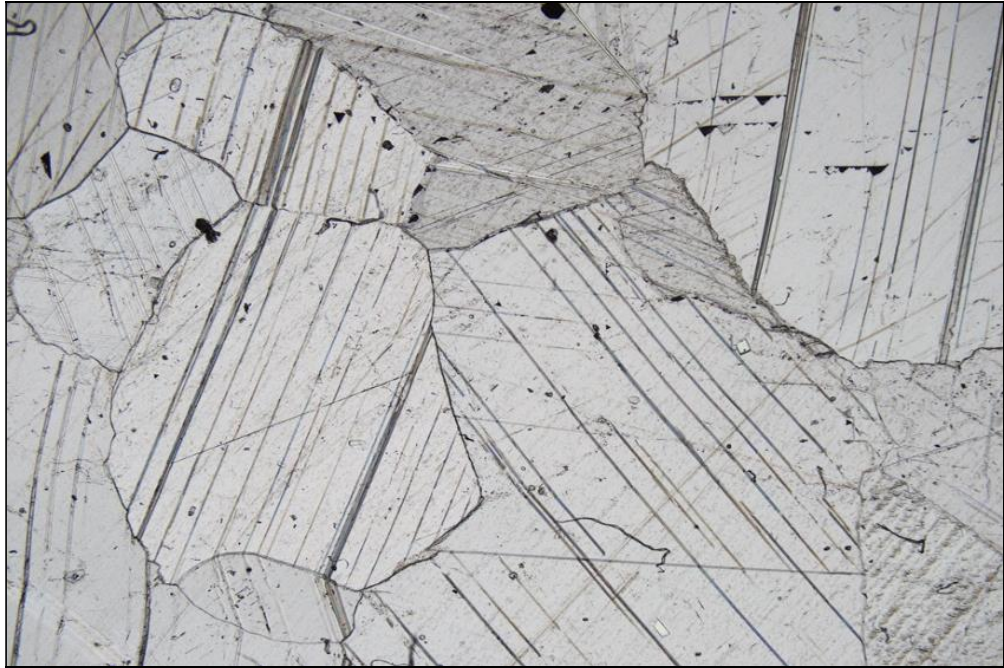


Figure 4.3: Photomicrograph of Marble Area 1 in Transmitted Plane Polarized Light

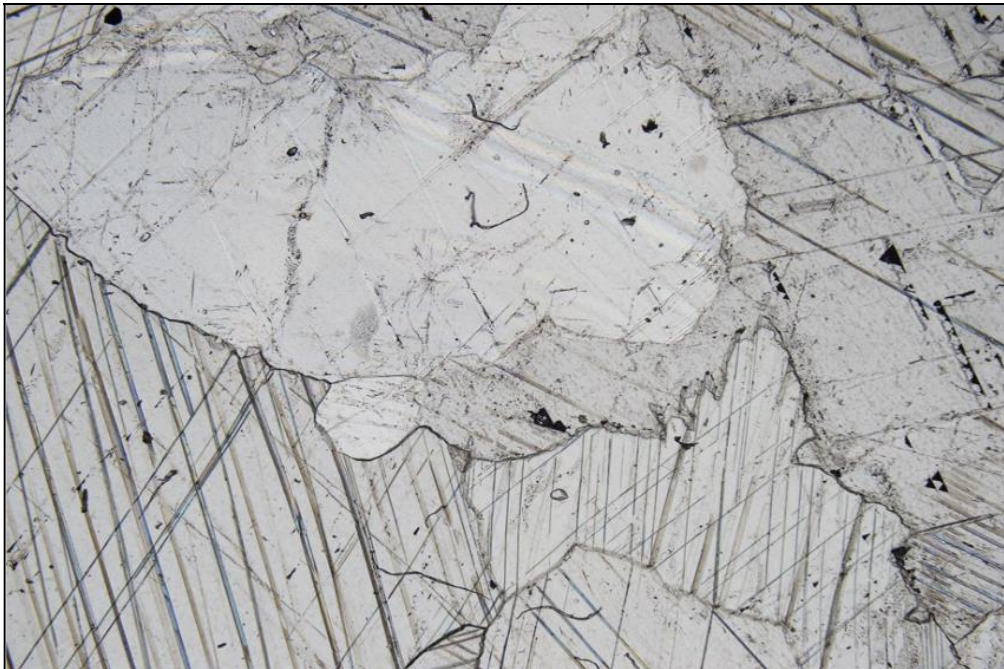


Figure 4.4: Photomicrograph of Marble Area 3 in Transmitted Plane Polarized Light

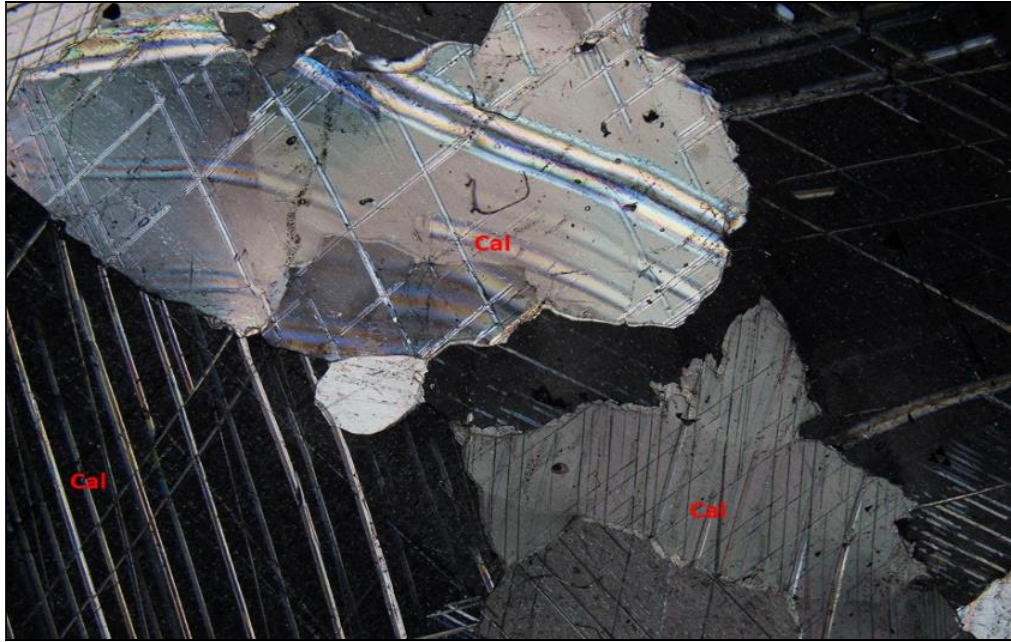


Figure 4.5: Photomicrograph of Marble Area 3 in Transmitted Cross Polarized Light Indicating Cal (Calcite)

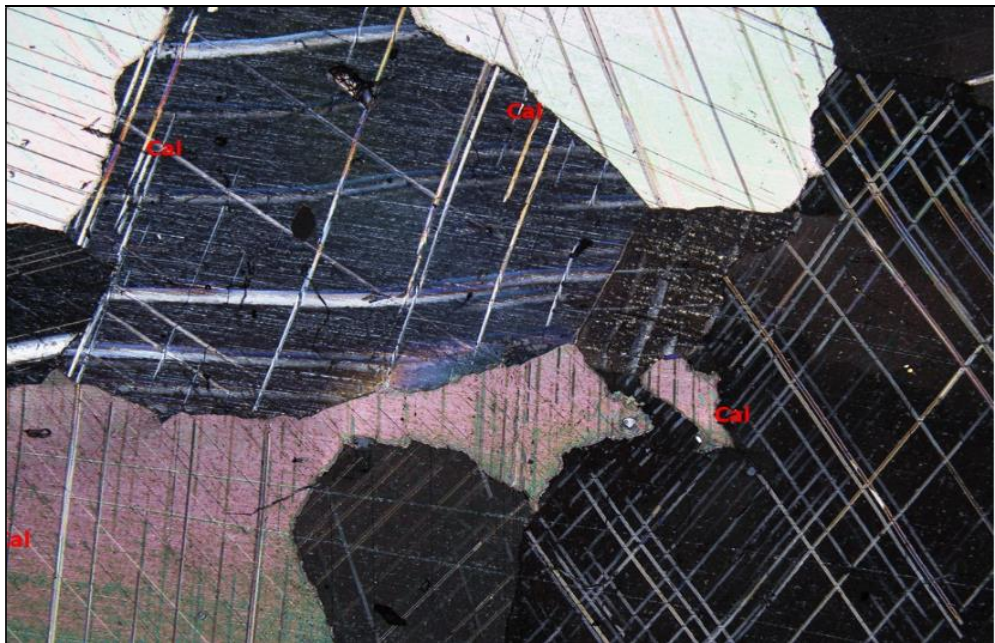


Figure 4.6: Photomicrograph of Marble Area 2 in Transmitted Cross Polarized Light Indicating Cal (Calcite)

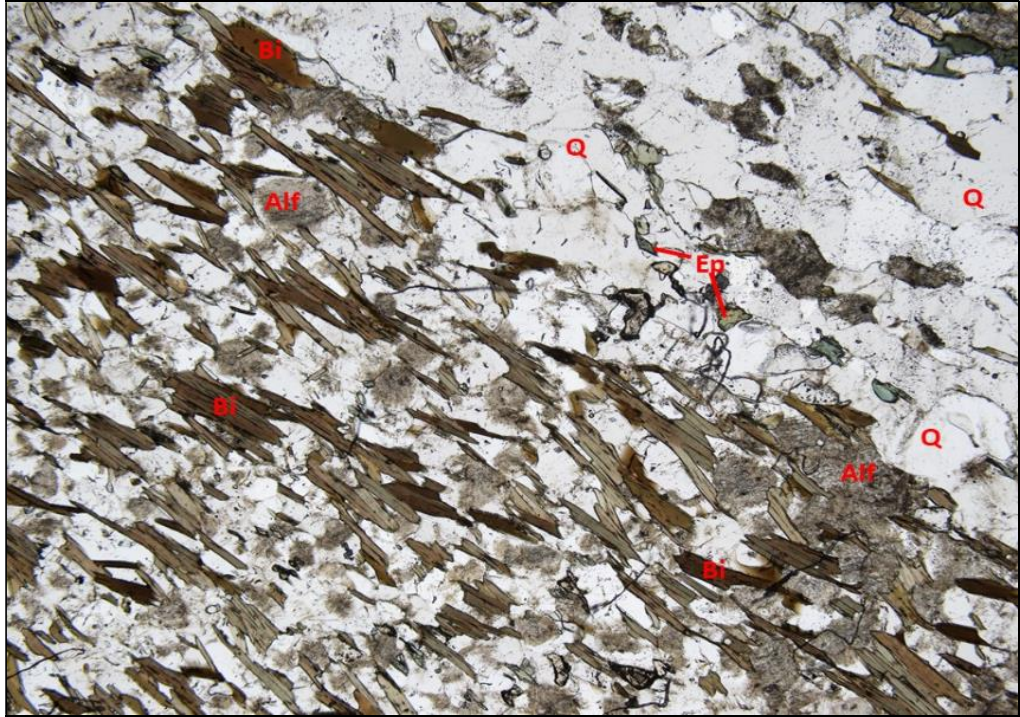


Figure 4.7: Photomicrograph of Intrusion 1 Area 1 in Transmitted Plane Polarized Light Indicating Q (Quartz), Alf (Alkali Feldspar), B (Biotite), Ep (Epidote)

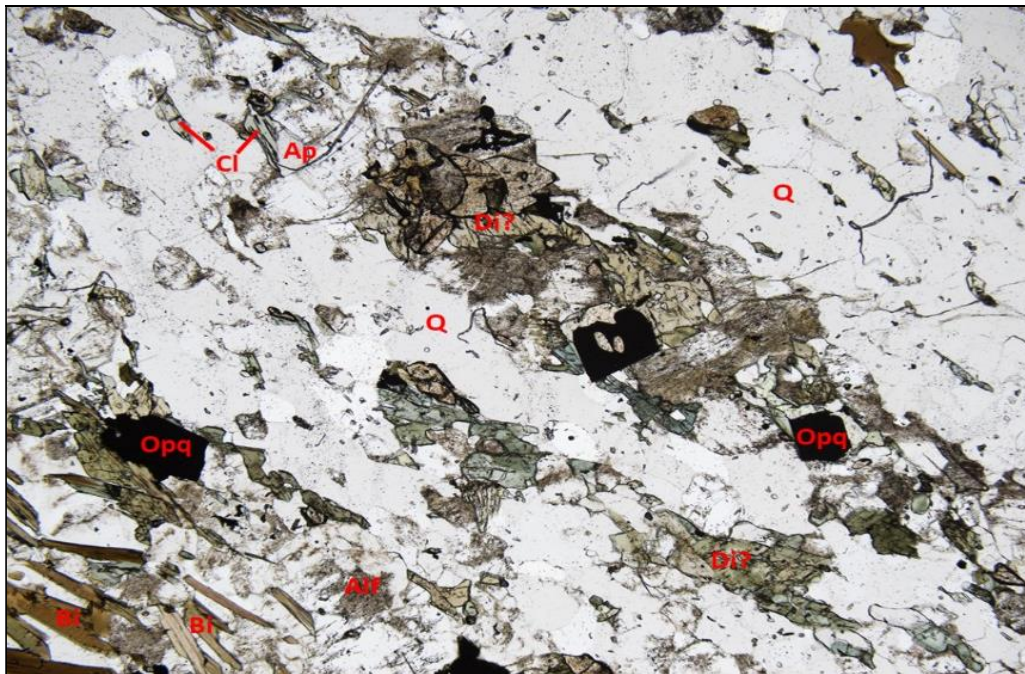


Figure 4.8: Photomicrograph of Intrusion 1 Area 2 in Transmitted Plane Polarized Light Indicating Q (Quartz), Alf (Alkali Feldspar), Bi (Biotite), Di (Diopside), Cl (Chlorite), Ap (Apatite), Opq (Opaque)

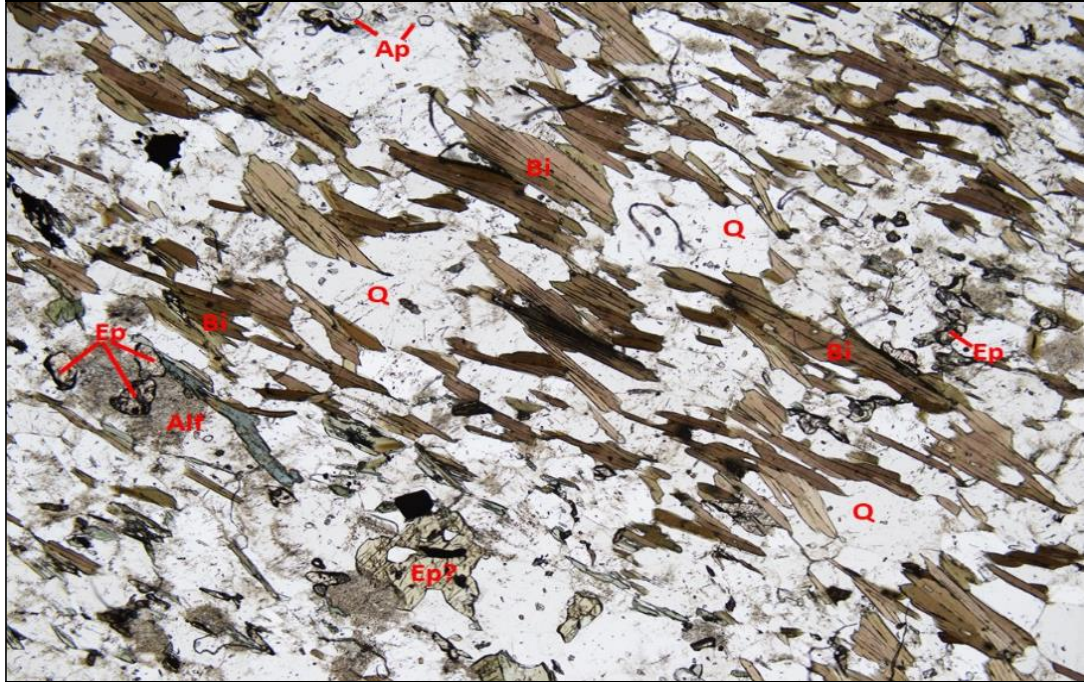


Figure 4.9: Photomicrograph of Intrusion 1 Area 3 in Transmitted Plane Polarized Light Indicating Q (Quartz), Alf/Plg (Alkali Feldspar)/ (Plagioclase), Bi (Biotite), Ep (Epidote), Ap (Apatite)

transmitted cross polarized light (Figures 4.10, 4.11 and 4.12). these analyses indicate Well-foliated metamorphic rock. Defined by aligned brown biotite and to a lesser degree by amphibole or diopside. Feldspar and quartz are present. Quartz is showing undulatory extinction. There appears to be siderite fine-grained, rounded, and anhedral, intergrown with pyrite in places.

Siderite is up to 0.5 mm. Quartz and feldspar are present. It is some sort of meta-sedimentary rock. The feldspars are moderately altered to fine-grained sericite. The petrographic analyses of thin section of intrusion 1 in six different areas of the thin section show the same minerals that are dominant in the rock which are Quartz (60 – 70%), Alkali Feldspar/ Plagioclase (25 – 35%) and Biotite (10 – 20%) and other minor minerals in that appear in some areas of the thin section with in small quantities (< 5 %) which are Diopside, Trace Apatite, Trace Opaque and Chlorite after Biotite that all appeared in the area 2 and area3 of the thin section I1 in transmitted plane polarized light. In area 1 and 2 in cross polarized light Trace Epidote appeared in less than 5% and in area 3 Trace Sphene and Trace Epidote are present in a less than 5% quantity (Table 4.2).

4.1.4.3 Thins Section from Intrusion 2 (I2)

Analyses of I2 thin section were done in six areas of the section, area 1, 2 and 3 in transmitted plane polarized light (Figures 4.13, 4.14 and 4.15) and area 1, 2, and 3 in transmitted cross polarized light (Figures 4.16, 4.17 and 4.18). These microscopic images indicate a Coarse grained, foliated (weakly to moderate), leucocratic (light-coloured) with quartz, orthoclase and plagioclase feldspars. Other minerals include biotite and possibly hornblende. The rock has been strongly altered where the feldspars show almost complete alteration to fine-grained sericite.

The biotites have been completely altered to chlorite. Other accessory phases include apatite, zircon, very rare muscovite and allanite with pleochroic halo. The feldspars show various types of twinning, Albite twinning, Carlsbad twinning, and possible Tartan twinning. Quartz shows various amounts of undulose extinction. Rare coarse grains of highly altered and composed of opaque minerals, possibly replaced hornblende or amphibole. Replaced by either magnetite, hematite, or some kind of iron oxide. The rock is a sort of meta-igneous rock most likely Metamorphosed granitic rock.



Figure 4.10: Photomicrograph of Intrusion 1 Area 1 in Transmitted Cross Polarized Light Indicating Q (Quartz), Alf (Alkali Feldspar), Bi (Biotite), Ep (Epidote).

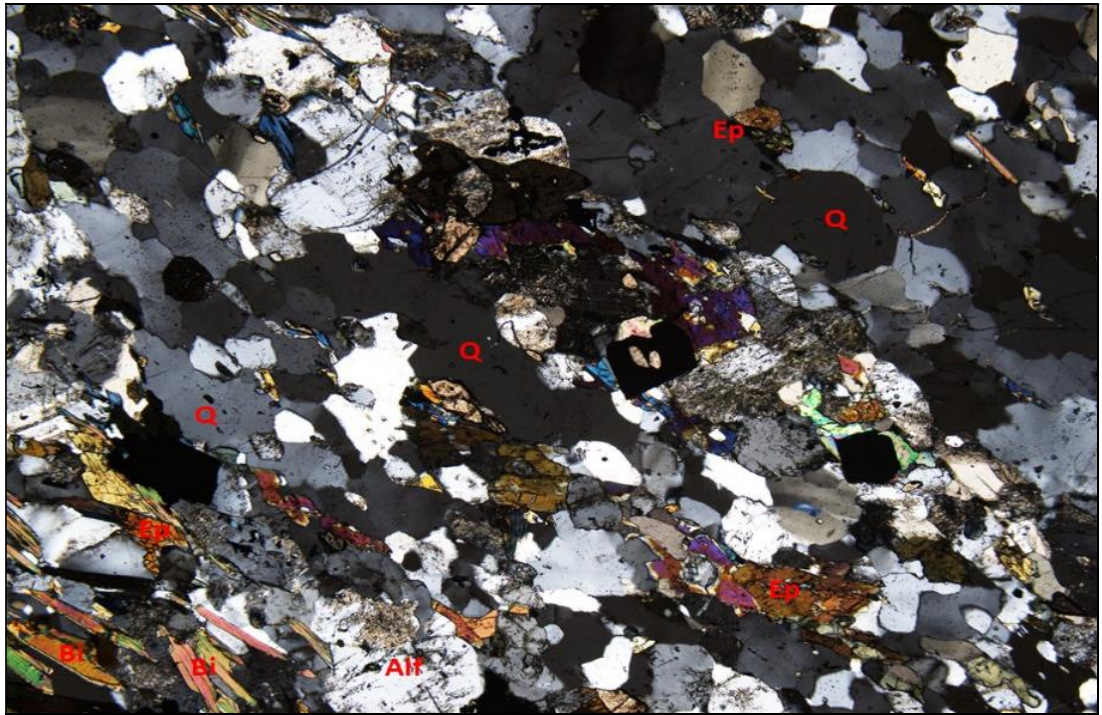


Figure 4.11: Photomicrograph of Intrusion 1 Area 2 in Transmitted Cross Polarized Light Indicating Q (Quartz), Alf/Plg (Alkali Feldspar)/ (Plagioclase), Bi (Biotite), Ep (Epidote).

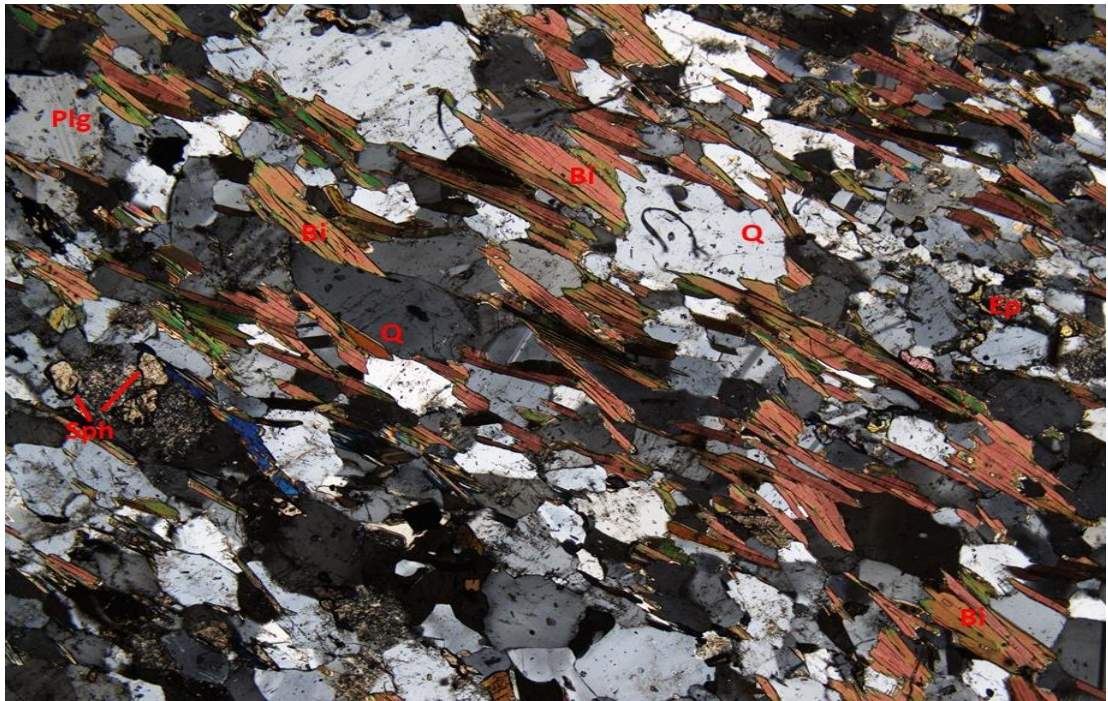


Figure 4.12: Photomicrograph of Intrusion 1 Area 3 in Transmitted Cross Polarized Light Indicating Q (Quartz), Alf/Plg (Alkali Feldspar)/ (Plagioclase), Bi (Biotite), Ep (Epidote), Sph (Sphene).

Table 4.2: Thin Section Analyses Results for Intrusion 1

Area	Mineral	Percentage %
I1 Area 1 PPI	Quartz (Q)	50 – 60
	Alkali Feldspar / Plagioclase (Alf/Plg)	30 – 35
	Biotite	10
I1 Area 2 PPI	Quartz (Q)	65
	Alkali Feldspar/ Plagioclase (Alf/Plg)	30 – 35
	Biotite (Bi)	1 – 5
	Diopside (Di)	1 – 5
	Trace Apatite (Ap), Trace Opaque (Opq), Chlorite (Cl) after Biotite	< 5
I1 Area 3 PPI	Quartz (Q)	60
	Alkali Feldspar/ Plagioclase (Alf/Plg)	25 – 35
	Biotite (Bi)	10 – 20
	Trace Apatite (Ap), Trace Opaque (Opq),	< 5
I1 Area 1 XPI	Quartz (Q)	65 – 75
	Alkali Feldspar (Alf)/ Plagioclase (Plg)	20 – 25
	Biotite	5 – 10
	Trace Epidote (Ep)	< 5
I1 Area 2 XPI	Quartz (Q)	60 – 65
	Alkali Feldspar (Alf)	25 – 30
	Biotite (Bi)	<10
	Trace Epidote (Ep)	< 5
I1 Area 3 XPI	Quartz (Q)	60 – 70
	Biotite (Bi)	20 – 25
	Plagioclase / Alkali Feldspar (Plg/Alf)	15 – 20
	Trace Sphene (Sph), Trace Epidote (Ep),	< 5

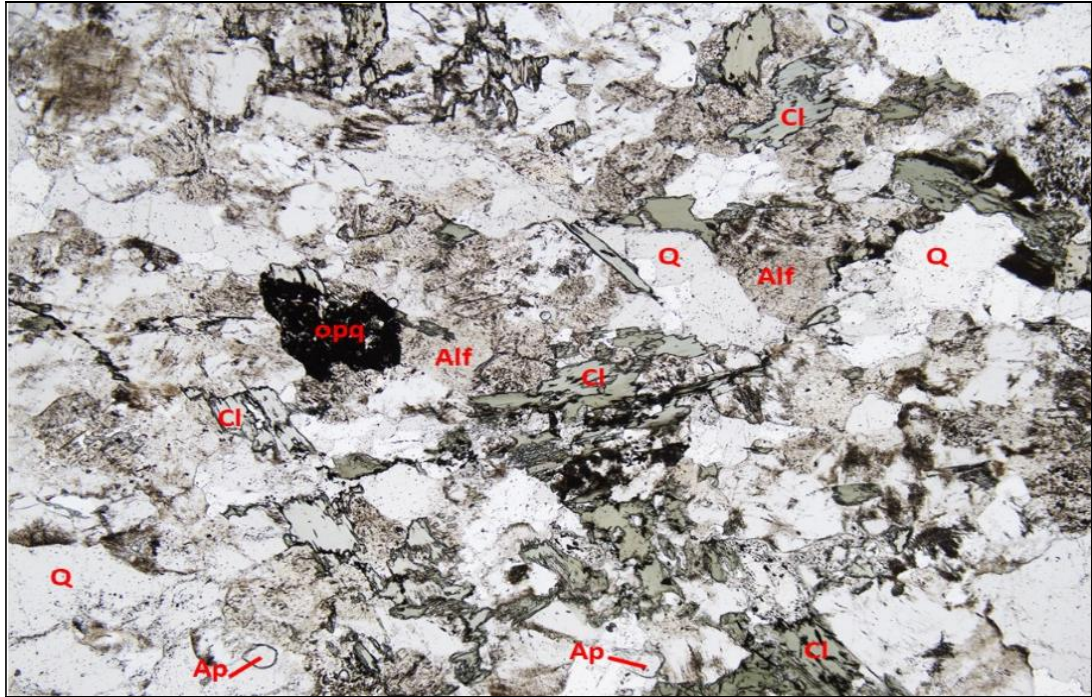


Figure 4.13: Photomicrograph of Intrusion 2 Area 1 in Transmitted Plane Polarized Light Indicating Q (Quartz), Alf (Alkali Feldspar), Cl (Chlorite), Ap (Apatite), Opq (Opaque).

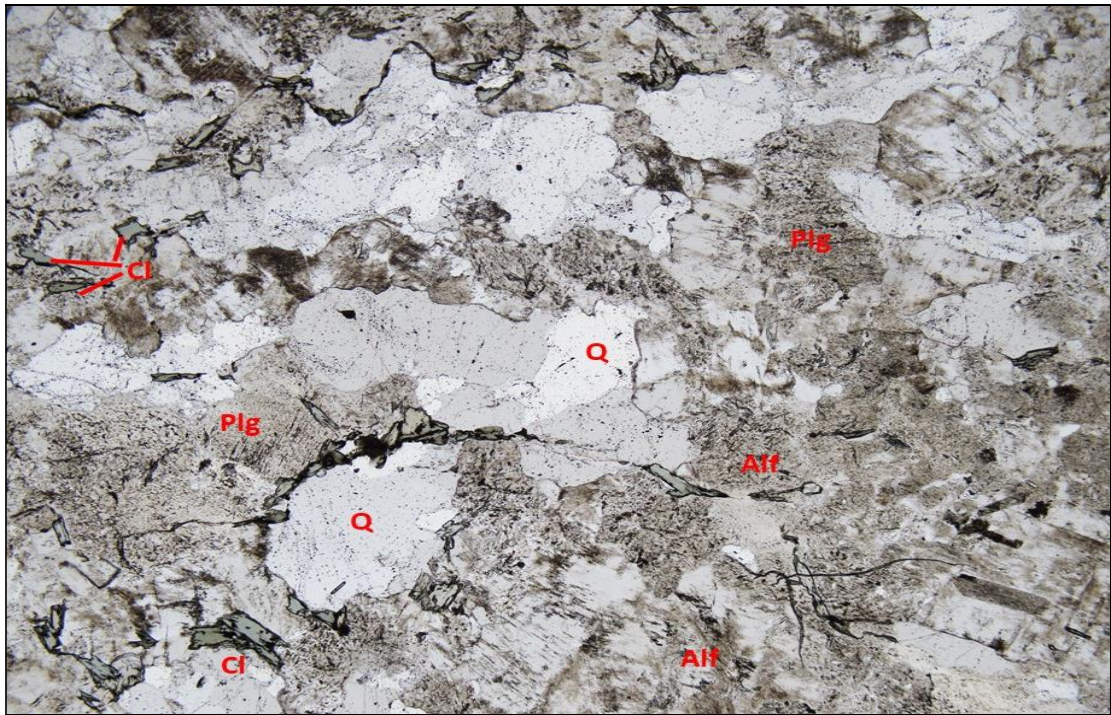


Figure 4.14: Photomicrograph of Intrusion 2 Area 2 in Transmitted Plane Polarized Light Indicating Q (Quartz), Plg/Alf (Plagioclase/Alkali Feldspar), Cl (Chlorite).

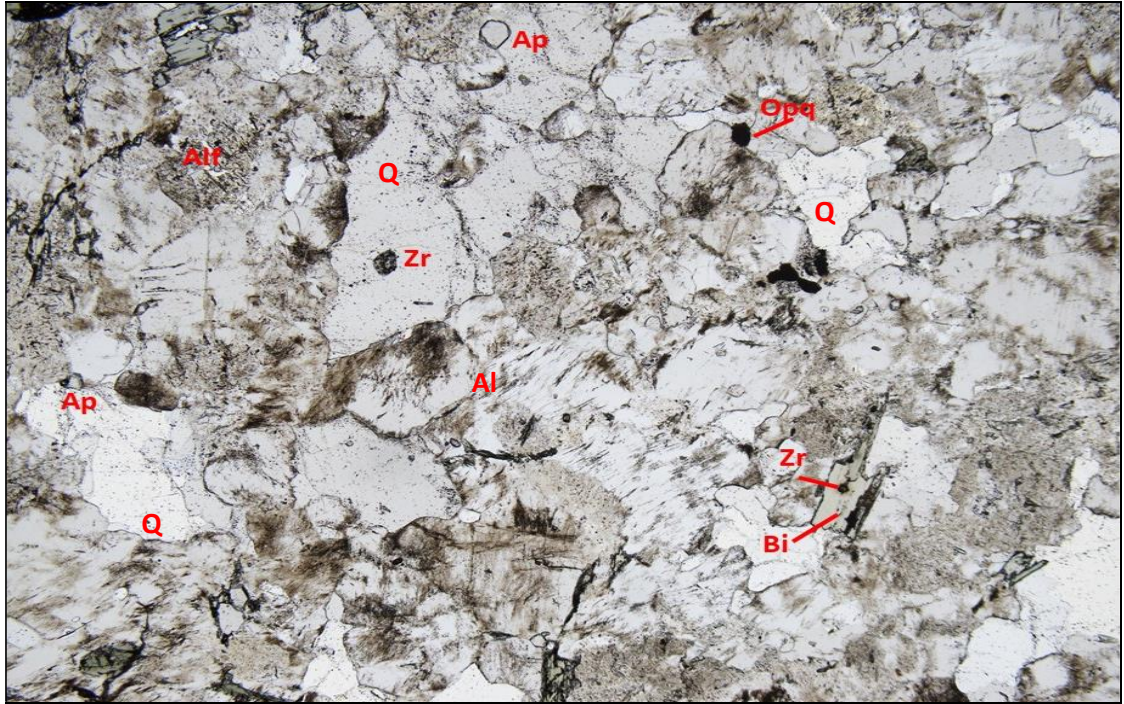


Figure 4.15: Photomicrograph of Intrusion 2 Area 3 in Transmitted Plane Polarized Light Indicating Q (Quartz), Alf (Alkali Feldspar), Bi (Biotite), Zr (Zircon), Ap (Apatite), Opq (Opaque).

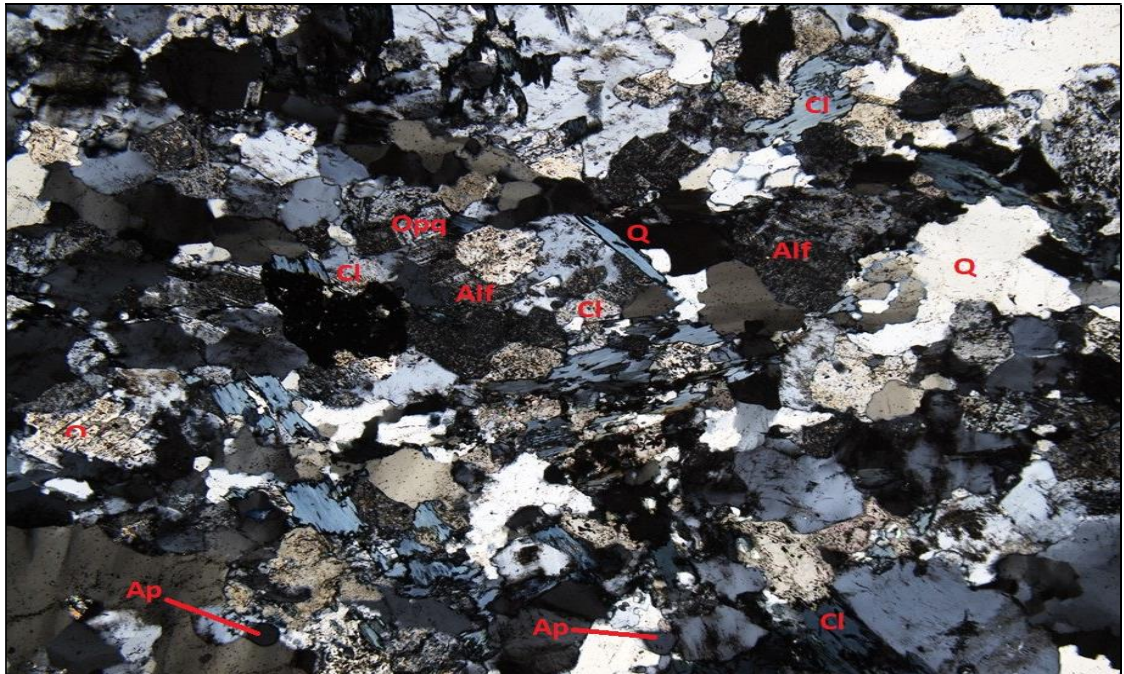


Figure 4.16: Photomicrograph of Intrusion 2 Area 1 in Transmitted Cross Polarized Light Indicating Q (Quartz), Alf (Alkali Feldspar), Cl (Chlorite), Ap (Apatite), Opq (Opaque).

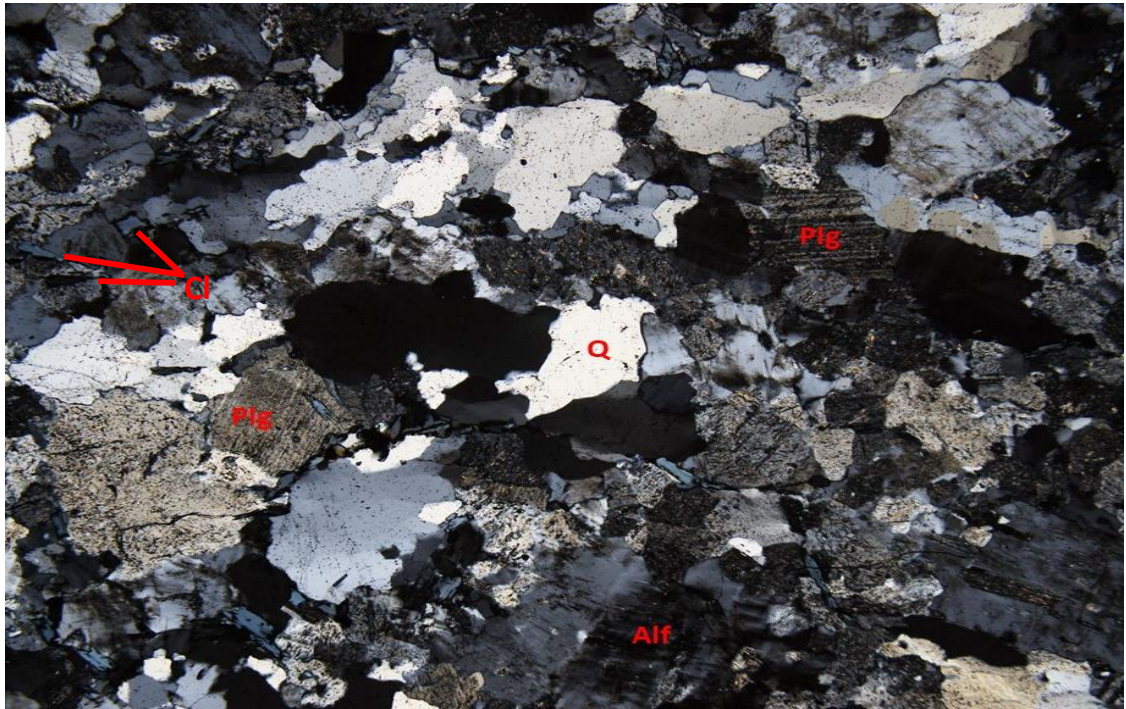


Figure 4.17: Photomicrograph of Intrusion 2 Area 2 in Transmitted Cross Polarized Light Indicating Q (Quartz), Plg/Alf (Plagioclase/Alkali Feldspar), Cl (Chlorite).

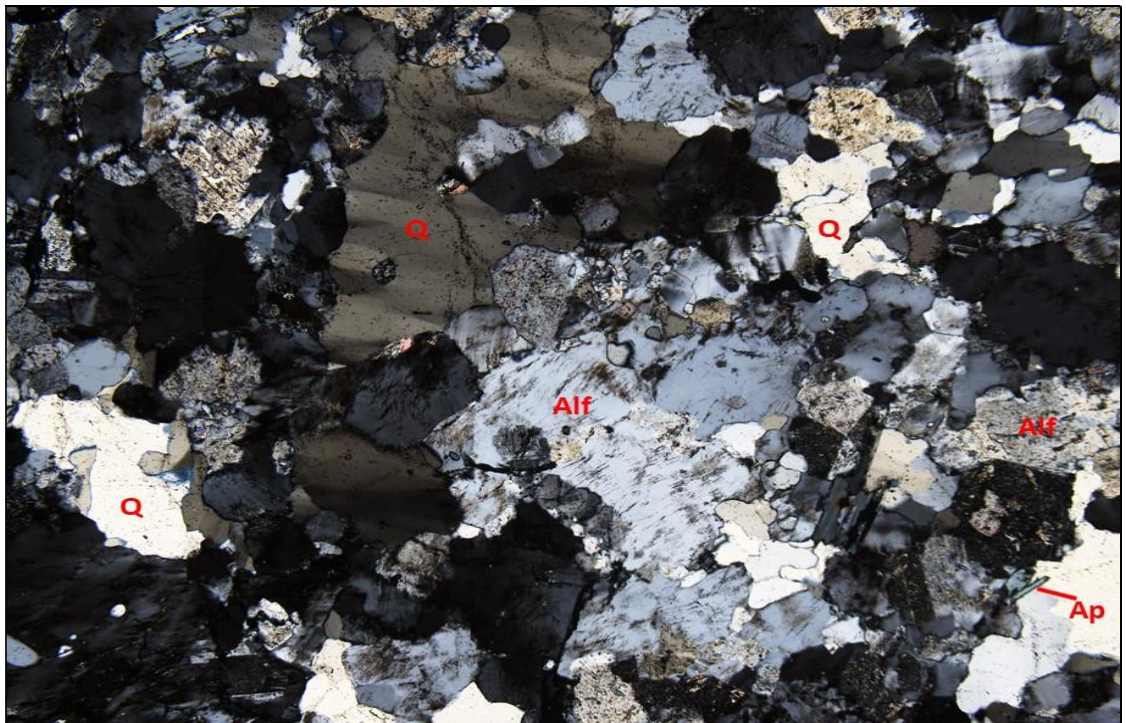


Figure 4.18: Photomicrograph of Intrusion 2 Area 3 In Transmitted Cross Polarized Light Indicating Q (Quartz), Alf (Alkali Feldspar), Ap (Apatite).

It is observed from the microscopic images that there are three minerals that are present in all the areas two are in a significant quantity, Quartz (60 – 70%) and Alkali Feldspar (25 – 30%), and Chlorite mineral that is present but, in less quantity, (5 – 10%). And other minor minerals that appeared in some of the areas in small quantities (less than 5%) which are Trace Apatite, Trace Opaque and a very minor quantity of Zircon that appears in area 3, Table 4.3 represents the thin section analyses results for Intrusion 2.

4.1.4.4 Thins Section from Intrusion 3 (I3)

Analyses of I3 thin section were done in six areas of the section, area 1, 2 and 3 in transmitted plane polarized light (Figures 4.19, 4.20 and 4.21) and area 1, 2, and 3 in transmitted cross polarized light (Figures 4.22, 4.23 and 4.24). These microscopic images indicate a significant similarity to I2. Coarse-grained, leucocratic (light-colored) with quartz, orthoclase, and plagioclase. Shows weak foliation. The orthoclase shows micropertite and Carlsbad twinning. The plagioclase shows Albite twinning. Feldspars have been variably altered to fine-grained sericite and contain inclusions of quartz and biotite. Quartz exhibits undulatory extinction. Biotite is brown to light-brown in colour, anhedral to subhedral. Biotites include inclusions of zircon with pleochroic halos. Feldspars contain inclusions of quartz and biotite. Accessory or trace minerals include apatite, calcite, zircon, muscovite, and possible rare allanite and rare opaque oxides or iron oxides. The biotite is weakly altered to chlorite. Myrmekite occurs in association with feldspars. Calcite replaces plagioclase and appears as an interstitial mineral phase.

It is observed from the microscopic images that there are three minerals that are present in all the areas but differ in concentration from area to another one, just like I2, two are in a significant quantity, Quartz (50 – 65%) and Plagioclase/Alkali Feldspar (20 – 35%). Some other different minerals are present but, in minor quantities like Biotite (< 5%), Muscovite (< 5%), Chlorite (< 5%), Epidote (< 5%) Trace Apatite (< 5%) and Trace Opaque (< 5%) Table 4.4 represents the results of thin section analyses for Intrusion 3.

Table 4.3: Results of Thin Section Analyses for Intrusion 2

Area	Mineral	Percentage %
I2 Area 1 PPI	Quartz (Q)	60 – 70
	Alkali Feldspar (Alf)	25 – 30
	Chlorite (Cl) after Biotite	5 – 10
	Trace Apatite (Ap), Trace Opaque (Opq)	< 5
I2 Area 2 PPI	Quartz (Q)	60
	Plagioclase/Alkali Feldspar (Plg/Alf)	30 – 35
	Chlorite (Cl) after Biotite	< 5
I2 Area 3 PPI	Quartz (Q)	60 – 70
	Alkali Feldspar (Alf)	25 – 30
	Chlorite (Cl) after Biotite	5 – 10
	Trace Apatite (Ap), Trace Opaque (Opq)	< 5 %
I2 Area 1 XPI	Quartz (Q)	65 – 75
	Alkali Feldspar (Alf)/ Plagioclase (Plg)	20 – 25
	Chlorite (Cl) after Biotite	5 – 10
	Trace Apatite (Ap), Trace Opaque (Opq)	< 5 %
I2 Area 2 XPI	Quartz (Q)	60 – 70
	Alkali Feldspar (Alf)	25 – 30
	Chlorite (Cl) after Biotite	5
I2 Area 3 XPI	Quartz (Q)	60 – 70
	Alkali Feldspar (Alf)	25 – 30
	Trace Apatite (Ap), Trace Opaque (Opq)	< 5 %

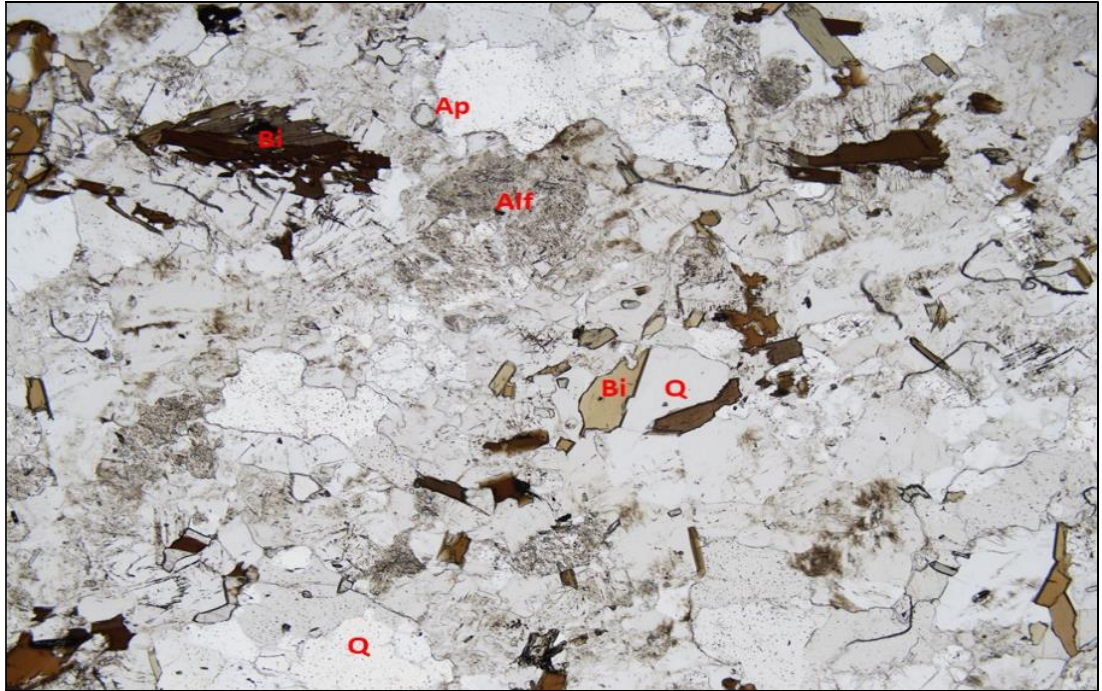


Figure 4.19: Photomicrograph of Intrusion 3 Area 1 in Transmitted Plane Polarized Light Indicating Q (Quartz), Alf (Alkali Feldspar), Biotite (Bi) and Ap (Apatite)

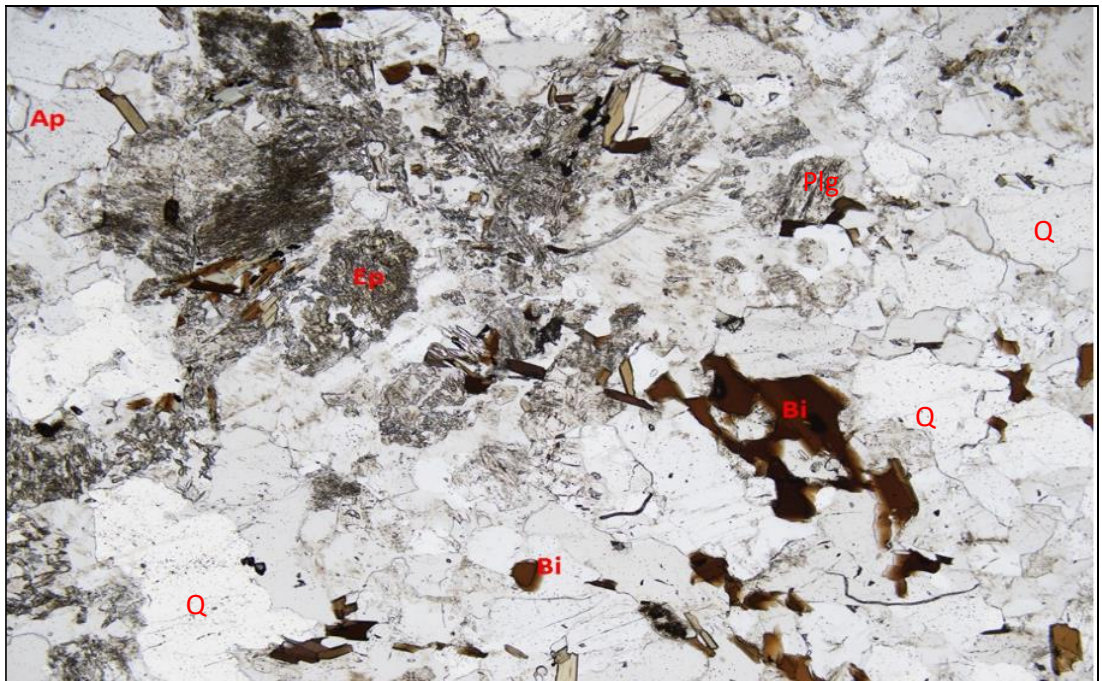


Figure 4.20: Photomicrograph of Intrusion 3 Area 2 in Transmitted Plane Polarized Light Indicating Q (Quartz), Plg (Plagioclase), Biotite (Bi), Ap (Apatite) and Ep (Epidote)

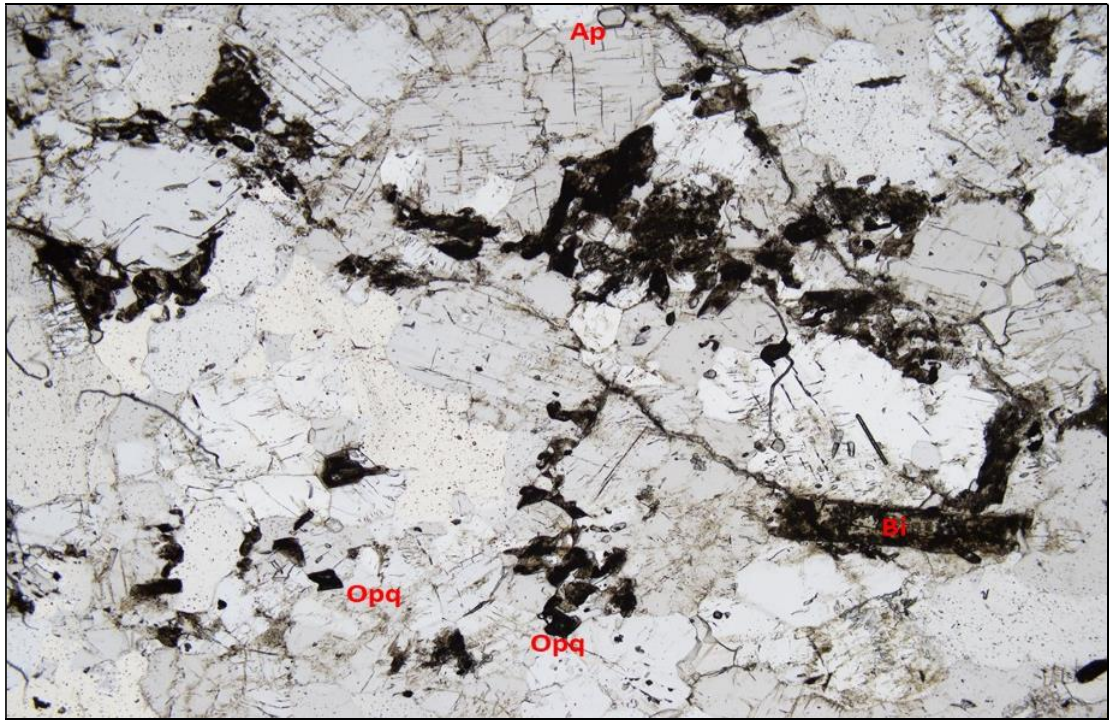


Figure 4.21: Photomicrograph of Intrusion 3 Area 3 in Transmitted Plane Polarized Light Indicating Bi (Biotite), Ap (Apatite) and Opq (Opaque)

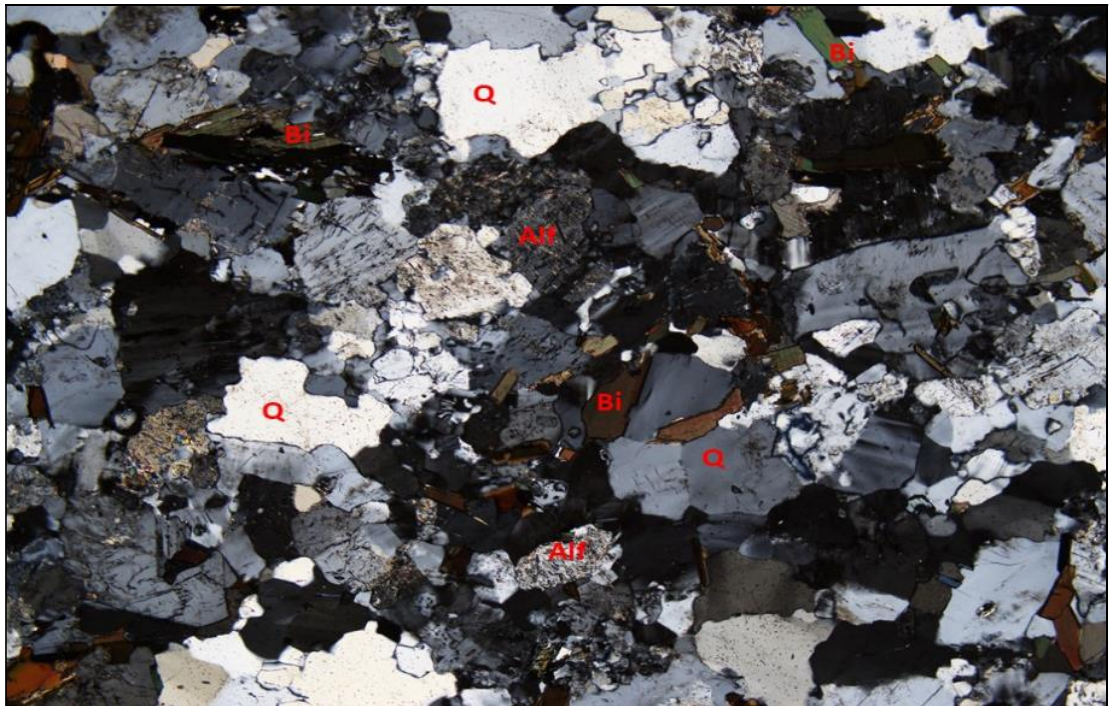


Figure 4.22: Photomicrograph of Intrusion 3 Area 1 in Transmitted Cross Polarized Light Indicating Q (Quartz), Alf (Alkali Feldspar) and Bi (Biotite)

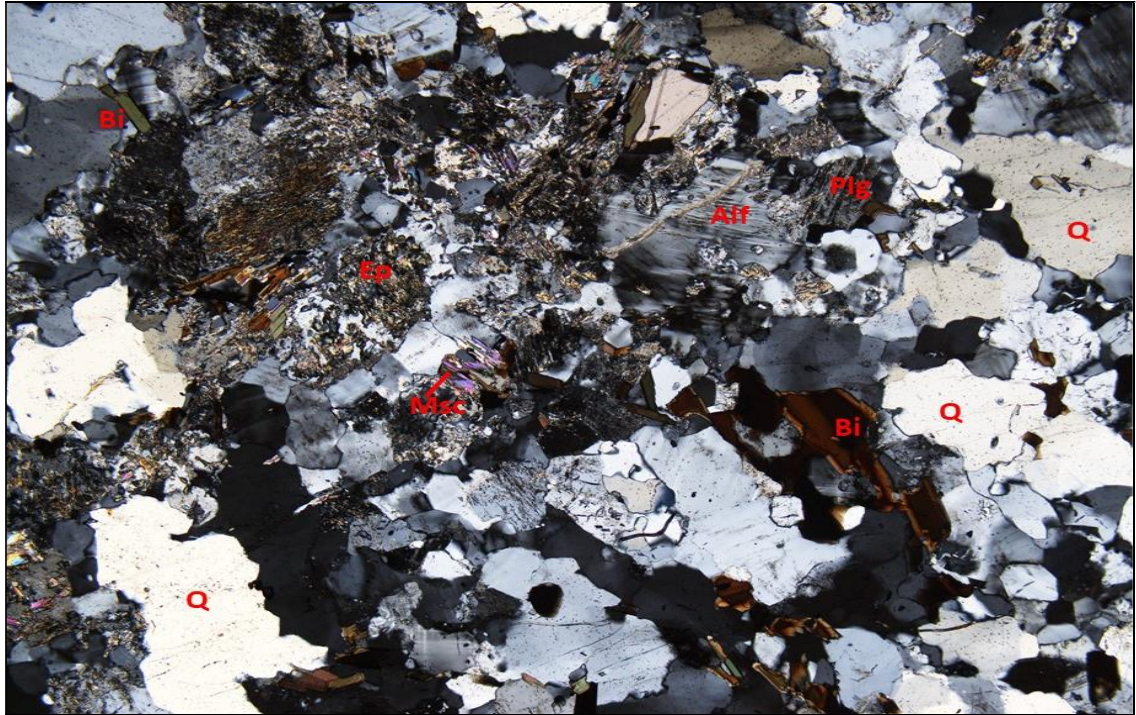


Figure 4.23: Photomicrograph of Intrusion 3 Area 2 in Transmitted Cross Polarized Light Indicating Q (Quartz), Alf (Alkali Feldspar), Plagioclase (Plg), Bi (Biotite) and Trace Muscovite (Msc)

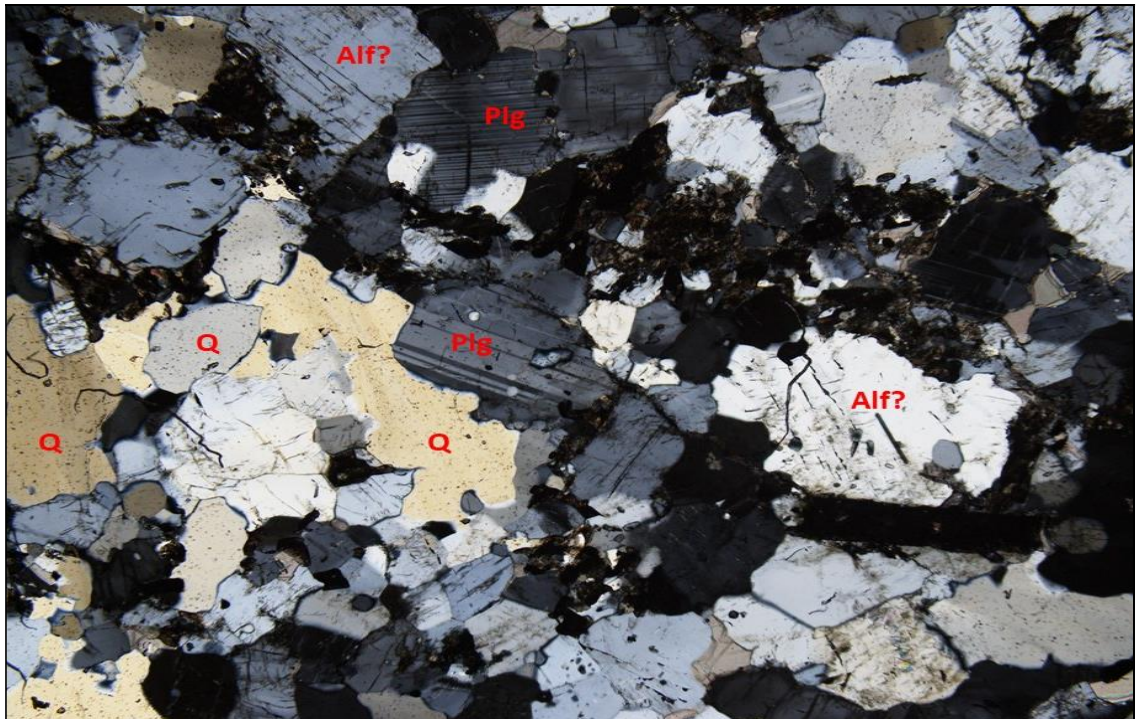


Figure 4.24: Photomicrograph of Intrusion 3 Area 3 in Transmitted Cross Polarized Light Indicating Q (Quartz), Alf (Alkali Feldspar), Plagioclase (Plg)

Table 4.4: Results of Thin Section Analyses for Intrusion 3

Area	Mineral	Percentage %
I3 Area 1 PPI	Quartz (Q)	60 – 65
	Plagioclase / Alkali Feldspar (Plg/Alf)	30 – 35
	Biotite (Bi)	< 5
	Trace Apatite (Ap)	< 5
I3 Area 2 PPI	Quartz (Q)	60 – 65
	Plagioclase/Alkali Feldspar (Plg/Alf)	30 – 35
	Biotite (Bi)	< 5
	Trace Apatite (Ap)	< 5
	Muscovite (Msc)	< 5
	Epidote (Ep* after Plg)	5 – 10
I3 Area 3 PPI	Quartz (Q)	50 – 60
	Plagioclase (Plg)	20 – 25
	Biotite (Bi)	10
	Trace Apatite (Ap), Trace Opaque (Opq)	< 5
I3 Area 1 XPI	Quartz (Q)	60 – 65
	Plagioclase/ Alkali Feldspar (Plg/Alf)	20 – 25
	Biotite	< 5
I3 Area 2 XPI	Quartz (Q)	60 – 65
	Plagioclase/ Alkali Feldspar (Plg/Alf)	30 – 35
	Biotite	< 5 %
	Chlorite (Cl)	< 5 %
I3 Area 3 XPI	Quartz (Q)	50 – 60
	Plagioclase/ Alkali Feldspar (Plg/Alf)	20 – 25
	Biotite	< 10
	Trace Apatite (Ap), Trace Opaque (Opq)	< 5

4.1.4.5 Summary of the Petrographic Analyses

It appears from all the results of the petrographic analyses that I1 and the marble are strongly metamorphosed. The marble is originated from limestone. And I2 and I3 intruded later. The presence of siderite and possible diopside supports the idea that I1 is a meta-sedimentary rock, possibly it was an interbed of limestone. The domination of Calcite in the marble (99%) calls for attention in this research project that deals with slope stability. Calcite disintegrates when exposed to rain water, and produces calcium hydroxide and carbon dioxide. Rainwater and carbon dioxide react to produce carbonic acid which reacts with calcite causing dissolution of calcite. Therefore, dissolution of marble that causes caverns, sinkholes and other features, hence, the slope instability and failure.

4.1.5 Geological 3D Model of the Deposit

The geological 3D model of the deposit at Ikpobia Quarry shows the concentration of marble and limestone which is mainly at the centre and to the western parts of the quarry with a depth of around 80 meters and in lesser concentration at the eastern part where the depth of marble and limestone is around 70 meters. It is remarkable that the eastern part has less concentration of marble and limestone and the depth reduces the more it goes to the west (Figures 4.25 and 4.26). This also appears on the fence diagram (Figure 4.27) but with some granite, gneiss and micrite intrusions that are mostly in the eastern part of the quarry. All this implicates that the depth of the pit will continue increasing at the centre and to the west of the quarry where the pit slope will be riskier and more prone to failure and instability which gives an early idea about the future failure possible locations.

4.1.6 Geophysical, Hydrogeological and Groundwater Investigation

The geophysical investigation in this research project tends to characterise the internal structure and the lithological properties of the soil and rock mass which play a significant role in the determination of geomechanical characterisation and the groundwater flow through the vertical electrical sounds VES which is based on the difference in resistivity between different sub-surface materials. The results of this method provided data that helped to enhance the understanding of geology and groundwater of the site because it covers a larger area and gives a continues information of the soil profile that can be used in predicting the slope behaviour.

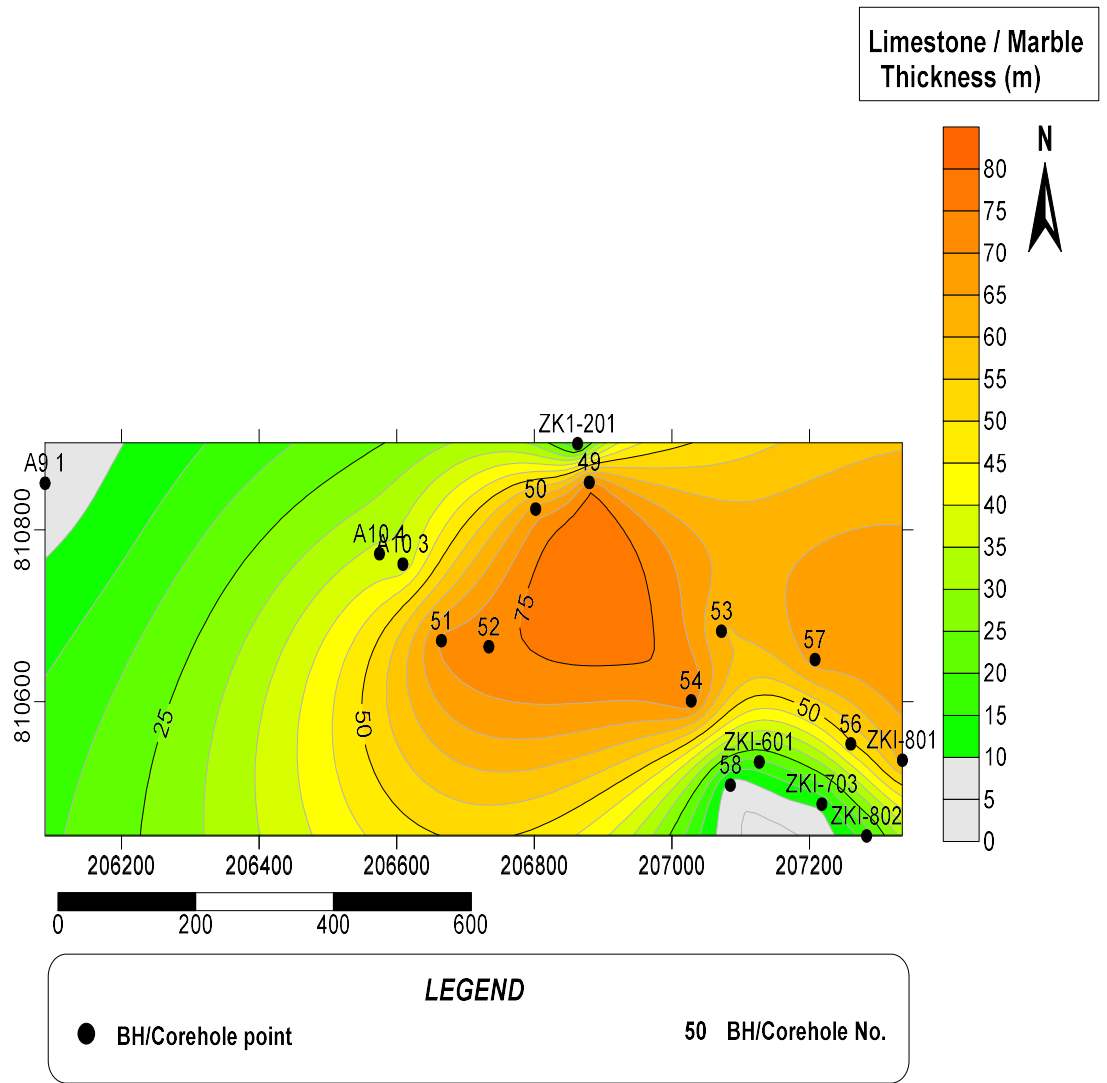


Figure 4.25: Concentration Map the Deposit with Coreholes Superimposed

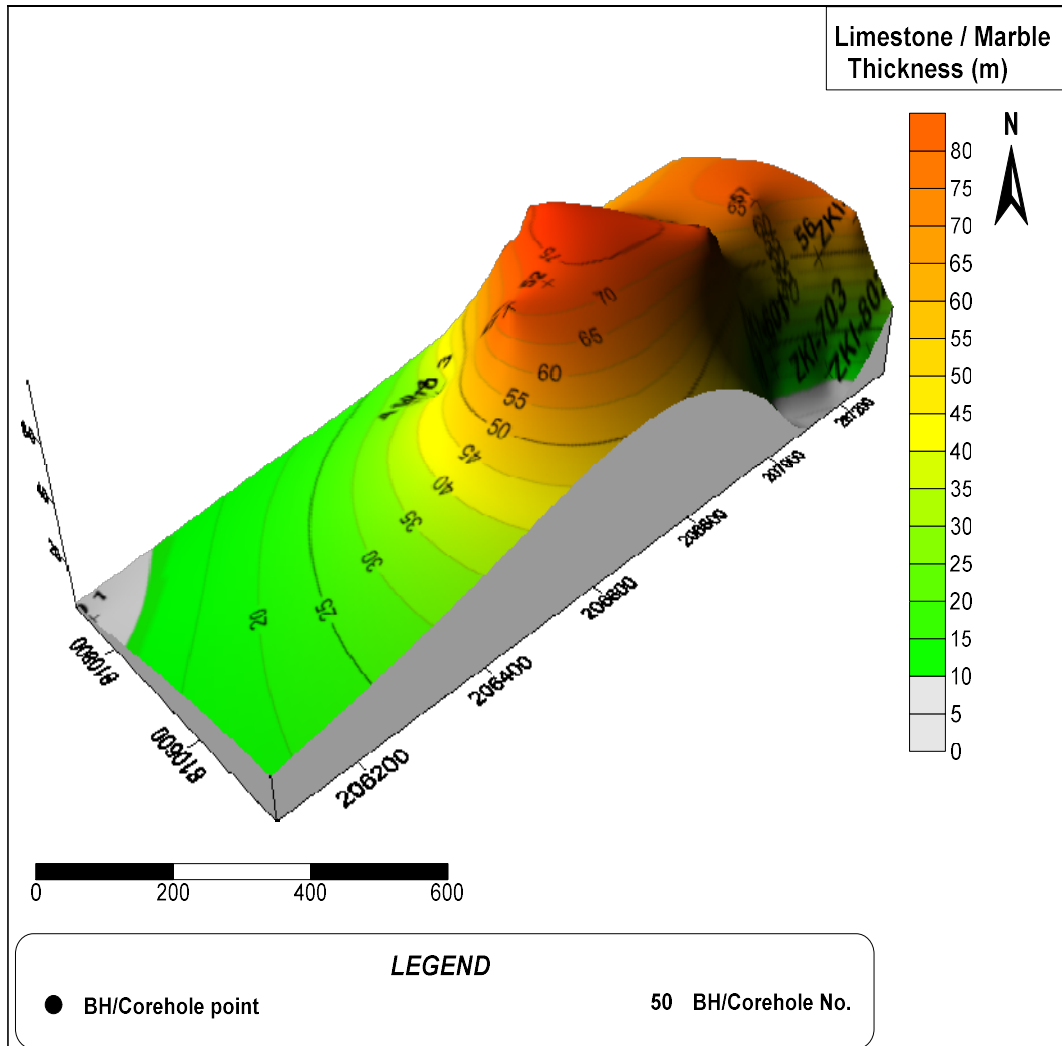


Figure 4.26: 3-D Geological Model of the Deposit with Coreholes Superimposed

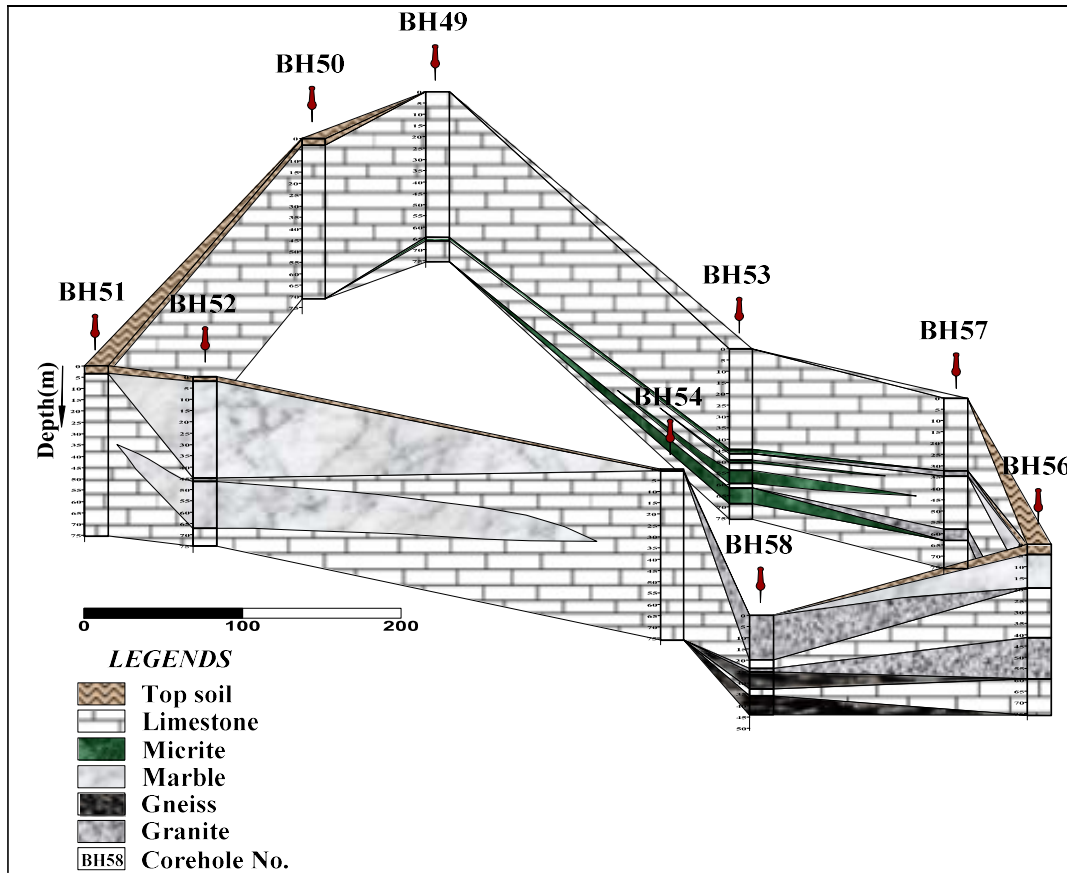


Figure 4.27: Fence Diagram of the Deposit

4.1.6.1 Data Processing and Interpretation of VES Results

The Vertical Electrical Sounding (VES) that was used is the conventional Schlumberger array method which is based on the gradual increasing of interelectrode spacing about fixed center of array. For processing data of Schlumberger method, it is needed to calculate the apparent resistivity (ρ_a) through the multiplication of the resistance got from the field and the geometric factors $\rho_a = 2\pi(a^2/b - b/4)R$.

4.1.6.2 Qualitative Interpretation

The first stage of the interpretation of resistivity sounding curve is noting the curve shape. This is categorised for three electrical layers in one of four basic curve shapes which are H, A, K and Q and can be combined to describe more complex field curves that may have several layers. In this study the model curves obtained have Root Mean Square error (RMS) of less than 5% in the majority of the curves, which is the total squared error between the field data and the fitted curves, and show A, HA, HK, KH, and K with H dominating. Some representatives of different curve types that were obtained at the pit are shown in (Figure 4.28), while the rest are shown in APPENDIX A. The quantitative analyses which refer to the proportion of curves of each type, relative to the total number of curves (26 curves of 26 VES points), showed that the A curves constitute 18% and are characterized by an increase in resistivity from topsoil to the bedrock, HA type represents 4%, HK 4%, KH 4%, K 8% and H 62% of the total (Figure 4.29). In the Ikpobia site the dominant type of curves is the type H (62%) that implies that the quarry site is water saturated, according to Jones and Jovanovich, (1985), who reported that in the H type, the intermediate layer is usually water saturated and has low resistivity, high porosity, and low permeability. The interpretation of the sounding curves permitted their classification which is illustrated in Table 4.5.

4.1.6.3 Relationship of the Curve Types with Geology

The distribution of the curve types across the area shows that the H related curves are the dominant types and it is common to all the rock types of granodiorite tonalite gneiss, augen gneiss, hypersthene granite, older granite, pegmatite, quartzite, pelitic metasediments.

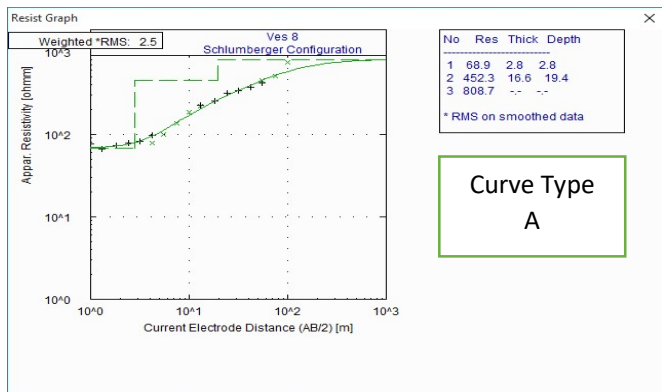
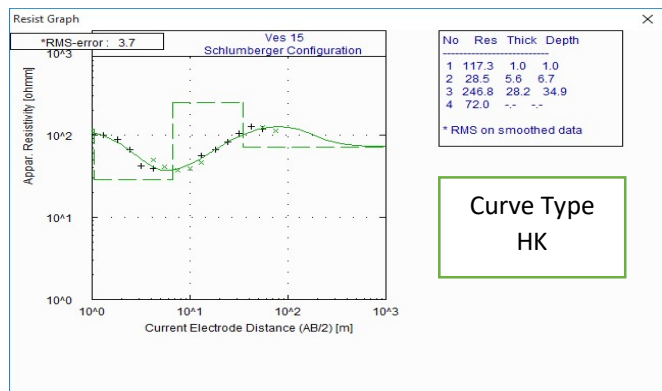
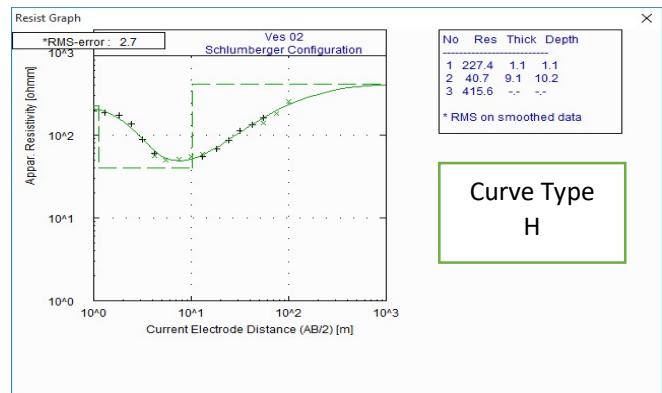
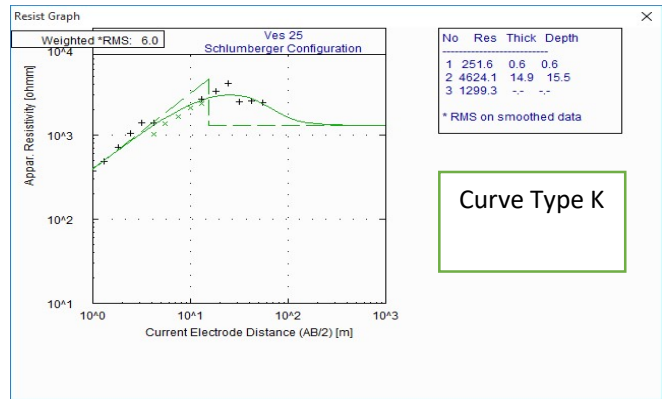


Figure 4.28: Representative VES Curves for Some Different Curve Types

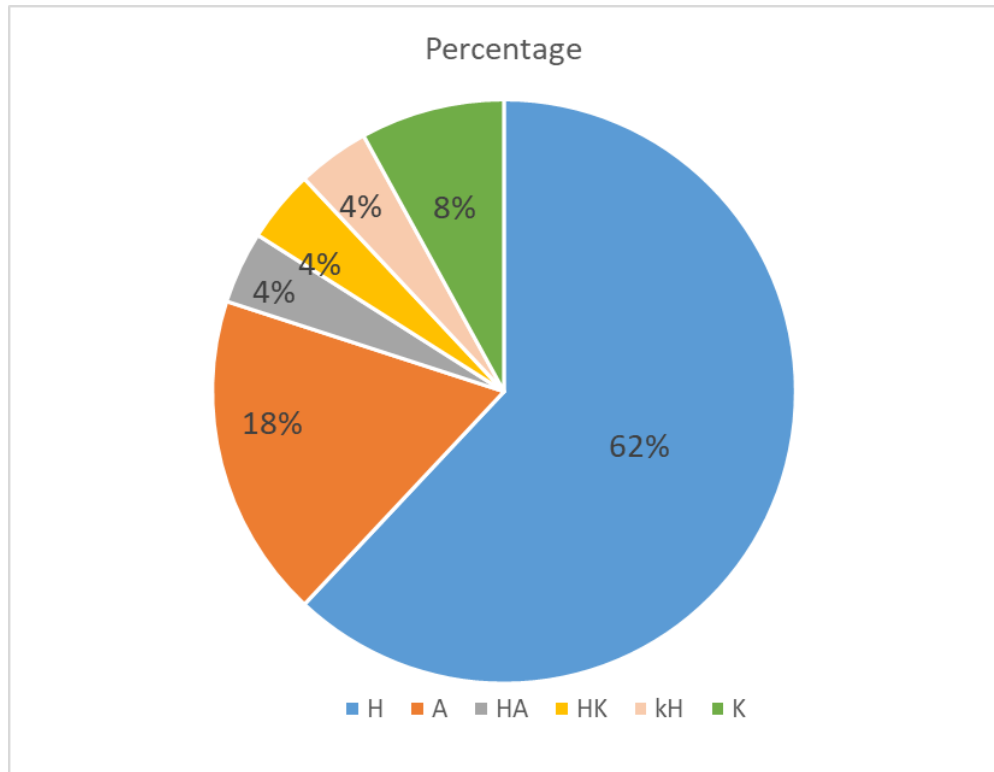


Figure 4.29: The Distribution of the Curve Types

Table 4.5: Quantitative Interpretation of the VES Data from the Quarry

VES No	Layer Resistivity(Ω m)	Thickness(m)	Depth(m)	Probable Lithology	Curve Type	RMS Error%
1	96	0.9	0.9	<i>Top Soil</i>	H	2.6
	56	14.9	15.8	<i>Weathered Bedrock</i>	–	
	2704			<i>Fresh Bedrock (Granite)</i>	–	
2	227	1.1	1.1	<i>Top Soil</i>	H	2.7
	41	9.1	10.2	<i>Weathered Bedrock</i>	–	
	416			<i>Fractured Bedrock (Limestone)</i>		
3	184	0.5	0.5	<i>Top Soil</i>	H	3.5
	35	15.6	16.1	<i>Weathered Bedrock</i>	–	
	704			<i>Fractured Bedrock (Limestone)</i>		
4	141	0.4	0.4	<i>Top Soil</i>	H	4.6
	12	6.6	7.0	<i>Weathered Bedrock(saturated clay)</i>	–	
	1716			<i>Fresh Bedrock (Limestone)</i>	–	
5	116	0.8	0.8	<i>Top Soil</i>	H	2.5
	34	14.4	15.2	<i>Weathered Bedrock</i>	–	
	396			<i>Fractured Bedrock (Marble)</i>		
6	50	1.3	1.3	<i>Top Soil</i>	H	2.4
	26	7.1	8.4	<i>Weathered Bedrock(saturated clay)</i>	–	
	495			<i>Fractured Bedrock (Marble)</i>	–	
7	71	0.7	0.7	<i>Top Soil</i>	H	2.5
	33	2.1	2.8	<i>Weathered Bedrock</i>	–	
	345			<i>Fractured Bedrock (Marble)</i>	–	
8	69	2.8	2.8	<i>Top Soil</i>	A	2.5
	452	16.6	19.4	<i>Weathered Bedrock</i>	–	
	809			<i>Fractured Bedrock (Limestone)</i>	–	

Table 4.5: Quantitative Interpretation of the VES Data from the Quarry (Continued)

9	56	10.2	10.2	<i>Top Soil</i>	A	2.6
	1702			<i>Fresh Bedrock (Limestone)</i>	–	
					–	
10	40	0.7	0.7	<i>Top Soil</i>	HA	3.4
	15	1.2	1.9	<i>Saturated Clay</i>	–	
	133	26	27.8	<i>Weathered Bedrock</i>	–	
	845			<i>Fractured Bedrock (Limestone)</i>		
11	140	0.8	0.8	<i>Top Soil</i>	H	2.9
	68	2.6	3.4	<i>Weathered Bedrock</i>	–	
	777			<i>Fractured Bedrock(Limestone)</i>	–	
12	31	1.3	1.3	<i>Top Soil</i>	A	8.7
	258	1.5	2.8	<i>Weathered Bedrock</i>	–	
	13335			<i>Fresh Bedrock (Granite)</i>		
13	61	3.8	3.8	<i>Top Soil</i>	A	4.4
	5757			<i>Fresh Bedrock (Limestone)</i>	–	
					–	
14	130	0.7	0.7	<i>Top Soil</i>	H	3.6
	75	1.1	1.8	<i>Weathered Bedrock</i>	–	
	1748			<i>Fresh Bedrock (Limestone)</i>		
15	117	1.0	1.0	<i>Top Soil</i>	HK	3.7
	29	5.6	6.6	<i>Saturated Clay</i>	–	
	247	28.2	34.8	<i>Weathered Bedrock</i>		
	72			<i>Fractured Bedrock (Limestone)</i>		
16	94	1.9	1.9	<i>Top Soil</i>	H	3.9
	59	13.5	15.4	<i>Weathered Bedrock</i>	–	
	689			<i>Fresh Bedrock (Limestone)</i>	–	

Table 4.5: Quantitative Interpretation of the VES Data from the Quarry (Continued)

17	79	0.7	0.7	<i>Top Soil</i>	H	4.0
	59	4.3	5.0	<i>Weathered Bedrock</i>	–	
	1032			<i>Fresh Bedrock</i>		
18	58	1.2	1.2	<i>Top Soil</i>	H	5.1
	17	8.6	9.8	<i>Weathered Bedrock</i>	–	
	3629			<i>Fresh Bedrock (Limestone)</i>	–	
19	101	1.2	1.2	<i>Top Soil</i>	H	2.5
	71	11.8	13.0	<i>Weathered Bedrock</i>	–	
	1532			<i>Fresh Bedrock (Limestone)</i>	–	
20	71	1.7	1.7	<i>Top Soil</i>	H	2.5
	33	7.3	9.0	<i>Weathered Bedrock</i>	–	
	709			<i>Fractured Bedrock (Limestone)</i>	–	
21	356	2.0	2.0	<i>Top Soil</i>	K	2.5
	3890	17.8	19.8	<i>Fresh Bedrock (Marble)</i>	–	
	937			<i>Fractured Bedrock (Marble)</i>	–	
22	93	0.5	0.5	<i>Top Soil</i>	KH	6.7
	3024	5.3	5.8	<i>Bedrock (Marble)</i>	–	
	187	17.3	23.1	<i>Fractured Bedrock (Marble)</i>	–	
	3924			<i>Fresh Bedrock (Marble)</i>		
23	745	2.0	2.0	<i>Top Soil (Marble)</i>	H	2.4
	255	5.1	7.1	<i>Weathered Bedrock (Marble)</i>	–	
	4215			<i>Fresh Bedrock (Marble)</i>	–	
24	96	0.8	0.8	<i>Top Soil (Marble)</i>	H	3.2
	43	1.7	2.5	<i>Fractured Bedrock (Marble)</i>	–	
	644			<i>Fresh Bedrock (Marble)</i>		
25	252	0.6	0.6	<i>Top Soil</i>	K	6.0
	4624	14.9	15.5	<i>Fresh Bedrock (Limestone)</i>	–	
	1299			<i>Fresh Bedrock (Limestone)</i>	–	
26	739	3.7	3.7	<i>Top Soil</i>	A	4.9
	69950			<i>Fresh Bedrock (Marble)</i>	–	

4.1.6.4 Geoelectric Sections

Geoelectric sections along profiles 1, 2, 3, 4 and 5 were drawn for the study area using the VES results supplied by geological information, Figure 4.30 shows the geoelectric profile lines and their positions relative to each other. In more detailed the dispositions of these sections are shown in Figures 4.31 – 4.35. The geoelectric sections show alternations of bedrock ridges and depressions. The fractured basement has resistivity value of less than 1000 ohm-m (Verma et al, 1980) and the fresh basement has resistivity value of greater than 1000 ohm-m.

4.1.6.4.1 Geoelectric Section Along Profile 1

Probable geoelectric sequence along this section is shown in (Figure 4.31). It shows a sequence of three geoelectric layers which represent clay/ clayey sand topsoil, with resistivity ranges between 96 - 101 ohm m and a mean thickness of 0.9 – 2.0 m, weathered bedrock, a fractured bedrock and fresh bedrock. The weathered bedrock directly underlies the topsoil with a resistivity ranging between 33 – 71 ohm m and a thickness between 7.3 – 14.9 m, underlined by weathered layer that is partly fractured/fresh bedrock of limestone with a resistivity that ranges between 709 - 3629 ohm m and a small occurrence of granite at the extreme left end of the profile under the VES point 1.

4.1.6.4.2 Geoelectric Section Along Profile 2

Three layers were equally recognized along this profile (Fig. 4.32). The clayey topsoil which has resistivity of between 69 – 227 ohm- m and a thickness of between 0.4 and 2.8 m. The weathered basement has resistivity of between 12 and 452 ohm- m with thickness extending from 2.1 – 16.6 m. This layer rest on top of the fractured/fresh basement rock of marble and limestone of resistivity ranging from 345 - 2704 ohm –m and occurrence of granite at the extreme right end of the profile under the VES point 1.

4.1.6.4.3 Geoelectric Section Along Profile 3

The profile along this section is shown in Figure 4.34. It shows a sequence of three geoelectric layers which comprises of clayey topsoil with resistivity ranged from 79 – 745 ohm-m, and a thickness that ranges between 0.4 - 2 m. The weathered layer with resistivity varying from 12 – 937 ohm – m and thickness ranges between 4.3 – 17.8 m.

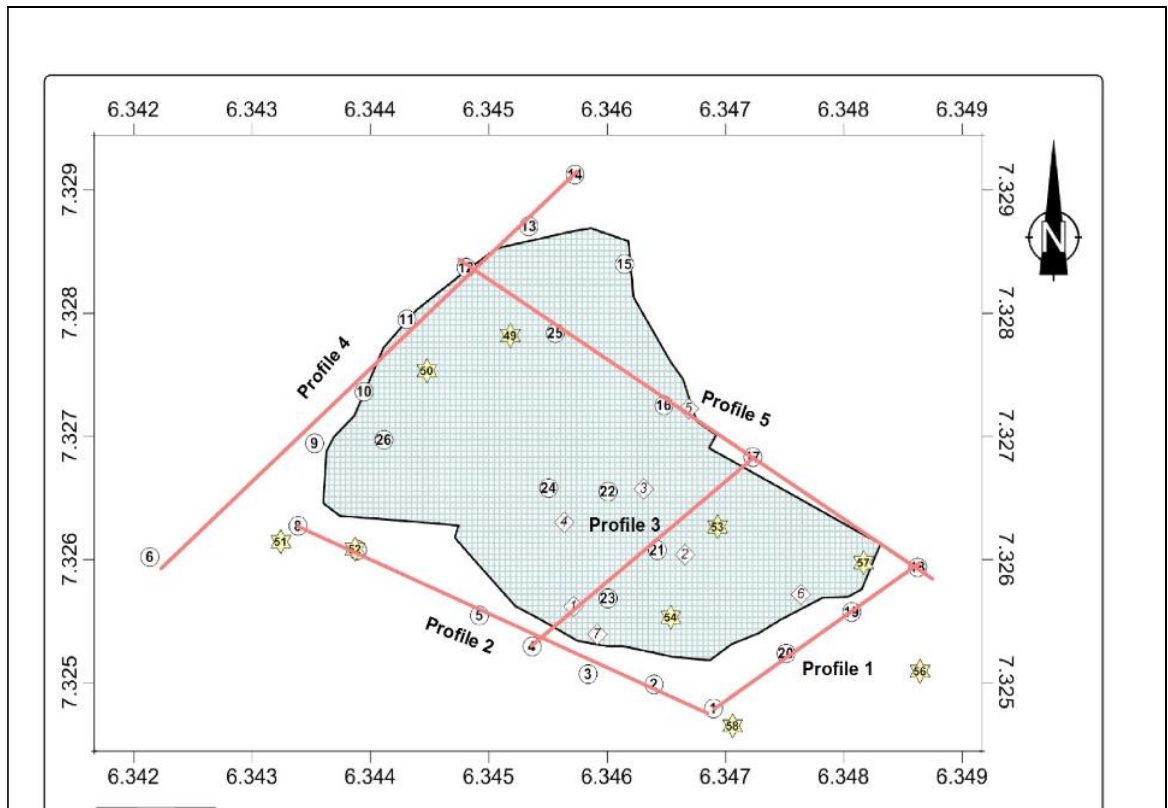


Figure 4.30: Geoelectric Profile Lines in the Ikpobia Quarry

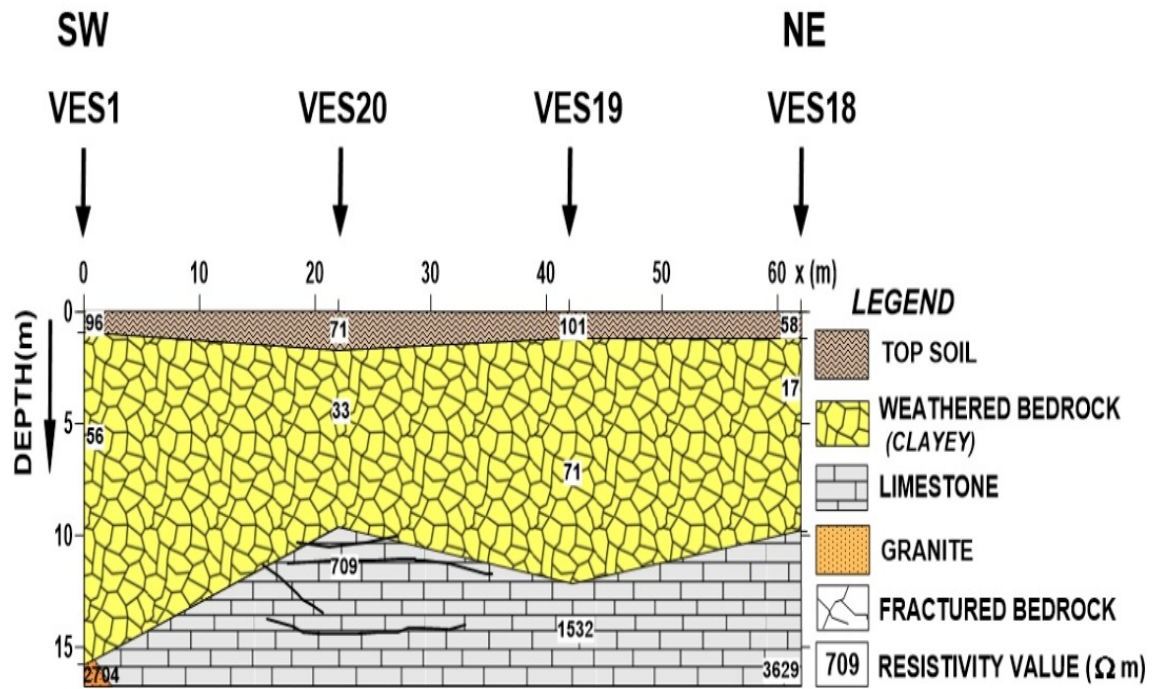


Figure 4.31: Geoelectric Section Along Profile1 (VES1, VES20, VES19, VES18)

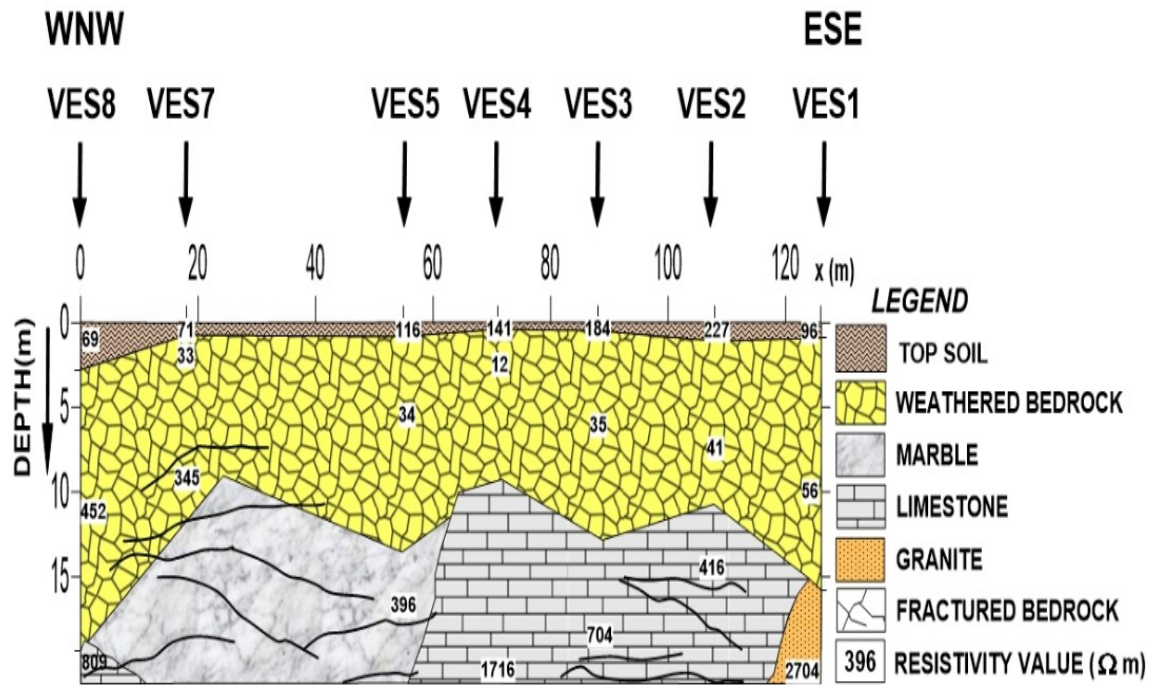


Figure 4.32: Geoelectric Section along Profile 2 (VES8, VES7, VES5, VES4, VES3, VES2, VES1)

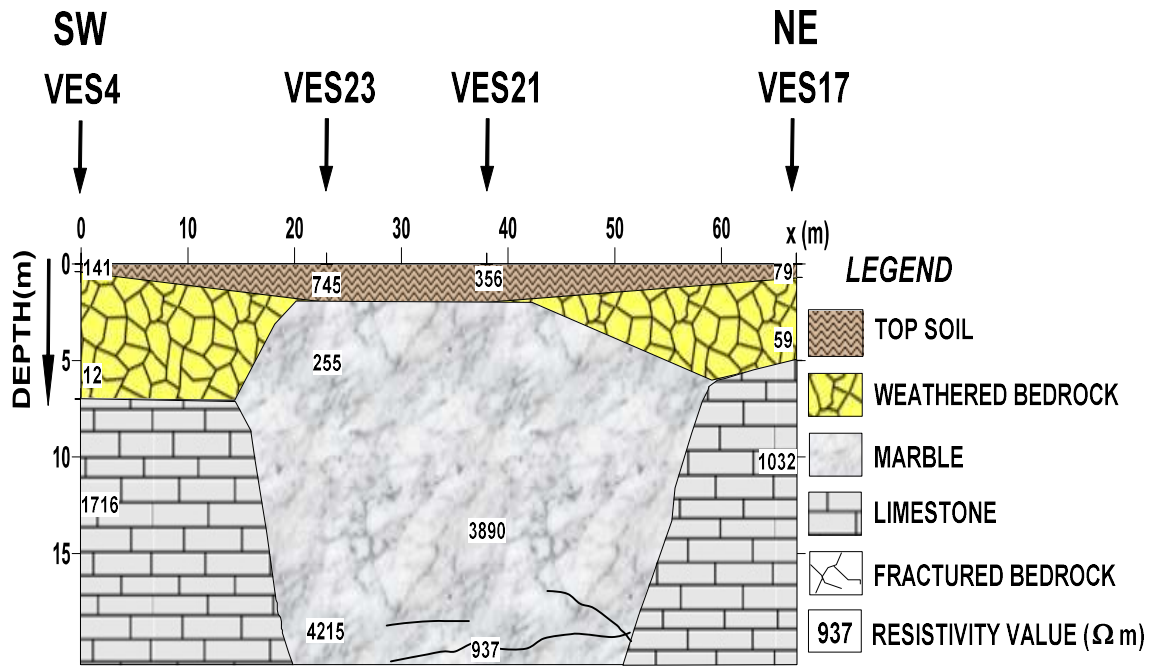


Figure 4.33: Geoelectric section along profile 3 (VES4, VES23, VES21 & VES17)

The last layer is the partly fractured/fresh basement of marble and limestone with resistivity between 937 – 4215 ohm-m.

4.1.6.4.4 Geoelectric Section Along Profile 4

This profile comprises mostly three layers with a small layer of saturated clay between the topsoil and the weathered bedrock under VES 10 and VES 11 as shown in Figure 4.34. The topsoil comprises clay soil with a resistivity that ranges between 8.0 and 24.0 ohm. The weathered layer has resistivity of between 31 and 140 ohm – m, and thickness ranging from 6.7 – 17.5 m with resistivity of between 98.0 and 4504.0 ohm - m. The overburden thickness has a mean of 12.2 m.

4.1.6.4.5 Geoelectric Section Along Profile 5

The geoelectric sequence along this profile is shown in Figure 4.35. It shows a system of three layers. The topsoil comprises lateritic soil, the weathered layer has resistivity of between 8.0 – 204.0 ohm - m. The depth to bedrock along this profile ranged from 2.6 – 12.7 m with a mean of 7.9 m. The underlying bedrock is mostly fresh granite gneiss which are resistant to weathering and this account for the shallow overburden thickness in some parts. The resistivity of the bedrock varied from 287.0 – 6394.0 ohm-m.

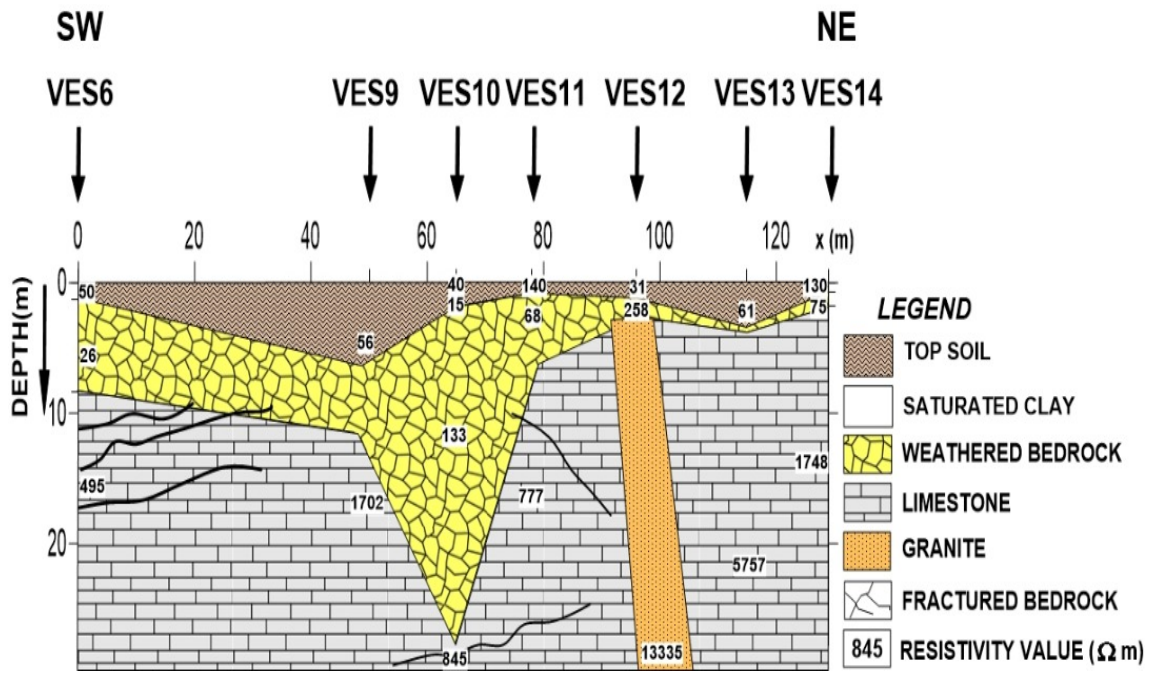


Figure 4.34: Geoelectric section along profile 4 (VES6, VES9, VES10, VES11, VES12, VES13 VES14)

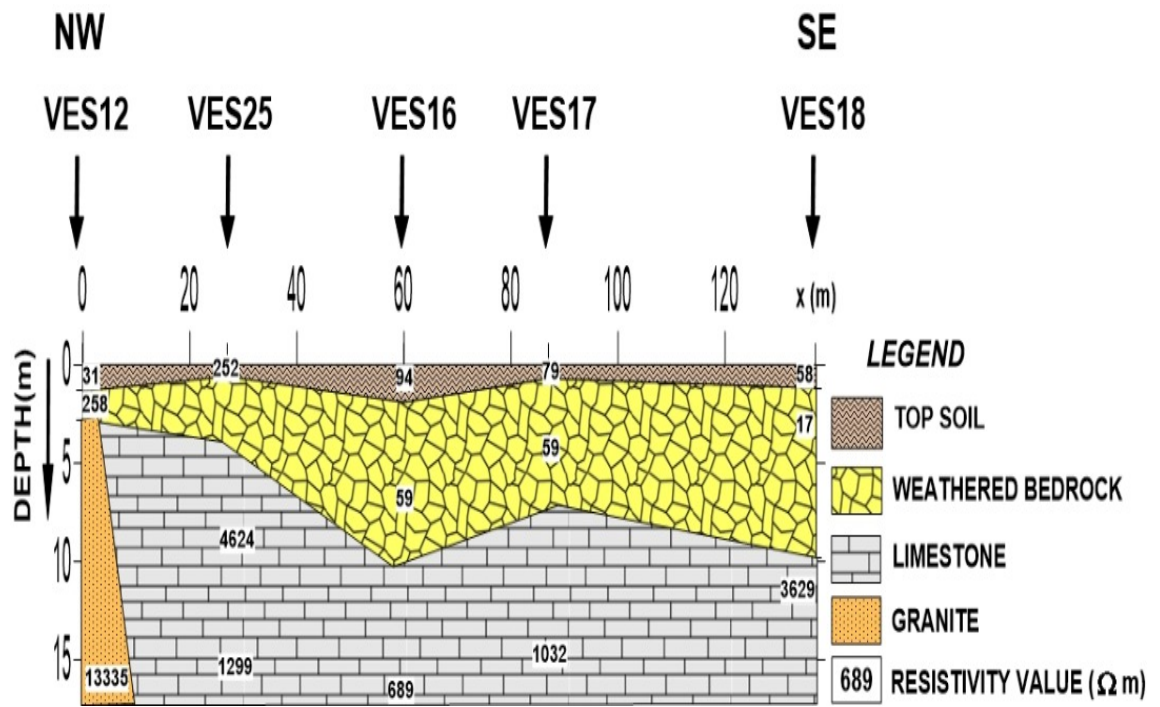


Figure 4.35: Geoelectric Section along Profile 5 (VES12, VES25, VES16, VES17, VES18)

4.1.6.5 Hydrogeology and Groundwater Flow

The metacarbonate marble in Okpella is a Proterozoic fragment of Nigeria's Basement complex. Which comprises of high-grade metavolcanics and metasedimentary rocks (Obaje, 2009). The geophysical investigation through VES has revealed the subsurface geology of the area in details. The majority of geoelectric sections show that the weathered bedrock ranges from a depth of less than 1 meter to a depth from 10 to 15 meters in all the subsurface of the quarry, which implies that all the water that is running on the surface like streams or rain water is possible to charge aquifers on this weathered bedrock of the pit through receiving water along distance mountain fronts and by leakage. Figure 4.36 represents the digital topographic picture from Shuttle Radar Topography Mission, SRTM, which is an international research effort that obtains Digital Elevation Models, DEM, on a near global scale to generate the most complete high resolution digital topographic database of the earth. The GIS advances and increasing quality of DEM have significantly extended the application potential of DEM to many hydrologic, hydraulic, water resources and environmental investigations (Moore *et al.*, 1991). The figure 4.36 shows the drainage system of about 25 Km surrounding the pit area to the east and to the west and about 20 Km surrounding the pit area to the north and to the south to demonstrate streams network in the area and to know how many streams is the pit receiving water from. The topography of the area ranges from 26 m to 671 m above sea level. The eastern part of the area shows maximum relief (from dark red 400 m to white 671 m) and the pit is located in the dark red area (about 400 m) which makes it a moderate to poor groundwater prospective zone but the map shows that the pit is receiving water from three streams and knowing that the pit rock mass is fractured it is possible that the aquifer is likely to produce significant pressure that can affect the slope stability. The geophysical investigation was also aimed to represent the groundwater flow that is not only affecting the slope stability but is also obstructing the daily operations at the quarry and causing a significant economic cost to pump the water outside the pit which is a cause of the water leakage through fractures inside the pit (Figure 4.37). The groundwater flow map Figure 4.38 shows that all the subsurface water in the saturated layer flows towards the pit because of the difference in the topography which makes fractures slope to the pit location. And mainly, the water is flowing to two points in of the pit, the eastern part and western part of the pit (Figure 4.38), which makes failure of pit slopes in the two parts more potential.

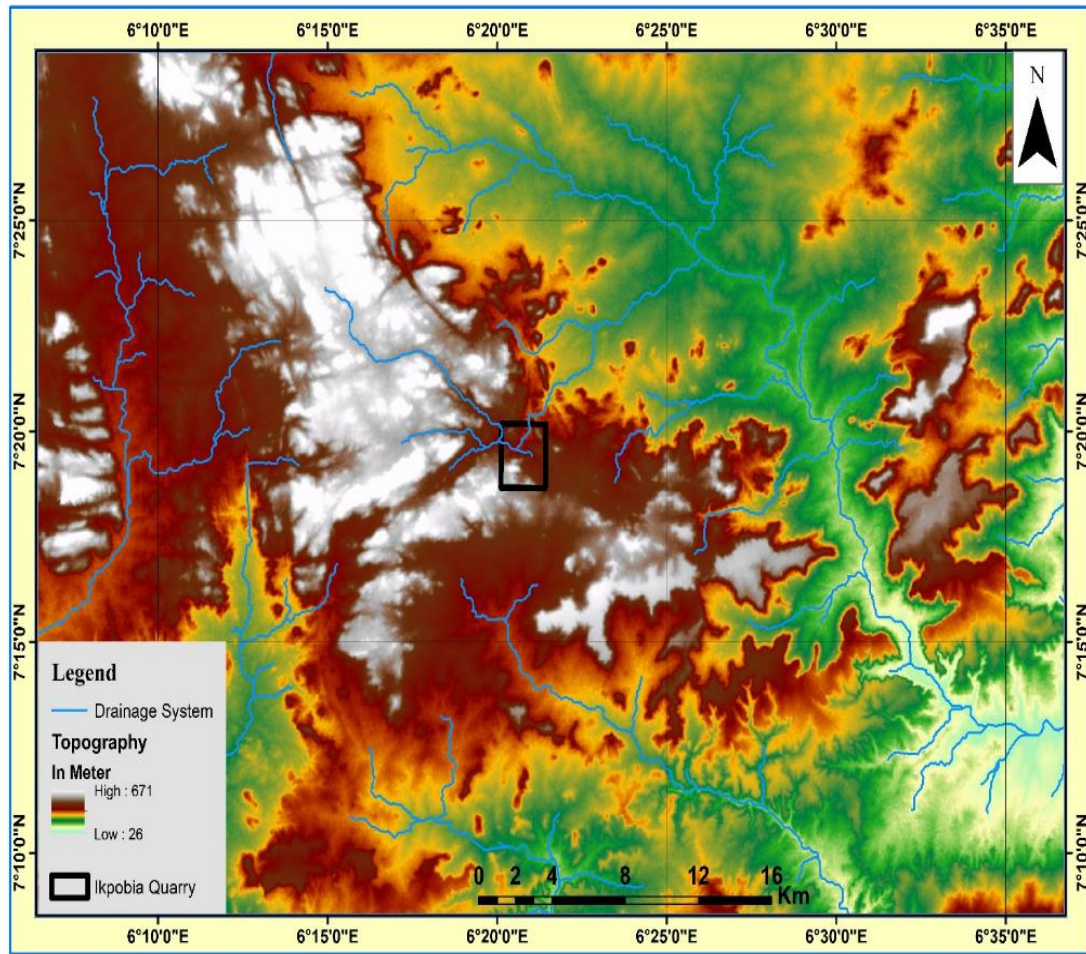


Figure 4.36: Representative View of Digital Topographic Picture of the Study Area



Figure 4.37: Pit Slope Picture Illustrating the Water Leakage Through Fractures

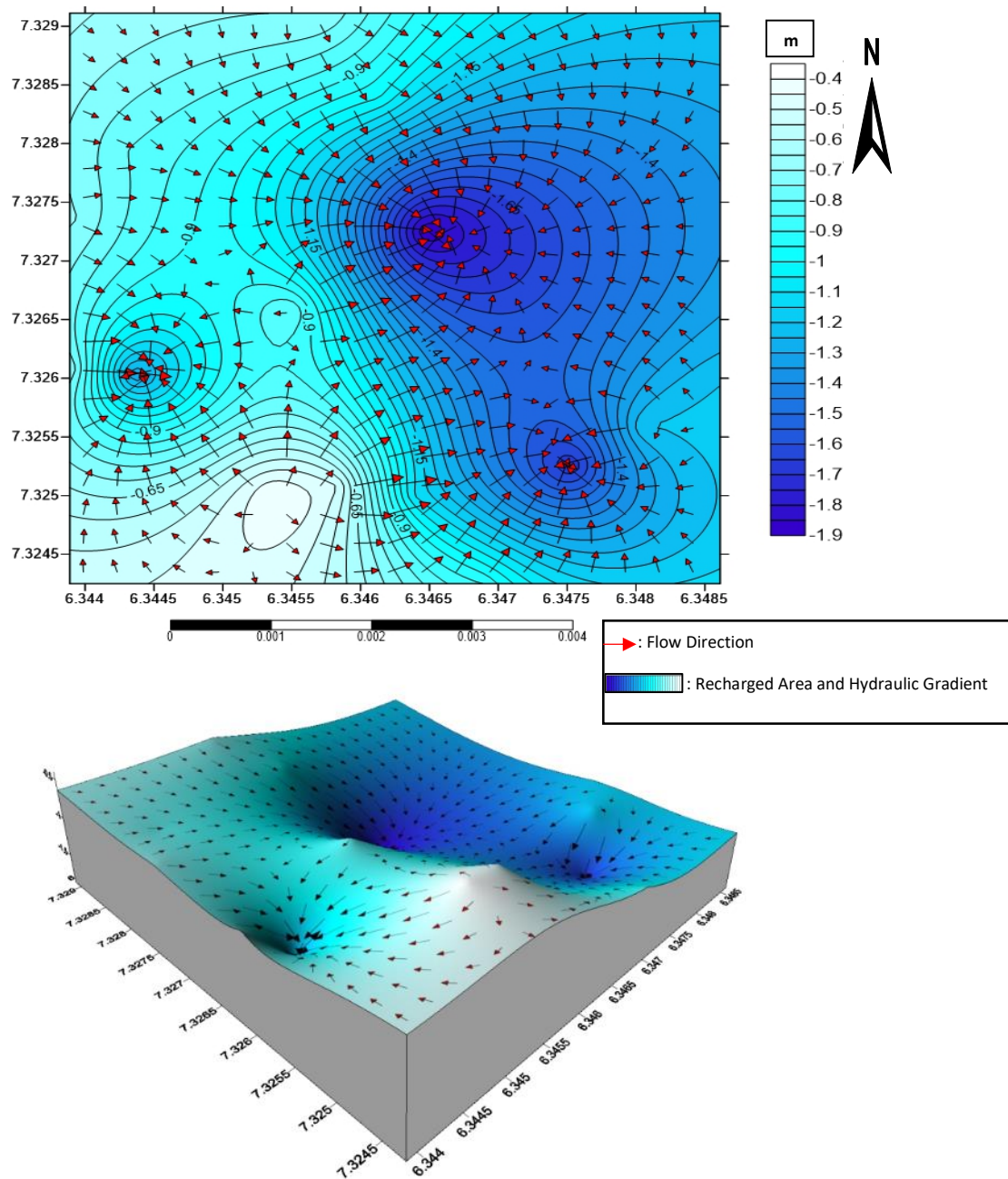


Figure 4.38: The Groundwater Flow Map Showing Recharged Area, Flow Direction and Hydraulic Gradient at the Quarry Site

4.1.7 Geomechanical Investigation

This includes structural investigation (joint data collection) and rock mass classification which requires strong observation and attention to the field data gathering.

4.1.7.1 Joint Data Collection (Photogrammetric Modelling)

Using photogrammetric techniques, the seven zones faces of the quarry were photographed and the data was digitally analysed using 3DF Zephyr Free Software to form a well-designed structural model. Which described discontinuities in the rock mass of the quarry face to get the joints information (Strikes and Dips).

4.1.7.1.1 Zone 1

There are five 5 major joint sets that were observed in the zone 1 (Figure 4.39). The joint sets are dipping in different directions and are different the dominant trending of each. Some are perpendicular to the face bench like joint 2 and others are parallel to the bench face like joints 1 and 4. The photogrammetric analysis of the joints gave the results in Table 4.6.

4.1.7.1.2 Zone 2

This zone is in-between zone 1 and zone 3 in the western part of the quarry pit. The difference between zones 1, 2 and 3 is in the bench orientation. It was observed, after projecting the joint sets of the zones 1 and 3, that there six joint sets that permeate zones 1 and 3, and by association, it can be assumed that the same common joint sets are present in zone 2. From plotting the joint sets in the Stereonet Software, Figure 4.40, it is observed that joint 5 of zone 3 is the same as joint 1 of zone 1 and joint 3 of zone 3 is the same as joint 5 of zone 1 and joint 6 of zone 3 is the same as joint 2 of zone 1. The properties of the joint sets in zone 2 are presented in Table 4.7.

4.1.7.1.3 Zone 3

There are six 6 major joint sets that were observed in the zone 3 (Figure 4.41). The joint sets are dipping in different directions, but, the dominant direction is the South West, though some of them are the same as others of zone 1. The majority of these joint sets are diagonal and intersect which give an idea from the first sight about

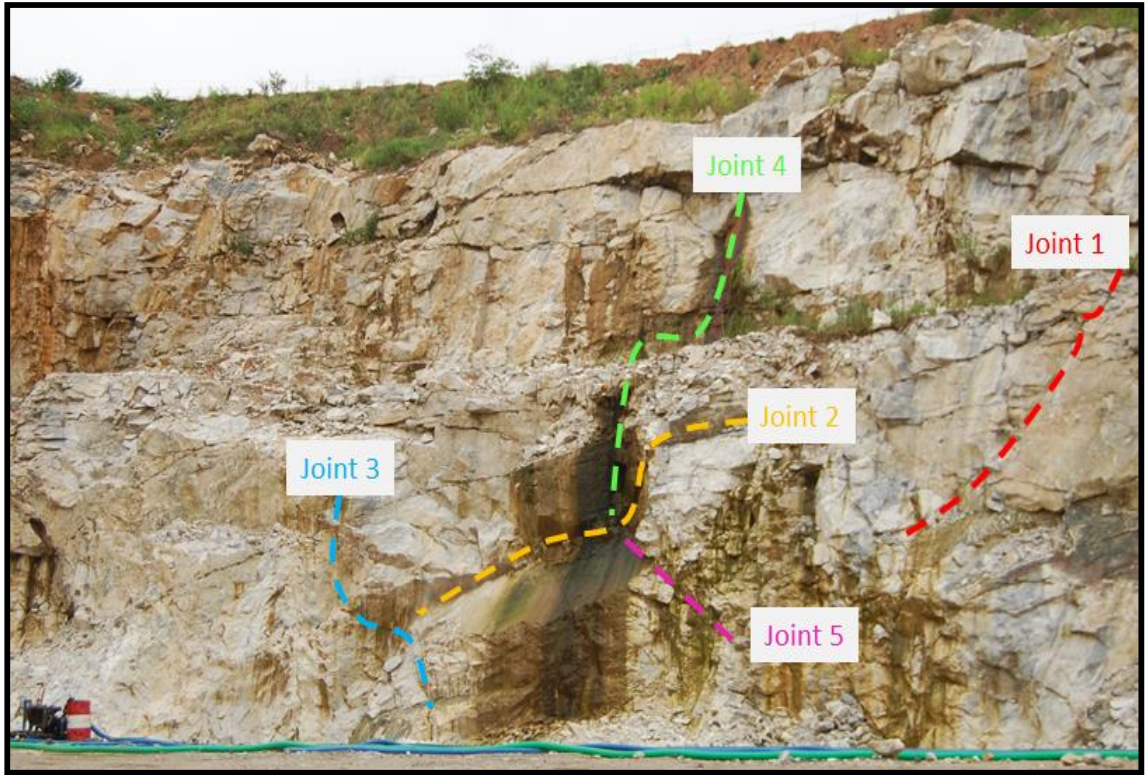


Figure 4.39: Illustration of Joint Sets in Zone 1

Table 4.6: Major Joint Sets of Zone 1

Joint number	Azimuth in NEV coordinates, deg	Pole dip, deg	Plane Strike, deg	Plane dip, deg	Plane dip dir., deg	Dip Quadrant
Joint 1	147.6	41.7	237.6	48.3	327.6	NW
Joint 2	166.8	42.4	256.8	47.6	346.8	NW
Joint 3	342.8	24.8	72.8	65.2	162.8	SE
Joint 4	318	19.1	48	70.9	138	SE
Joint 5	11.2	43	101.2	47	191.2	SW
Average Bench Orientation:		Face strike, deg	Dip Direction, deg			
		280.2	10.2			

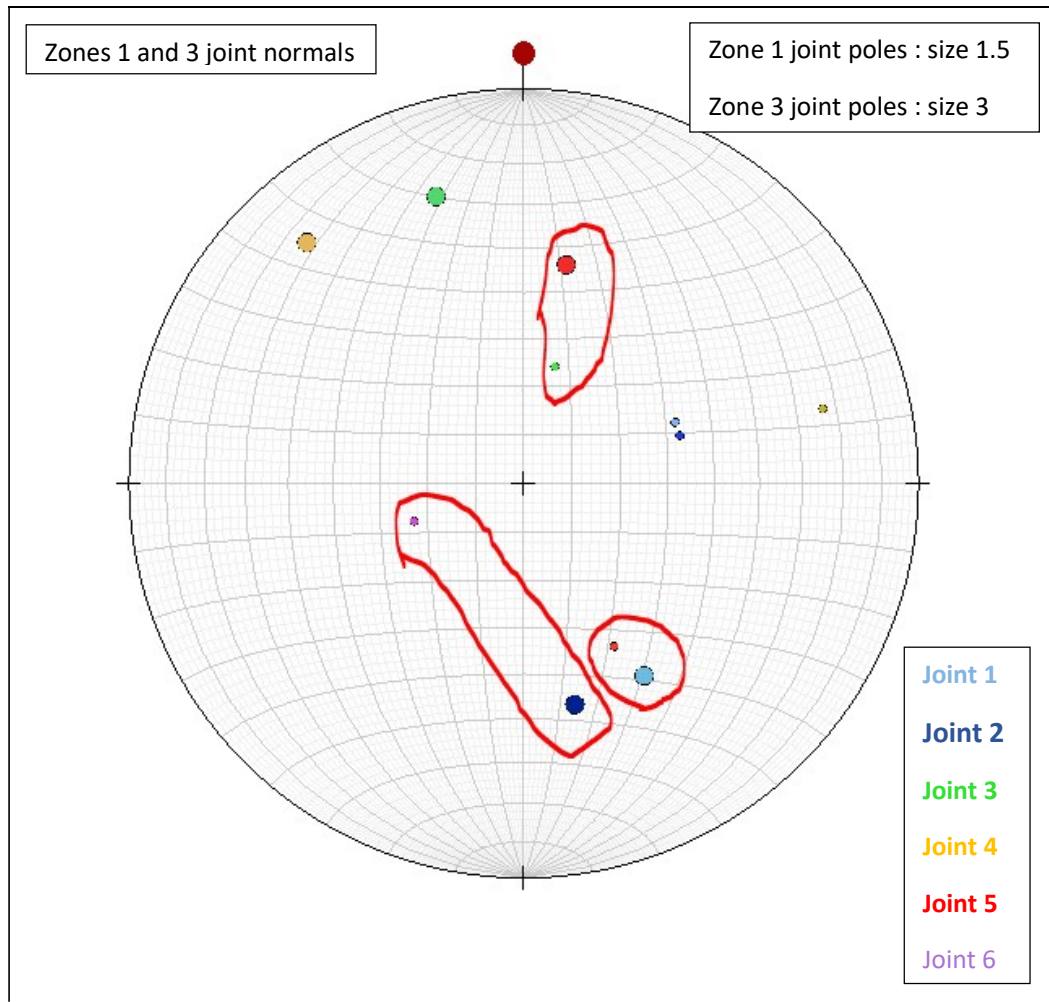


Figure 4.40: Projection of joint sets of zones 1 and 3 in Stereonet Software

Table 4.7: Major Joint Sets of Zone 2

Joint number	Azimuth in NEV coordinates, deg	Pole dip, deg	Plane Strike, deg	Plane dip, deg	Plane dip dir., deg	Dip Quadrant
Joint 1	206.2	41.7	296.2	48.3	26.2	NE
Joint 2	456.7	51	186.7	39	276.7	NW
Joint 3	69.8	43	159.8	47	249.8	SW
Joint 4	320.5	65.3	50.5	24.7	140.5	SE
Joint 5	225.4	42.4	315.4	47.6	45.4	NE
Joint 6	196.9	66.1	286.9	23.9	16.9	NE
Average Bench Orientation:		Face strike, deg	Dip Direction, deg			
		325	55			

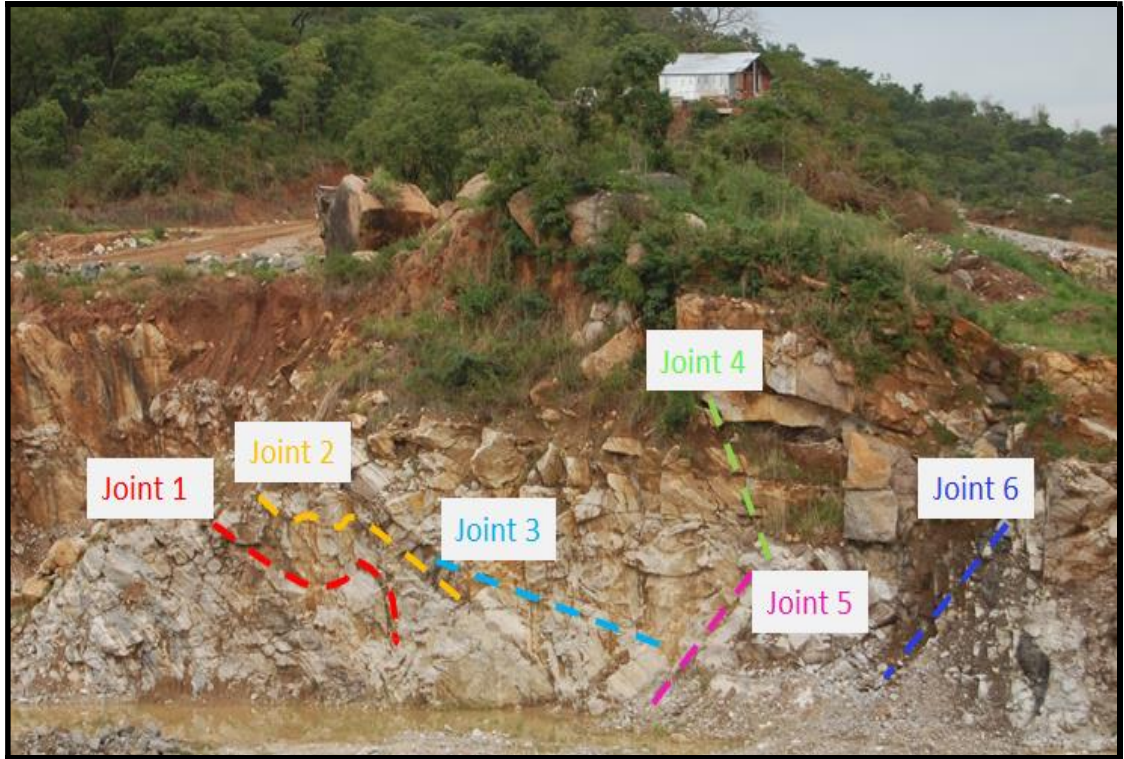


Figure 4.41: Illustration of Joint Sets in Zone 3

potential slope failures. The photogrammetric analysis of the joints gave the results in Table 4.8.

4.1.7.1.4 Zone 4

There are six 6 major joint sets that were observed in the zone 4 (Figure 4.42). The joint sets are dipping in different directions and are different in the dominant trending of each. Some are perpendicular to the face bench like joint 2 and others are parallel to the bench face like joints 1 and 4. The photogrammetric analysis of the joints gave the results in Table 4.9.

4.1.7.1.5 Zone 5

There are four 4 major joint sets that were observed in the zone 5 (Figure 4.43). The joint sets are dipping in different directions, but, the dominant trending is to the North West. The photogrammetric analysis of the joints gave the results in Table 4.10.

4.1.7.1.6 Zone 6

This zone has the same situation as zone 2. Where is located in-between zone 5 and zone 7 in the eastern part of the quarry pit. The difference between zones 5, 6 and 7 is in the bench orientation. It was observed, after projecting the joint sets of the zones 5 and 7, that there are five joint sets that permeate zones 5 and 7, and by association, it can be assumed that the same common joint sets are present in zone 6. From plotting the joint sets in the Stereonet Software, Figure 4.44, it is observed that joint 3 of the two zones 5 and 7 is the same, and joint 4 is also the same in the two zones, and joint 2 of zone 5 is the same as joint 8 of zone 7. The properties of the joint sets in zone 6 are presented in Table 4.11.

4.1.7.1.7 Zone 7

There are eight 8 major joint sets that were observed in the zone 7 (Figure 4.45). The joint sets are dipping in different directions, but, the dominant direction in this zone is the South East, four joint sets. The joint sets in this zone are large and distance which gives and an idea about the big risk if failure occurs along them. The photogrammetric analysis of the joints gave the results in Table 4.12.

Table 4.8: Major Joint Sets of Zone 3

Joint number	Azimuth in NEV coordinates, deg	Pole dip, deg	Plane Strike, deg	Plane dip, deg	Plane dip dir., deg	Dip Quadrant
Joint 1	68.1	55.8	158.1	34.2	248.1	SW
Joint 2	73.5	56.4	163.5	33.6	253.5	SW
Joint 3	14.9	65.3	104.9	24.7	194.9	SW
Joint 4	75.6	23.2	165.6	66.8	255.6	SW
Joint 5	151.1	51	241.1	39	331.1	NW
Joint 6	251.3	66.1	341.3	23.9	71.3	NE
Average Bench Orientation:		Face strike, deg	Dip Direction, deg			
		25.6	-64.4			

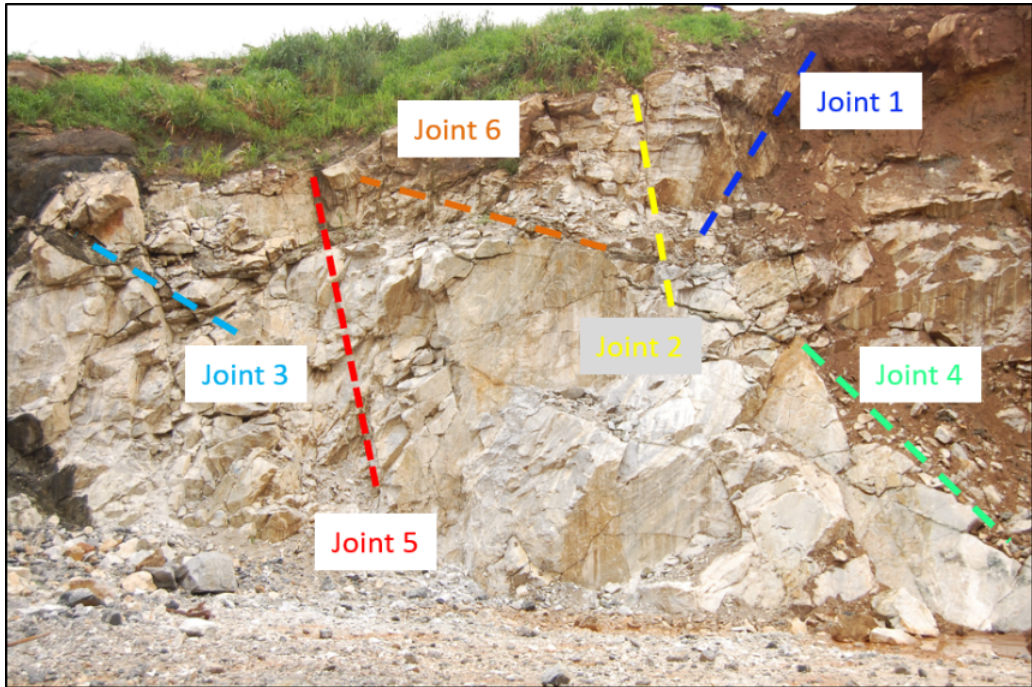


Figure 4.42: Illustration of Joint Sets in Zone 4

Table 4.9: Major Joint Sets of Zone 4

Joint number	Azimuth in NEV coordinates, deg	Pole dip, deg	Plane Strike, deg	Plane dip, deg	Plane dip dir., deg	Dip Quadrant
Joint 1	202.5	39.8	292.5	50.2	22.5	NE
Joint 2	109.2	44.6	199.2	45.4	289.2	NW
Joint 3	79.3	47.6	169.3	42.4	259.3	SW
Joint 4	107.5	40.7	197.5	49.3	287.5	NW
Joint 5	95.3	38.1	185.3	51.9	275.3	NW
Joint 6	309.9	60.4	39.9	29.6	129.9	SE
Average Bench Orientation:		Face strike, deg	Dip Direction, deg			
		12.6	-77.4			

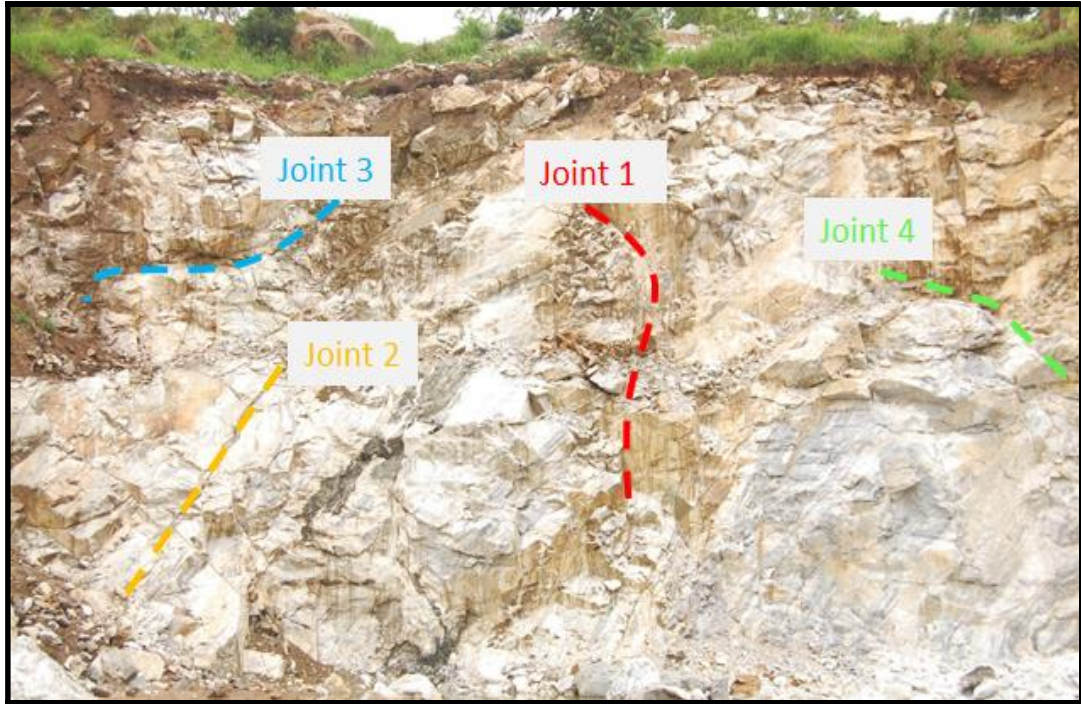


Figure 4.43: Illustration of Joint Sets in Zone 5

Table 4.10: Major Joint Sets of Zone 5

Joint number	Azimuth in NEV coordinates, deg	Pole dip, deg	Plane Strike, deg	Plane dip, deg	Plane dip dir., deg	Dip Quadrant
Joint 1	138.9	20.4	228.9	69.6	318.9	NW
Joint 2	104.4	54.9	194.4	35.1	284.4	NW
Joint 3	187.9	56.3	277.9	33.7	7.9	NE
Joint 4	160.9	55.7	250.9	34.3	340.9	NW
Average Bench Orientation:		Face strike, deg	Dip Direction, deg			
		112.2	202.2			

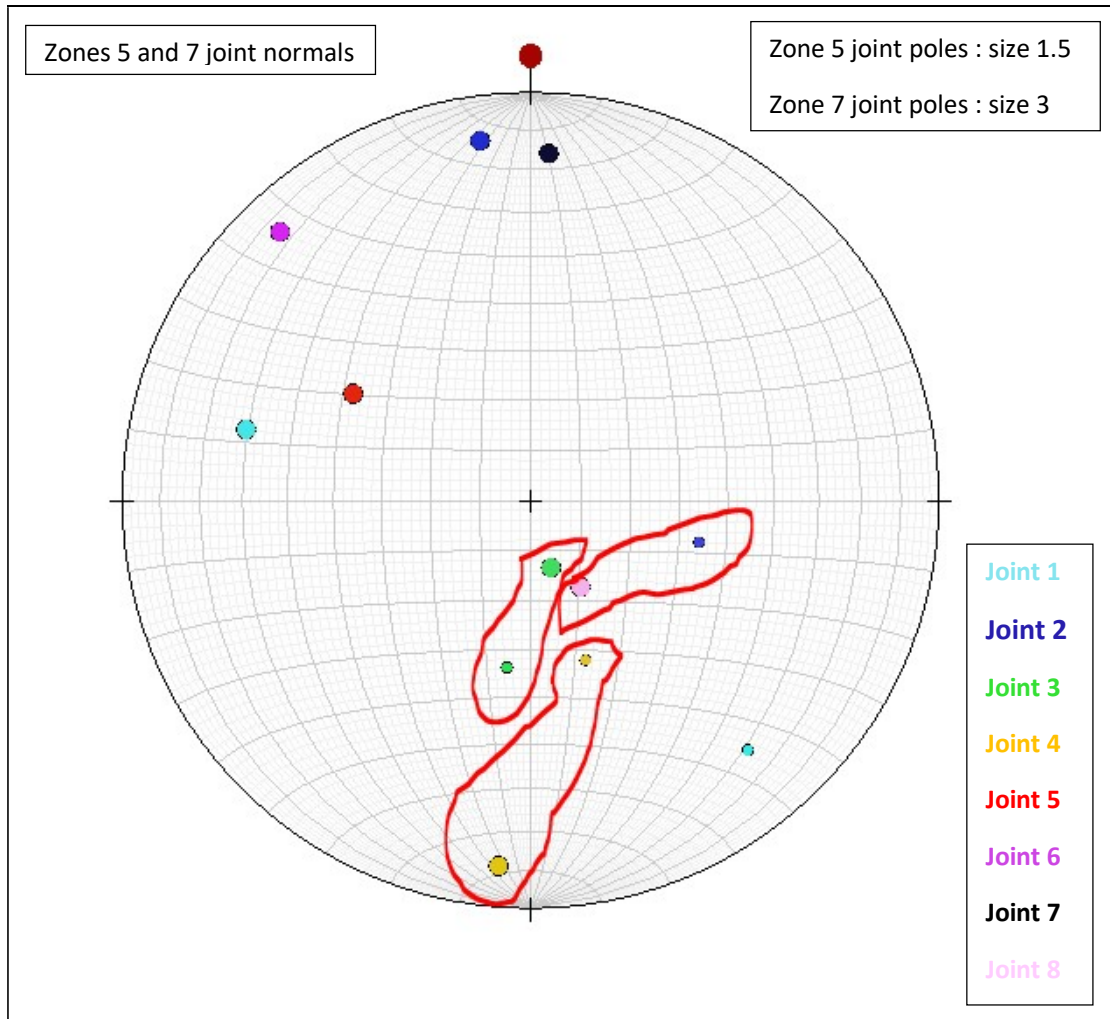


Figure 4.44: Projection of joint sets of zones 5 and 7 in Stereonet Software

Table 4.11: Major Joint Sets of Zone 6

iJoint number	Azimuth in NEV coordinates, deg	Pole dip, deg	Plane Strike, deg	Plane dip, deg	Plane dip dir., deg	Dip Quadrant
Joint 1	327	56.3	57	33.7	147	SE
Joint 2	300	55.7	30	34.3	120	SE
Joint 3	243.5	54.9	333.5	35.1	63.5	NE
Joint 4	170.6	10.8	260.6	79.2	350.6	NW
Joint 5	149.5	76.4	239.5	13.6	329.5	NW
Joint 6	135.8	70.3	225.8	19.7	315.8	NW
Average Bench Orientation:		Face strike, deg	Dip Direction, deg			
		230	320			

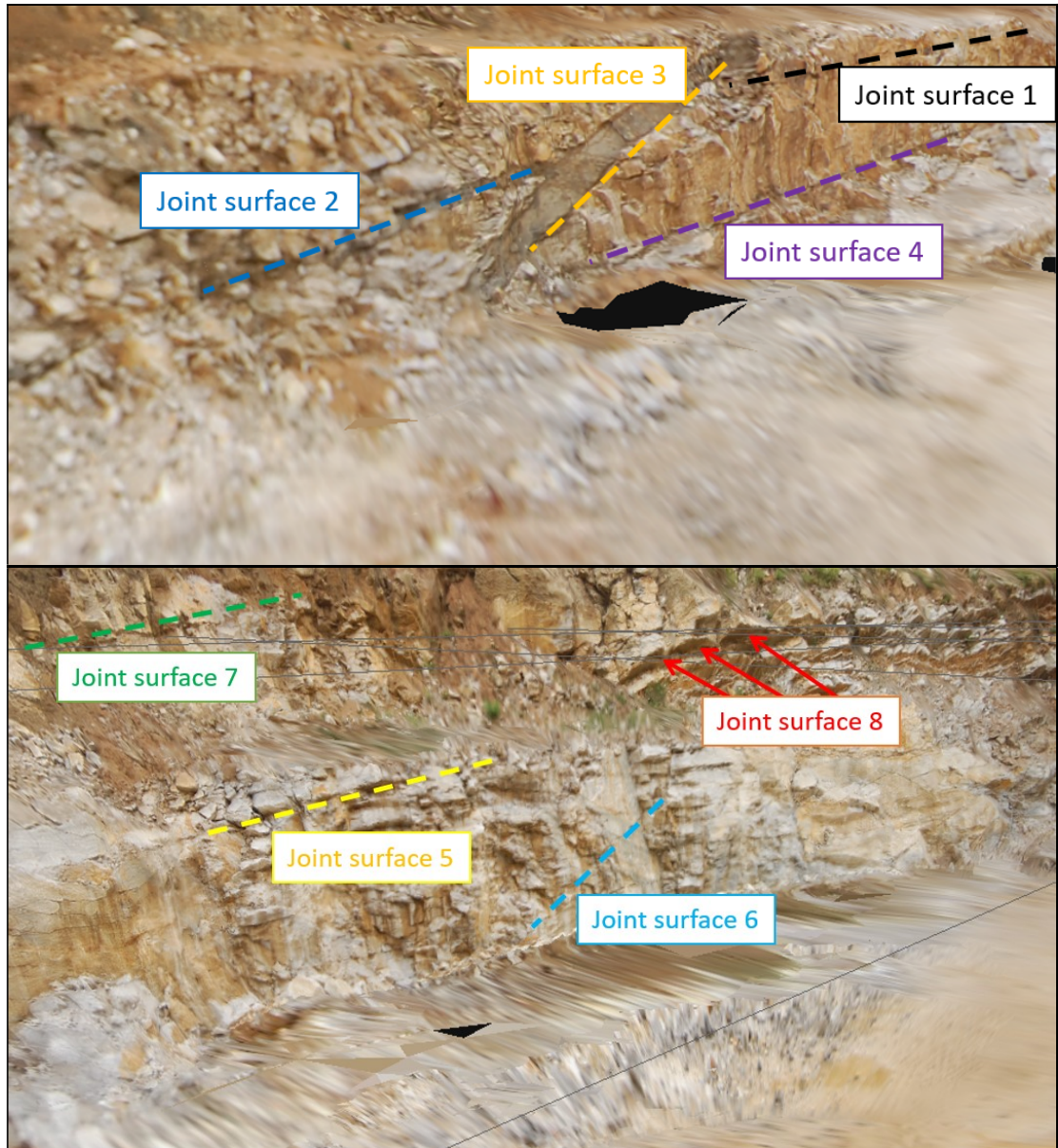


Figure 4.45: Illustration of Joint Sets in Zone 7

Table 4.12: Major Joint Sets of Zone 7

Joint number	Azimuth in NEV coordinates, deg	Pole dip, deg	Plane Strike, deg	Plane dip, deg	Plane dip dir., deg	Dip Quadrant
Joint 1	284.1	28.5	14.1	61.5	104.1	SE
Joint 2	352	11.6	82	78.4	172	SE
Joint 3	163.5	76.4	253.5	13.6	343.5	NW
Joint 4	184.6	10.8	274.6	79.2	4.6	NE
Joint 5	301.3	47.5	31.3	42.5	121.3	SE
Joint 6	316.9	10.7	46.9	79.3	136.9	SE
Joint 7	363.2	15.6	93.2	74.4	183.2	SW
Joint 8	149.8	70.3	239.8	19.7	329.8	NW
Average Bench Orientation:		Face strike, deg	Dip Direction, deg			
		249.7	339.7			

4.1.7.2 Rock Mass Classification

The most recent GSI chart introduced by (Marinos and Hoek, 2000) which uses the qualitative description to identify the state of the structure and rock surface, and relies more on the observation and the engineering and professional experience. The GSI value is widely used together with the intact rock properties to estimate deformation properties and rock mass strength. The GSI chart that is used to classify rock mass quality of each zone in the Ikpobia quarry is presented in Figure 4.46. The estimated GSI values are also listed in Table 4.13. The values presented in table 4.13 demonstrate that the GSI of the quarry ranges from 30 for the disturbed rock masses to 40 for Blocky/Very Blocky rock masses. Which is a result of the structure of various masses in the quarry with interlocked and disturbed mass with multi-faced angular blocks formed by 4 or more joint sets, while the conditions of discontinuities are fair to poor in surfaces that are moderately to highly weathered.

4.2 Geomechanics Study

To determine the properties of rock mass and analyse the slope stability of Ikpobia Quarry it is important to obtain the physical and mechanical properties of the intact rock through laboratory tests. The tests for this research were conducted at the Geomechanics Laboratory at Mining Engineering Department, University of Utah. The marble rock samples were prepared and subjected to different laboratory tests.

4.2.1 Uniaxial Compressive Strength

Three samples that were tested under the uniaxial compression conditions C7A, C8A and C9A are represented in the Table 4.14. It summarizes the dimensions and some properties of samples that were tested under the UCS conditions. The samples did not have a Length-to-Diameter ratio of 2:1 which is important to get correct UCS results. When the length/diameter ratio of a rock specimen is less than 2, a correction factor is usually applied. The form correction of the unconfined compressive strength, according to ASTM 1986, is:

$$C = Ca \div \left(0.88 + \left(0.24 \times \frac{D}{L} \right) \right) \quad (4.1)$$

Where Ca: measured compressive strength of specimen

C: calculated compressive strength of an equivalent 2:1 length/diameter specimen

Table 4.13: Estimated GSI Values for Rock Masses in Ikpobia Quarry

Zone	GSI Value
Zone 1	40
Zone 2	35
Zone 3	30
Zone 4	35
Zone 5	35
Zone 6	30
Zone 7	40

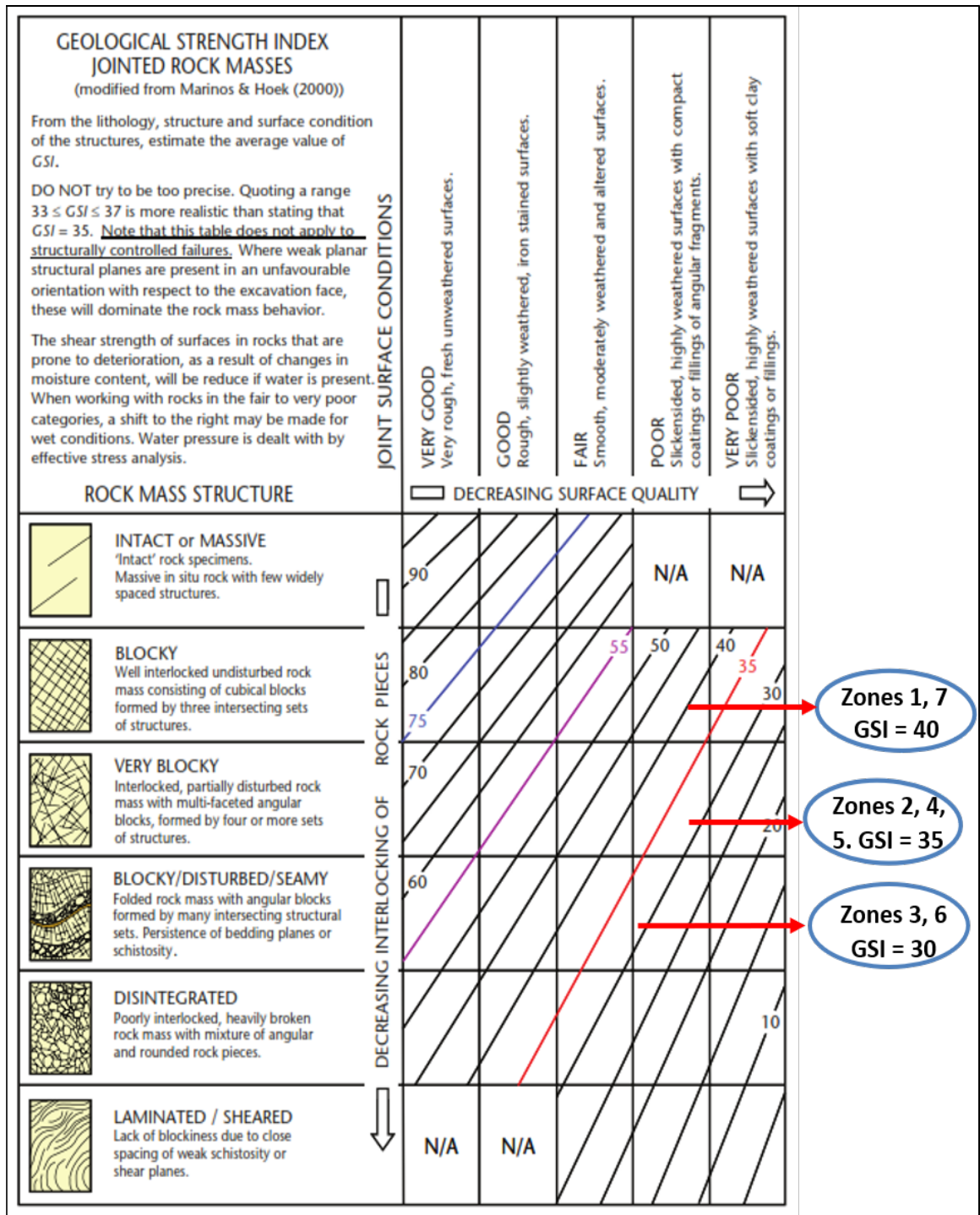


Figure 4.46: Estimation of the Range of Geological Strength Index in Ikpobia Quarry

Table 4.14: Dimensions and Some Properties of Specimens Prepared for UCS

Sample	C7A	C8A	C9A
End parallelism End 1, mm	0.01016	0.0127	0.0127
End parallelism End 2, mm	0.01016	0.00762	0.0127
Mass, g	1736.7	1503.8	1693.2
Length 1, cm	13.4264	12.8117	13.1851
Length 2, cm	13.4251	12.8054	13.1838
Length 3, cm	13.4213	12.8079	13.1838
Average Length, cm	13.4244	12.8084	13.1843
Diameter 1, cm	7.7533	7.3545	7.7724
Diameter 2, cm	7.7825	7.4460	7.7622
Diameter 3, cm	7.7495	7.3431	7.7597
Diameter 4, cm (smallest diameter about 2.5 inch from top)	0	7.3304	0
Diameter 5, cm (smallest diameter about 2.5 inch from top)	0	7.4523	0
Diameter 6, cm (smallest diameter about 2.5 inch from top)	0	7.3520	0
Average diameter, cm	7.7618	7.3797	7.7647
Volume of sample, cm ³	635.1979	547.8582	624.3168

D: diameter of the specimen

L: length of the specimen

Figure 4.47 presents an example of the uniaxial compression test of sample C9A before, during and after the test as an example. Figure 4.48, Figure 4.49 and Figure 4.50 show the obtained experimental diagrams of the UCS tests on the three samples. The diagrams show relatively high strength for the stresses at the mine, a high degree of nonlinearity up to the ultimate strength and a manifestation of ductile behavior and a large plastic deformation, instead of brittle behavior. Table 4.15 lists the uniaxial compression's results tests for the three samples. Where the average UCS is 48.47 MPa and the average Young's modulus and Poisson's ratio are 55.22 GPa and 0.2433 respectively with a reasonable standard deviation of all the results (less than 10 %).

4.2.2 Triaxial Compression Test

Six standard triaxial compression tests were conducted on C1A, C1B, C2A, C3A, C4A and C5A cylinders to determine the Mohr-Coulomb parameters of the rocks, which are, cohesion and friction angle. For this purpose, the peak stresses were plotted against the confining pressures and the tangent of the slope of the best fit line drawn across the points was used for the calculation of the internal friction angle, ϕ , and the cohesion c (Figure 4.51). Table 4.16 represents the dimensions of each sample that were prepared for the triaxial tests to estimate the cohesion and internal friction. Figure 4.52 presents an example of the Triaxial compression test of sample C1B before, during and after the test as an example. All the samples had diagonal shear plane failure except C4A that failed across a horizontal plane which was caused by tapping the specimen out of the triaxial cell. Figure 4.53 presents the Triaxial compression test of sample C4A before, during and after the test. Figure 4.54 shows the obtained experimental diagrams of the Triaxial tests on the six samples. Failure occurs at the pick of the graphs and it is observed from the graphs that all the samples had a ductile behaviour or ductile behaviour to brittle failure except the sample C5A that had a brittle failure. The results obtained for the triaxial compression test are listed in Table 4.17.

4.2.3 Brazil (Indirect Tensile) Test

Seven cylindrical samples were subjected to the Brazilian splitting test D1A, D2A, D2B, D3A, D5A, D11A and D11B in order to obtain the tensile strength of rocks.

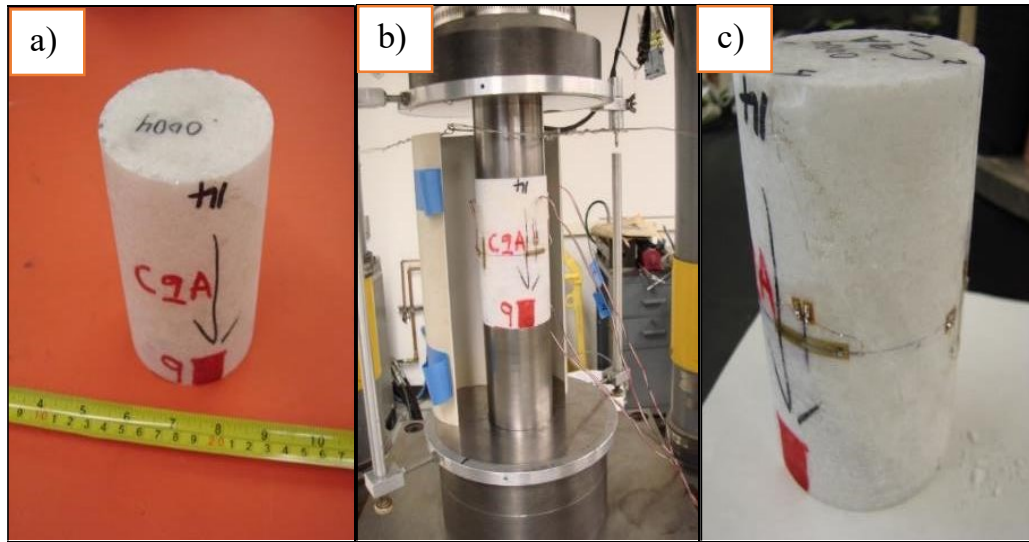


Figure 4.47: Sample C9A Before, During And After The Uniaxial Compression Test

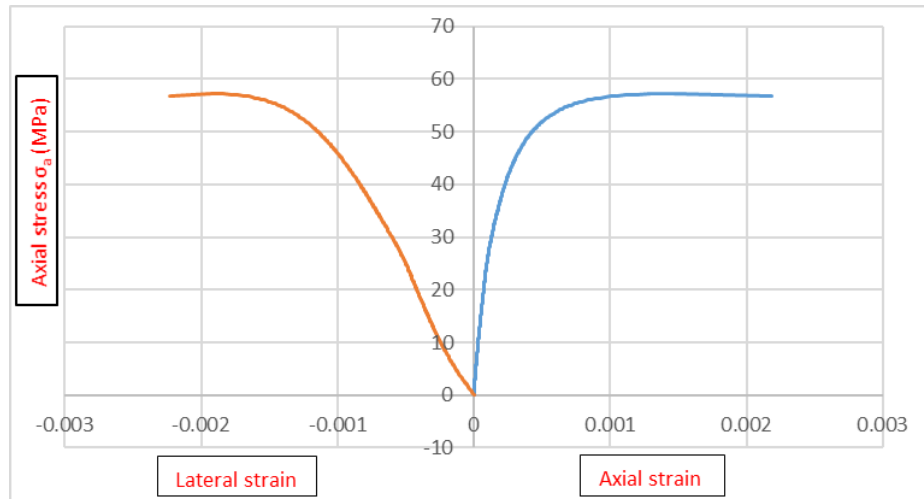


Figure 4.48: Experimental Stress-Strain Diagram of Sample CA9

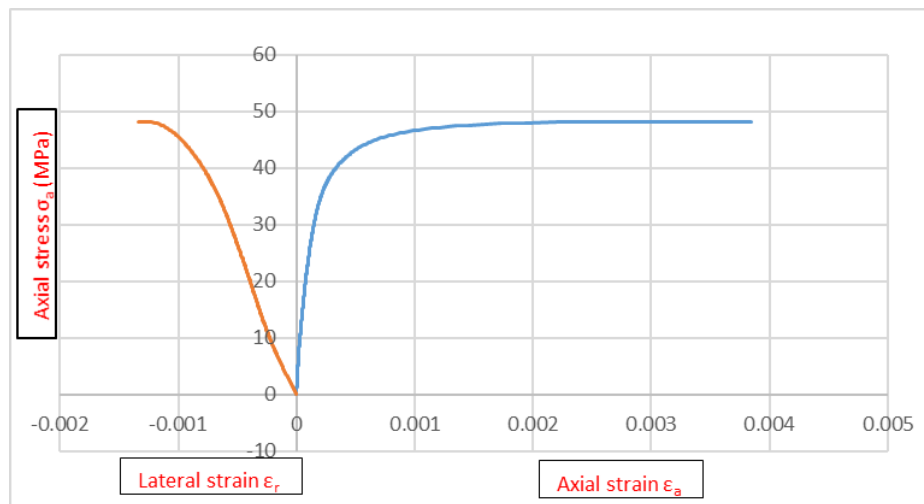


Figure 4.49: Experimental Stress-Strain Diagram of Sample C8A

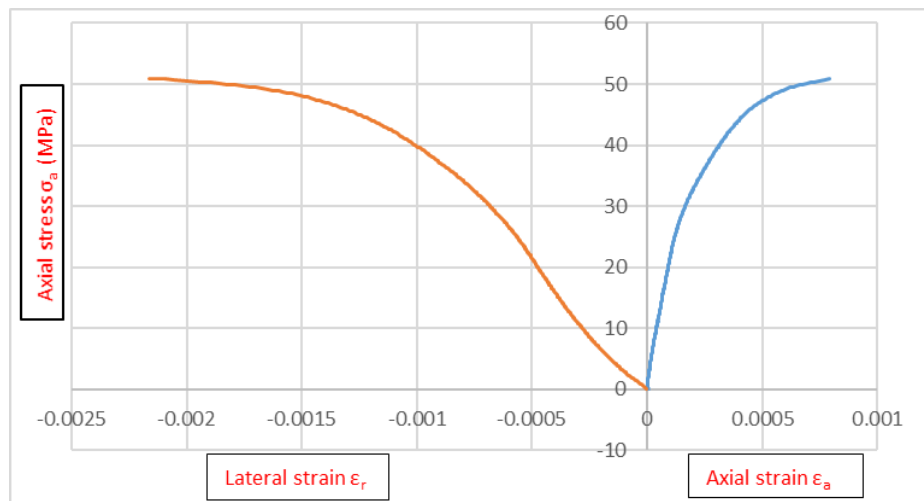


Figure 4.50: Experimental Stress-Strain Diagram of Sample C7A

Table 4.15: Uniaxial Compression Tests Results for the Ikpobia Quarry samples

Sample	UCS, psi	UCS, MPa	D/L	Corrected UCS, psi	Corrected UCS, MPa	E, psi	E, GPa	Poisson's ratio
C9A	7445	51.33	0.5779	7584	52.29	7,640,000	52.68	0.2246
C8A	6757	46.59	0.5761	6880	47.44	8,853,000	61.04	0.2631
C7A	6488	44.73	0.5889	6626	45.68	7,534,000	51.94	0.2422
Average	6897	47.55		7030	48.47	8,009,000	55.22	0.2433
St. Dev	494	3.40		496	3.42	732,844	5.05	0.0193

UCS = Uniaxial Compressive Strength, E = Young modulus,

St. Dev. = standard deviation

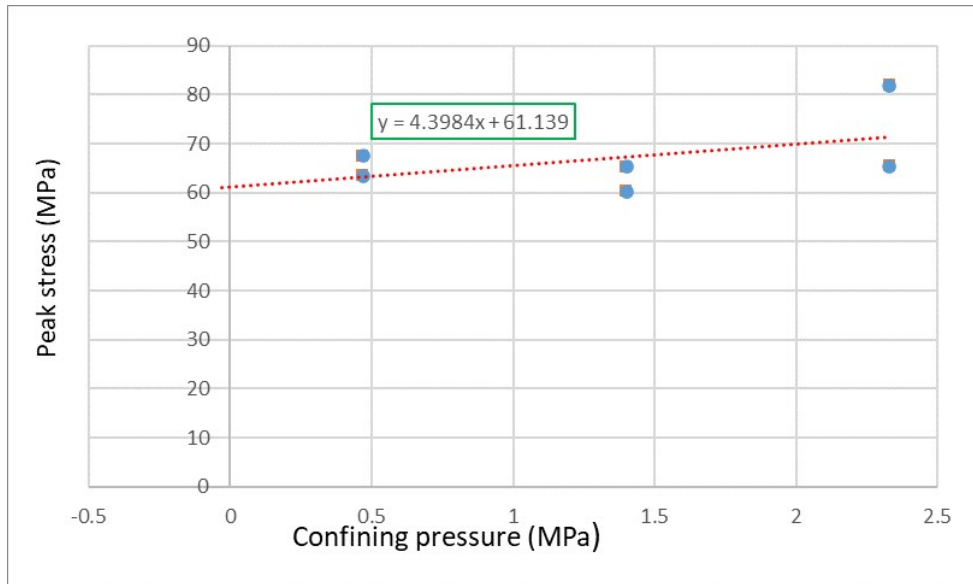


Figure 4.51: Plot of Peak Stresses Versus Confining Pressures



Figure 4.52: Sample C1B Before, During and After the Triaxial Compression Test at Geomechanics Laboratory, Mining Engineering Department of University of Utah, USA



Figure 4.53: Sample C4A Before, During and After the Triaxial Compression Test at Geomechanics Laboratory, Mining Engineering Department of University of Utah, USA

Table 4.16: Dimensions of samples prepared for triaxial test

Sample	C1A	C1B	C2A	C3A	C4A	C5A
Diameter at 0 deg, cm	7.6885	7.68858	7.73557	7.71144	7.72668	7.72668
Diameter at 60 deg, cm	7.6809	7.69112	7.77367	7.68604	7.72668	7.6708
Diameter at 120 deg, cm	7.6860	5.14731	7.73303	7.72922	7.68096	7.72668
Average diameter, cm	7.6851	6.842337	7.747423	7.7089	7.71144	7.70805
Length at 0 deg, cm	15.13078	15.36192	15.24889	15.22603	15.01013	15.30477
Length at 120 deg, cm	15.12316	15.38605	15.25143	15.2273	15.00759	15.30604
Length at 240 deg, cm	15.12316	15.35557	15.25016	15.22857	15.00632	15.3035
Average length, cm	15.1257	15.36785	15.25016	15.2273	15.00801	15.30477
Parallel tolerance of top, cm	0.001016	0.00127	0.002794	0.000508	0.000508	0.000762
Parallel tolerance of bottom, cm	0.000762	0.001016	0.00254	0.000762	0.000762	0.000762

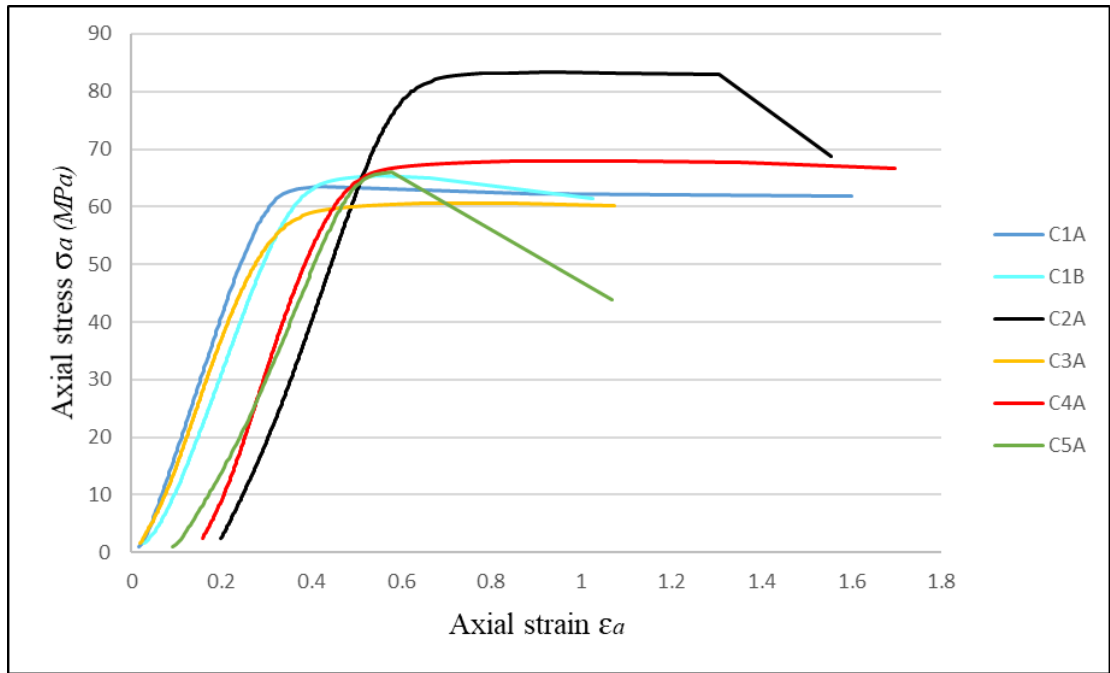


Figure 4.54: Experimental stress-strain diagram of sample C7A

Table 4.17: Summary of the Triaxial Compression Test Results for the Ikpobia Quarry

Sample	Confining stress, $\sigma_2 = \sigma_3$ (psi)	Confining stress, $\sigma_2 = \sigma_3$ (MPa)	Measured Triaxial compressive strength, σ_1 (MPa)	Corrected Triaxial compressive strength, σ_1 (MPa)	Cohesion, c (MPa)	Internal friction angle, ϕ (°)
C1A	68	0.4688	63.58	63.46	61.14	66.20
C1B	203	1.3996	65.33	65.33		
C2A	338	2.3304	82.02	81.86		
C3A	203	1.3996	60.36	60.27		
C4A	68	0.469	67.5	67.44		
C5A	338	2.330	65.62	65.41		
Average	203	1.40	67.402	67.295		

Table 4.18 represents the dimensions of each of the disks that were prepared for the Brazil tests. Figure 4.55 represents an example of Brazil test of sample D11B before, during and after the test as an example. Table 4.19 presents the tensile strength results obtained from the Brazil test. It was observed from the table of results that there was a significant variability in the tensile strength because of the difference in size of samples. Sample D11B had the smallest tensile strength, 1.5023 MPa, and sample D2A had the highest tensile strength, 4.6255 MPa.

4.2.4 Density Test

The three samples that were tested under the uniaxial compression conditions C7A, C8A and C9A were measured to determine the density of the marble at Ikpobia Quarry. The results are listed in the Table 4.20. The average of density is 2730.4 kg / m³ which is considered high value compared to the types of rocks and it gives an idea that the porosity of the marble of Ikpobia Quarry is small because of the reverse relationship between density and porosity (the increment of density implies the decrement of porosity).

Table 4.18: Dimensions of Disk Samples Prepared for Brazil test

Sample	D1A	D2A	D2B	D3A	D5A	D11A	D11B
Diameter, in	3.0340	3.0375	3.0410	3.0310	3.0455	3.0190	2.9990
Diameter, mm	77.064	77.153	77.241	76.987	77.356	76.683	76.175
Average Thickness, In	1.0073	1.0060	1.0095	0.9983	1.0150	1.0285	1.0100
Average Thickness, Mm	25.584	25.552	25.641	25.356	25.781	26.124	25.654
Mass, g	326.1	326.8	327.8	321.5	328.4	325.9	317.4
Area in²	3.0560	3.0557	3.0699	3.0257	3.0912	3.1050	3.0290
Area mm²	1971.6	1971.4	1980.6	1952.1	1994.3	2003.2	1954.2
Sample volume, in³	7.2821	7.2899	7.3321	7.2028	7.3939	7.3624	7.1345
Sample volume, m³	0.000119	0.000119	0.00012	0.000118	0.000121	0.000121	0.000117



Figure 4.55: The sample D11B Before, During and After the Brazil Test at Geomechanics Laboratory, Mining Engineering Department of University of Utah, USA

Table 4.19: Summary of the Brazil Test Results for the Ikpobia Quarry

Sample	Load at failure, KN	Time to failure, s	Average loading rate, KN/s	σ_t , psi	σ_t , MPa
D1A	6.583	72	0.091431	484.29	3.3391
D2A	9.119	101	0.090287	670.87	4.6255
D2B	8.452	127	0.066551	618.91	4.2672
D3A	6.8895	89	0.077472	512.28	3.5320
D5A	6.272	76	0.082526	456.14	3.1450
D11A	5.605	76	0.07375	405.79	2.7978
D11B	2.936	38	0.077263	217.89	1.5023
Average	6.552	82.71	0.79897	480.88	3.3156

σ_t = Tensile strength,

Table 4.20: Summary of the Density Results for the Ikpobia Quarry

Sample	V, cm ³	ρ , g/cm ³	ρ , Kg/m ³
C9A	635.1979	2.7341	2734.1
C8A	547.8582	2.7449	2744.9
C7A	624.3168	2.7121	2712.1
Average	602.4576	2.7304	2730.4

V = Volume

P = Density

4.3 Pit Slope Stability Analysis

In this study, different slope stability analyses were used to assess the stability at BUA Ikpobia Quarry. Kinematic analysis was used to investigate the possible failure modes, and Hoek-Brown failure criterion was used to estimate the rock mass properties that were used as inputs to the numerical analysis which is the most accurate mean to assess the stability through the calculation of the stress and the displacement of rock masses.

4.3.1 Kinematic Analysis Stability

The kinematic analysis was performed for bench faces of the zones 1 – 7 to estimate the possibility of slope failure. The analyses and results are presented in Figures 4.56 – 4.62. Table 4.21 summarises the kinematic analysis results, it was observed that in zone 1 there was small possibility of the occurrence of planar sliding failure (20%), no possibility for flexural toppling failure mode, a possibility for wedge sliding failures to occur (30%), while the dominant mode of failure was direct toppling which had a high possibility of occurrence (60%). In zone 2, there was no direct toppling failure, and very small possibility of planar and flexural failures (16.67%) and a small possibility of wedge failure. The modes of failure that were present in zone 3 are planar, direct toppling and wedge failure with 16.67%, 33.33% and 20% possibility of occurrence while there was no flexural toppling. Zone 4 had no possibility of flexural and direct toppling failures and a small possibility of plan and wedge failures with possibility of (16.67%) and (20%) respectively. In zone 5 there was no possibility of planar and direct toppling failures and a possibility of flexural toppling failure, while the most probable mode of failure in this zone was the wedge sliding (50%). In zone 6, it was observed that there was no existence of flexural and direct toppling modes of failure, but a very small possibility of wedge sliding (6.67%) and a small possibility of planar sliding mode of failure. Zone 7 had no possibility of wedge sliding but a very small possibility of occurrence of planar and flexural toppling modes of failure. The most probable mode of failure in this zone was the direct toppling mode of failure (50%). The summarized results in Table 4.21 show that with some differences in orientations and joint set orientations, different failure modes are possible. Some zones with the joint sets present pose the risk of some degree of failure. The state of the pit shows some smaller degrees of failure. The possibility to use such results to change design in

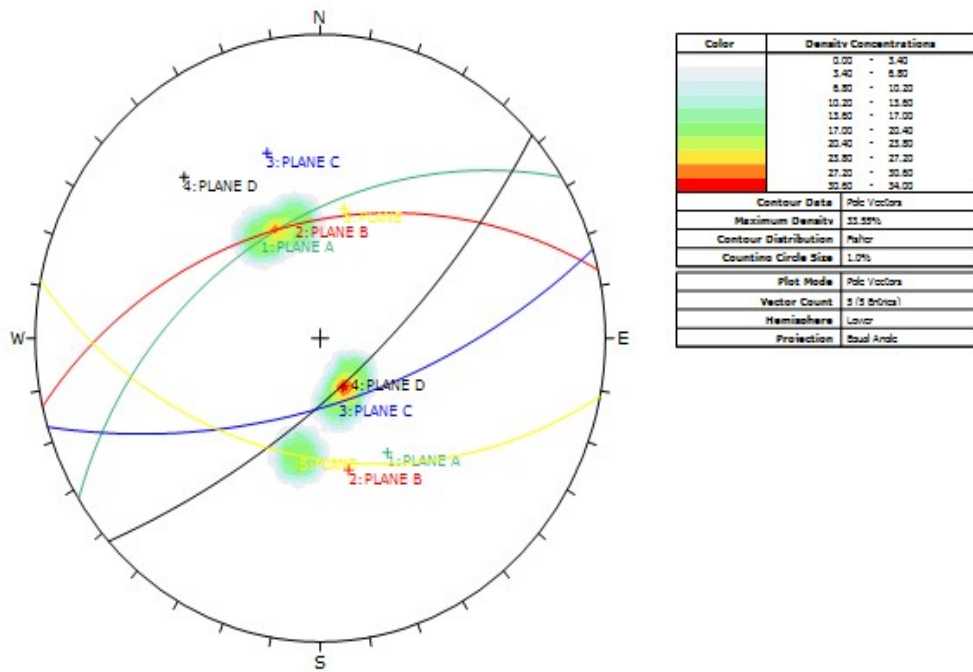


Figure 4.56: Kinematic Analysis for Zone 1

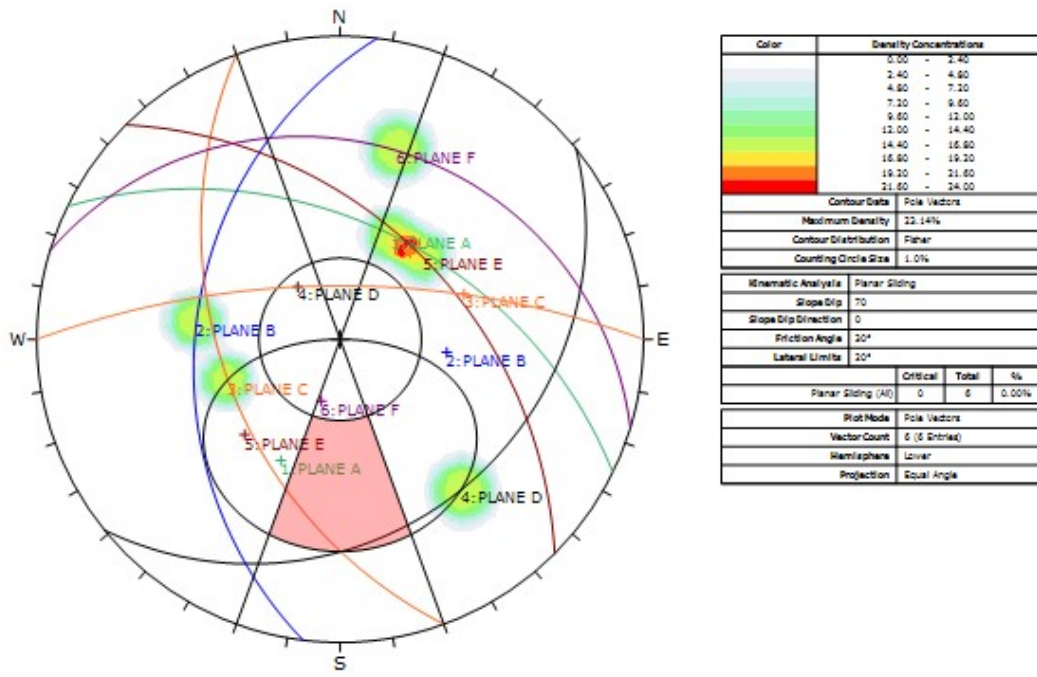


Figure 4.57: Kinematic Analysis for Zone 2

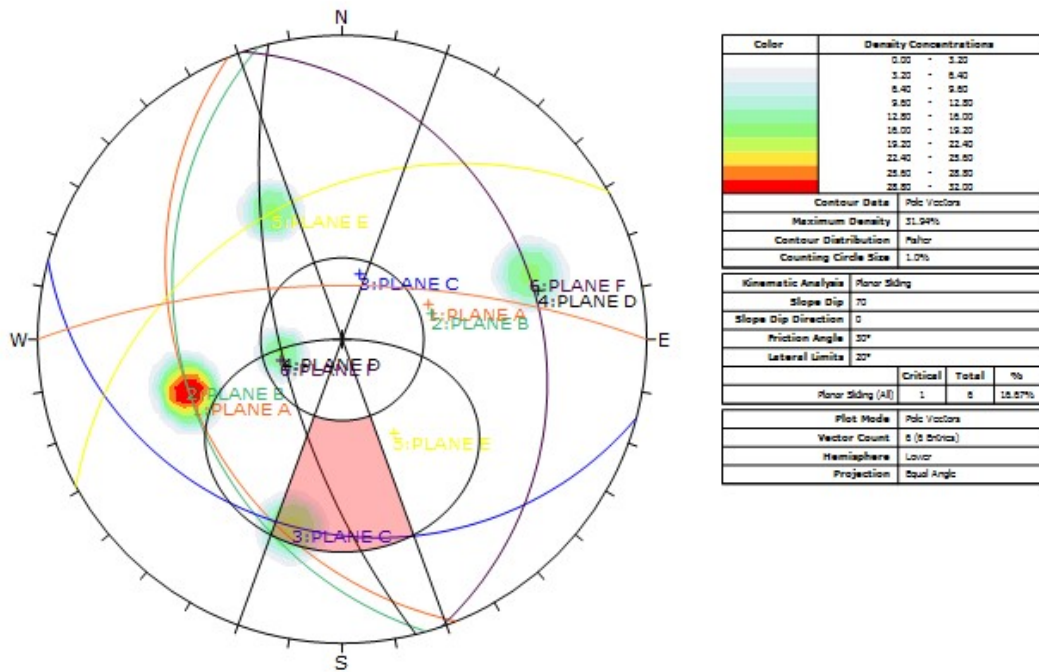


Figure 4.58: Kinematic Analysis for Zone 3

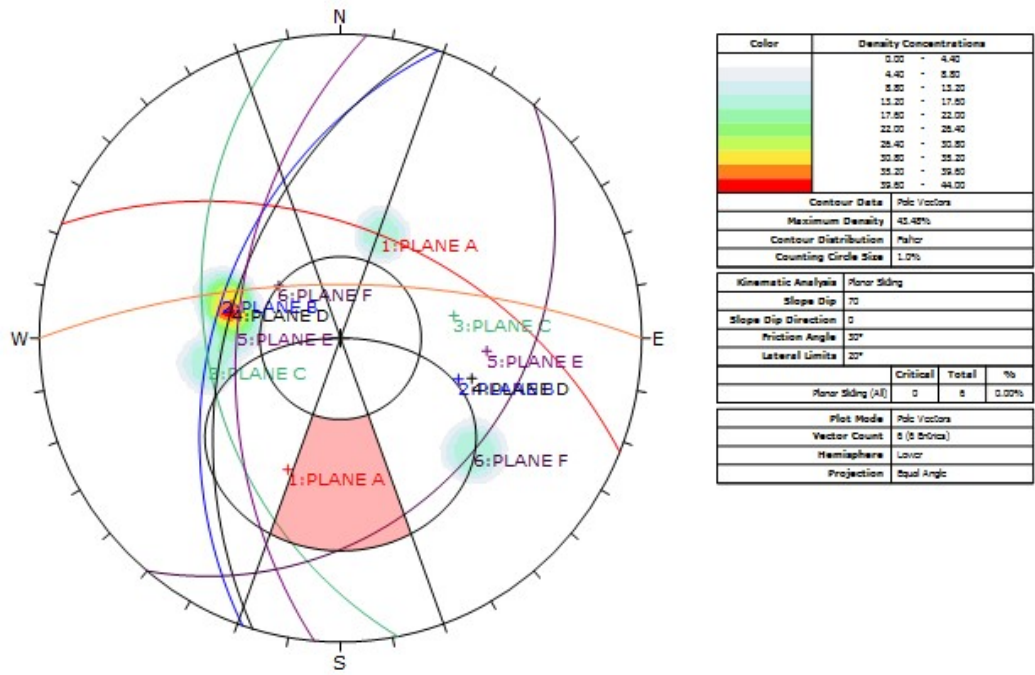


Figure 4.59: Kinematic Analysis for Zone 4

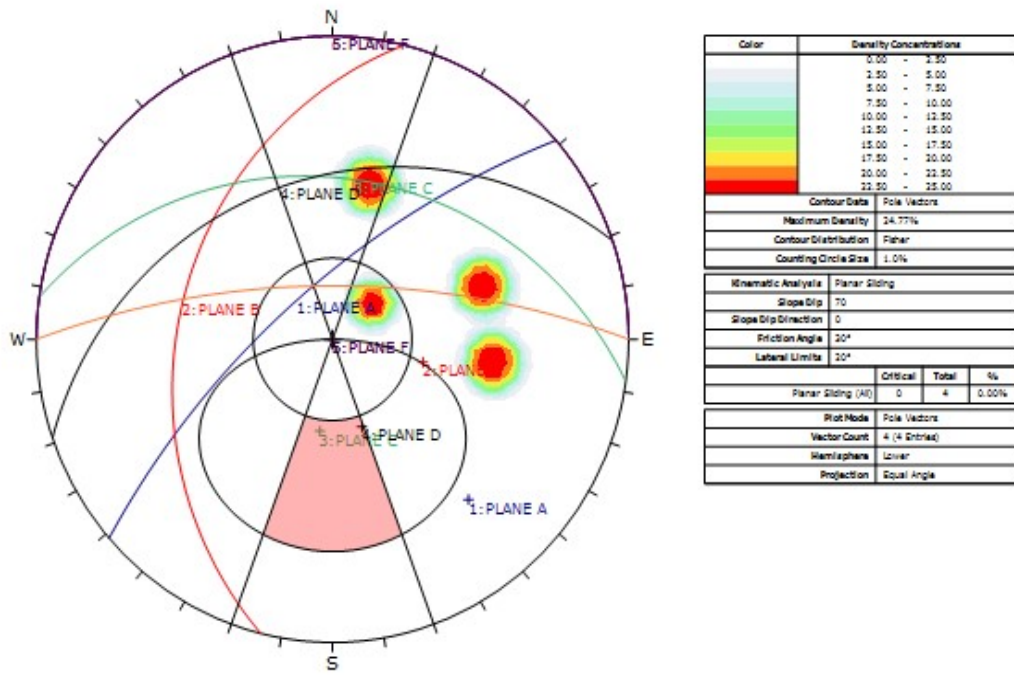


Figure 4.60: Kinematic Analysis for Zone 5

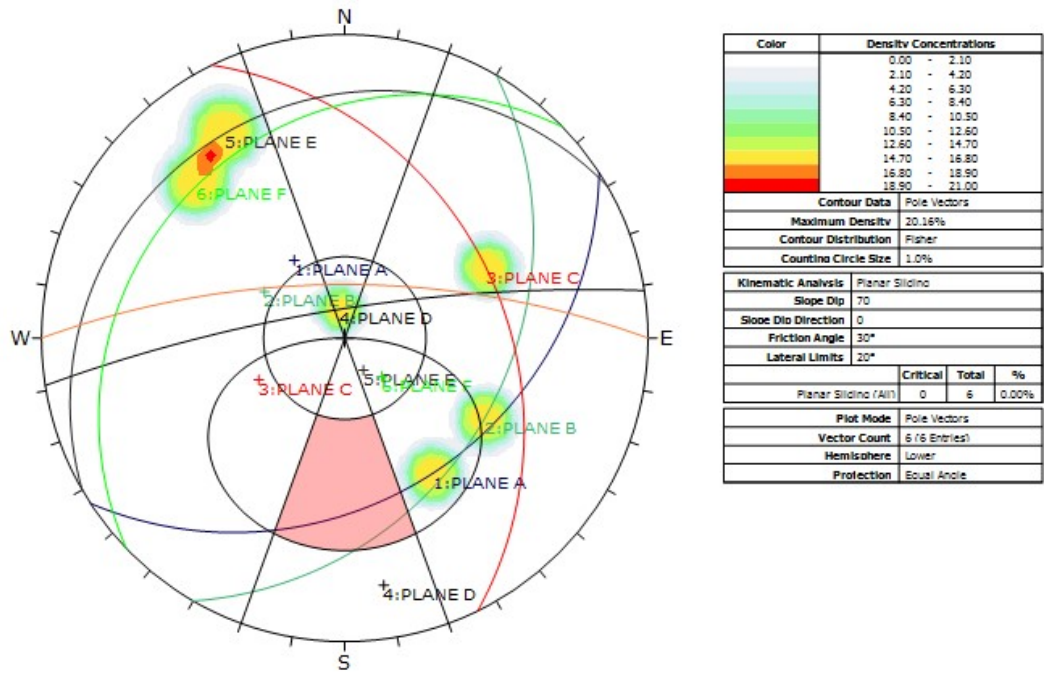


Figure 4.61: Kinematic Analysis for Zone 6

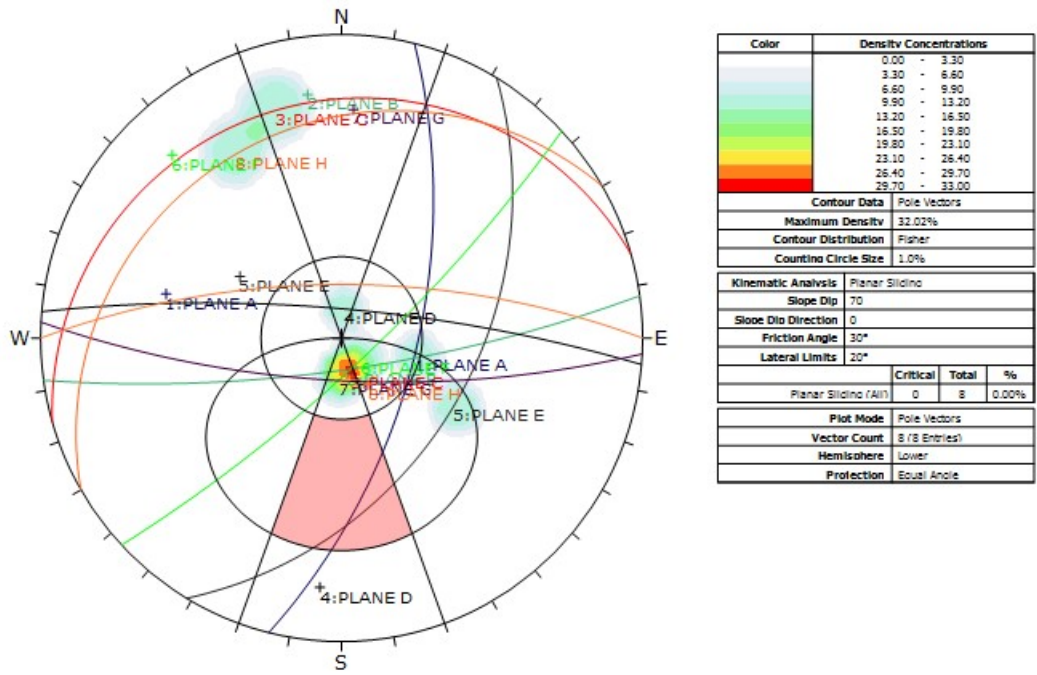


Figure 4.62: Kinematic Analysis for Zone 7

Table 4.21: Summary of Kinematic Analysis Results

Type of Failure	Planar Sliding	Flexural Toppling	Direct Toppling	Wedge Sliding
Zone 1	There was small possibility of plane failure 20%	There was no possibility of Flexural Toppling 0%	There was much possibility of the Direct Toppling failure 60%	There was possibility of the Wedge Sliding failure 30%
Zone 2	There was small possibility of plane failure 16.67%	There was small possibility of such failure 16.67%	There was no possibility of the Direct Toppling 0%	There was small possibility of the Wedge Sliding failure 20%
Zone 3	There was small possibility of plane failure 16.67%	No possibility of the Flexural Toppling 0%	There was possibility of the Direct Toppling 33.33%	There was small possibility of the Wedge Sliding failure 20%
Zone 4	There was small possibility of plane failure 16.67%	There was no possibility of Flexural Toppling 0%	There was no possibility of the Direct Toppling 0%	There was small possibility of the Wedge Sliding failure 20%
Zone 5	There was no possibility of plane failure as 0%	There was a possibility of Flexural Toppling failure 25%	There was no possibility of the Direct Toppling 0%	There was possibility of the Wedge Sliding failure 50%
Zone 6	There was small possibility of plane failure 16.67%	There was no possibility of Flexural Toppling 0%	There was no possibility of the Direct Toppling 0%	There was very small possibility of the Wedge Sliding failure 6.67%
Zone 7	There was very small possibility of plane failure 12.5%	There was very small possibility of the Flexural Toppling failure 12.5%	There was possibility of the Direct Toppling failure 50%	There was no possibility of Wedge Sliding failure 0%

different areas of the pit to increase stability or to optimize resource extraction might be considered. The results of this technique show its usefulness not only to BUA company but also to other mining companies in the area which can help to increase the safety of workers.

4.3.2 Estimation of Rock Mass Properties Using Hoek-Brown Failure Criterion

Rock mass properties were determined based on the geological visual observation of (GSI), Disturbance factor (D), Slope height and laboratory analysis results. They were used as inputs for free RocLab Software (Rocscience, 2007) in order to have the generalized Hoek-Brown failure criterion to estimate the rock mass properties. The analyses were done for each zone separately. The input parameters of RocLab software are:

Sigci: Intact Uniaxial Compressive Strength, GSI: Geologic Strength Index, D: Disturbance factor, m_i : the intact rock parameter, γ = Unit weight and the slope height. The rock mass input parameters are presented in Table 4.22.

The analytical results of the rock mass failure criterion that were obtained from the RocLab software are presented in Table 4.23. It was observed from the results that the friction angle varies from 35.27° to 39.45° and the cohesion varies from 0.103 to 0.169 MPa which show that there were some differences of the rock properties from zone to other that can be significant in terms of the stability of slope.

This estimation of rock mass using RocLab software produced Mohr-Coulomb failure envelope from Hoek-Brown failure criterion. The failure envelopes of zone 1 are presented in Figures 4.63 and 4.64 as example. The Hoek brown describes a nonlinear rise in strength as confinement increases in the form of a nonlinear envelope from which the best fit of the Mohr-Coulomb strength envelope is projected over a stress range of low to high confinement.

4.4.3 Numerical Analysis

The uniaxial compressive strength of the intact rock and other rock mass properties like Deformation modulus (Young modulus), friction angle, cohesion, unit weight, Poisson's ratio, tensile strength, GSI and the Slope height of the Ikpobia Quarry which were determined from the laboratory tests and RocLab software were employed in the numerical modelling of the quarry slope stability as input parameters. The default

Table 4.22: The Rock Mass Input Parameters of RocLab software

Parameters	Sigci MPa	GSI	D	Mi	v MN/m³	Slope height M
Zone 1	48.47	40	0.8	9	0.027	25
Zone 2	48.47	35	0.8	9	0.027	25
Zone 3	48.47	30	0.8	9	0.027	20
Zone 4	48.47	35	0.8	9	0.027	20
Zone 5	48.47	35	0.8	9	0.027	30
Zone 6	48.47	30	0.8	9	0.027	20
Zone 7	48.47	40	0.8	9	0.027	25

Sigci = Intact Uniaxial Compressive Strength

v = Unit weight

Table 4.23: The Analytical Results of the Rock Mass Failure Criterion from RocLab

	Internal friction angle ϕ (°)	Cohesion. c_0 (MPa)	Sig3max MPa	Deformation modulus MPa	Uniaxial compressive strength MPa	Tensile strength MPa
Zone 1	39.45	0.169	0.5568	612.28	0.464	0.0216
Zone 2	36.67	0.141	0.5478	480.85	0.301	0.014
Zone 3	35.27	0.103	0.4393	394.77	0.190	0.0086
Zone 4	38.31	0.125	0.4471	480.85	0.301	0.0136
Zone 5	35.32	0.156	0.6466	480.85	0.301	0.0136
Zone 6	35.27	0.103	0.4393	394.77	0.190	0.0086
Zone 7	39.45	0.169	0.5568	612.28	0.464	0.0216

Sig3max = Major principal stress

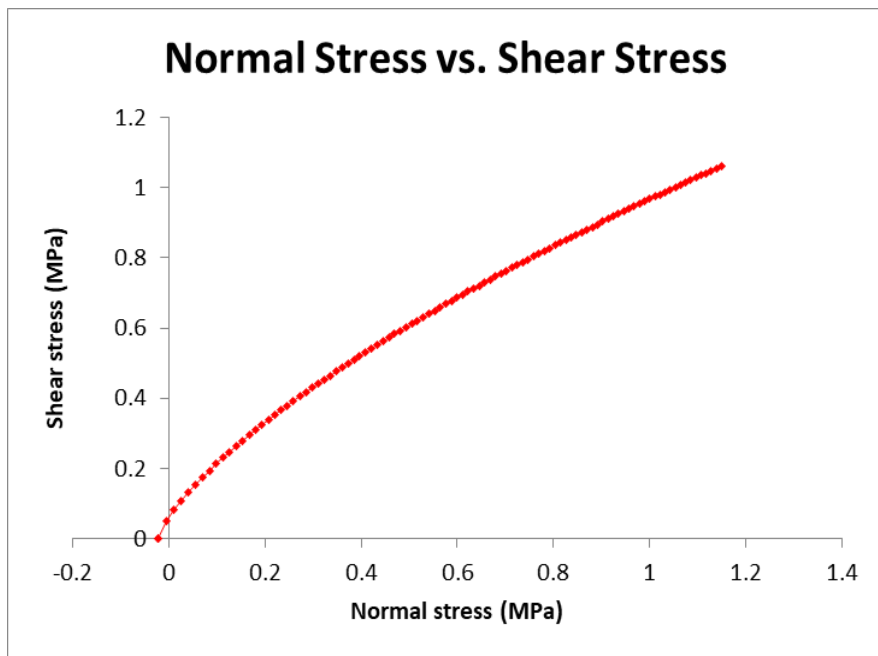
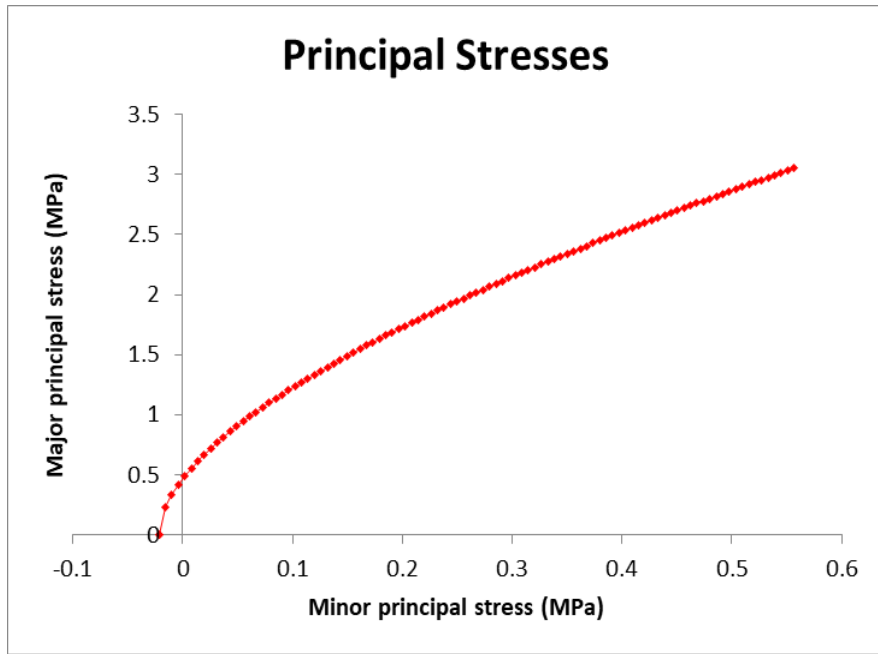


Figure 4.63: Hoek Brown Failure Envelope for Zone 1 Representing Principal Stresses and Normal Stress vs. Shear Stress

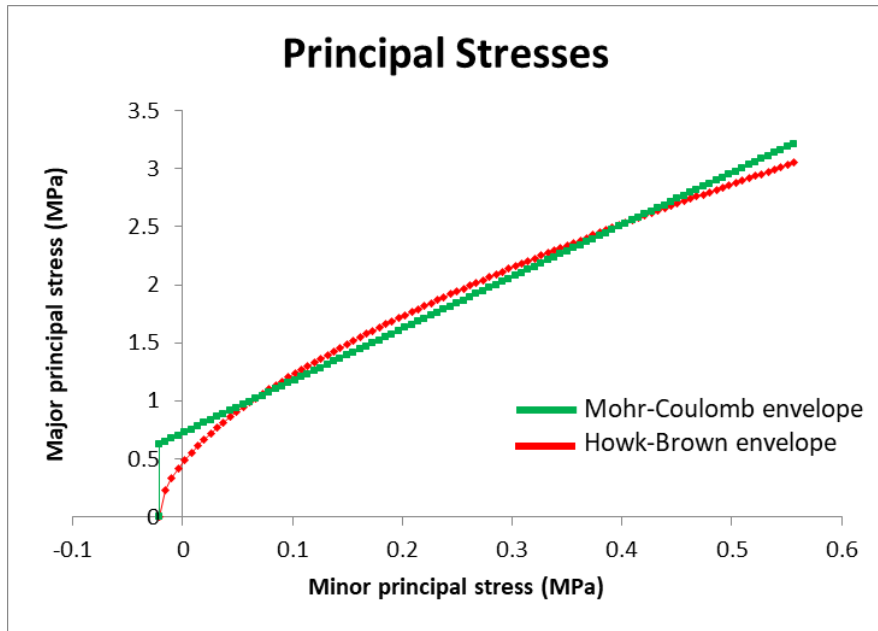


Figure 4.64: Mohr-Coulomb and Hoek Brown Failure Envelopes for Zone 1

values of the other parameters such as the dilation angle, the horizontal to vertical stress ratio (k ratio), and the locked-in horizontal stresses were used for the numerical modelling. The input parameters for deterministic numerical modelling are presented in Table 4.24. The slopes at the seven zones in the quarry were analysed using three criteria, the maximum shear strain plot, displacement plot and the SRF.

4.4.3.1 Maximum Shear Strain Plots

Figures 4.65 - 4.71 show the maximum shear plots for the slopes at zones 1 – 7 respectively which represent the present state of the stability at the BUA Ikpobia Quarry. There was also about 1 % shear strain at the toes of slopes of zones 2 and 5. Shear strain ranges between 1 and 2 % in the zones 1, 3, 4, 6 and 7. The contours of the maximum shear strain obtained at all the zones has a diagonal shape, though was still small because the slope was stable, but indicated the presence of circular failure, which is common in highly weathered slopes.

4.4.3.2 Total Displacement Plots

The total displacement plots and obtained from the numerical modelling for the slopes of zones 1 to 7 are shown in Figures 4.72 to 4.78 respectively. It was observed from the figures that the total displacement of zones 1, 3, 6 and 7 was the lowest in the quarry and ranges from 15 – 20 mm, and was a little bit higher than 20 mm in zones 2 and 4. Meanwhile, it was very high at the zone 5 where it reaches 60 mm at the crest. This gives the idea about the early failure detection at the quarry site and calls attention for reviewing the slope design.

4.4.3.3 Strength Reduction Factor

Strength Reduction Factor (SRF) is equivalent to limit equilibrium factor of safety. The SRF values obtained from the numerical modelling of the slopes of zones 1 to 7 are presented in Table 4.25. The SRF for each zone was compared with the recommended critical factor of safety (F_c) (1.3). The results show that all the slopes of Ikpobia Quarry were stable during the field study because the SRF was higher than 1.3. It was observed from the table that the most current stable slope was the one of zone 4 (1.69) and that is because its angle is flatter than others (75°). Others differed but zones 3 and 6 were the closest to the critical factor of safety hence were the closest to the instability (1.34). All SRF values were obtained during the field study while

Table 4.24: Input Parameters for the Phase 2 Software for All the Zones

	Internal friction angle ϕ (°)	Cohesion c_0 (MPa)	Poisson's ratio	Deformation modulus Mpa	Unit weight (KN)	Slope geometry		Tensile strength MPa
						Slope angle (°)	Slope height (m)	
Zone 1	39.45	0.169	0.2433	612.28	0.027	85	25	0.0216
Zone 2	36.67	0.141	0.2433	480.85	0.027	80	25	0.014
Zone 3	35.27	0.103	0.2433	394.77	0.027	80	20	0.0086
Zone 4	38.31	0.125	0.2433	480.85	0.027	75	20	0.0136
Zone 5	35.32	0.156	0.2433	480.85	0.027	80	30	0.0136
Zone 6	35.27	0.103	0.2433	394.77	0.027	80	20	0.0086
Zone 7	39.45	0.169	0.2433	612.28	0.027	85	25	0.0216

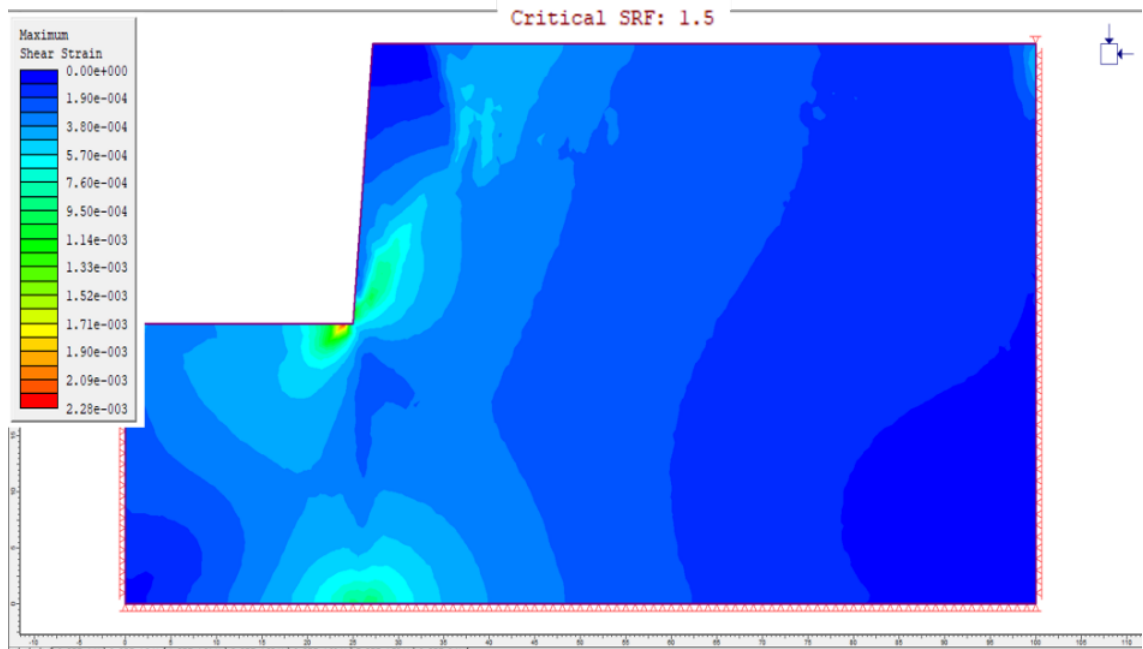


Figure 4.65: Maximum Shear Strain for Slope at Zone 1

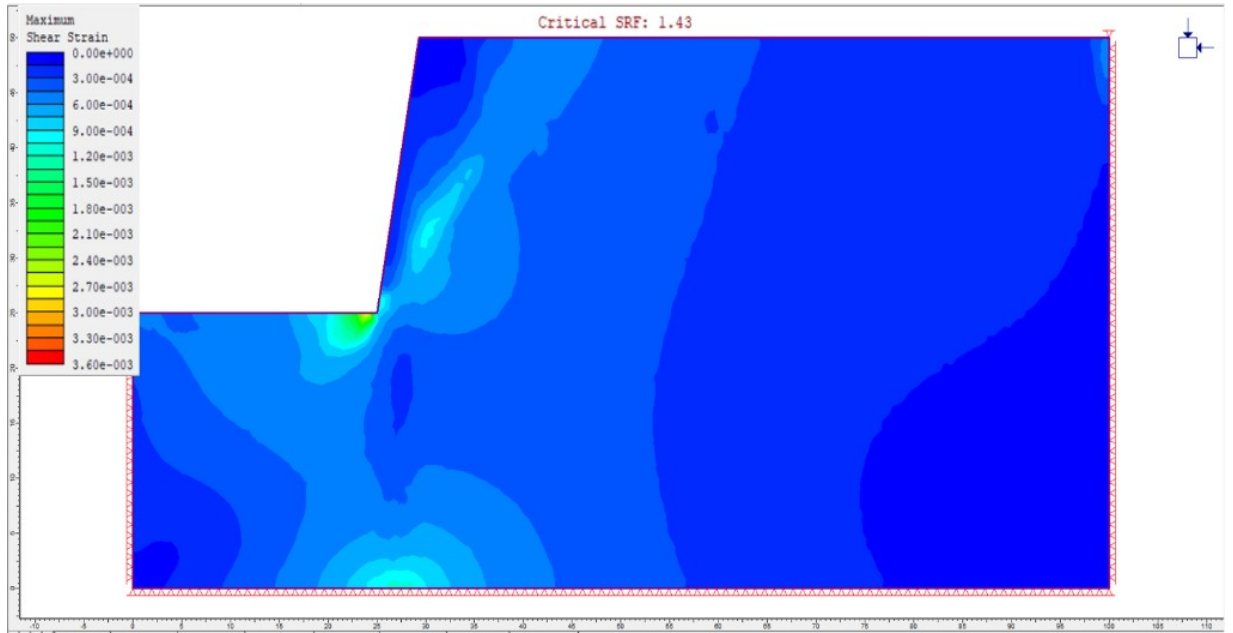


Figure 4.66: Maximum Shear Strain for Slope at Zone 2

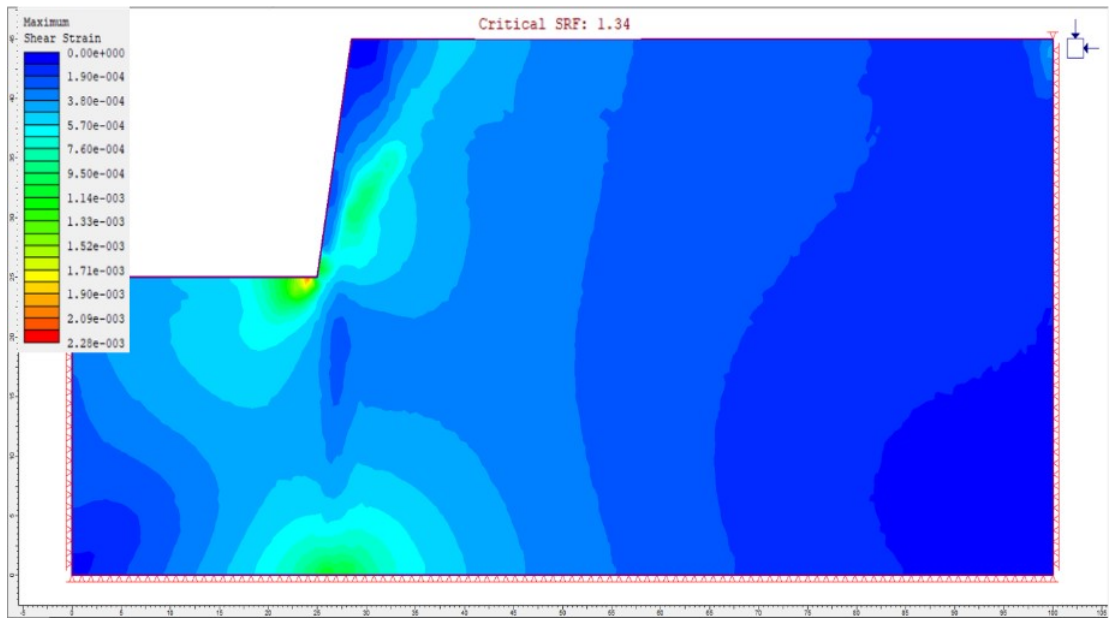


Figure 4.67: Maximum Shear Strain for Slope at Zone 3

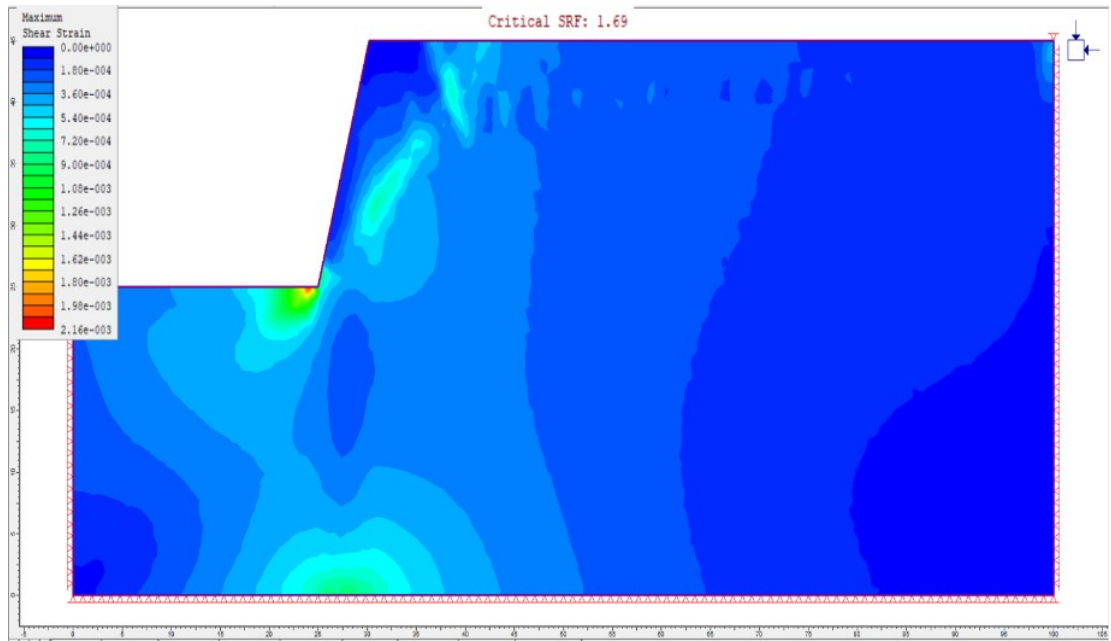


Figure 4.68: Maximum Shear Strain for Slope at Zone 4

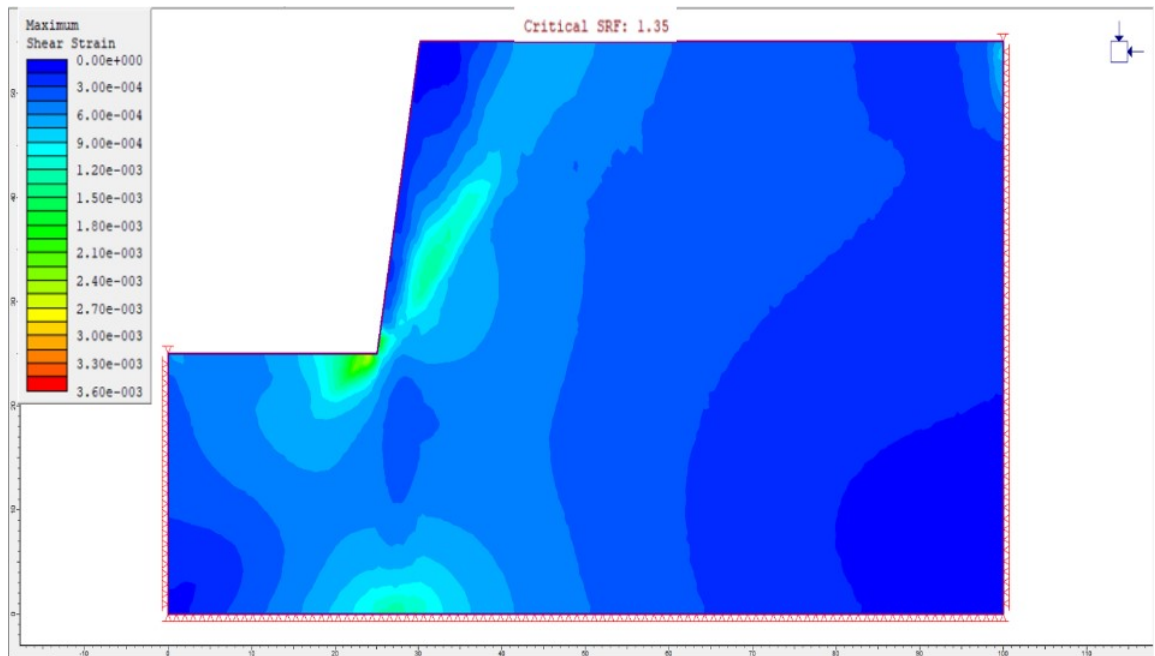


Figure 4.69: Maximum Shear Strain for Slope at Zone 5

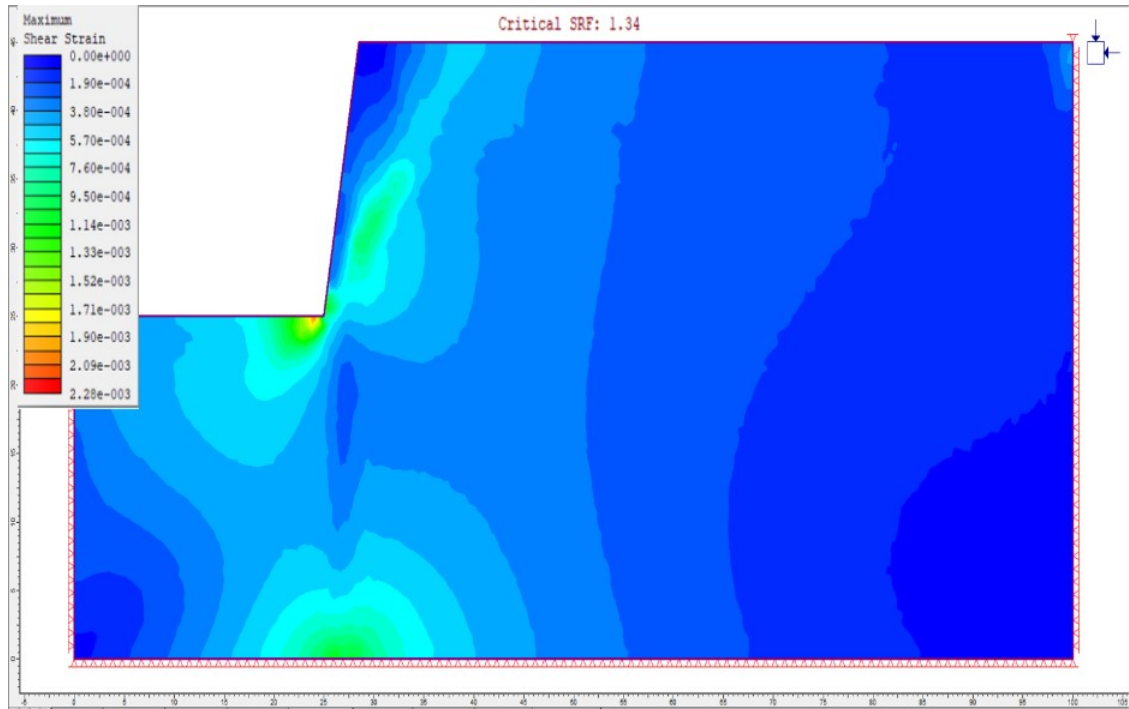


Figure 4.70: Maximum Shear Strain for Slope at Zone 6

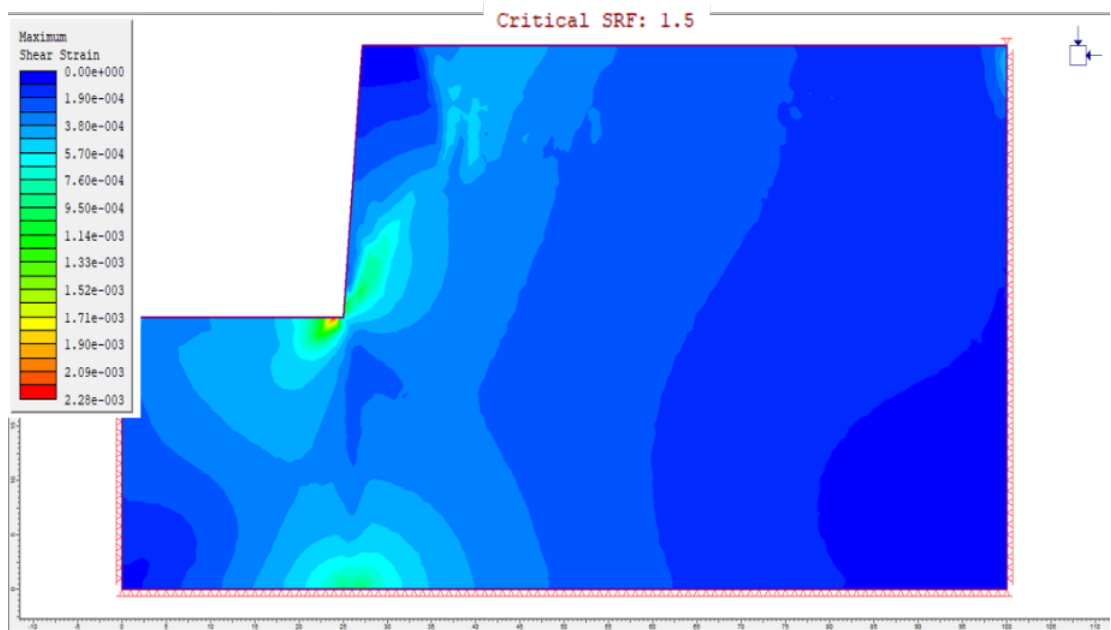


Figure 4.71: Maximum Shear Strain for Slope at Zone 7

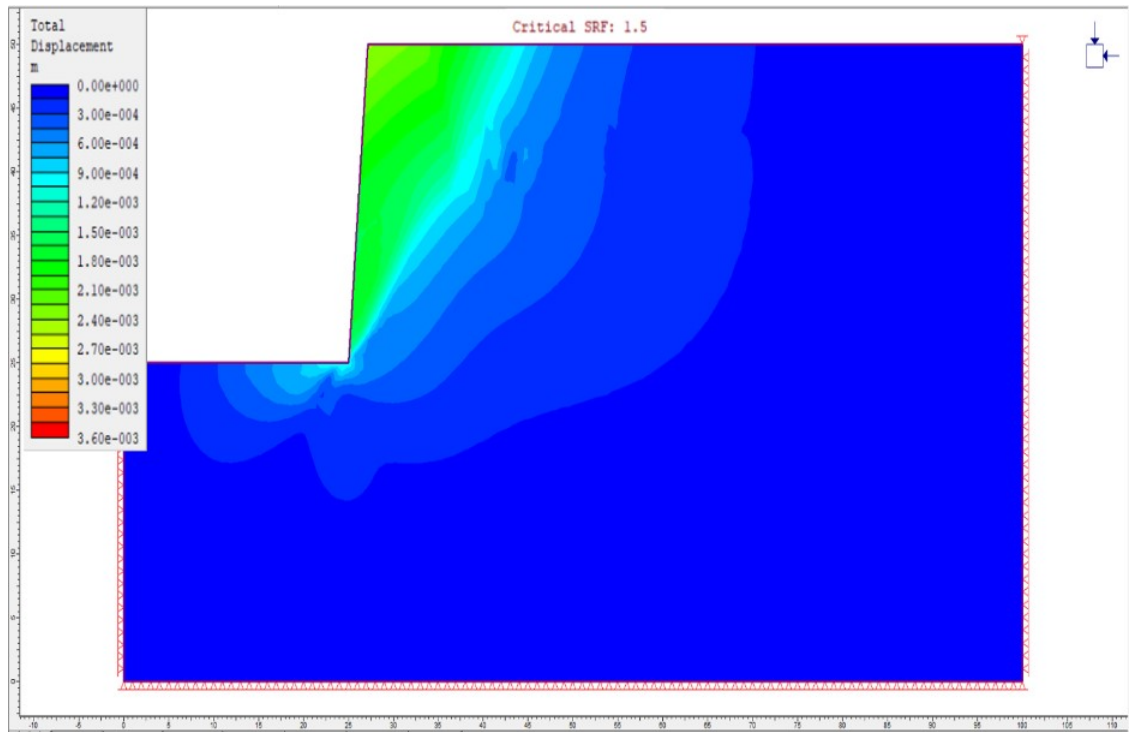


Figure 4.72: Total Displacement for Slope of Zone 1

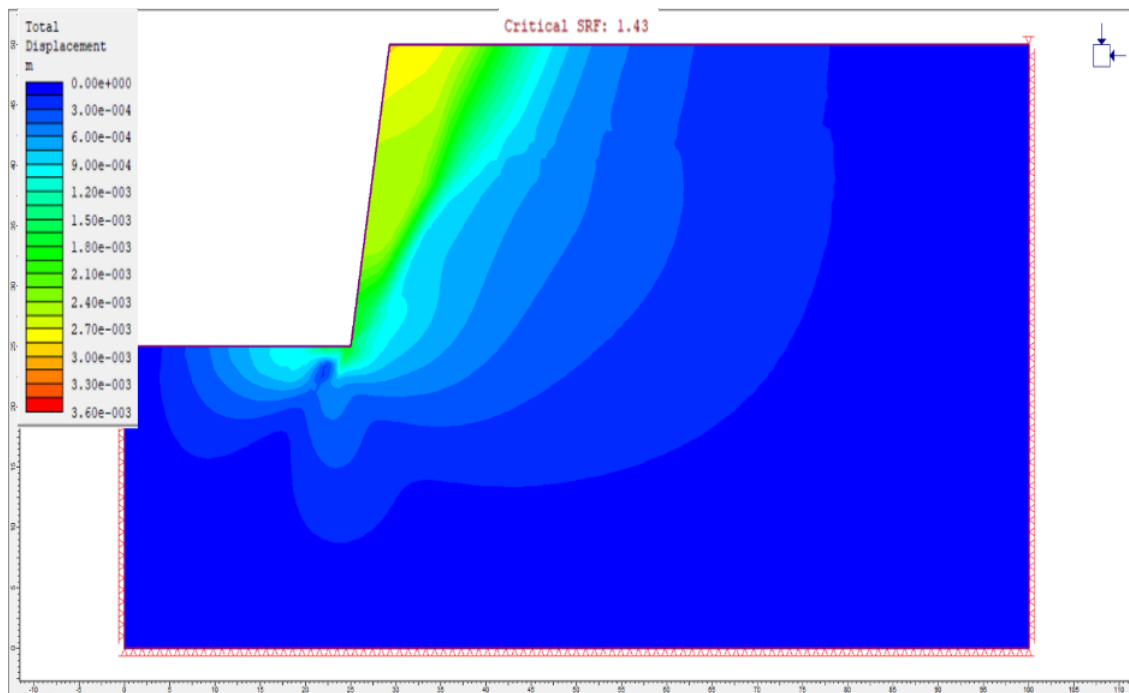


Figure 4.73: Total Displacement for Slope of Zone 2

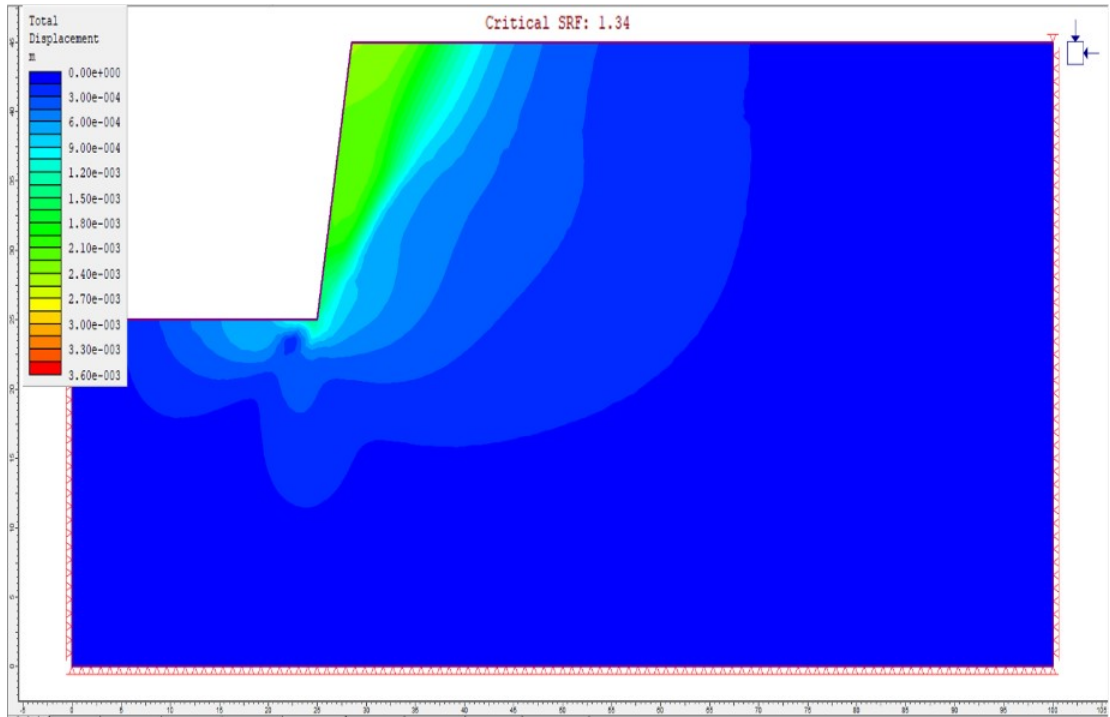


Figure 4.74: Total Displacement for Slope of Zone 3

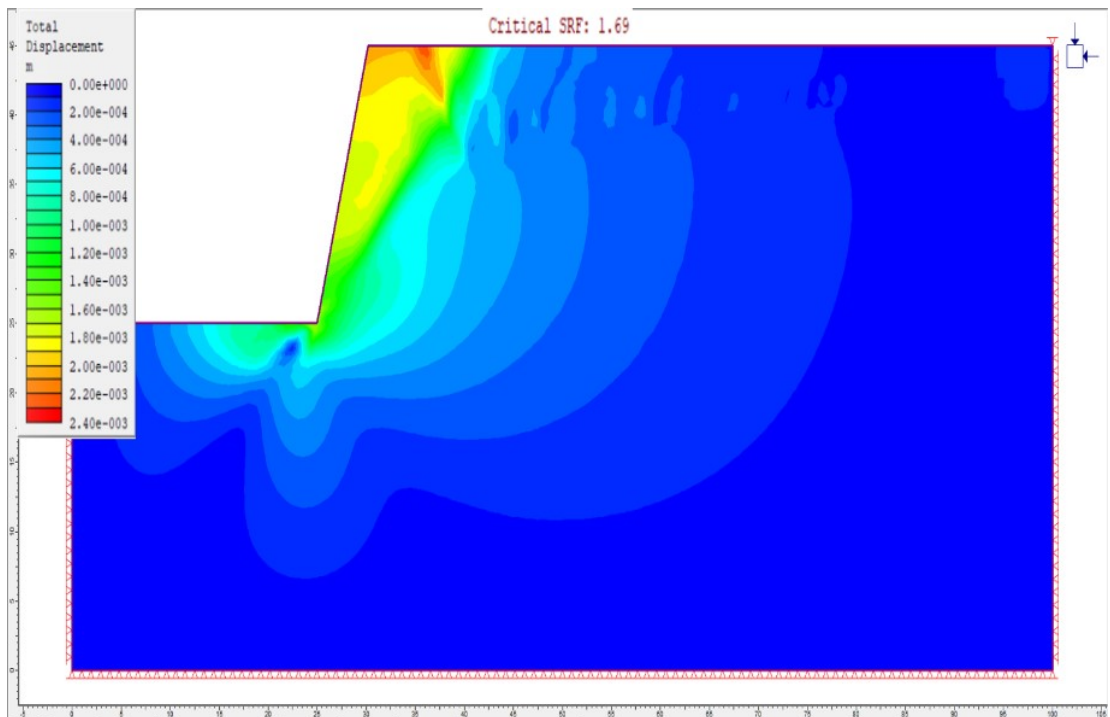


Figure 4.75: Total Displacement for Slope of Zone 4

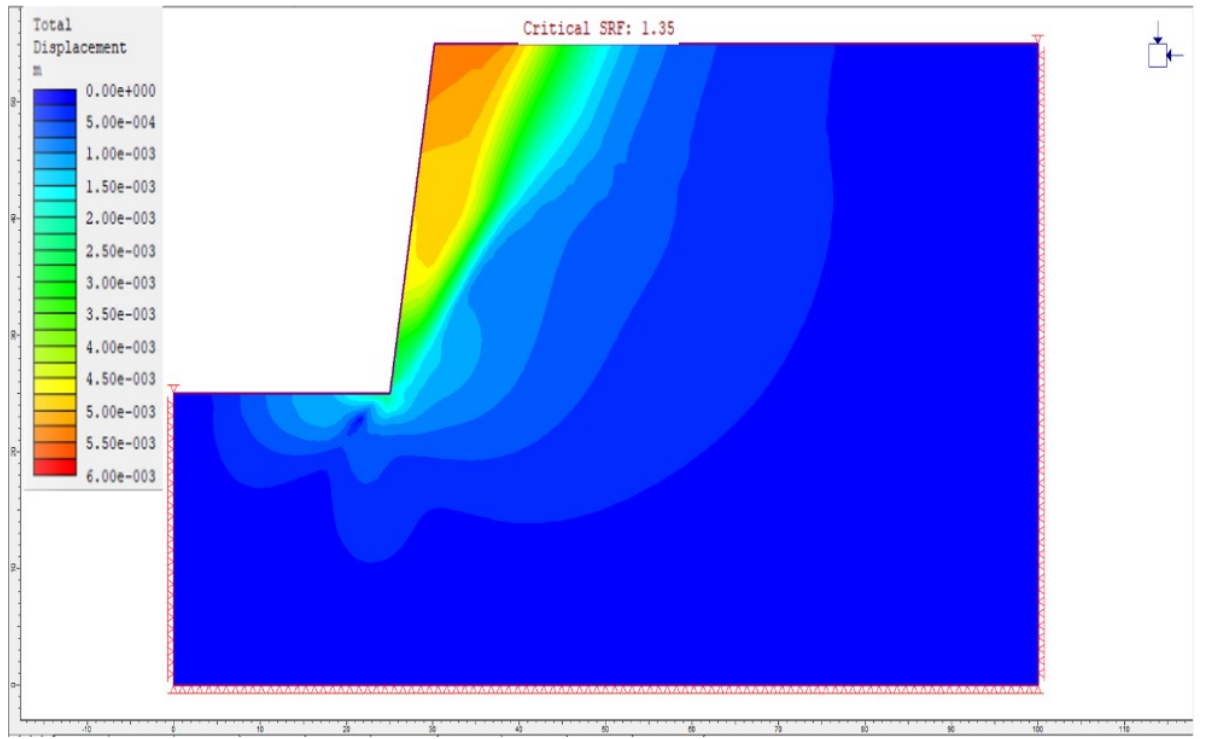


Figure 4.76: Total Displacement for Slope of Zone 5

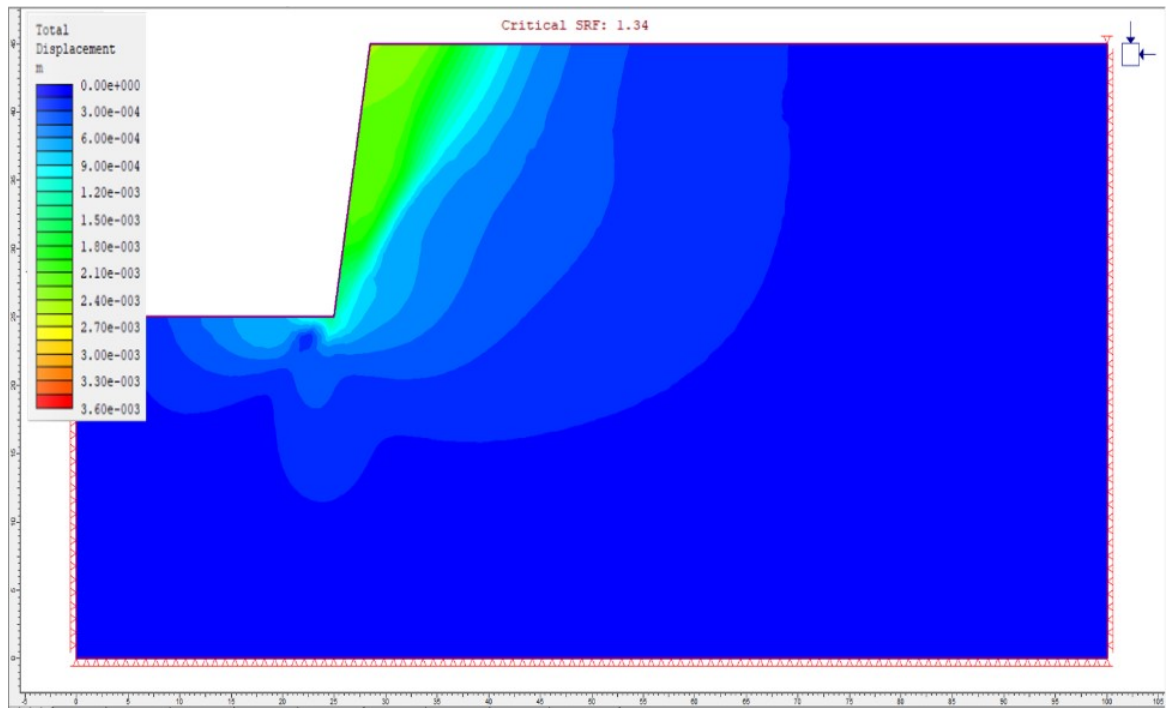


Figure 4.77: Total Displacement for Slope of Zone 6

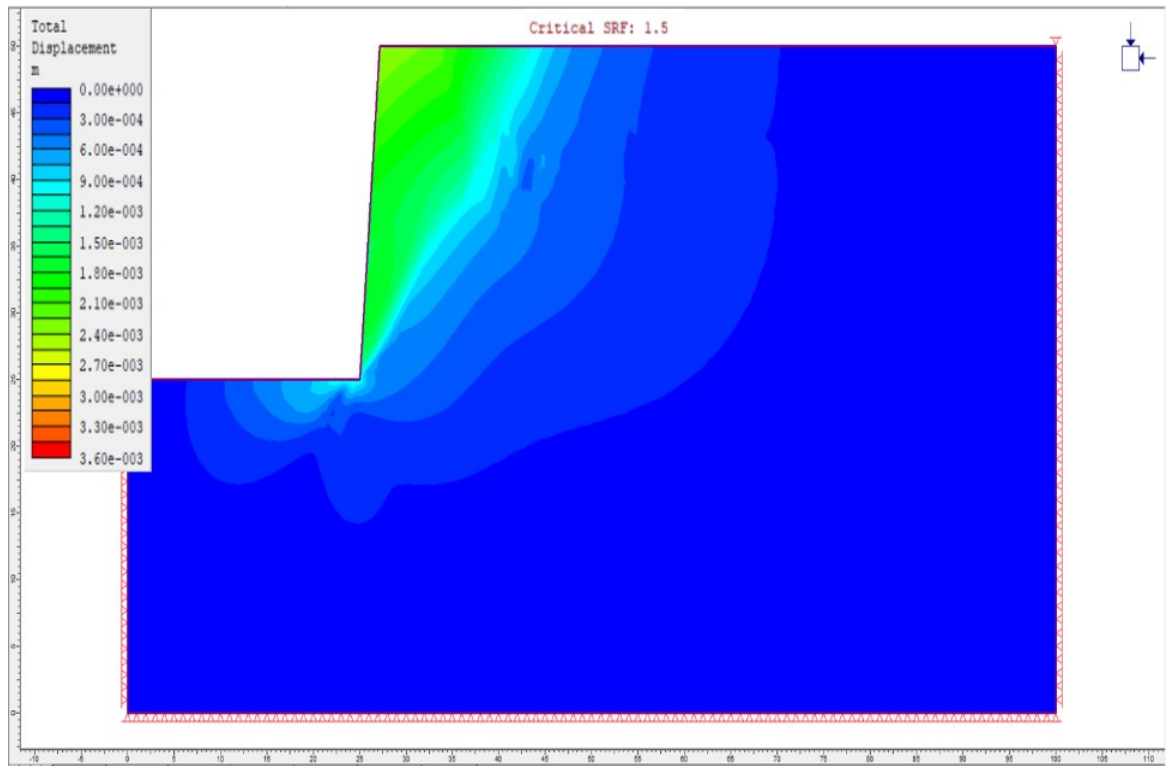


Figure 4.78: Total Displacement for Slope of Zone 7

Table 4.25: Critical SRF of the Seven Zones of Ikpobia Quarry

Slope Zone	Critical SRF	Recommended Fc	Current State
1	1.5	1.3	Stable
2	1.43	1.3	Stable
3	1.34	1.3	Stable
4	1.69	1.3	Stable
5	1.35	1.3	Stable
6	1.34	1.3	Stable
7	1.5	1.3	Stable

works were progressing which makes those values keep changing as the pit gets deeper, which calls for sensitivity studies to be able to predict SRF at deeper slopes. Generally, it can be deduced from the Phase 2 inputs and SRF results that the friction angle and cohesion play an important role in determining the SRF (the higher friction angle and cohesion the higher SRF).

4.4.3.4 Sensitivity Analyses for the Deterministic Modelling

Sensitivity analyses were performed to determine the influence of slope height and slope angle variations on the slope failure. This was done by fixing the slope angle and increasing the slope height till it reaches 70 m which is the expected maximum slope height because this was the depth of the marble deposit. Then decreasing the slope angle until getting a stable slope that has a critical SRF of 1.3 or above. This simulation analysis was repeated for the 7 zones and results are presented below in Tables 4.26 – 4.39. The critical SRF obtained from the analysis results of zone 1 are presented in Table 4.26 which represents a summary of sensitivity analysis of zone 1 slope at 85° angle. The analysis started from the present SRF at the zone 1 slope height which shows that it was stable (1.5). It then simulated the stability after the work progress at the quarry with the increasing of the slope and the simulation at different heights, from 25 to 70 m, shows that the slope will remain stable till the height of 35 m. Any height more than this will be unstable. Knowing that the deposit has a depth of 70 m, the slope will reach a 70 m height and it will not be stable at the current angle (85). The simulation of different angles at the height of 70 m shows that the best angle of stability for the slope is 55 and any angle higher than this will make the slope unstable (Table 4.27 and Figures 4.79 – 92). The analyses of zone 2 show that the slope will fail if it passes 35 m height because it has a critical SRF of 1.3 at 35 m and the optimum angle of slope in this zone is 40° where the slope has a critical SRF of 1.37 at the height of 70 m (Tables 4.28 and 4.29). At zone 3, the sensitivity analysis show that the slope was stable at the present state but it doesn't support a more increment because it shows the critical SRF was 1.06 at the height of 30 which was not far from the current height (Table 4.30). It was observed from Table 4.31, that the minimum slope angle that will ensure stability at zone 3 is less than 25 because the SRF at 25 was 1.29 which was less than the recommended SRF 1.3 and the best angle that ensures stability in this case is angle 20 where SRF equals to 1.33. The sensitive analysis at zones 4, 5, 6 and 7 show that the slopes at the zones cannot exceed the

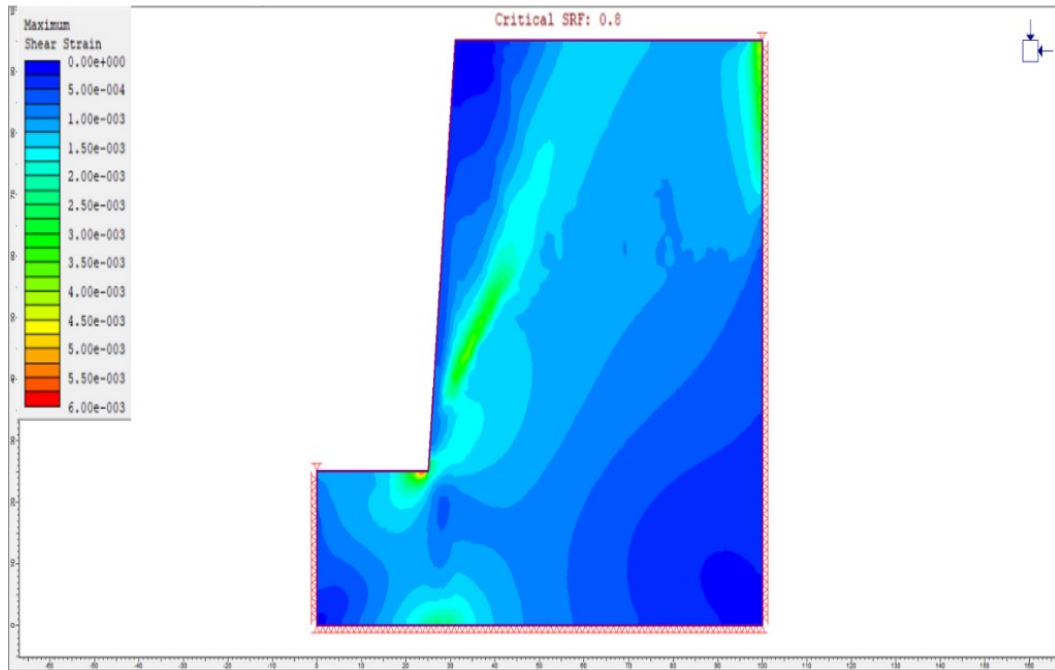


Figure 4.79: Maximum Shear Strain Plot for the Slope of Zone 1 at 70 m Height and Angle of 85°

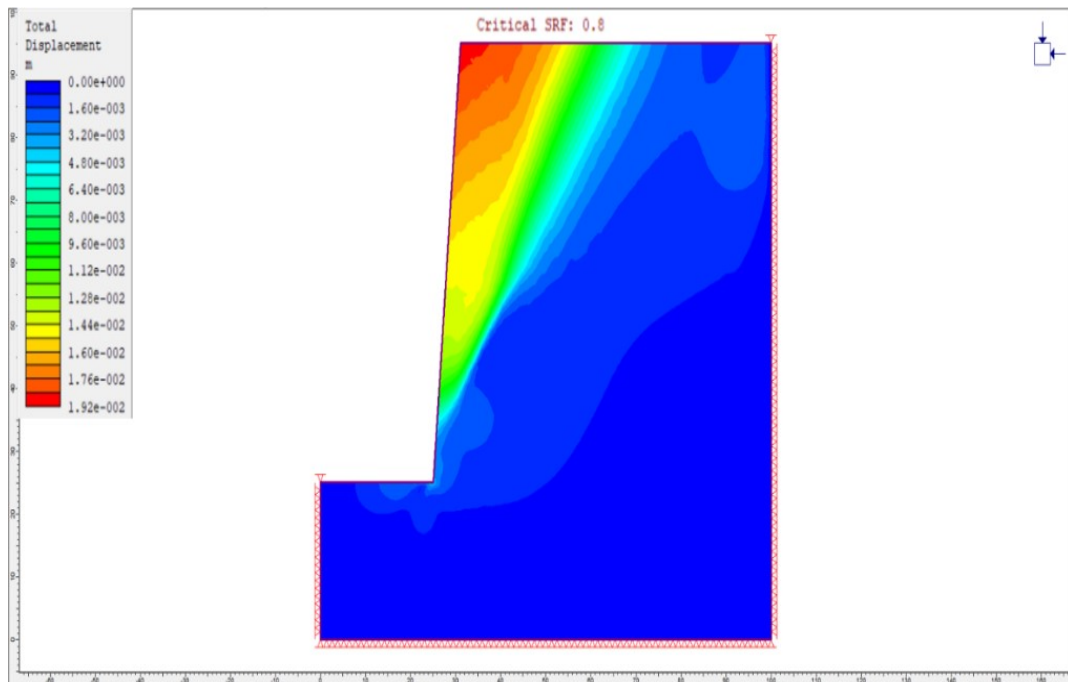


Figure 4.80: Total Displacement Plot for Slope at 70 m Height and Angle of 85°

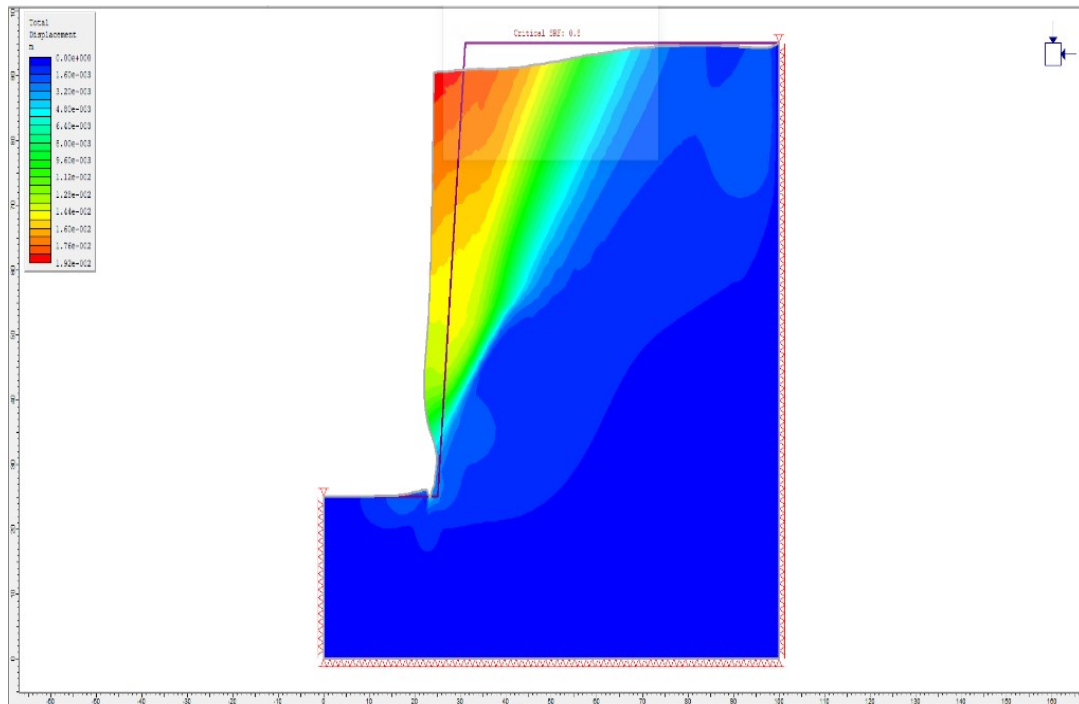


Figure 4.81: Deformation Contour for the Slope of Zone 1 at 70 m Height and Angle of 85°

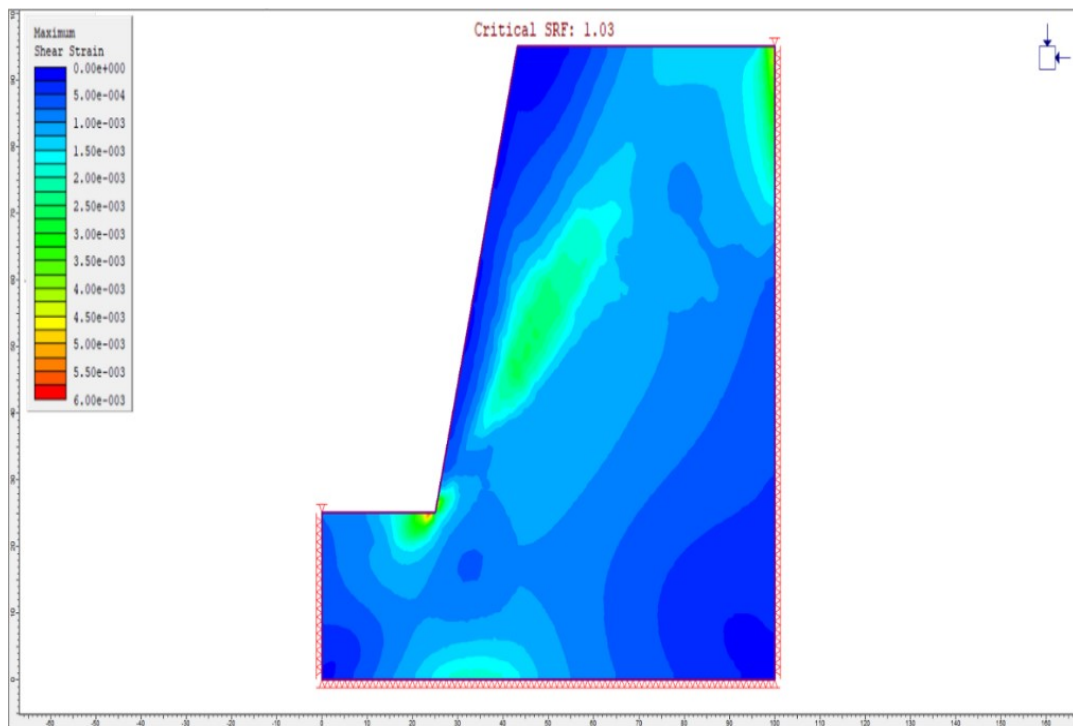


Figure 4.82: Maximum Shear Strain Plot for the Slope of Zone 1 at 70 m Height and Angle of 75°

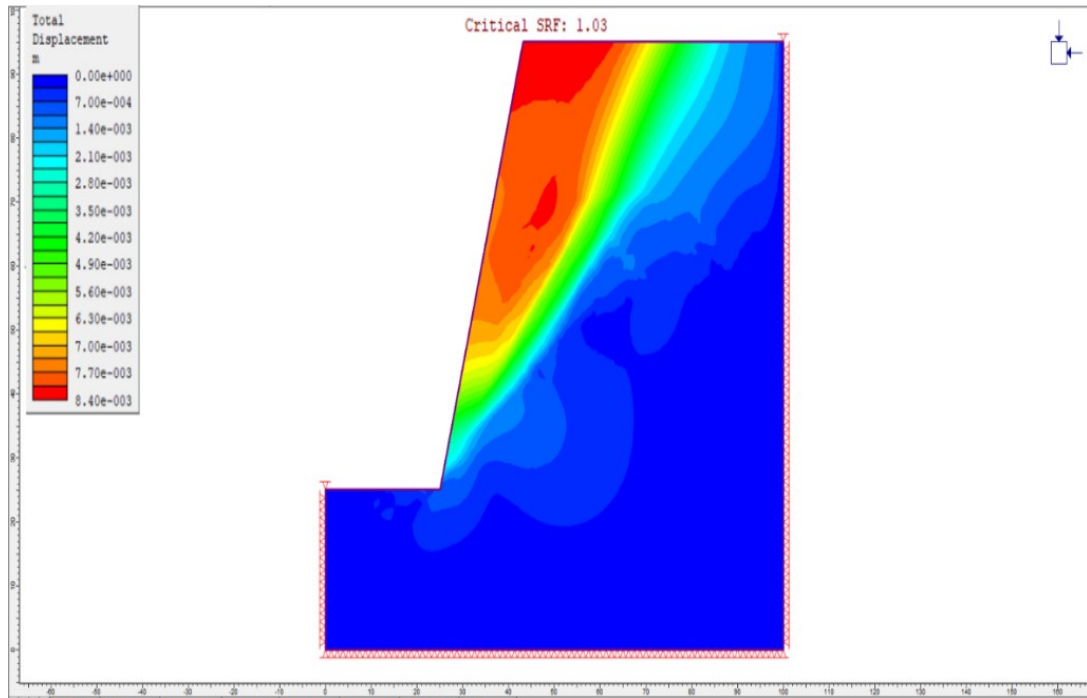


Figure 4.83: Total Displacement Plot for Slope at 70 m Height and Angle of 75

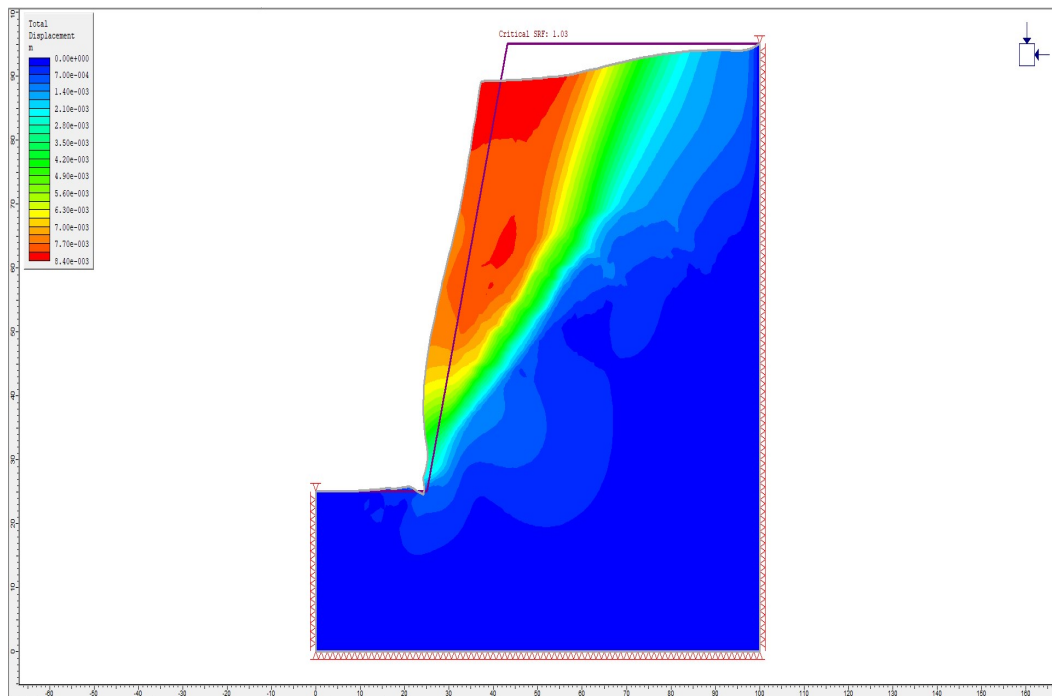
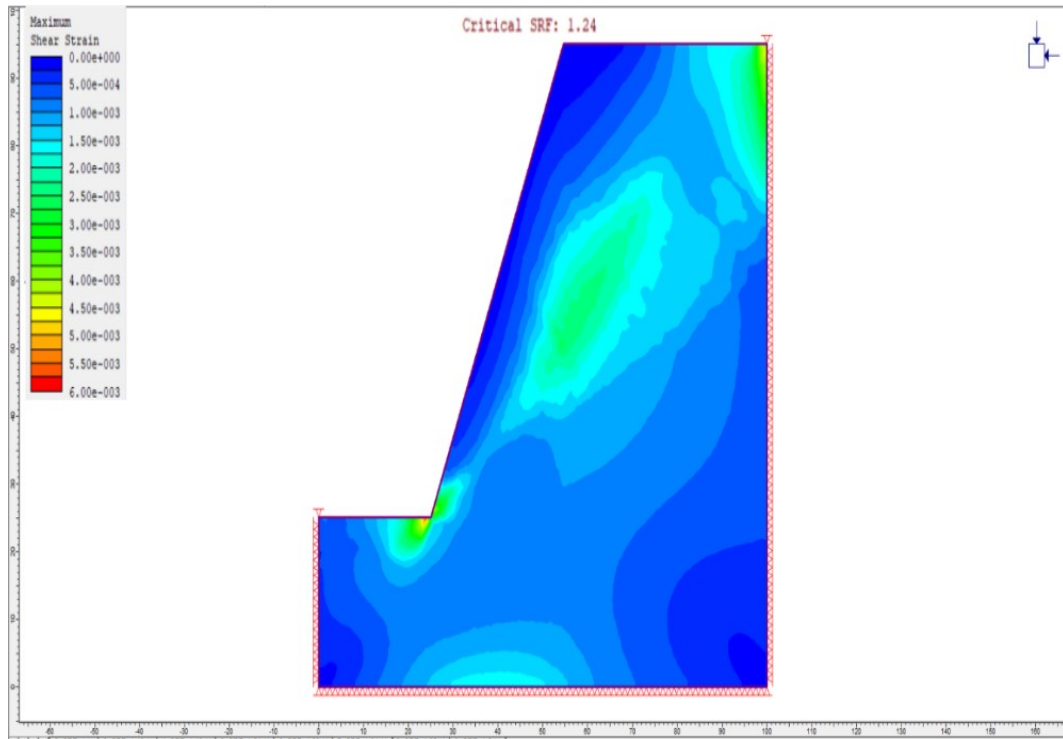


Figure 4.84: Deformation Contour for the Slope of Zone 1 at 70 m Height and Angle of 75°



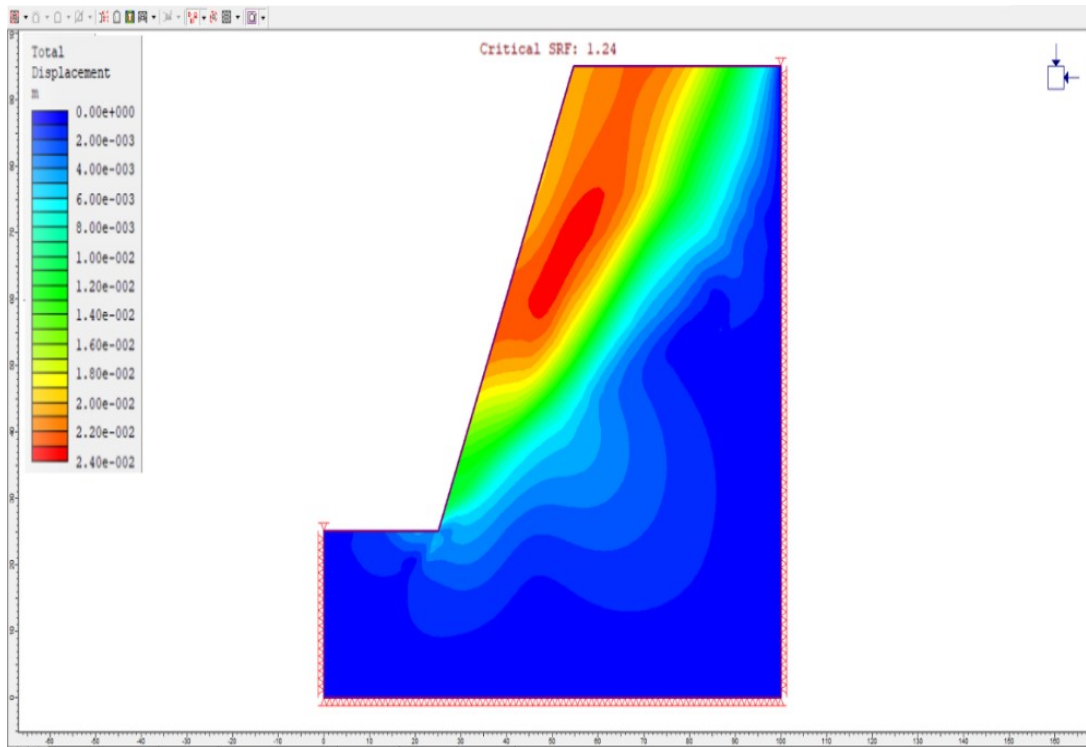


Figure 4.86: Total Displacement Plot for Slope at 70 m Height and Angle of 65

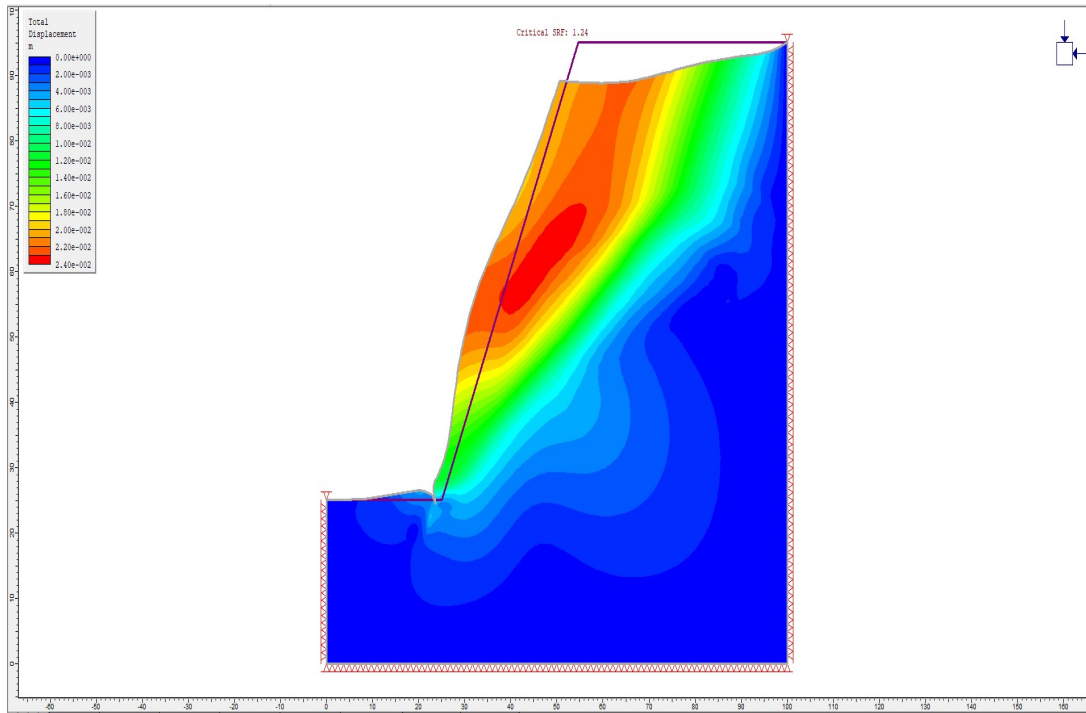


Figure 4.87: Deformation Contour for the Slope of Zone 1 at 70 m Height and Angle of 65°

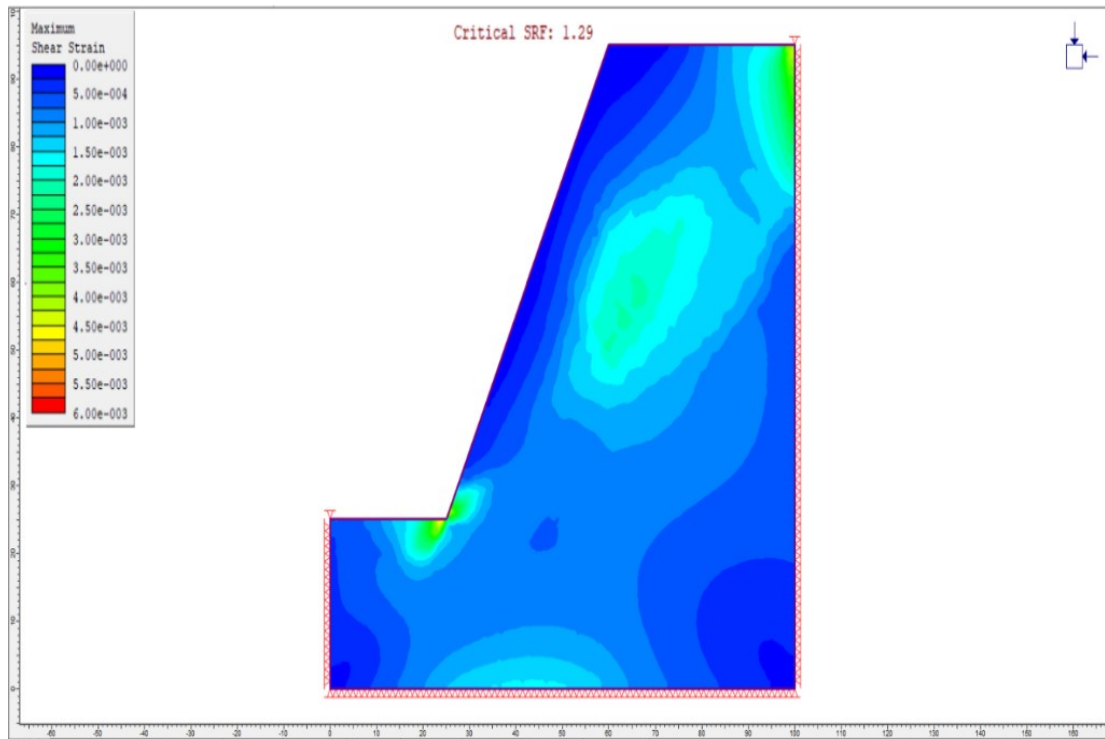


Figure 4.88: Maximum Shear Strain Plot for the Slope of Zone 1 at 70 m Height and Angle of 60°

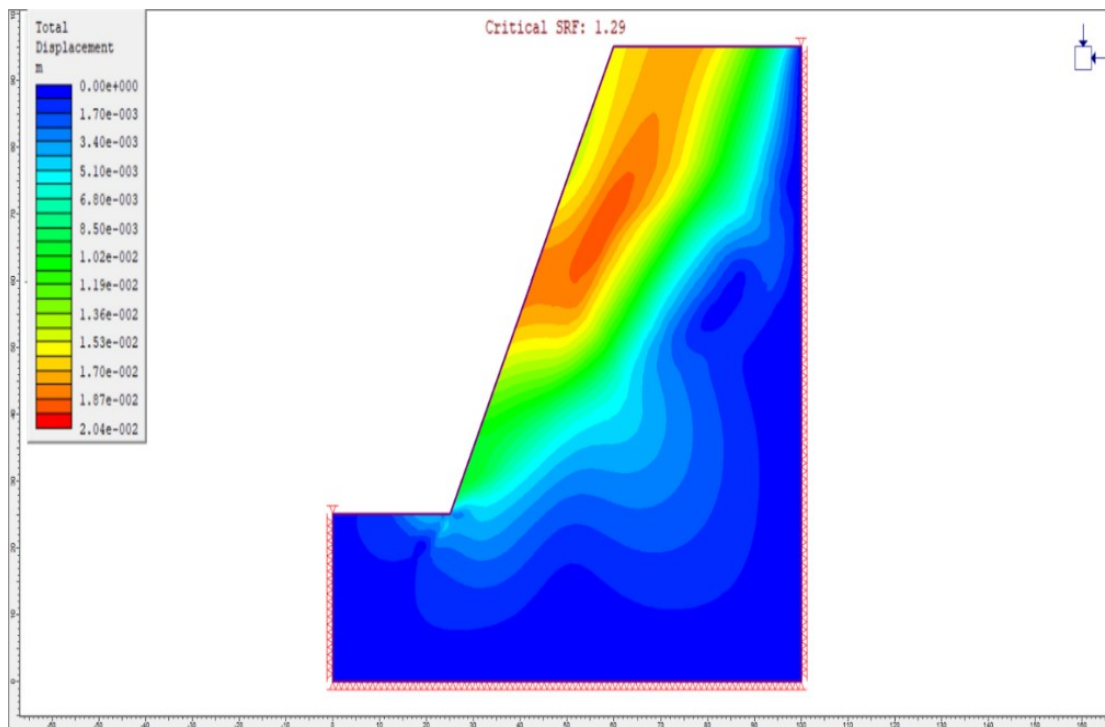


Figure 4.89: Total Displacement Plot for Slope at 70 m Height and Angle of 60°

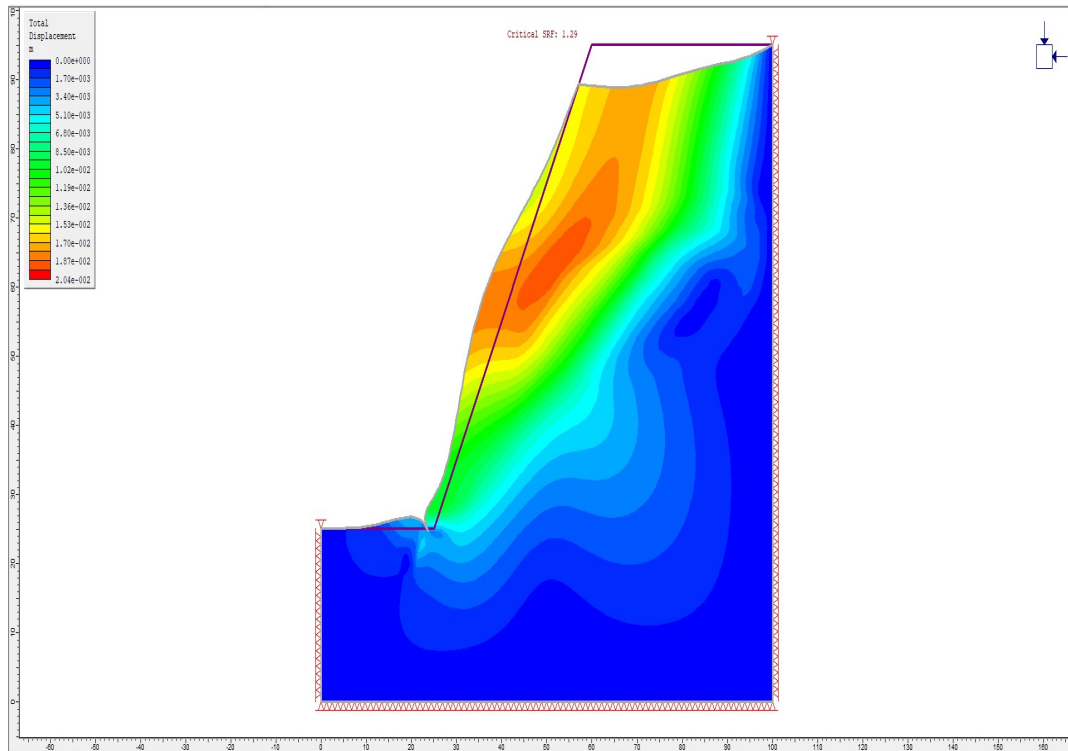


Figure 4.90: Deformation Contour for the Slope of Zone 1 at 70 m Height and Angle of 60°

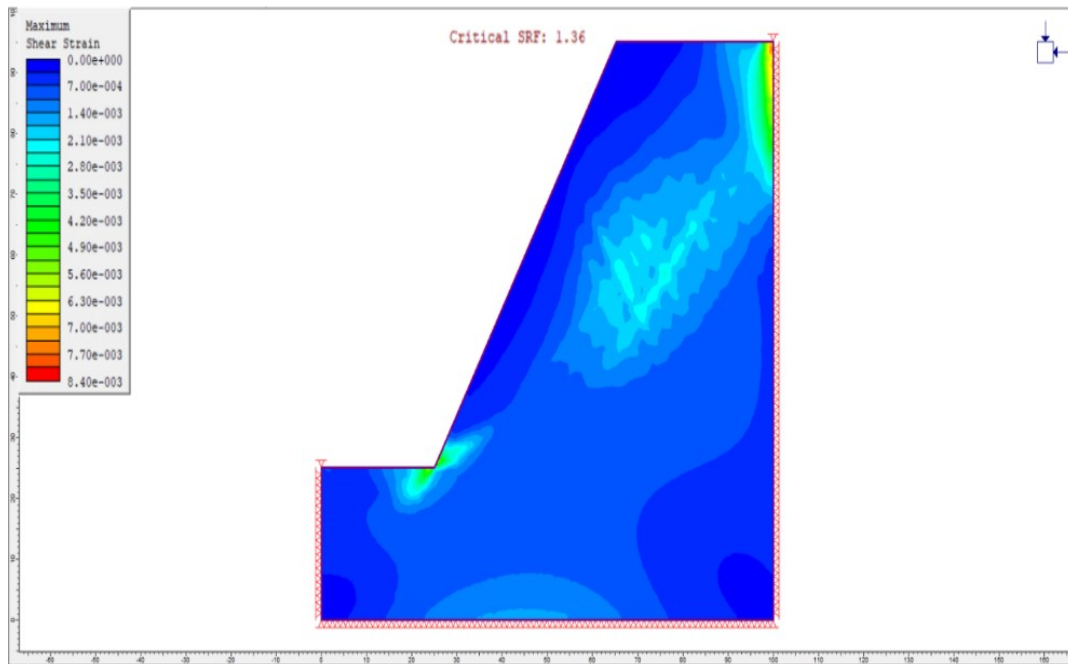


Figure 4.91: Maximum Shear Strain Plot for the Slope of Zone 1 at 70 m Height and Angle of 55°

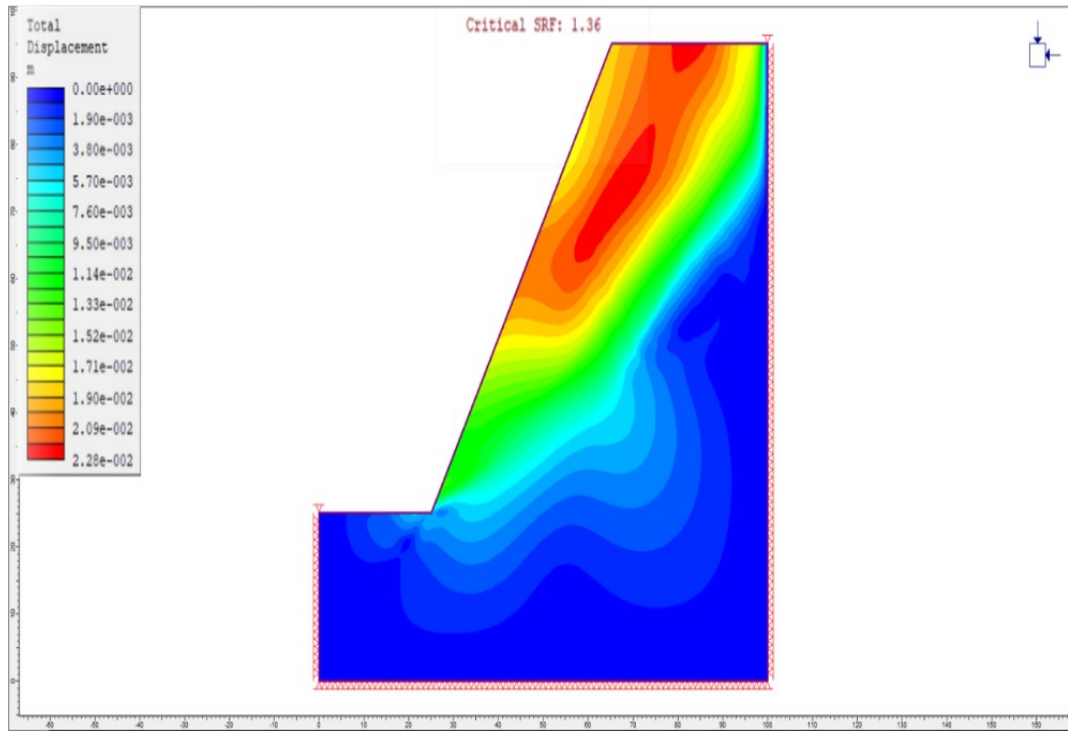


Figure 4.92: Total Displacement Plot for Slope at 70 m Height and Angle of 55°

Table 4.26: Summary of Sensitivity Analysis for Slope of the Zone 1 at Angle of 85°

Slope angle (°)	Slope height (m)	SRF
85	25	1.5
85	35	1.30
85	45	1.17
85	55	1.07
85	65	1.01
85	70	0.8

Table 4.27: Summary of Sensitivity Analysis for Slope of the Zone 1 at 70 m Height

Slope angle (°)	Slope height (m)	SRF
85	70	0.8
75	70	1.03
65	70	1.24
60	70	1.29
55	70	1.36

Table 4.28: Summary of Sensitivity Analysis for Slope of the Zone 2 at Angle of 80°

Slope angle (°)	Slope height (m)	SRF
80	25	1.5
80	35	1.30
80	40	1.17

Table 4.29: Summary of Sensitivity Analysis for Slope of the Zone 2 at 70 m Height

Slope angle (°)	Slope height (m)	SRF
80	70	0.70
70	70	0.87
60	70	1.15
40	70	1.37

Table 4.30: Summary of Sensitivity Analysis for Slope of the Zone 3 at Angle of 80°

Slope angle (°)	Slope height (m)	SRF
80	20	1.34
80	30	1.06
80	70	0.64

Table 4.31: Summary of Sensitivity Analysis for Slope of the Zone 3 at 70 m Height

Slope angle (°)	Slope height (m)	SRF
80	70	0.64
70	70	0.82
50	70	0.98
30	70	1.25
25	70	1.29
20	70	1.33

heights 20, 30, 20 and 25 meters respectively which means the need of reducing the slope angle to be able to go deeper in the exploitation of the deposit which has a depth of 70 m. The sensitivity analysis estimated the optimum angles were the slopes can maintain stability with increase depths till 70 m are 40°, 45°, 20°, 55° for zones 4, 5, 6 and 7 respectively. These are presented in Tables 4.32 – 4.49. The graph in Figure 4.93 summarises the results of the optimum angle of the 7 zones at the quarry.

Table 4.32: Summary of Sensitivity Analysis for Slope of the Zone 4 at Angle of 75°

Slope angle (°)	Slope height (m)	SRF
75	20	1.69
75	45	1.09
75	70	0.85

Table 4.33: Summary of Sensitivity Analysis for Slope of the Zone 4 at 70 m Height

Slope angle (°)	Slope height (m)	SRF
75	70	0.85
55	70	1.13
45	70	0.29
40	70	1.35

Table 4.34: Summary of Sensitivity Analysis for Slope of the Zone 5 at Angle of 80°

Slope angle (°)	Slope height (m)	SRF
80	30	1.35
80	50	0.98
80	70	0.8

Table 4.35: Summary of Sensitivity Analysis for Slope of the Zone 5 at 70 m Height

Slope angle (°)	Slope height (m)	SRF
70	70	0.8
50	70	1.27
45	70	1.33

Table 4.36: Summary of Sensitivity Analysis for Slope of the Zone 6 at Angle of 80°

Slope angle (°)	Slope height (m)	SRF
80	20	1.34
80	40	0.89
80	70	0.64

Table 4.37: Summary of Sensitivity Analysis for Slope of the Zone 6 at 70 m Height

Slope angle (°)	Slope height (m)	SRF
80	70	0.64
60	70	0.98
40	70	1.17
20	70	1.33

Table 4.38: Summary of Sensitivity Analysis for Slope of the Zone 7 at Angle of 85°

Slope angle (°)	Slope height (m)	SRF
85	25	1.5
85	40	1.11
85	70	0.80

Table 4.39: Summary of Sensitivity Analysis for Slope of the Zone 7 at 70 m Height

Slope angle (°)	Slope height (m)	SRF
85	70	0.8
65	70	1.24
60	70	1.29
55	70	1.36

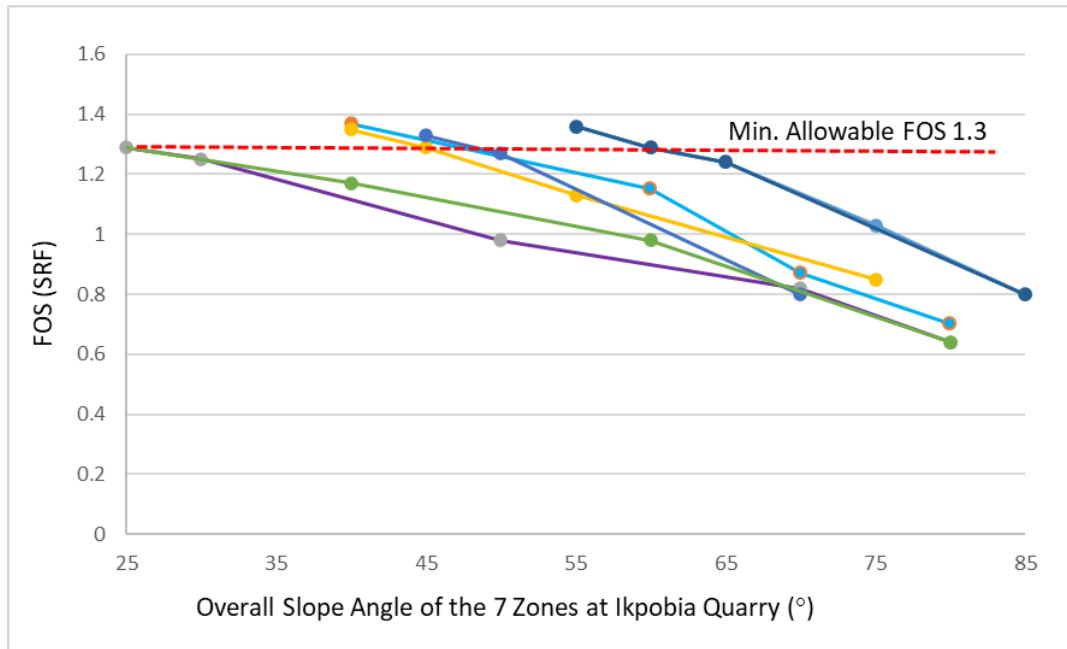


Figure 4.93: SRF Results of the Slope Angle Optimization Analyses for the Ikpobia Quarry

CHAPTER FIVE

CONCLUSIONS AND RECOMMENDATIONS

5.1 CONCLUSIONS

This research covers some aspects of geology and engineering that have influence on the slope stability and design optimization. The key findings of the research study is that it has identified the geological and geomechanical characteristics of the quarry pit that can affect the slope stability at Ikpobia Quarry with the increasing depth of mining. The importance of slope design optimization for open pit mines and quarries can be briefed in the production optimization and the safety insurance. High slope angles can reduce the stripping ratio, hence, increase economic profit but also increases the risk of slope failure. The optimized slope angle insures the maximum profit and the stable slope. In order to optimize the slope angles, at the BUA Ikpobia Quarry, different site investigations and laboratory analyses and numerical modelling were carried out. The following conclusions can be drawn from this research project:

1. The geological investigation has helped in the determination of the maximum depth of the pit that is the depth of the deposit which was used to determine the height of the slope for the slope design.
2. The geological investigation of the deposit has increased the knowledge of the pit quarry which has helped in understanding the mineralogy and its effects on the slope stability.
3. The geophysical investigation helped in understanding the subsurface structure and the groundwater flow which gave an important idea about the possible situations and movements of the groundwater and how can that affect the slope stability.
4. The DEM investigation helped in understanding the topography of the area and the flow of surface and groundwater which made a contribution to the slope stability analysis and design which is expecting the surface water and groundwater effects on the slope stability.
5. The use of 3D Zephyr free software for the photogrammetry analysis was a new attempt in the field of mining and was of many benefits because it insured safety and saved time and efforts.

6. 3D Zephyr free software helped in the structural analysis through determining the properties of joint sets at slopes faces in the quarry accurately.
7. The determination of joint sets properties showed the importance of discontinuity orientation to the stability of slopes from the results of kinematic analyses.
8. The kinematic analysis is a simple and important analytical method used for slope stability investigation.
9. The kinematic analysis showed the possible mode of failure in each zone depending on the discontinuity measurements with respect to the bench face orientation only.
10. The kinematic analysis showed the importance of joint set measurements for slope stability analysis, hence, the importance of structural investigation for slope stability and design.
11. The rock mass properties estimation is one of the most important aspect for the slope stability and design.
12. The estimation of the rock mass properties gives an idea about the rock mass behaviour.
13. The determination of physical and mechanical properties intact rock is important for the estimation of rock mass properties.
14. Geological observations at the site such as the evaluation of GSI and D are important in the determination of rock mass.
15. Hoek-Brown failure criterion was used to determine the rock mass properties through the use of Rocscience software RocLab.
16. The rock mass properties obtained from RocLab software were used as inputs of the Phase 2 Rocscience software for the Finite Element analysis.
17. The Rocscience Phase 2 software was used for the assessment of slope stability at the present state of the seven zones of the pit.
18. The Rocscience Phase 2 software was used to design the pit slope and obtain the optimum slope angle at all the seven zones of the BUA Ikpobia Quarry.

5.2 RECOMMENDATIONS

The following recommendations were drawn from the different results of the different steps that were followed in this study:

- I. The company should use the results of the geomechanical investigations in this research as part of the data base that can be reached by its engineers. Which will increase their knowledge and understanding of the pit quarry and deposit, hence, increases their confidence on any analysis done.
- II. The company should take into consideration the results of the slope stability in this research and take action particularly at zones 3 and 6 slopes that are currently stable with SRF 1.34 at 20 m but with progress of works the slope height will increase and then the failure will occur. Hence, the urgent need to decrease the slope angle.
- III. It is recommended decreasing the slope angles of all the slopes because the height of the slope will reach 70 m based on the deposit depth, and the angles at which the slope will remain stable even at 70 m are: 55° for slopes at zone 1 and 7 and 40° for slopes at zones 2 and 4 and 20° for slopes at 3 and 6 and an angle of 45° for the slope at zone 5.
- IV. The results of the slope design can be implemented in other quarries in Okpella region because all the deposits in the area have the same characteristics.

5.3 CONTRIBUTION TO KNOWLEDGE

The research reported in this thesis contributes to knowledge with the following:

1. The provision of a data base of geological, geophysical and geomechanical information.
2. The determination of rock mass properties and characteristics.
3. The design of a slope for the quarry that can be used in neighboring quarries with similar characteristics.

REFERENCES

- Adebimpe, R. A., and Akande, J. M. 2014. Open Pit Slope Design of Ajabanoko Iron Ore Deposit, Kogi State, Nigeria. *Journal of Mining World Express* v. 3 25-32.
- Adiuku-Brown, M. 1999. The dangers posed by the abandoned mine ponds and Lotto mines on the Jos Plateau. *Journal of environmental sciences* v. 3 no. 2 258-265.
- Ajibade, A. 1980. Geotectonic evolution of the Zungeru Region, Nigeria. Unpubl. PhD thesis, Univ. Wales, Aberystwyth.
- Ajibade, A., Fitches, W., and Wright, J. 1979. The Zungeru Mylonites, Nigeria: recognition of a major tectonic unit. *Revue de géologie dynamique et de géographie physique Paris* v. 21 no. 5 359-363.
- Ajibade, A., Woakes, M., and Rahaman, M. 1987. Proterozoic Crustal Development in the Pan-African Regime of Nigeria. *Proterozoic Lithospheric Evolution* 259-271.
- Ajibade, A., and Wright, J. 1988. Structural Relationship in the Schist Belts of North Western Nigeria. *Precambrian geology of Nigeria. A publication of Geological Survey* 103-109.
- Akinniyi Akinjide, A., and Ola Samuel, A. 2016. Investigation of Certain Engineering Properties of Some Nigerian Limestone Deposits For Cement Production. 1-12.
- ASTM, D. 1986. 790 M-86. Standard test method for flexural properties of un-reinforced and reinforced plastics and electrical insulating materials (METRIC).
- Bieniawski, Z. Year. Published. Engineering classification in rock engineering. in *Proceedings of the symposium on exploration for rock engineering, Johannesburg 1976.* 97-106.
- Black, R. 1980. Precambrian of west Africa. *Episodes Journal of International Geoscience* v. 3 no. 4 3-8.
- Breuer, J., Höffer, E.-M., and Hummitzsch, W. 2002. Rate of occupational accidents in the mining industry since 1950—a successful approach to prevention policy. *Journal of Safety Research* v. 33 no. 1 129-141.

- Burke, K., and Dewey, J., 1972, Orogeny in Africa: In Dessauvague TFJ, Whiteman AJ (Eds.), African Geology (pp. 583-608), Ibadan: University of Ibadan Press.
- Call, R., Nicholas, D., and Savely, J. 1976. Aitik Slope Stability Study. Pincock, Allen & Holt, Inc. Report to Boliden Aktiebolag, Gällivare, Sweden.
- Call, R., Savely, J., and Nicholas, D. Year. Published. Probabilistic approach to slope design for the Aitik mine, Sweden: Bergmekanikdagen 1977. in Proceedings Rock Mechanics Meeting1977. 37-62.
- Call, R. D. 1972. Analysis of geologic structure for open pit slope design. Citeseer.
- Chowdhury, R., Flentje, P., and Bhattacharya, G. 2009. Geotechnical slope analysis. Crc Press, Taylor and Francis, UK.
- Cooray, P. 1972. Hornblende–garnet Granulites from Hatton, Ceylon. Geological Magazine v. 109 no. 1 37-44.
- Dada, S. 1998. Crust-forming ages and proterozoic crustal evolution in Nigeria: a reappraisal of current interpretations. Precambrian research v. 87 no. 1-2 65-74.
- Dawson, E., Roth, W., and Drescher, A. 1999. Slope stability analysis by strength reduction. Geotechnique v. 49 no. 6 835-840.
- Dempers, G., Seymour, C., and Jenkins, P. 2011. A New Approach to Assess Open Pit Slope Stability. Proceedings, Slope Stability 18-21.
- Dempster, A. N. 1967. Geophysical Survey of Nigeria 1:250,000 Sheet 61 Akure.
- Dhillon, B. S. 2010. Mine safety: a modern approach. Springer science & business media.
- Dorin, I., Diaconescu, C., and Topor, D. I. 2014. The role of mining in national economies. International Journal of Academic Research in Accounting, Finance and Management Sciences v. 4 no. 3 155-160.
- Dunn, M. 2014. Geotechnical Models and Data Confidence in Mining Geotechnical Design.
- Eberhardt, E. 2003. Rock slope stability analysis–utilization of advanced numerical techniques. Earth and Ocean sciences at UBC.

- Eberhardt, O., and Wallmersperger, T. 2015. Energy consistent modified molecular structural mechanics model for the determination of the elastic properties of single wall carbon nanotubes. *Carbon* v. 95 166-180.
- Ekwueme, B. N. 1987. Structural orientations and Precambrian deformational episodes of Uwet area Oban massif, SE Nigeria. *Precambrian Research* v. 34 no. 3-4 269-289.
- Elueze, A., and Okunlola, O. 2003. Petrochemical and petrogenetic characteristics of metasedimentary rocks of Lokoja-jakura schist belt, central Nigeria. *Journal of Mining and Geology* v. 39 no. 1.
- Elueze, A. A. 1982. Mineralogy and chemical nature of metaultramafites in Nigerian schist belts. *Journal of Mining and Geology*.
- Ericsson, M. 2012. Mining technology—trends and development. POLINARES Consortium.
- Fadugba, O. G., Oluyemi-Ayibiowu, B. D., Owolabi, T. A., and Olowoselu A. S 2015. Strength Characteristics of Lateritic Soils Stabilized with Locally Manufactured and Imported Hydrated Lime v. 7(10) 4-15.
- Falconer, J. D., and Woods, H. 1911. The geology and geography of northern Nigeria. Macmillan and Company, limited.
- Fatoye, F. B., and Gideon, Y. B. 2013. Geology and occurrences of limestone and marble in Nigeria. *Geology* v. 3 no. 11.
- Fillion, M., and Hadjigeorgiou, J. 2013. Reliability of strength estimates based on limited laboratory data. *Proceedings Slope Stability* 163-176.
- Fleurisson, J.-A. 2012. Slope Design and Implementation in Open Pit Mines: Geological and Geomechanical Approach. *Procedia Engineering* v. 46 27-38.
- Fleuty, M. 1964. The description of folds. *Proceedings of the Geologists' Association* v. 75 no. 4 461-492.
- FMMP 1974. Geological map of Nigeria, 1:2,000,000 scale. Federal Ministry of Mines and Power, Nigeria.

- Girard, J. M., and McHugh, E. 2000. Detecting problems with mine slope stability. 31st Annual Institute on Mining Health, Safety, and Research, Roanoke, VA, Also NIOSHTIC Report no. 10006193.
- Grant, N. K. 1970. Geochronology of Precambrian basement rocks from Ibadan, southwestern Nigeria. *Earth and Planetary Science Letters* v. 10 no. 1 29-38.
- Grant, N. K. 1971. South Atlantic, Benue Trough, and Gulf of Guinea Cretaceous Triple Junction. *Geological Society of America Bulletin* v. 82 no. 8 2295-2298.
- Grant, N. K., Hickman, M. H., Burkholder, F. R., and Powell, J. L. 1972. Kibaran metamorphic belt in Pan-African domain of West Africa? *Nature Physical Science* v. 238 no. 84 90-91.
- Griffiths, D., and Lane, P. 2000. Slope stability analysis by finite elements. *Geotechnique* v. 49 no. 3 387-403.
- Hartman, H. L., and Britton, S. G. 1992. *SME mining engineering handbook*. Society for Mining, Metallurgy, and Exploration Denver.
- Hartman, H. L., and Mutmanský, J. M. 2002. *Introductory mining engineering*. John Wiley & Sons.
- Hawley, R., and Stewart, A. 1987. Design of open pit coal mine slopes: an integrated approach. *International Journal of Surface Mining, Reclamation and Environment* v. 1 no. 3 179-185.
- Hoek, E. 1965. *Rock fracture under static stress conditions*. CSIR.
- Hoek, E., 2007, *Analysis of Rockfall Hazards, Practical Rock Engineering*, Electronic document.
- Hoek, E. 2009. *Fundamentals of slope design*. Keynote address at Slope Stability 9-11.
- Hoek, E., 2010, *Practical rock engineering*, Evert Hoek Consulting Engineer Inc.
- Hoek, E., and Bray, J. 1981. *Rock slope engineering*. Inst. Mining and metallurgy, London.

- Hoek, E., and Brown, E. 2019. The Hoek–Brown failure criterion and GSI–2018 edition. *Journal of Rock Mechanics and Geotechnical Engineering* v. 11 no. 3 445-463.
- Hoek, E., and Brown, E. T. 1980. Empirical strength criterion for rock masses. *Journal of Geotechnical and Geoenvironmental Engineering* v. 106 no. ASCE 15715.
- Hoek, E., and Brown, E. T. 1997. Practical estimates of rock mass strength. *International journal of rock mechanics and mining sciences* v. 34 no. 8 1165-1186.
- Hoek, E., Carranza, C., and Corkum, B., 2002, Hoek–Brown failure criterion, 2002 edition. Narms-Tac, University of Toronto Press.
- Hoek, E., Wood, D., and Shah, S. Year. Published. A modified Hoek–Brown failure criterion for jointed rock masses. in *Proceedings Rock Characterization: ISRM Symposium, Eurock'92, Chester, UK, 14–17 September 1992*. Thomas Telford Publishing. 209-214.
- Hubbard, F. 1968. The association charnockite-Older granite in South-Western Nigeria. *Niger J Min Geol* v. 3 25-32.
- Hubbard, F. H. 1975. Precambrian crustal development in western Nigeria: indications from the Iwo region. *Geological Society of America Bulletin* v. 86 no. 4 548-554.
- Hustrulid, W., and Kuchta, M. 1995. Open pit mine. *PLANNING & DESIGN.*: SME.
- Hustrulid, W. A. 1982. *Underground mining methods handbook*.
- Hustrulid, W. A., McCarter, M. K., and Van Zyl, D. J. 2001. *Slope stability in surface mining*. SME.
- Ibrahim, S., Egesi, C., and Tukur, A. 2010. "Nigeria: How Illegal Mining Deplete our Population".
- Igwe, O., and Una, C. O. 2019. Landslide impacts and management in Nanka area, Southeast Nigeria. *Geoenvironmental Disasters* v. 6 no. 1 1-12.
- ISRM, International Society of Rock Mechanics, 2007. *The complete ISRM suggested methods for rock characterization, testing and monitoring: 1974-2006*. International Soc. for Rock Mechanics, Commission on Testing Methods.

- Jimoh, O. A., Ariffin, K. S., Hussin, H. B., and Habeeb, A. A. 2017. Characterization and assessment of Okpella metacarbonate deposit in Nigeria. *Carbonates and Evaporites* v. 32 no. 4 513-524.
- Jing, L. 2003. A review of techniques, advances and outstanding issues in numerical modelling for rock mechanics and rock engineering. *International Journal of Rock Mechanics and Mining Sciences* v. 40 no. 3 283-353.
- Jones, G., and Hockey, R. 1964. Geology of parts of Southwestern Nigeria *Bull. Geol. Surv.* no. 31.
- Jones, H., and Jovanovich, D. 1985. A ray inversion method for refraction analysis. *Journal of Geophysics*. V.50 no. 11 1701-1720.
- Keller, G. V., and Frischknecht, F. C. 1966. *Electrical methods in geophysical prospecting*.
- Kennedy, B. A. 1990. *Surface mining*. 2nd. SME.
- Kogbe, C. A. 1989. *Geology of Nigeria*. Rock View (Nigeria) Limited. Jos, Nigeria. 325-334.
- Kucuker, H. 2006. Occupational fatalities among coal mine workers in Zonguldak, Turkey, 1994–2003. *Occupational Medicine* v. 56 no. 2 144-146.
- Le Maitre, R. W., Streckeisen, A., Zanettin, B., Le Bas, M., Bonin, B., and Bateman, P. 2005. *Igneous rocks: a classification and glossary of terms: recommendations of the International Union of Geological Sciences Subcommittee on the Systematics of Igneous Rocks*. Cambridge University Press.
- Little, M. 2006. The benefit to open pit rock slope design of geotechnical databases. *Proceedings of international symposium on stability of rock slopes in open pit mining and civil engineering*. SAIMM 97-116.
- Liu, Y., Lee, F.-H., Quek, S.-T., and Beer, M. 2014. Modified linear estimation method for generating multi-dimensional multi-variate Gaussian field in modelling material properties. *Probabilistic Engineering Mechanics* v. 38 42-53.
- Llano-Serna, M., Williams, D. J., and Ruest, M. 2016. Analysis of Kennecott Utah Copper's Bingham Canyon Mine Pit Wall Slides. *Tailings and Mine Waste*'16.

- Mallo, S. J. 2012. Mitigating the activities of artisanal and small-scale miners in Africa: challenges for engineering and technological institutions. *International Journal of Modern Engineering Research* v. 2 no. 6 4714-4725.
- Mallo, S. J., and Wazoh, H. N. 2014. Reclamation of abandoned mined-out areas of Bukuru-Rayfield. *Journal of Environmental Science, Toxicology and Food Technology* v. 8 no. 2 25-34.
- Mallo, S. J., and Yarekes, P. 2012. Preliminary Study of Rocks and Soils Types in Mangun, Plateau State, North Central Nigeria. *Continental Journal of Earth Sciences* v. 7 no. 1 19 - 28.
- Marinos, P., and Hoek, E. Year. Published. GSI: a geologically friendly tool for rock mass strength estimation. in *Proceedings ISRM international symposium2000*. International Society for Rock Mechanics.
- Marinos, V. 2019. A revised, geotechnical classification GSI system for tectonically disturbed heterogeneous rock masses, such as flysch. *Bulletin of Engineering Geology and the Environment* v. 78 no. 2 899-912.
- Marinos, V., and Carter, T. G. 2018. Maintaining geological reality in application of GSI for design of engineering structures in rock. *Engineering Geology* v. 239 282-297.
- Mathis, J. I., Geotechnical, Z., and Ellensburg, W. 2009. Bench-Inter-ramp-Overall: a guide to statistically designing a rock slope. *Slope Stability, Conference*. Santiago, Chile.
- McClintock, F. Year. Published. Friction on Griffith cracks in rocks under pressure. in *Proceedings Proc. 4th US Nat. Congr. Appl. Mech.*1962. Volume 2. 1015-1022.
- Moore, I. D., Grayson, R., and Ladson, A. 1991. Digital terrain modelling: a review of hydrological, geomorphological, and biological applications. *Hydrological processes* v. 5 no. 1 3-30.
- National Research Council, 2002. *Evolutionary and revolutionary technologies for mining*. National Academies Press.

- Nicholas, O., 1986, Schlumberger Vertical Soundings: Techniques and Interpretations with Examples from Krfsluvlk and Glerardalur, Iceland and Olkaria, Kenya, Geothermal Training Programme—United Nations University.
- Obaje, N. G. 2009. Geology and mineral resources of Nigeria. Springer.
- Obiora, S., and Umeji, A. 2004. Petrographic evidence for regional burial metamorphism of the sedimentary rocks in the lower Benue Rift. *Journal of African Earth Sciences* v. 38 no. 3 269-277.
- Odeyemi, I. 1979. Orogenic events in the Precambrian basement of Nigeria, West Africa. *Precambrian geology of Nigeria. PAOB Newsletter I. Yace (ed) no. 3* 18-24.
- Odeyemi, I. 1988. Lithostratigraphy and structural relationships of the Upper Precambrian Metasediments in Igarra area, southwestern Nigeria. *Precambrian geology of Nigeria. Publ. GSN* 111.
- Ogezi, A. 1977. Geochemistry and geochronology of basement rocks from northwestern Nigeria. Unpubl. PhD thesis, Univ. Leeds.
- Okagbue, C.O. 1992. The 1988 Nanka landslide, Anambra state, Nigeria. *Bulletin of the International Association of Engineering Geology* 46 (1): 79-87.
- Okunlola, O. A. 2005. Metallogeny of tantalum-niobium mineralization of precambrian pegmatites of Nigeria. *Ορυκτός Πλούτος* v. 2005 no. 137 38-50.
- Okunlola, O. A., Alabi, M. O., and Idakwo, S. O. 2015. Testing Pre-Cambrian Marble Bodies in the Oreke and OwaKajola Areas, North Central Nigeria for Multiple Industrial Applications. *Journal of Environment and Earth Science* v. 5 no. 15.
- Okunola, O., Akintola, A., and Egbeyemi, R. 2006. Compositional features and petrogenetic affinity of precambrian amphibolitic-schist of Sepeteri are South western Nigeria. *Global Journal of Geological Sciences* v. 4 no. 2.
- Oladunjoye, M., and Jekayinfa, S. 2015. Efficacy of Hummel (modified Schlumberger) arrays of vertical electrical sounding in groundwater exploration: case study of parts of Ibadan Metropolis, Southwestern Nigeria. *International Journal of Geophysics* v. 2015.

- Oluyide, P. O., Nwajide, C. S., and Oni, A. O. 1998. The geology of the Ilorin area. Nigerian Geological Survey Bulletin no. 42 84.
- Opafunso, Z. O. 2002a. Application of Pincock Software Model in Gold Mining Economics. Science, Engineering and Technology v. 9 no. 3 4373 - 4382.
- Opafunso, Z. O. 2002b. Design of a Stable Overburden Heap in Feldspar Open Pit Mine. Journal of Science, Engineering and Technology v. 9 no. 1 3865 - 3873.
- Opafunso, Z. O. 2011. Overview of Artisanal and Small Scale Mining of Gold Operations in Nigeria. Lecture at Federal University of Technology, Akure, Ondo State, Nigeria.
- Opafunso, Z. O., and Ozigis, I. I. 2008. Dimension Stone Drilling Pattern Design, Equipment and Performance. Environmental Science, University of Jos v. 12 no. 1-2 114 -121.
- Oversby, V. 1975. Lead isotopic study of aplites from the Precambrian basement rocks near Ibadan, southwestern Nigeria. Earth and Planetary Science Letters v. 27 no. 2 177-180.
- Oyawoye, M. 1972. The basement complex of Nigeria. African geology 67-99.
- 1972. The basement complex of Nigeria. African geology 67-99.
- Pankow, K. L., Moore, J. R., Hale, J. M., Koper, K. D., Kubacki, T., Whidden, K. M., and McCarter, M. K. 2014. Massive landslide at Utah copper mine generates wealth of geophysical data. GSA Today v. 24 no. 1 4-9.
- Parasnis, D. S. 2012. Principles of applied geophysics. Springer Science & Business Media.
- Piper, D. 2012. Mining in Africa a Legal Overview. Retrieved Nov. 20, 2019. from www.dlapiper.com. 1-68.
- Qudrat-Ullah, H., and Panthallor, P. N. 2020. Operational Sustainability in the Mining Industry: The Case of Large-Scale Open-Pit Mining (LSOPM) Operations. Springer Nature.
- Rahaman, M. 1973. The Geology of the district around Iseyin, Western Nigeria: Unpublished Ph. D. D Thesis, University of Ibadan 268.

- Rahaman, M. 1988. Recent advances in the study of the basement complex of Nigeria. Pre Cambrian geology of Nigeria 11-41.
- Rahaman, M., and Ocan, O. 1978. On relationship in the Precambrian migmatitic gneisses of Nigeria J. Min. and Geol v. 15 no. 1.
- Rahaman, M. A. 1978. Geochemistry of some gneiss from parts of Southern Nigeria. Journal of Mining and Geology.
- Rahaman, M. 1989. Review of the Basement Geology of Southwestern Nigeria. Geology of Nigeria (Kogbe CA Ed.). Elizabeth Publishing. Co. Nigeria 41-58.
- Read, J., and Ogden, A. 2006. Developing new approaches to rock slope stability analyses. Int Symp Stab Rock Slopes, South African Inst Min Metall Symp Ser S v. 44 3-10.
- Read, J., and Stacey, P. 2009. Guidelines for open pit slope design.
- Rocscience, 2009. Phase2 version 7.0 User Manual. Computer software. Toronto, Ontario, Canada: Rocscience, Inc., <https://www.rocscience.com/software/dips>.
- Rocscience, 2019. Dips, ver. 7.0, Computer software. Toronto, Ontario, Canada: Rocscience, Inc. <https://www.rocscience.com/software/dips>.
- Rocscience, 2007. RocLab Version 1.031—Rock mass strength analysis using the Hoek–Brown failure criterion. Online.
- Russ, W. 1957. The geology of parts of Niger, Zaria and Sokoto Provinces, with special reference to the occurrence of gold. authority of the Federal Government of Nigeria.
- Satyanarayana, I., and Sinha, A. K. 2018. A Critical Review of Stability Analysis and Design of Pit Slopes in Indian Opencast Coal Mines. Chemical Engineering Transactions v. 66 1231-1236.
- Scoffin, T. P. 1986. An introduction to carbonate sediments and rocks.
- Senouci, O., and Okunlola, O. A., 2019, The Importance of Joint Set Measurements for Slope Stability and Design Case Study: BUA Quarry, Okpella, Edo State, Nigeria, 55th Nigerian Mining and Geosciences Society (NMGS) Annual International Conference and Exhibitions : Coal City, Enugu, Nigeria, p. 134-135.

- Sivakugan, N., Shukla, S. K., and Das, B. M. 2013. Rock mechanics: An introduction. Crc Press.
- Sjöberg, J. 1997. Estimating rock mass strength using the Hoek–Brown failure criterion and rock mass classification—a review and application to the Aznalcollar open pit. Division of Rock Mechanics, Department of Civil and Mining Engineering, Lulea University of Technology v. 154.
- Sjöberg, J. 1999. Analysis of large scale rock slopes. Luleå tekniska universitet.
- Sjöberg, J., Sharp, J., and Malorey, D. 2001. Slope stability at Aznalcóllar. Slope stability in surface mining 183-202.
- Stacey, P. 2006. Factors in the design of open pit slopes-A reviewer's perspective. International Symposium on Stability of Rock Slopes in Open Pit Mining and Civil Engineering. Cape Town 1-2.
- Stacey, T. 2004. The link between the design process in rock engineering and the code of practice to combat rock fall and rockburst accidents. Journal of the Southern African Institute of Mining and Metallurgy v. 104 no. 1 29-33.
- Standard, A. 2008. D4543. Standard Practices for Preparing Rock Core as Cylindrical Test Specimens and Verifying Conformance to Dimensional and Shape Tolerances. Annual Book of ASTM Standards, American Society for Testing and Materials, West Conshohocken, PA.
- Standard, 2010. D7012–10 (2010) Standard test method for compressive strength and elastic moduli of intact rock core specimens under varying states of stress and temperatures. Annual Book of ASTM Standards, American Society for Testing and Materials, West Conshohocken, PA 495-498.
- Steffen, O., Contreras, L., Terbrugge, P., and Venter, J. Year. Published. A risk evaluation approach for pit slope design. in Proceedings The 42nd US Rock Mechanics Symposium (USRMS)2008. American Rock Mechanics Association.

- Sternik, K. 2013. Comparison of slope stability predictions by gravity increase and shear strength reduction methods. *Czasopismo Techniczne. Środowisko* v. 110 no. 1-Ś 121--130.
- Stewart, A., Wessels, F., and Bird, S. 2000. Design, implementation, and assessment of open-pit slopes at Palabora over the last 20 years. *Slope Stability in Surface Mining* 177-181.
- Stewart, S. W. 2007. Rock mass strength and deformability of unweathered closely jointed New Zealand greywacke.
- Sullivan, T. 2006. Pit slope design and risk—A view of the current state of the art. *Proceeding of the Int. Symposium on Stability of Rock Slopes in Open Pit Mining and Civil Engineering Situations*.
- Taseko Mines Limited. 2012. New Prosperity Gold Copper Mine Project British Columbia, Canada: Environmental Impact Statement. September, 2012.
- Terazawa, K., Takatori, T., Tomii, S., and Nakano, K. 1985. Methane asphyxia. Coal mine accident investigation of distribution of gas. *The American journal of forensic medicine and pathology* v. 6 no. 3 211-214.
- Trewin, B. 2007. The role of climatological normals in a changing climate. *World Climate Data and Monitoring Program* no. 61, WMO-TD no. 1377.
- Twerefou, D. K. 2009. Mineral Exploitation, Environmental Sustainability and Sustainable Development in EAC, SADC, and ECOWAS Regions. African Trade Policy Centre, Economic Commission for Africa.
- UNECA. 2011. Minerals and Africa's development: The International Study Group Report on Africa's Mineral Regimes.
- Valdivia, C., and Lorig, L. 2000. Slope stability at Escondida mine. *Slope Stability in Surface Mining*, Littleton. SME, Colorado 153-162.
- Valerio, M., D'Ambra, S., Castro, L., and Woodward, R. Year. Published. Evaluation of Rock Bridges Through DFN Models to Improve Pit Slope Design in the Absence of Joint

- Persistence Data. in Proceedings 51st US Rock Mechanics/Geomechanics Symposium2017. American Rock Mechanics Association.
- Varnier, J.-B., Cremeens, J., and Overton, D. 2018. Three-dimensional slope stability analysis of block sliding slope failure at the Pikeview Quarry, El Paso County, Colorado. *Mining Engineering* v. 70 no. 3.
- Verma, R., Rao, M., and Rao, C. 1980. Resistivity investigations for ground water in metamorphic areas near Dhanbad, India. *Groundwater* v. 18 no. 1 46-55.
- Warhurst, A. 1999. Environmental Regulation, Innovation and Sustainable Development. In a Warhurst (ed), *Mining and Environment: Case Studies from the Americas*, Internatinal Development Research Center, Ottawa, Canada.
- Wesseloo, J., and Dight, P. Year. Published. Rock mass damage in hard rock open pit mine slopes. in Proceedings Rock mass damage in hard rock open pit mine slopes2009. University de los Andes, Chile. 7.
- West, R., Larson, N., Visca, P., Nicholas, D., and Call, R. 1985. Aitik slope stability study. Call & Nicholas, Inc. Report to Boliden Mineral AB, Aitik Mine.
- Woods, J., and Lane, A. 2015. State of Mining in Africa in the spotlight.
- Wyllie, D. C., and Mah, C. 2004. *Rock slope engineering*. CRC Press.
- Zheng, Y., Tang, X., Zhao, S., Deng, C., and Lei, W. 2009. Strength reduction and step-loading finite element approaches in geotechnical engineering. *Journal of Rock Mechanics and Geotechnical Engineering* v. 1 no. 1 21-30.
- Zienkiewicz, O. C., Humpheson, C., and Lewis, R. 1975. Associated and non-associated visco-plasticity and plasticity in soil mechanics. *Geotechnique* v. 25 no. 4 671-689.